A Novel Electrochemical Technique for Mineral Scale Coverage and Scaling Tendency Quantification

Tong H Teh

Submitted for the degree of Doctor of Philosophy

Heriot-Watt University

School of Engineering and Physical Sciences

September 2011

ABSTRACT

Mineral scaling poses a far greater problem to any industry that uses or produces water. The quality of water used by industry varies widely and gives rise to numerous scaling problems. Mineral scale formation and deposition on equipment surface causes major flow assurance concerns particularly apparent in the offshore oil and gas industry. An improper of scale management programmes could lead to a rapid mineral scale build up and subsequently significant reductions in productivity and compromises the operational safety of process equipment (i.e. safety valves) as a result of blockage.

The result is costly workovers increasing project operating costs (OPEX) due to the need for scale dissolver treatments and significant production losses. As part of scale management programme, it is desirable to be able to quantify the extent of the mineral scale that has deposited on component surface and also to be able to monitor the changes of likelihood that a production fluid will precipitate out mineral scale.

The nature of this research is focus on exploring a simple approach or a methodology to detect the mineral scale formed specifically for calcium carbonate on the electrode surface. The application of a submerged impinging jet (SIJ) in conjunction with an electrochemical technique was developed. The development of this technique has been taken into the consideration of advantages and disadvantages of the current available scale detection techniques. Not only has the complexity of equipment and facilities been considered during the development stage, but the data interpretation of the existing technologies has been considered.

In general, efforts have concentrated upon strategies to develop and to validate this methodology for the scale coverage on the electrode surface as well as monitoring the scaling tendency through the electrochemical technique measurement. Various verifications and experiments were undertaken to ensure the reliability of the use of electrochemical measurement and SIJ geometry configurations. The influence of surface condition on the sensitivity of this technique were also assessed

This technique clearly demonstrated that various levels of mineral deposition on the surface could be quantified. This included the calcium carbonate deposition in the presence and absence of magnesium ions. In this study, a similar SIJ set up

configuration was used for scaling tendency measurement to quantify and predict whether scaling will occur in water or brine solution. The scaling tendency results illustrated that there was a good correlation between the saturation ratio and the scaling tendency slope measurement by an electrochemical analysis.

The contribution main of this research contributes to a better understanding of the used of SIJ for scale detection, monitoring and quantification of calcium carbonate scale formation.

ACKNOWLEDGEMENT

Firstly, I would like to express my thanks to my supervisors, Professor Anne Neville and Dr Gillian Thomson for the assistance and trust during this research, without their support this thesis would not be been possible. I sincerely acknowledge Heriot-Watt University for giving me the opportunity to carry this research.

I appreciate the help provided by staff in the department, thanks for their attention and assistance especially Marian Millar, Ronald Millar, Malcolm McWilliams, Richard Kinsella, Cameron Smith, John Pritchard, Paul Glynn, Aftab Aziz, Mark, Josie and Mary.

Warm thanks to my work mates and special friends who helped me keep faith and maintain a healthy balance between work and leisure. I appreciate the helping hand given by Catherine Fitzgerald, special thank to her.

Finally, I would like to thank my family, in particular my parents and my brothers, for their constant support and advice. Most of all, I am grateful to Ms An T Liao for her continuous incessant encouragement, patience, but mainly for sharing her life and ideas with me during my research. This thesis is dedicated to them.

ACADEMIC REGISTRY
Research Thesis Submission

Name*:*	Tong H Teh		
School/PGI:	School of Engineering and Physical Sciences		
Version: *(i.e. First, Resubmission, Final)*	Final	Degree Sought (Award and Subject area)	PhD

Declaration

In accordance with the appropriate regulations I hereby submit my thesis and I declare that:

1) the thesis embodies the results of my own work and has been composed by myself
2) where appropriate, I have made acknowledgement of the work of others and have made reference to work carried out in collaboration with other persons
3) the thesis is the correct version of the thesis for submission and is the same version as any electronic versions submitted*.
4) my thesis for the award referred to, deposited in the Heriot-Watt University Library, should be made available for loan or photocopying and be available via the Institutional Repository, subject to such conditions as the Librarian may require
5) I understand that as a student of the University I am required to abide by the Regulations of the University and to conform to its discipline.

* *Please note that it is the responsibility of the candidate to ensure that the correct version of the thesis is submitted.*

Signature of Candidate*:*		Date:	

Submission

Submitted By *(name in capitals):*	
Signature of Individual Submitting:	
Date Submitted:	

For Completion in the Student Service Centre (SSC)

Received in the SSC by *(name in capitals):*			
Method of Submission (Handed in to SSC; posted through internal/external mail):			
E-thesis Submitted (mandatory for final theses)			
Signature:		Date:	

TABLE OF CONTENT

CHAPTER 1 INTRODUCTION AND OBJECTIVES 1

1.1 INTRODUCTION 1

1.2 OBJECTIVES 2

1.3 THESIS LAYOUT 2

CHAPTER 2 SCALE MONITORING TECHNOLOGIES 4

2.1 INTRODUCTION 4

2.2 SCALE PREDICTION 5

2.3 SCALE DETECTION TECHNIQUES 8

2.3.1 Electrochemical Monitoring Techniques 9
2.3.2 Ultrasonic Methods 13
2.3.3 Temperature/Heat Sensors 15
2.3.4 Radioactive Detectors 16
2.3.5 Common Practices of Scale Monitoring 17

2.4 SCALE DETECTION TECHNOLOGIES 18

2.4.1 Thickness Shear Mode Resonator (TSMR) 18
2.4.2 Dual/ Triple Gamma Ray Attenuation 19
2.4.3 Attenuated Total Reflectance (ATR) 20

2.5 SUMMARY OF THE TECHNOLOGIES 21

CHAPTER 3 REVIEW OF MINERAL GROWTH AND SCALING 23

3.1 INTRODUCTION 23

3.2 BACKGROUND OF SCALE 23

3.2.1 Organic Scale 23
3.2.2 Inorganic Scale 24

3.3 MINERAL SCALING AND PRECIPITATION 27

3.3.1 The Kinetics of Crystal Nucleation 29
3.3.2 Review of the Crystal Growth and Kinetics 31

3.4 CRYSTAL DISSOLUTION 34

3.4.1 Industry Cleaning/ Scale Removal 38
3.4.2 Scale Control 39

3.5 REVIEW OF SURFACE SCALING 40

3.5.1 London-Van der Waals Forces 40
3.5.2 Electrostatic Double-layer Force 41
3.5.3 Characteristics of Surface Scaling 41
3.5.4 Electrochemically Accelerated Scaling Tests 43

CHAPTER 4 REVIEW AND DEVELOPMENT OF A SUBMERGED IMPINGING JET AS A MONITORING SENSOR 50

4.1 INTRODUCTION 50

4.2 REVIEW OF THE ELECTROCHEMICAL MEASUREMENT....53
4.3 REVIEW OF A SUBMERGED IMPINGING JET (SIJ)....54
4.4 BACKGROUND TECHNIQUE OF SCALE DETECTION....59
4.5 BACKGROUND TECHNIQUE OF SCALING TENDENCY....61
4.6 BACKGROUND OF SCALE REMOVAL/CLEANING....63
4.7 DESIGN OF THE SUBMERGED IMPINGING JET (SIJ) AND EQUIPMENT SET-UP....65

CHAPTER 5 EXPERIMENTAL PROCEDURES AND CALIBRATIONS...67

5.1 INTRODUCTION....67
5.2 STUDY AND INVESTIGATION OF SCALE COVERAGE....68
5.2.1 Sample Preparation and Mechanical Polishing....69
5.2.2 Initial Analysis....70
5.2.3 Scale Deposition (Normal Deposition)....72
5.2.4 Final Analysis....74
5.2.5 Post Analysis of Scale Coverage....74
5.3 STUDY AND INVESTIGATION OF SCALING TENDENCY....77
5.3.1 Scale Deposition (Electrochemical Deposition)....77
5.3.2 Post Analysis of Scaling Tendency....79
5.4 STUDY AND INVESTIGATION OF SCALE REMOVAL/CLEANING....81
5.4.1 Initial Analysis....81
5.4.2 Scale Deposition (Not Electrochemical Deposition)....81
5.4.3 Final Analysis....81
5.4.4 Cleaning Analysis....82
5.4.5 Post Analysis....83
5.5 CALIBRATION OF THE SYSTEM PARAMETERS AND TECHNIQUE FOR ELECTROCHEMICAL MEASUREMENT....86
5.5.1 Calibration of the SIJ Set-up and Its Associated Equipment....86
5.5.2 Optimising the Experimental Conditions....89
5.5.3 Calibrations of the Electrochemical Technique....98
5.6 CONCLUSIONS OF THE DEVELOPMENT AND VERIFICATIONS OF THE ELECTROCHEMICAL MEASUREMENT USING A SIJ CELL RIG....110

CHAPTER 6 AN INVESTIGATION OF SIJ AS A MEANS OF DETECTING MINERAL SCALING....111

6.1 INTRODUCTION....111
6.2 AN INTRODUCTION OF SCALE COVERAGE INVESTIGATION....114
6.3 THE USE OF SIJ TO DETECT CALCIUM CARBONATE....114
6.3.1 Calcium Carbonate with the Presence of Magnesium Ions....115
6.3.2 Calcium Carbonate with the Absence of Magnesium Ions....121
6.3.3 The Effect of Magnesium Ions on Scale Coverage Quantification....125
6.4 FURTHER INVESTIGATION OF SCALE COVERAGE DISCREPANCY BETWEEN THE IMAGE ANALYSIS AND ELECTROCHEMICAL TECHNIQUE....129

6.4.1 The Effect of Brine Solution on Surface Coverage *130*
6.4.2 Overall Effect of the Brine Composition on Scale Coverage *137*
6.4.3 Comparison of Scale Coverage Quantified By the RDE to SIJ *139*
6.4.4 The Influence of Crystal Deposited on Electrochemical Measurement *146*
6.4.5 Investigations of Scale Coverage Discrepancy between the Electrochemical Versus the Image Analysis *149*
6.4.6 Summary of Investigation of Scale Coverage Discrepancy between Electrochemical Technique and Image Analysis *152*
6.5 CONCLUDING REMARKS ON CALCIUM CARBONATE DETECTION 154

CHAPTER 7 AN INVESTIGATION OF SCALING TENDENCY 155

7.1 INTRODUCTION 155
7.2 A BRIEF INTRODUCTION OF BACKGROUND TECHNIQUE OF SCALING TENDENCY MEASUREMENT 156
7.3 THE INFLUENCE OF BRINE COMPOSITIONS ON SCALING TENDENCY 158
7.3.1 The Effect of Bicarbonate Ions on Polarisation *161*
7.3.2 The Effect of Magnesium Ions on Polarisation *162*
7.3.3 Conclusion of the Effect of Brine Solution Composition *164*
7.4 FEASIBILITY STUDY AND INVESTIGATION OF SCALING TENDENCY 165
7.4.1 Understanding the Various Regimes of Current Response Prior to Scaling Tendency Quantification *166*
7.4.2 Summary of the Scaling Tendency Measurement Determination *172*
7.5 SCALING TENDENCY QUANTIFICATION OF VARIOUS SATURATED BRINE SOLUTION (DIFFERENT SATURATION RATIO) 175
7.5.1 Saturated Brine Solutions *175*
7.5.2 Undersaturated Brine (Saturation Ratio 0.27) *180*
7.5.3 Crystal Morphology Formation by Polarisation Process *183*
7.5.4 The Effect of Flow rate on Scaling Tendency Slope Measurement *186*
7.5.5 Scaling Time Quantification *187*
7.6 VERIFICATION OF THE RELATIONSHIP OF THE SCALING TENDENCY SLOPE AND THE SATURATION RATIO 190
7.6.1 Conclusions of the Scaling Tendency Slope Measurement *194*
7.7 THE PRACTICAL APPLICATION OF SIJ TECHNIQUE 195

CHAPTER 8 AN INVESTIGATION OF SURFACE CLEANING AND SURFACE SENSIVITY 196

8.1 INTRODUCTION AND OBJECTIVE 196
8.2 SURFACE SENSIVITY AFTER SCALE REMOVAL/CLEANING TECHNIQUE 197
8.2.1 Electrochemical-Cathodic Polarisation *197*
8.2.2 The Understanding and Effect of Electrochemical Cleaning on Surface Coverage Quantification *204*
8.2.3 The Effectiveness of Electrochemical Cleaning *206*
8.2.4 Acid Cleaning *207*
8.2.5 The Effect of Acid Cleaning On Surface Coverage Quantification *217*
8.2.6 The Effectiveness of Scale Removal by Acid Cleaning *218*

8.3 UNDERSTAND THE SENSIVITY OF ELECTROCHEMICAL MEASUREMENT ON SURFACE MODIFICATIONS 220

8.3.1 Conclusions of the Sensivity of the Electrochemical Measurement on Surface Modifications 223
8.3.2 An Investigation of Different Materials 224
8.3.3 The Use of Different Materials on Oxygen Reduction 227
8.3.4 Conclusion of Acid Cleaning and Electrochemical Polarisation 228

CHAPTER 9 CONCLUSIONS AND FUTURE WORK 229

9.1 INTRODUCTION 229

9.1.1 Summary of Scale Detection and Quantification 229
9.1.2 Summary of Scale Detection and Quantification 229
9.1.3 Summary of Scaling Tendency Quantification 230
9.1.4 Summary of Surface Cleaning and Surface Sensivity 230

9.2 CONTRIBUTIONS OF THIS RESEARCH WORK TOWARD INDUSTRY AND ACADEMICS 231

9.3 CONCEPT THE USE OF SIJ UNIT IN A FIELD TRIAL 232

9.4 FUTURE WORK 235

REFERENCES 237

THESIS RELATED PUBLICATIONS

Tong TEH and Anne NEVILLE, *Electrochemical Sensor For Scaling Building Up Measurements*. (WO/2005/054837) International Application No.: PCT/GB2004/005060. Publication Date: 16-06-2005

Chapter 1 Introduction and Objectives

1.1 Introduction

Scale deposition causes a major practical problem in many process industries, particularly in oil recovery, power and desalination plants. Usually, mineral scale can be found in reservoirs, perforations, process equipment tubing, valves, pumps and separators. In Canada and the North Sea, the main production challenge is mineral scale deposition on process equipment. A fall of production from 30,000 BPD to 0 BPD in 24 hours due to scaling problems was reported in the Miller well [1]. The consequences of scaling are massive in terms of economic and technical challenges. From an economic aspect, it increases OPEX (operating expenditure) through costs associated with chemical treatments to remove and prevent scaling. From a technical view, it lowers the heat transfer coefficient and imposes a range of flow assurance problems. Tjomsland *et al.* reported about $1.1 bn US was being invested to control scale in Veslefrikk field Norway [2]. It is estimated that the overall cost of fouling to industry in the UK per year, has been between £1,000 and £1,200 million. Problems arise with encrustation of tubing, boilers, coils, jets, sprinklers, cooling towers and heat exchangers or wherever the industry is forced to use heated hard water, the heat transfer performance is often affected by scale deposition. Energy losses due to poor heat transfer efficiency has been reported as costing approximately £1,000 million. A 1 mm and 1.5 mm layer of scale was shown to add 7.5 % and 15 % to energy costs respectively. A thickness of 7 mm of scale could increase costs by over 70 % [3].

During the past decade, extensive research has been concentrated in areas such as precipitation kinetics, prediction models, the development of scale inhibitors and treatments. This research has significantly increased and contributed to the scientific understanding on mechanisms of mineral precipitation under various conditions. However, mineral deposition continues to impose massive costs associated with flow assurance problems. This is mainly due to the lack of monitoring development, especially for the reliable on-line monitoring technology to enable the detection of scale at its onset. The development of such a sensor would give better cost savings as well as improve the overall scale management programmes through chemical injection optimisation.

1.2 Objectives

As described in the previous section, any improvement or research activities that focus on scale monitoring processes would be beneficial to many process industries. Hence, the principal aim of this work is to develop a reliable methodology to detect and monitor scale deposited on the component surfaces. In addition, a methodology to quantify and provide an indication of how likely a system is susceptible to scaling is the focus in this research. A novel technique based on the combination of electrochemical measurement and the SIJ (submerged impinging jet) methodology was developed. This technique is capable of detecting the mineral scale deposited on sensor surfaces and the scaling tendency of a system.

This research work focuses and contributes to the understanding of the development of this novel technique. The reliability and validity of this methodology as a means of sensor relies on ability of the sensor to be calibrated and the sensor assessed under various operational environments (such as various saturation brine solutions, types of mineral scale etc.).

As part of a reliable technique to quantify the mineral scaling, different surface cleaning techniques, such as the electrochemical and acid cleanings have been explored. This is an important factor that will contribute to a better understanding of the capability as well as the sensitivity of the sensor after having been subjected to cleaning. Furthermore, the robustness of the sensor can be significantly increased by reducing the frequency of replacing a new the sensor.

1.3 Thesis Layout

The thesis layout is as follows:

Chapter 1 is the general introduction of mineral scaling and the objectives of this project. The summary and layout of each chapter for this thesis are defined.

In Chapter 2, the review of the current monitoring technologies available for laboratory studies and in industry is presented. The current practices to monitor the extent of mineral scale deposited on the component surfaces are reviewed.

Chapter 3 is concerned with the basic knowledge needed to understand mineral scale. The overview relating to mineral scale, such as morphologies, kinetics factors, precipitation and dissolution is reviewed in this chapter.

In Chapter 4, technical background details of a submerged impinging jet (SIJ) in combination with the electrochemical technique use to study mineral scaling are outlined.

The development of essential experimental procedures throughout the thesis is described in Chapter 5. Basically, the procedures can be divided into 3 main related sections investigating (i) scale coverage, (ii) scaling tendency and (iii) scale removal. The development of the SIJ methodology, such as calibration and validation of this technique to ensure the reliability as a monitoring tool is also addressed in this section.

Chapter 6 shows the results of the SIJ technique as a means of accessing the extent of scale formed on metallic surfaces. The most common inorganic minerals found in the oil and gas industry e.g. calcium carbonate are included. Most of the research in this chapter is concerned with calcium carbonate scale with and without the presence of Mg^{2+} ions.

In Chapter 7, the result of the electrochemical measurements to access the scaling tendency of calcium carbonate in the presence of Mg^{2+} ions is described. The scaling tendency is accessed using a novel electrochemical technique. Various parameters such as chemical composition, flow rate and saturation ratio which can influence the scaling tendency measurement have been used to assess the scaling tendency.

Chapter 8 outlines the results of a preliminary investigation showing possible ways to remove calcium carbonate scale deposited on the sensor surfaces. The influence of various cleaning techniques on the sensitivity of this sensor has been assessed.

Chapter 9 summarises the main conclusions and contributions of this research work to academic and industry. Recommendations of future work are also presented in this chapter.

Chapter 2 Scale Monitoring Technologies

2.1 Introduction

Mineral scaling on the surface of heat exchangers, evaporators, water cooling towers and pipelines is one of the major problems encountered in industrial processes. The formation and deposition of mineral scale on process equipment surfaces causes a significant decrease of the flow rate, as well as heat transfer. For many industries, scaling problems continue to impose massive costs. Therefore, the improvement of scale monitoring processes such as the development of a robust on-line monitoring system or new technology is a major challenge.

Mineral scaling on the surface of equipment causing loss of efficiency or production can be addressed through either a monitoring technique, water chemistry prediction or combination of both. Scale prediction models have been widely used in industry as recommended practice especially during the design stage, where the deployment of a scale detection technique is impossible. However, the change of the operational conditions such as pressure, temperature, pH, water content etc. can significantly influence the accuracy of the prediction models. The consequence of underestimating the prediction may have a significant impact on production as result of scale deposition on the process equipment surface where data is collected and sent to a third party for analysis may take days for critical data to be noted. Hence, the development of an *in-situ* technique to monitor the scaling tendency of a system would be a major advantage to a production process where operational parameters may be expected to change as a result of field aging. This also applies to any scale detection technique where the measurement of the real extent of mineral scale formed on the component surface may differ from predicted levels. However, the challenge to have a reliable mineral scale detection technique remains a major issue that needs to be addressed in most of the water related industrial processes.

In this chapter, a brief review of the development of scale detection techniques available in the laboratory and in industry is presented. This chapter is divided into two main sections, prediction models and scale detection techniques. An overview of these will give a better understanding of the technologies and their limitations for the studies of mineral scale precipitation and deposition. Some of these scale detection techniques

have been developed into scale monitoring technologies, which are currently being used in industry.

2.2 Scale Prediction

Numerous saturation indexes and computer algorithms have been developed to determine the scaling potential of particular waters in a process system. The most common scale prediction models are the Langelier Index [4, 5], Ryznar Solubility Index [6] or the Stiff and Davis Index [7]. These models have been used to determine scale forming or corrosive tendencies of water qualitatively. Langelier Saturation Index (LSI) is defined as the difference between the actual pH and the calculated saturated pHs. It has been used to calculate the scaling tendency of water at any given temperature and water composition. The equation used is as follows:

$LSI = pH - pHs$ Equation 2-1

where $pHs = pCa + palk + C$

pHs = saturated pH

pCa = calcium hardness factor (expressed as ppm $CaCO_3$,)

palk = M alkalinity factor (expressed as ppm $CaCO_3$)

C = total solids (expressed as ppm at the temperature of the water)

All the pH values above are expressed in logarithmic form (log [H+]). When the actual pH is equal to the calculated pHs, the Langelier Saturation Index (LSI) is zero, a saturation equilibrium exists and there is no scale formation or corrosive attack is minimised. Supersaturation of $CaCO_3$ exists with respect to alkalinity and total solids at that temperature when the Langelier Saturation Index is positive (pH>pHs). However, when the Langelier Saturation Index indicates a negative value (pH<pHs), any scale previously formed will be dissolved. When the unprotected or bare metal exposed to the brine solution, corrosion could occur and the corrosion rate is higher in an acidity environment compared to a neutral environment. The prediction of water characteristics by LSI appears in the Table 2-1

LSI	Tendency of Water
+2.0	Scale-forming and for practical purposes non-corrosive
+0.5	Slight scaling and non-corrosive
0.0	Balanced but pitting corrosion possible
-0.5	Slightly corrosive and no scale-forming
-2.0	Highly corrosive

Table 2-1 Prediction of water characteristics by the Langelier Index

One of the limitations of the LSI is the possibility of having the same LSI value for a low hardness water and a high hardness water. Hence, this leads to the development of the Ryznar Stability Index (RSI) to distinguish between the two waters having the same LSI value. The Ryznar equation is given in Equation 2-2

Ryznar Stability Index (RSI) = 2pHs – pH Equation 2-2

Ryznar Stability Index (RSI)	Tendency of Water
4.0 – 5.0	Heavy Scale
5.0 – 6.0	Light Scale
6.0 – 7.0	Little Scale or Corrosion
7.0 – 7.5	Significant Corrosion
7.5 – 9.0	Heavy Corrosion
9.0 and Higher	Intolerable Corrosion

Table 2-2 Prediction of Water Characteristics by the Ryznar Index

Both models (LSI and RSI) are very basic and provide a fast approach to determine scaling tendency in a fairly clean water environment. A more advanced scale prediction model is needed to achieve accurate prediction in tougher environments, often associated with oilfield brines consisting of high ionic strength, the presence of impurities such as iron ions, inhibitors and oil. A further modification of RSI, taking into account the influence of high levels of dissolved solids on the solubility of calcium carbonate has been developed by Stiff and Davis [7]. The SDI Index is developed for use in high saline waters or brines in the oilfield. The index is defined as in Equation 2-3

SDI = pH - pCa - palk – K Equation 2-3

where K is a constant based on the total ionic strength and temperature.

Other prediction models such as Oddo-Tomson saturation indices are among some of the prediction models most widely used in the oil industry [8, 9]. There are several commercial and non-commercial computer programmes available to predict scale formation, for example SOLMINEQ88, PHREQ.PITZ, EQ3/EQ6 and EQPITZER. However, all of these are general-purpose chemical speciation codes and are not intended for oilfield brine conditions. In studies of the kinetics of precipitation by applying prediction models, the focus has been on assessing the kinetics of homogenous and heterogeneous precipitation. These models predict the scaling tendency of the system and the amount of scale that is expected to precipitate in a system. The application of these models requires input of certain operational parameters such as ion content e.g. Ca, HCO_3^-, CO_2, temperature, pressure, flow rate, the presence of organic acids and inhibitors. The scaling tendency is the output result from the prediction models and the amount of mineral scale is likely to be precipitated in these conditions. Numerous corrections, which account for temperature, pressure and ionic strength in the prediction model has been reported in literature [9]. However, most of the prediction models often ignore the kinetic factors in the rate of precipitation.

ScaleSoftPitzer software has been developed to model the mineral scale precipitation [10]. This program is written in Microsoft Excel, designed to calculate the pH scaling tendency and inhibitors needed for oil and gas fields. The temperature and pressure dependence of the solubility product is incorporated in this software. The saturation index is given in Equation 2-4

$$SI = Log_{10}\left[\frac{\left(Me^{2+}\right)\left(A^{2-}\right)}{K_{sp}\left(T,P,S_i\right)}\right] \quad \text{Equation 2-4}$$

where SI is the saturation index, $Me = Mg^{2+}, Ca^{2+}, Sr^{2+}, Ba^{2+}$ and $A = CO_3^{2-}, SO_4^{2-}$

$K_{sp}(T,P,S_i)$ is the solubility constant term that is a function of temperature (T), pressure (P) and ionic strength (S_i)

Normal operational conditions such as temperature, pressure and flow rate are used as input parameters in the software. Also incorporated is the presence of different types

and concentrations of inhibitors to determine the amount of mineral scale that will be precipitated in a system. The main drawback is an approximate prediction of the amount of scale precipitated in the bulk solution without indicating any information on surface scaling (the amount of scale deposited on the component surfaces). This is an important factor, since often in industries scale deposition on component surfaces (surface scaling) is more of a problem than bulk precipitation in a system.

For all of the above discussed indices models, accurate analytical values for the reactant used as the input values are important in order accurately predict the conditions. This in particular to the use of solution pH value as an input data. However, in oil and gas production, a realistic pH measurement is rarely possible. A complex pH environment in oilfield brine is often affected by the changes in CO_2 fugacity, partitioning of CO_2 and operational conditions. These changes cause difficulties in measuring pH. The presence of other weak acids in the system may also have an effect on the alkalinity in the prediction models. Furthermore, not all the ions in the system are free, ion pairings such as calcium associated with sulphate and other ions like bicarbonate, carbonate have to be taken into consideration when using these models. The ignorance of ion pairing leads to over-prediction of the scaling tendency of a system even in high ionic strength waters. Neglecting the common ion effect in low ionic water can lead to great errors in high ionic strength brine [11]. Again, all the predictions and sample analyses are based on the scaling of bulk solution rather than metallic surface scaling. Often, laboratory data does not reproduce the same trends created in a real working environment. Hasson *et al.* [12] has demonstrated that there can be wide anomalies between actual deposition and rates estimated by the models.

2.3 Scale Detection Techniques

Traditional methods to study scale formation have concentrated on bulk solution by using beaker tests where the nucleation and growth of mineral crystals are measured by bulk chemical analysis. Study of the relationship between precipitation and scaling of metal surfaces has received less attention. There are only a few techniques available that enable surface scale monitoring in a system. Those that do exist are mainly based on the electrochemical technique in combination with other techniques such as the quartz crystal microbalance (QCM) [13], electrochemical impedance spectroscopy (EIS) [14] and rotating disc electrode (RDE) [15]. Moreover, there are a few additional

techniques based on acoustic and non-acoustic techniques, which monitor scale deposition. The details of each technique are described in sections 2.3.1 to 2.3.5.

2.3.1 Electrochemical Monitoring Techniques

Extensive work relating to the use of an electrochemical technique as a means of investigation and study of calcium carbonate under laboratory conditions has already been reported. The electrochemical techniques are used in conjunction with quartz crystal microbalance (QCM) [13] and rotating disc electrode (RDE) [15]. Other electrochemical techniques, such as the chronoamperometry, chronoelectrogravimetry [13, 16, 17] and electrochemical impedance [18, 19] have been described by research staff in the Pierre et Marie Curie University and Laboratoire de Chimie Analytique des Process Industriels in France. The following section gives a brief description of some of the electrochemical techniques used to study mineral scaling.

2.3.1.1 Electrochemical Quartz Crystal Microbalance (EQCM)

Generally, QCM also refers to piezoelectric sensors. The combination of QCM and the electrochemical technique is known as Electrochemical Quartz Crystal Microbalance (EQCM) [13]. The technique has been widely employed, not only in the investigation of crystal depositions on metal surfaces but also in the studies of ion-transport processes in the polymer films. Figure 2-1 represents a schematic of EQCM instrument set-up to investigate and study mineral scaling.

EQCM is a technique based on the measurement the change in frequency of a quartz crystal resonator, Δf assigned with the mass changes that is associated with dissolution or the deposition of scale during an electrochemical process. The shift to a quartz crystal resonator frequency, Δf is proportional to the change of the mass Δm when scale is deposited onto the surfaces of quartz crystal according to the Sauerbrey relation

$$\Delta f = k_s \Delta m \qquad \text{Equation 2-5}$$

where, k_s is Sauerbrey coefficient.

EQCM is adapted to be used in a submerged impinging jet set-up, which allows *in-situ* mass measurement in a well-defined flowing electrolyte conditions [16]. EQCM associated with chronoelectrogravimetry is one technique that enables the nucleation induction time (induction time is defined as the time elapsed between establishment of

the supersaturation and the appearance of first crystal) to be evaluated. It is a highly sensitive sensor that capable of detecting a film with a thickness as small as a single layer of atoms and it also provides real-time feedback [17]. However, the sensitivity is affected by the presence of chemicals, sand and oil [20]. In addition, this technique does not provide any distinction between the species, the frequency change is dependent on the location of the deposit. The surface of the sensor is easily saturated with scale since it has a limited area and weight (lower than 2 % of the total mass of the crystal).

There are also some other issue using quartz crystal coated with a dielectric material coating such as silicon dioxide or magnesium fluoride. It generates a strong tension or compression, which can affect the measurement. Some quartzes are heat sensitive. The practical upper limit of quartz resonators is approximately 150 ºC, therefore it is not suitable to use in high temperature environment. It has also limited application in some of the thermal and chemical vapour depositions where the temperatures are often exceeded 150 ºC for both processes. As quartz is heated, it undergoes a change in frequency, the slope of which gets steeper with increases temperature. A small rise in temperature leads to a large change in resonant frequency (slope value). This makes frequency measurement difficult and inaccurate.

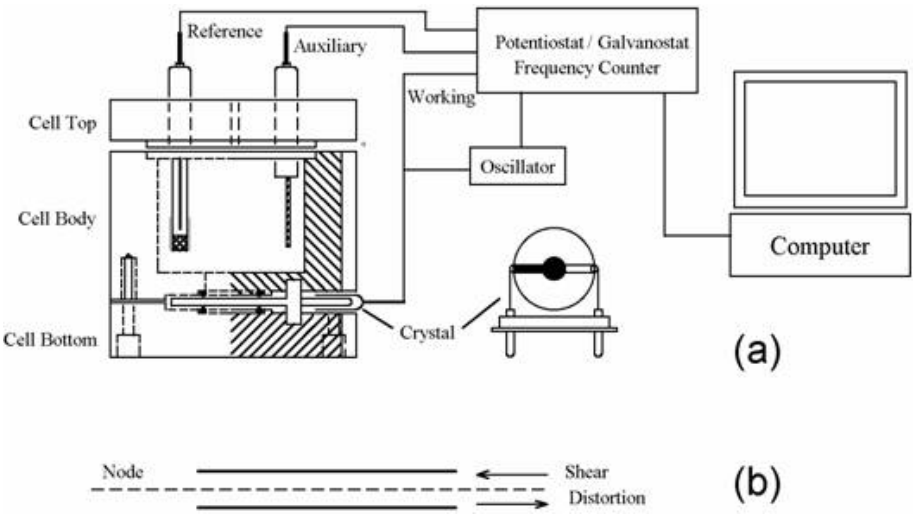

Figure 2-1 Schematic representation of a typical EQCM instrument set-up (a) The quartz crystal is coated with thin gold films on both sides.(b) The side view of the QCM crystal depicts the shear deformation [21]

2.3.1.2 Rotating Disc /Cylinder Electrode (RDE/ RCE)

The use of RDE was first proposed as a technique to detect mineral scale by Neville and Morizot [22]. This technique is based on the analysis of mass transport to an unscaled and scaled surface of a metallic. The scale deposition on metallic surfaces can be estimated through an assessment of the kinetics of the oxygen reduction process as is described in Equation 2-6

$$O_2 + 2H_2O + 4e^- \rightarrow 4OH^- \qquad \text{Equation 2-6}$$

The percentage of the working electrode covered by mineral scale deposits indicates the scale intensity. Using this technique, the well defined hydrodynamics (laminar flow regimes) ensures that a uniform coverage of the surface electrode condition is generated and can be controlled by changing the rotation speed. The limiting current at a specified constant potential increases linearly with the square root of rotational speed according to Levich's equation

$$i_L = 0.62\, nFCD^{2/3}\nu^{-1/6}\omega^{1/2} \qquad \text{Equation 2-7}$$

i_L = Limiting current, mA
n = number of electron
F = Faraday constant, $C.mol^{-1}$
C = concentration of electroactive species, $mol.dm^{-3}$
D = diffusion coefficient, $cm^2.s^{-1}$
ω = angular speed of RDE, $rads^{-1}$
A = area of the electrode, cm^2
ν = kinematics viscosity of the electrolyte, $cm^2 s^{-1}$

The deposition of the scale is followed by calculating the change of electrode area. As scale is deposited, the active surface area changes from an initial bare electrode to a final value, which is covered by scale. This technique gives a good correlation and reproducible result. Although the RDE is a compact, inexpensive, simple and reliable technique, there are difficulties for use at high temperatures and pressure conditions. Under conditions of high pressure, it subjected to sealing problems at the rotating parts of the equipment. Further development of such methodology would be needed to ensure it has a viable optimum for scale detection in the field rather than as a laboratory test.

The major advantage of the rotating disk arrangement is that the rate of mass transfer may be easily manipulated by adjusting the rotational speed of the disk. Furthermore, the flow characteristics of this system are well defined and the surface area available for reaction may be calculated since the dimensions of the mineral disk are known.

This approach is complicated, particularly in the interpretation of the information recorded. It is also a time consuming analysis meaning that the technique is often not appropriate for use in practical situations. Measuring an EIS spectrum takes time (often many hours) since the system must be at a steady state prior to any electrochemical measurement taken. In practice, a steady state can be difficult to achieve due the changes of an adsorption of solution impurities, growth of an oxide layer, coating degradation and temperature changes etc. Even this simple model has been the cause of some controversy in literature. Most researchers agree that this model can be used to evaluate the quality of a coating. However, they do not agree on the physical processes that create the equivalent circuit elements.

2.3.1.3 Chronoamperometry (CA)

This is another basic electrochemical technique which has been widely used to investigate crystal scaling [19]. It is an accelerated test as the electrode is cathodically polarised. The limiting current is recorded against time. A decrease of current is obtained when scale is deposited on the active surface. Often scaling time is the main parameter in this study where the scaling time represents the time required to reach the lowest and stable value of the current. A large scaling power indicates a smaller scaling time t_s. It is a simple and easy technique. However, the current is not directly proportional to the active free surface when scale partially blocks the surface. The actual scale coverage is often under-estimated by this technique. In addition, no information on the thickness or type of scale formed can be interpreted by this technique [23].

2.3.1.4 Electrochemical Impedance Spectroscopy (EIS)

EIS has been used to monitor corrosion processes and has been used extensively for characterising the performance of protective polymer coatings [24]. Studies on the corrosion of ferrous metal and porosity of coating or film layer have been widely reported using this technique [25]. This method has also been used for porous electrode studies to investigate the scaling rate and morphology of the calcareous deposits [26,

27]. With this technique, impedance measurements employ small AC excitation signals with magnitude (I_o) and frequency as input. The output is recorded as a voltage response and an equivalent circuit of the partially block scale is proposed. Information on the compactness and the thickness of the deposit can be obtained through the EIS technique [28].

Typically, EIS spectra are analysed by fitting equivalent electrical circuits, containing elements such as resistors and capacitors, to the data [14, 18, 19]. This allows the determination of trends in diffusion time constants of an ion/species and changes in high and low frequency resistance limits. However, it may be possible to fit several different circuit models to the data, which may or may not explain the physical phenomena occurring within an electrochemical cell. The impedance of a totally blocked electrode by crystal scale takes into account the impedance of the scale film as given below:

$$Z_b = \frac{R_f}{1 + j\omega R_f C_f} + Z_c \qquad \text{Equation 2-8}$$

where Z_b is the impedance of a totally blocked electrode, Z_c impedance of the cavity under the scale block, R_f and C_f are the resistance of porous film and the dielectric capacitance of the scale layer respectively Z_c and ω is the radial frequency.

2.3.2 Ultrasonic Methods

Mineral scaling of an inner pipe can be detected by non-destructive ultrasonic techniques. The application of ultrasonic as a means to detect and monitor mineral scale on the component surfaces has been widely patented [29, 30]. The ultrasound signal is generated by a transducer that is capable of transmitting and receiving ultrasonic energy. When an acoustic wave travels through the wall of a tube and scale, most of it is reflected away. However, there are some energy losses because of absorption, which is greatly influenced by the amount and density of the scale at the inner surface. A method of determining low density deposits on an inner surface of a boiler tube through an ultrasound technique was patented in US Patent 4872347 [30]. An ultrasonic transducer is placed on the outer surface toward inner surface of the tube. Ultrasound is generated by the transducer and its energy is reflected back and forth between the outer and inner metal/deposit surface. The signals are then received by the same transducer, which is connected to a PC. The signals are then processed and

analysed to quantify the amount of inner surface deposit on a standard tube. An application of the ultrasound technique is illustrated in Figure 2-2

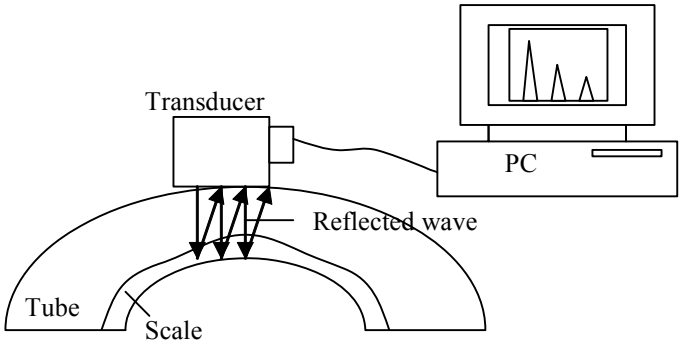

Figure 2-2 Schematic representation of ultrasound to detect scale deposition on a section of tube

US Patent 5,092,176 claimed a poor sensitivity has been observed when applying a frequency below 3 MHz. This is mainly due to beam spreading and the optimum frequency range is between 3-7 MHz. This technology claimed to detect scale that build up in an empty tube and an oxide scale thickness of 0.1 mm can be detected with a high frequency technique (50 MHz) [29].

However, there are two main reasons for the conventional ultrasonic techniques not being applicable in scale detection. Firstly, the speed of sound in the deposits is initially unknown and can vary. Secondly, the coupling ultrasound to the pipe results in the generation of strong reverberating signals that mask the echoes reflected off the lower boundary of the deposits, making it impossible to extract timing information. However, Gunarathne and Keatch [31] claimed that by analysing the decay pattern of the reverberating signals, scale deposits could be identified by comparing results to a standard test specimen. The velocity of sound obtained from the analysis is then used to calculate the thickness of the scale. They have also reported that this technique could detect 0.5 mm of barium sulphate at a frequency of 5 MHz. Therefore, this technique potentially can be developed further to use in oilfield for scale monitoring. In addition, this technique can be used as a de-scaling tool to remove any scale formed on a component surface. The application of chemical scale removal under a higher power level of ultrasound to generate cavitations has been reported successfully in cleaning processes. A significant increase of $BaSO_4$ dissolution rate from 4 to 17 times for an

ultrasound intensity of 10 % to 55 % was claimed. The estimated power density required to remove scale is 100 mW/cm^2. This is a proven technology that can be used to identify the type and thickness of scale deposited under laboratory condition [31]. However, the accuracy of the measurement is strongly influenced by the presence of void in the medium (mineral scale or pipeline or interface between both).

2.3.3 Temperature/Heat Sensors

Temperature and heat sensors are based on the temperature difference between the sensor and the scale formed on a metal surface. The arrangement of the heating element and the sensor is such that there is a heat transfer from or to crude oil. Once mineral scale is deposited on the metal surface, the heat transfer is impeded from the heating element to crude oil. Then the temperature is measured by a heat sensor [32].

A clean temperature probe is placed to ensure good contact to the crude oil. It allows the sensor to achieve equilibrium with the crude oil, (T1). Then it is heated to a few degrees higher than T1 by a direct current and the temperature is measured as T2. This result in different temperatures recorded between the probe and the crude oil. When scale is deposited on the probe, the temperature increase can be monitored continuously since all other factors are maintained essentially constant. The measurement theory of the test is as follows

$$Q_c = U_c A_c \Delta T_c \qquad \text{Equation 2-9}$$

For the natural convection process, the heat transfer coefficient is equal to

$$\frac{1}{U_c} = \frac{1}{h} \qquad \text{Equation 2-10}$$

As scale is deposited, it acts a resistance to the heat transfer hence,

$$Q_d = U_d A_d \Delta T_d \qquad \text{Equation 2-11}$$

$$\frac{1}{U_d} = \frac{1}{h} + \frac{x}{k} \qquad \text{Equation 2-12}$$

Where c is under clean condition, d is with scale deposited condition, $Q_{c,d}$ is the heat flux (W), $U_{c,d}$ is the overall heat transfer coefficient (W/m^2K), h is the convective heat transfer coefficient, $A_{c,d}$ is the area of heat transfer (m^2) and $\Delta T_{c,d}$ is the

temperature difference between the probe and oil (K). x/k is defined as the fouling factor where k is denoted as deposit thermal conductivity and x is the deposit thickness.

Since the heat flux is constant and the heat transfer area remains the same throughout the experiment, substitute Equation 2-9, Equation 2-10, Equation 2-11 and Equation 2-12, it leads to

$$\frac{x}{k} = (\frac{A}{Q})(\Delta T_d - \Delta T_c) \qquad \text{Equation 2-13}$$

Although the thickness of the scale deposit or fouling factor can be monitored through this technique [33, 34], application is more suited to the water or power industry and much more research is needed before applying this technology to oil and gas fields.

Recently a similar technology, analysing the temperature profile of a low thermal conductivity of a mineral scale layer known as a Distributed Temperature Sensor (DTS), was developed [35]. The basic principle is based on the thermal conductivity the various scale deposits such calcium carbonate ($CaCO_3$) has a thermal conductivity that ranges between 2215.6 Joule to 3376.2 Joule; while the barium sulphate scales have an even lower thermal conductivity around 1477.1 Joule. The differences between the thermal properties of oil, gas and water allow the detection of unwanted fluids using DTS. The thermal insulation provided by the scale causes a unique temperature profile and quantitative analysis allows the scale thickness can be determined.

2.3.4 Radioactive Detectors

This technique is based on recordings of the radioactive form NORM (Naturally Occurring Radioactive Material) scale [36]. A radioactive detector is inserted into a system to measure and record any radioactivity of the scale. Usually, natural gamma (γ) radiation is emitted from the Radium-266, Radium-288 and Bismuth. These radioactive elements do not precipitate directly but are co-precipitated with $BaSO_4$ scale, causing the scale to be radioactive as in the following equation [10],

$$Ba^{2+} + Ra^{2+} + SO_4^{2-} \rightarrow Ba(Ra)SO_4 \ (barite\ solid) \qquad \text{Equation 2-14}$$

An increase in radioactive levels in the system indicated NORM scale build up on the wall of a tubing. Bamforth *et al.* [36] reported using gamma ray logs to detect

radioactive mineral scale deposited on tubing or pipeline surfaces. This technique uses the presence of natural radioactivity such as Ra-266 in normal mineral scale as a means to detect mineral scale deposition [36]. Furthermore, this technique is only suitable for NORM and it cannot detect normal scale such as $CaCO_3$ [37] which usually does not contain any radioactive elements. This technique is generally not sensitive enough to detect a low level of radiation emitted by the scales.

2.3.5 Common Practices of Scale Monitoring

Pressure monitoring is perhaps the most common practice method used by oil and gas industry to detect any scale formation. It is a common and easy method monitoring technique. Often, a section of a pipeline length is monitored to determine the scale built up in a system. When mineral scale deposits on the pipeline surface, it causes a difference in pressure gradient in that section of the monitored pipe. Obviously, a fall of oil production can also be observed when mineral scale deposition occurs. However, scale detection often comes too late using this type of monitoring, only detected in changes after the decrease in production caused by the blockage of a very thick layer of scale. Furthermore, it is not the only possible symptoms and there may be other possibilities such as hydrate formation and drop of production as the field ages, hence *in-situ* monitoring can be used to eliminate the uncertainty [20].

Other monitoring techniques such as brine sampling and chemistry analysis are often used in the industry and the laboratory. Chemistry monitoring through sampling is carried out by analysing the brine composition or residual inhibitors. This can be done through the ICP wet chemical and tagging methods. Traces of residual inhibitor in the system are monitored to predict the potential of scaling. Low inhibitor concentrations may indicate insufficient inhibition and scaling may occur in a process system. One limitation of this technique is that the critical inhibitor concentration is susceptible to the change in environmental conditions (water compositions, pH and temperature). Brine monitoring also is common practice in industry, this is done by analysing the presence of ions such as calcium (Ca), magnesium (Mg), barium (Ba), ferrum (Fe) and organic acids. By monitoring the calcium (Ca) content, for high Ca brine, it is most likely that scale precipitation will occur. Both techniques are time consuming especially when time is lost whenever samples are sent out to the laboratory for analysis [17]. Usually, it takes a few days to obtain the analysis results and often they come to

too late to detect mineral scale deposition. Again, this is bulk precipitation monitoring rather than surface scaling on equipment surfaces.

2.4 Scale Detection Technologies

Currently only limited technologies are available for real-time or on-site monitoring of scale deposition. The reasons for having on-line monitoring are:

i.) Obtaining well system conditions without any delay, hence corrective action can be taken to prevent problems associated with scaling;

ii.) With feedback information from the well, an optimisation of scale treatment programme can be recommended. Subsequently, lower operation costs can be achieved by applying appropriate dosages of inhibitors without wastage and production shutdown.

2.4.1 Thickness Shear Mode Resonator (TSMR)

This technique is very similar to the QCM. The traditional QCM device does not provide an accurate and reliable mass measurement of biofouling, which is amorphous and crystalline. This issue is overcome by the application of TSMR. It consists of piezoelectric quartz wafer with metal electrodes coated on opposite faces. It also responds to the fluid viscosity and elasticity properties of the deposit. The application of electrical potential across the wafer results in its shear deformation at a resonant frequency. The resonant frequency and its oscillation magnitude of TSMR are proportional to the density, viscosity as well as type of properties of the wafer. Generally, a decrease in resonant frequency is observed when scale is deposited onto the wafer surface. One advantage of this technique is the ability to monitor scale formation on-line including biological, inorganic and organic scales [37]. This technique has also been used to trace any chemical contamination in the air or water, characterization of film viscoelastic properties, sensing change in material such as epoxy curing in the industrial process.

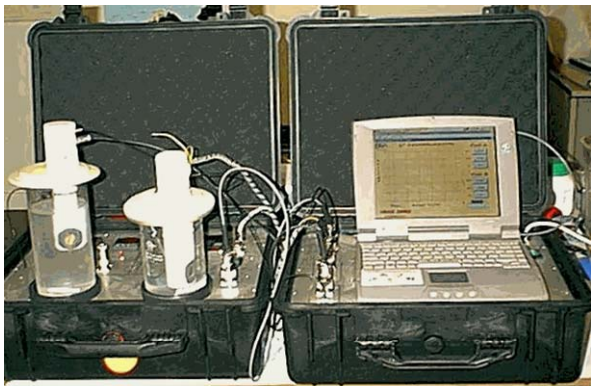

Figure 2-3 shows a commercial equipment set-up for the TSMR technique

Emmons and Jordon [38] conducted a number of experiments where a sensor is immersed into a 50/50 mix Forties formation brine and seawater. A known concentration of barium solution is added to precipitate barium sulphate scale. A decrease in the resonant frequency indicated the occurrence of scale deposition. However, this equipment set up is not *on-line* and not permanently installed in the production line. Nor does it measure the scale formation under flow dynamic conditions as well as in high pressure and temperature conditions. Hence, no field data is available for the application of this sensor operating in the production well. Furthermore, it is not integrated into the system but is a stand-alone unit connected to a laptop. The field test is carried out in an offshore production chemistry laboratory by sampling the water in the absence of oil, and then immediately performing the analysis. It is able to detect mineral scale formation and inhibitor dosage in the brine system rather than in the oil/water system.

2.4.2 Dual/ Triple Gamma Ray Attenuation

The presence of mineral scale can be identified by a dual energy/triple gamma ray attenuation measurement. This technology has been adapted from a nuclear measurement developed for the wire line and well logging during the drilling processes. A multiphase meter used to monitor the flow rate of the gas, oil and water has been deployed in combination of dual/triple gamma ray attenuation measurement to detect mineral scale on the component surfaces. This technology was developed by the Schlumberger Oilfield Service's research team [39].

The principle of this technique is based on an attenuation of nuclear spectrum to the density or composition of the subjected medium. It consists of a radioactive source (Ba-133) and a detector located opposite the radioactive source for detecting the gamma ray. A fraction of each medium (gas, oil, water) is determined as the gamma ray is emitted from the Ba-133. Attenuation of the gamma ray occurs as it crosses the three mediums. Since the scale composes a heavier atomic element than oil and water, an increase in attenuation is observed when scale is deposited.

The main advantage of this technique is that it has the ability to identify types and thickness of the scale by *in-situ* analysis without shutting down the production. Scale identification can be determined quickly in a few minutes. This technology was tested in a field trial where the technology was deployed in a North Sea production well that is operating in high temperature and pressure conditions.

2.4.3 Attenuated Total Reflectance (ATR)

Attenuated Total Reflectance (ATR) is a surface analysis technique based on the transmission of spectroscopic information in direct contact with sample [40]. An appropriate optical setup is where an infrared light is focused onto the end of the internal reflectance element (IRE). Then the light enters and reflects down the length of the IRE that is usually made of zinc selenide (ZnSe) or germanium (Ge). The light will totally reflect within the IRE if the angle θ at which the infrared light impinges upon the crystal-sample interface between the IRE crystal (the dense medium) and the air or water is greater than the critical angle. A portion of energy is reflected back into the crystal, while a small portion of energy is transferred from crystal to crystal-sample interface.

At each internal reflection, the IR radiation penetrates a short distance (~1 μm) from the surface of the IRE into the sample. A unique physical phenomenon (evanescent wave) that enables one to obtain the infrared spectra of samples placed in contact with the IRE. Figure 2-4 depicts this phenomenon known as an evanescent wave. Different wavelengths cause evanescent wave penetrating different distances into the sample. The principle of ATR measurement is based on the expression of the total absorption intensity (A) as a function of the incident angle

$$A(\theta) = \int_0^\infty \alpha\, z(e)^{-\beta z}\, dz \qquad \text{Equation 2-15}$$

where $\beta = \frac{4\pi\sqrt{n_1^2 \sin^2\theta - n_2^2}}{\lambda}$

n_1 and n_2 are the IRE and sample refraction indexes respectively, λ is the infrared ray wavelength, $\alpha(z)$ is the absorption coefficient of the sample as a function of the depth of z and θ is the angle of the infrared light impinges or incident beam.

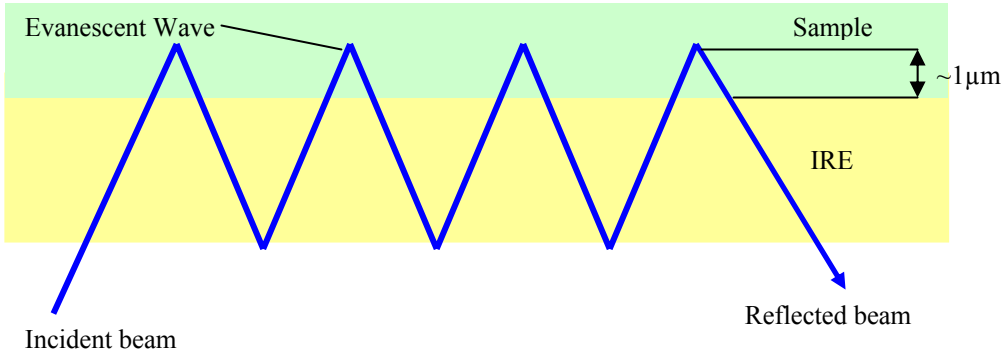

Figure 2-4 Total internal reflection at the interface of an internal reflection element. The evanescent wave is shown extending beyond the surface IRE

A novel technique utilising an attenuated total reflectance (ATR) probe to detect calcium carbonate scale from oilfield fluid was developed by Baker Petrolite [41, 42]. A field test experiment was carried out in the West of Texas oilfield. The company claimed that the ATR sensor enables the detection of calcium carbonate in a mixed production fluid system. Also, the measurement is not affected by the presence of crude oil, suspended particles and pH solution. Little support equipment is needed for the technology, therefore this monitoring device can be utilised in more places than the other techniques.

2.5 Summary of the Technologies

It is clear that there are techniques already in existence, which can monitor mineral scaling in a system. The extent of scale deposited on metal surfaces has been studied with various techniques and majority of the studies are mainly based on an electrochemical technique in a laboratory. Each of the scale detection technologies has their own benefits and limitations as presented in Table 2-3. There is a gap between technical needs and available technology to solve the scaling problems. Existing technology needs to be not only robust and reliable to succeed in normal and tough

environments but also be simple to use to and allow easy interpretation of the results. An increase in new development fields are in deepwater where tougher environments and HPHT (high-pressure high-temperature) are expected, such as in the Gulf of Mexico and West of Africa. Hence, any new sensor development fulfilling these conditions would be of a benefit to the industry. Consideration of the practicality should be taken into considerations at the early laboratory stage in order to be able to transform technology into commercial instrument.

Technique	Advantages	Disadvantages
Rotating Disc Electrode (RDE)	Easy to operate and setup Easy interpretation of data Mass transfer and flow characteristics are easily manipulated	Not suitable in high pressure condition as sealing at the rotating part may be an issue
Quartz Crystal Microbalance (QCM)	Highly sensitive (detecting a film with a thickness as small as a single layer of atoms)	Limited area and weight (<2% of the total mass of the crystal) Limited to high temperature Oscillation sensitive may affected by liquid flow
Electrochemical Impedance Spectroscopy (EIS)	Suitable for porous and perfect layer of scale formed	Difficult to obtain a represent model (especially at the early stage of scaling process Complicated technique particularly on data interpretation Time required to achieve steady state prior measurement is taken
Pressure Monitoring	Simple and easy Low cost	Often detect once a significant of mineral scale built up
Attenuation Technique	Proven technology as in Dual/Triple Gamma Ray Attenuation Ability to identify types and thickness of the scale	Expensive and complicated
Ultrasonic Technique	Can be use for surface cleaning	Required a significant thickness of layer for strong reverberating signals Complicated data interpretation

Table 2-3 Summary the benefits and limitations of the electrochemical techniques being used to investigate mineral scaling.

Chapter 3 Review of Mineral Growth and Scaling

3.1 Introduction

Prior to the development of using an electrochemical technique as a means of monitoring the extent of mineral scale deposited on the component surfaces, it is important to gain and access some of the knowledge regarding mineral scaling. Hence, the purpose of this chapter is to review the basics of mineral scaling. A brief introduction to mineral scale and various types of mineral scale found in industry are covered in the first few sections of this chapter. In addition, a basic overview of mineral scaling and precipitation is described consisting of crystal nucleation and growth. In the final section of this chapter, background knowledge of scale dissolution and surface scaling are also reviewed. Since the existing technique (SIJ in combination of electrochemical measurement) is strongly influenced by the surface conditions of the sensor, any knowledge or background information on surface conditions will provide a greater understanding and benefit to the study of mineral scaling using this technique.

3.2 Background of Scale

There are several types of scale formed during oil recovery. Basically, these can be divided into two main groups, organic and inorganic scales. The following section of the literature review describes the type of mineral scale, which is commonly found in the oil and gas industry.

3.2.1 Organic Scale

Paraffin waxes and asphaltenes are common organic scales found in oil and gas production processes. The formation of these types of scale is mainly due to the oil becoming unstable when the operational conditions change such as pressure and temperature. As result of these, solid organic carbon crystallises (wax) deposit on the walls of the pipeline or equipment surfaces. The wax present in crude petroleum primarily consists of paraffin hydrocarbons (C18-C36) known as paraffin wax and naphthenic hydrocarbons (C30-C60). When the wax freezes, it forms crystals, and the crystals forms of paraffin wax are known as macro-crystalline. Those formed from naphthenes are known as microcrystalline wax [43]. The structures of macro-crystalline, microcrystalline and the crystal deposit network of wax are shown in Figure 3-1.

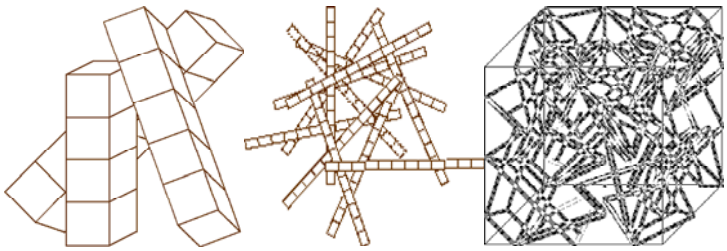

Figure 3-1 Macro-crystalline, Micro-crystalline, and Crystal Deposit Network of Wax [43]

Asphaltenes are defined as a black solid material that precipitates when an excess of n-heptanes or n-pentane is present in the crude oil. It has an amorphous solid structure, the heaviest and polar fractions found in the crude oil. Structurally, asphaltenes are condensed polynuclear aromatic ring systems bearing mainly alkyl side chains as shown in Figure 3-2. The number of rings in oil asphaltenes can vary from 6 to 15. The solubility of asphaltenes decreases until it reaches the bubble point. Eventually it precipitates out into the system as the pressure and pH drop.

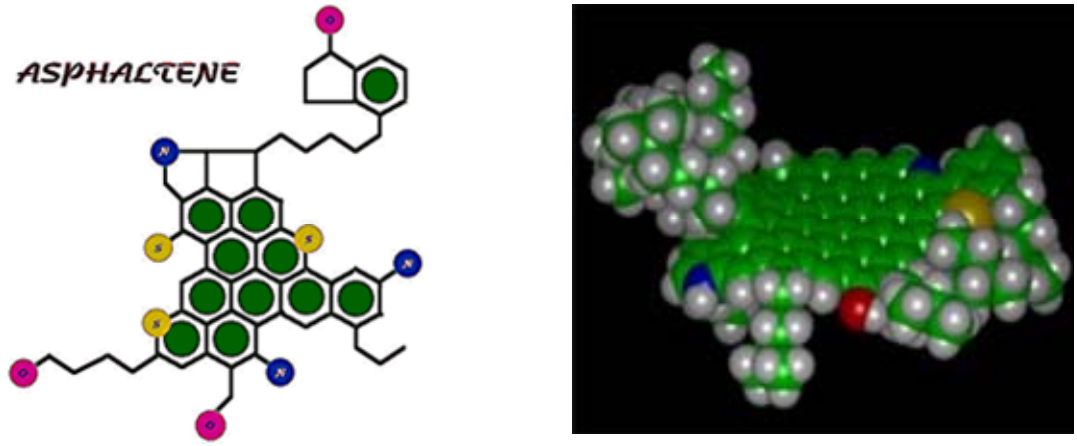

Figure 3-2 Structure of asphaltenes in 2 and 3 dimensions [43]

3.2.2 Inorganic Scale

There are a number of types of inorganic mineral scale discovered in the pipelines during oil recovery such as calcium carbonate ($CaCO_3$), calcium sulphate ($CaSO_4$, $CaSO_4.2H_2O$), barium sulphate ($BaSO_4$) and strontium sulphate ($SrSO_4$). Usually ferric oxide (Fe_2O_3), an inorganic scale deposits on the pipes due to corrosion problems [44]. However, the most commonly found inorganic mineral scale in the oil and gas industry is $CaCO_3$ and $BaSO_4$.

3.2.2.1 Calcium Carbonate ($CaCO_3$)

Calcium carbonate occurs as a mineral in nature. Usually it is divided into $CaCO_3$ polymorphs that are anhydrated and hydrated. The three anhydrate phases are calcite (the stable phase at room temperature and atmospheric pressure), aragonite (at high-pressure and temperature conditions) and vaterite (metastable with respect to calcite or aragonite). The amorphous calcium carbonate, monohydrate and hexahydrate (ikaite) calcium carbonate are the three hydrated forms of $CaCO_3$. As shown in Figure 3-3, different crystal structures can be found in crystallisation processes. Operational process conditions such as temperature, pressure and the presence of chemical substance have a great influence on the crystal structure. At room temperature, calcite is predominantly formed for the condition that is favourable to a fast nucleation rate, whereas a slow nucleation rate leads to vaterite nucleation. As the temperature increases formation of aragonite needles or vaterite crystals with different morphology occurs [16]. Usually calcium carbonate in calcite form has a cubic crystal and aragonite has a needle-like crystal. Vaterite has an ill-defined morphology and is rarely observed under normal conditions.

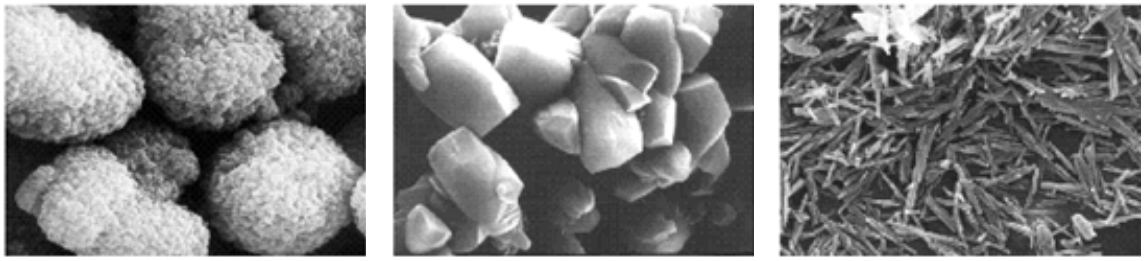

Figure 3-3 Polymorph structures of $CaCO_3$ in the forms of spherical calcite (left), rhombohedral calcite (middle) and discrete acicular aragonite (right) [3]

The presence of mineral ions or organic impurities cause a major influence on crystal growth processes. For example, magnesium ions inhibit calcite and promote aragonite. Tracy *et al.* [45] reported that when impurities exist, calcite that formed secondary after the amorphous phase exhibits a spherulitic shape. Aragonite has an elongated needle shape and the most common type of vaterite is in lenses or sometimes observed in clusters called sand rosettes. Some vaterites also exist in a spherical shape, as shown in Figure 3-4. Among the polymorphous calcium carbonate, calcite has the lowest solubility product and amorphous calcium carbonate (ACC) has the highest solubility.

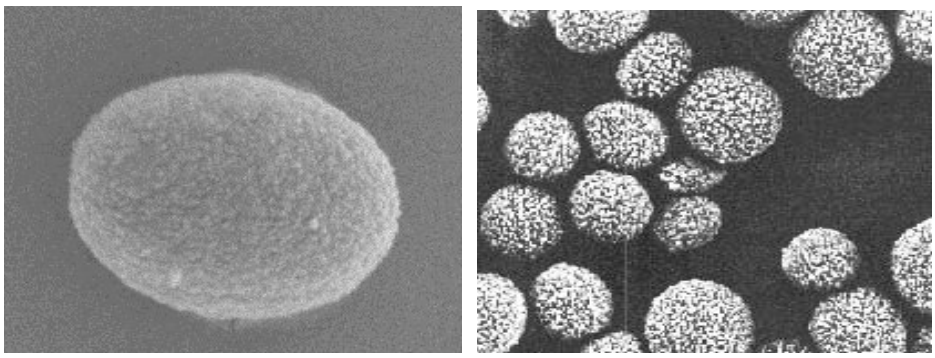

Figure 3-4 Structure of $CaCO_3$ in the form of vaterite [3]

3.2.2.2 Barium Sulphate ($BaSO_4$)

Most of the formation waters in the reservoir contain a high concentration of alkaline-earth-metals (Ba^{2+}) while seawater consists of a high content of SO_4^{2-}. When these two incompatible brines are mixed during water injection processes to improve or maintain the oil recovery, barium sulphate or barite ($BaSO_4$) precipitation and deposition on process equipment surfaces occurs. Barium sulphate is one of the typical mineral deposits and is extremely insoluble mineral. The solubility of $BaSO_4$ is about 2.5 mg/l at 25 ºC [46] in water and the solubility limit K_{sp} of $BaSO_4$ is about $10^{-9.99}$ [47]. However, the solubility of $BaSO_4$ increases as the temperature or pressure increases [48, 49]. pH has only a slight effect on the dissolution of $BaSO_4$ compared to calcium carbonate.

Several $BaSO_4$ morphologies such as spherical, spindle diamond, dentritic, rectangular and rhombohedral were reported in literature [50-53]. Generally, $BaSO_4$ exists as an orthorhombic crystal [54]. The experimental conditions such as temperature, pressure, pH, saturation ratio and presence of organic additives [55, 56] have a great influence on the shapes as well as the $BaSO_4$ morphologies during crystals growth. For example, barium sulphate exists in "rock roses" and "desert roses" shapes that are actually made up of tabular crystals as a result of randomly deposited and subsequently growth of smaller tabular crystal on larger tabular crystal on equipment surfaces [50]. Kai *et al.* [46] found that supersaturation ratio is a crucial factor affecting barite morphology. The crystal growth process at high degree of supersaturation (SI >3) is under diffusional control and dentritic morphologies (rod-like, spindle-like and star like) are observed. When low supersaturation aqueous solutions (SI<3) are used to precipitate $BaSO_4$,

rectangular and rhombohedra crystal are found. In this case, surface reactions are the controlling mechanisms.

3.3 Mineral Scaling and Precipitation

The most important property among the factors, which causes scale precipitation on metal surfaces, is the supersaturation index. It is a driving force for precipitation reactions. Once the solubility exceeds the saturation point, precipitation is thermodynamically favourable and whether it occurs or not depends on the kinetics factor. A high supersaturation index indicates a high possibility of mineral precipitation. However, it does not show how fast the precipitation will be nor the amount of scale precipitated. Usually a supersaturated solution can be induced via a variety of methods: temperature variation, pH variation, solvent evaporation and introduction of a co-miscible solvent in which the solute has limited solubility. Solubility is defined as the limiting amount of solute that can be dissolved in a solvent under a given set of physical conditions [15]. The solubility product of a compound $m_{v+}x_{v-}.\kappa H_2O$ can be expressed from the concentration of species by Equation 3-1. K_{sp} is the solubility product that can be calculated using the ionic concentration. For concentrations greater than this, it is necessary to adopt ionic activity as shown in Equation 3-1.

$$K_{sp} = m_M^{v+} m_x^{v-} (\gamma_{\pm m})^{v} (a_1)^{k} \qquad \text{Equation 3-1}$$

where a_i is the ionic activity, m_i^v is the concentration of species i expressed molarities, $\gamma_{\pm m}$ is the stoechiometric mean activity coefficients which correct for the solution being non-ideal. The activity of water can be assumed to be one since the amount of solute is negligible compared to the amount of solvent. The supersaturation of a solution can be expressed in terms of the saturation ratio. It is defined as the ratio of the ion product to the solubility product constant. Sometimes it is referred to as the supersaturation index, I_s where the saturation ratio value is expressed in logarithmic terms.

$$SR = \frac{m_M^{v+} m_x^{v-} \gamma_{\pm m}}{K_{sp}} \qquad \text{Equation 3-2}$$

$$I_s = Log(SR) \qquad \text{Equation 3-3}$$

where I_s is the supersaturation index and SR is the saturation ratio.

In a solution which contains a given amount of dissolved MX, where the activities of M^+ and X^- are a_m and a_x respectively, thermodynamically, if

i.) I_s=0 where SR=1 the solution is saturated with MX;

ii.) I_s<0 or SR<1 where the solution is under saturated with MX and precipitation is not thermodynamically possible;

iii.) I_s>0 or SR>1 where the solution is supersaturated with MX and precipitation is thermodynamically possible.

The solubility product of 3 crystal forms of calcium carbonate is not the same, as shown in Table 3-1. As opposed to most sulphate scale, the prediction of calcium carbonate scale requires not only the consideration of temperature, pressure, saturation ratio and pH, but also the knowledge of the presence of CO_2 in the aqueous solution.

$CaCO_3$ Polymorphs	Solubility Product at 25 °C
Calcite	$K_c = 3.16 \times 10^{-9}$
Aragonite	$K_a = 4.78 \times 10^{-9}$
Vaterite	$K_v = 12.6 \times 10^{-9}$

Table 3-1 represents the solubility product of 3 crystal forms of calcium carbonate, calcite, aragonite and vaterite at temperature 25 ° C [57]

According to the inorganic carbon equilibria, when CO_2 gas from the atmosphere dissolves in water, it forms a weak carbonic acid (CO_2 gas will be associated to a certain extent with water molecules to form CO_2 aqueous). Most of the carbonic acid exists as aqueous CO_2 and is usually written as $H_2CO_3^*$. The relevant chemical reaction involved and equilibrium constants for each process are presented in Table 3-2. Basically, the carbonate species can be divided into three regions as shown in Figure 3-5. At pH between 7 to 10 i.e. the most common pH for natural water, the stable species are in the form of bicarbonate. When the pH is above 10, carbonate exists as the stable species and the stable species carbonic acid is associated with a pH of below 7.

Chemical Reaction	Equilibrium	Equilibrium constant
$H_2O \leftrightarrow H^+ + OH^-$	$K_w = C_{H^+} C_{OH^-}$	$K_w = 10^{-14}$
$CO_{2(g)} \leftrightarrow H_2O + H_2CO_3^*$	$K_H = C_{H_2CO_3^*} / pCO_2$	$K_H = 10^{-1.47}$
$H_2CO_3^* \rightarrow H^+ + HCO_3^-$	$K_1 = C_{H^+} C_{HCO_3^-} / C_{H_2CO_3^*}$	$K_1 = 10^{-6.35}$
$HCO_3^- \rightarrow H^+ + CO_3^{2-}$	$K_2 = C_{H^+} C_{CO_3^{2-}} / C_{HCO_3^-}$	$K_2 = 10^{-10.33}$

Table 3-2 Equilibrium constants from dissolved carbon dioxide species at 25 ° C [58]

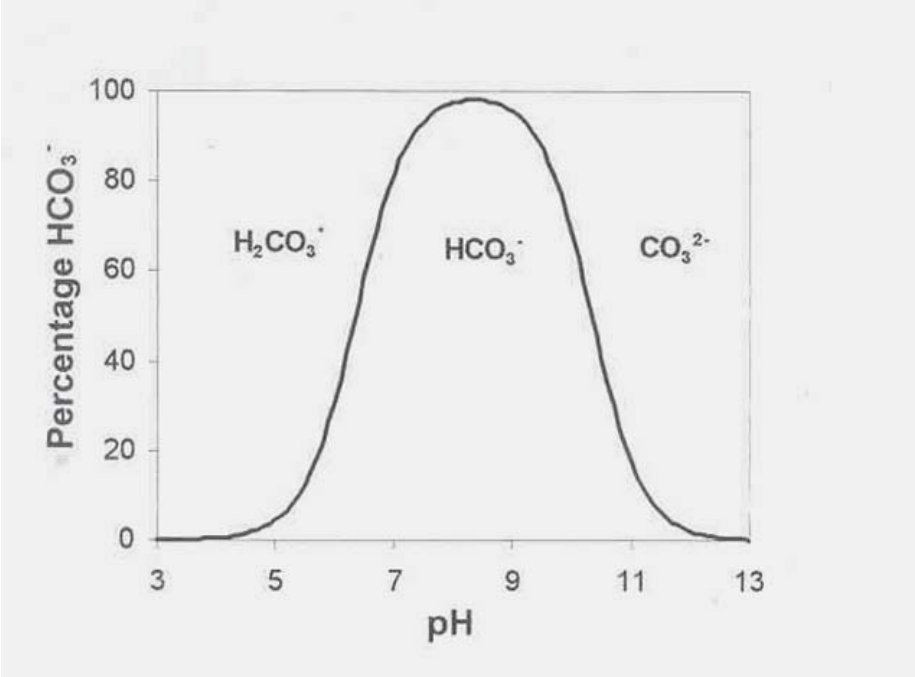

Figure 3-5 Percentage of HCO_3^- in total carbonate as a function of pH [58]

3.3.1 The Kinetics of Crystal Nucleation

The kinetics of mineral scale precipitation can be divided into two stages; nucleation and crystal growth. When the saturation ratio (SR) of the solution is above 1, from the thermodynamics point of view precipitation is possible, but from a kinetics point of view it may not occur. The kinetics of a reaction will determine the reaction rates (how fast the precipitation occurs). It depends on environmental conditions such as water chemistry, pH, CO_2/H_2S partial pressure, pressure and temperature, any changes in the variable will have a significant effect on mineral scaling [39].

Crystallisation is not caused by the supersaturation factor alone. Before a crystal can be developed, a number of minute solid bodies must exist (embryos, nuclei or seeds) that act as centres of crystallisation. Crystal nucleation can be divided into two separate categories: primary and secondary nucleations.

3.3.1.1 Primary Nucleation

Primary nucleation occurs in a system that does not contain crystalline matter. It can be sub-divided into homogenous and heterogeneous nucleation. Homogeneous nucleation is assumed to occur in a solution that is completely free of impurities [59] and is also known as spontaneous nucleation. Homogenous nucleation may occur spontaneously in the bulk solution if the saturation ratio is above a critical value. The classical theories of nucleation is based on thermodynamic approaches reported by Gibbs [60] and Volmer [61] with some modifications by Becker and Doring [62]. Nucleation occurs when the clusters or nuclei achieves a critical size. The free energy changes associated with homogeneous nucleation are as below

$$\Delta G = 4\pi r^2 \gamma + \frac{4}{3}\pi r^3 \Delta G_v \qquad \text{Equation 3-4}$$

where ΔG is the overall excess free energy and ΔG_v is the volume free energy. The $\Delta G_s = 4\pi r^2 \gamma$ is a positive quantity, the magnitude of which is proportional to r^2 and G_v is negative quantity proportional to r^3.

Generally, in practice, homogenous nucleation is not common because in almost all cases there is the presence of impurities in the solution such as atmospheric dust [59]. When particles are present in the solution, they act as hetero-nuclei sites and the nucleation rate can be lower than one required for homogeneous nucleation. In the presence of a solid wall, heterogeneous nucleation may occur due to a lower value of saturation ratio. This depends on the nature of the material, surface finish of the substrate [28, 63] and other parameters such as the presence of impurities. The overall free energy change associated with the formation of a critical nucleus under heterogeneous conditions $\Delta G'_{crit}$ must be less than the free energy associated with homogeneous nucleation ΔG_{crit}.

3.3.1.2 Secondary Nucleation

Secondary nucleation occurs when a source of crystals or impurities are introduced into supersaturation solution. The mechanism of nucleation resulting from the presence of crystals in supersaturated solutions is generally termed secondary nucleation i.e. at low supersaturation, when crystals of the solute are already present or deliberately induced into the solution. Secondary nucleation can be divided into two categories: contact nucleation and seeding [59]. Two examples of contact nucleation are crystal detachment and crystal fragmentation as a result of particle collision. Crystallisation solution is seeded with seed materials in order to control the distribution and sizes of the crystals.

3.3.2 Review of the Crystal Growth and Kinetics

Crystal growth takes place once the nuclei size from the nucleation process is larger than the critical nuclei size [59]. When a crystal grows, a series of different physical and chemical processes take place. This can be broken down into different events, as listed below:

i.) Bulk transport of reactants to the edge of the boundary;
ii.) Diffusion through the boundary layer to the solid surface;
iii.) Adsorption onto solid crystal surface;
iv.) Diffusion along the solid crystal surface;
v.) Attachment to the surface step;
vi.) Diffusion along step and;
vii.) Integration into the crystal at a kink.

Kossel [64] postulated that flat crystal surfaces are made up of moving layers (steps) of monatomic height, which contain one or more kinks. Crystal growth is advanced by atoms, molecules or ions absorbed and incorporated into the crystal especially at the energetically favourable sites (kink and vacancies sites). Figure 3-6 is a schematic diagram where ions are absorbed at different sites such as hole, kinks, steps etc during crystal growth.

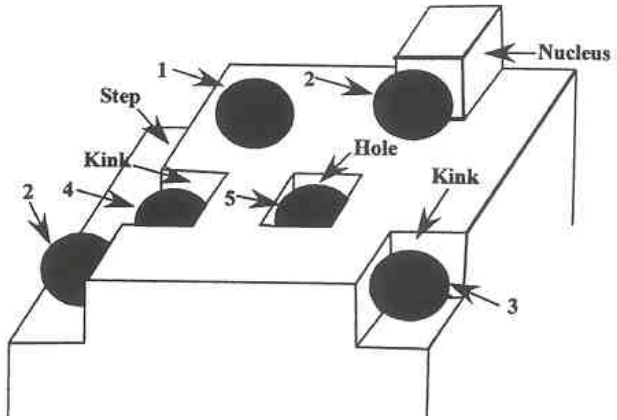

Figure 3-6 Absorption of ions (in black) at different sites such as step, hole and nucleus at solid crystal surface[65]

However, based on this postulation there is a major discrepancy between the predicted and actual growth rate at low supersaturation. This leads to the development of the kinetics theory for crystal growth by Burton, Cabrera and Frank [66]. This model enables prediction of the growth rate at low supersaturation and postulated that most crystals contain dislocations in which the crystal faces can be developed into a 'spiral staircase' from screw dislocations. The Burton, Cabrera and Frank (BCF) relationship stated

$$R = A\sigma^2 \tanh\left(\frac{B}{\sigma}\right) \qquad \text{Equation 3-5}$$

where R=crystal growth rate, the supersaturation σ=S-1 where S=c*/c. A and B are complex temperature and step spacing dependent constants respectively. The BCF equation changes from a parabolic (R proportional σ^2 at low supersaturation) to a linear growth (R proportional to σ at high supersaturation) as supersaturation increases.

The crystal growth process has also been linked to diffusional theory. The origin of diffusion theory was proposed by Noyes and Whitney [67] who considered crystal growth as essentially a diffusion process. The process is similar to a dissolution process. Berthoud [68] and Valeton [69] have reported that the process involved two steps where solute ions, atoms and molecules are transported to the crystal surface and follow a first order reaction when linked to the lattice.

Calcite precipitation kinetics and the mechanism of calcium carbonate precipitation from the solution is a surface controlled reaction that has been reported in many studies [70, 71]. The most successful models are the BCF [66], Davies and Jones [72], Reddy

and Nancollas [73] and Plummer *et al.* [74] models where all the models are based on the crystal growth rate laws. There are two general growth rate equations that can be represented as

$$r = k_p (S^{0.5} - 1)^n \quad \text{Equation 3-6}$$

$$r = k_p (S - 1)^n \quad \text{Equation 3-7}$$

where n is defined as reaction order. k_p is the precipitation rate constant (m/s) and S is the calcite supersaturation ratio.

Davies and Jones [72] developed a kinetic model based on the adsorption layer theory. This model is based on the assumption that there is a monolayer of hydrated ions covering the crystals in an aqueous solution. The hydration of lattice ions at surface sites precedes precipitation. The calcite growth follows a second order rate equation with respect to concentration. This suggests that the slowest step of the overall growth is a surface-controlled process. Adsorption, surface diffusion, dehydration of the lattice ions may cause the rate-limiting step to involve a surface reaction at the crystal surface. If the equilibrium at the crystal is achieved sufficiently rapid, crystal growth would be controlled by the bulk diffusion of material to the surface, this will lead to first-order dependence of the crystal growth rate [70]. Davies and Jones [72] also found that the calcite precipitation rate from supersaturated solutions at pH above 7 has a reaction order close to 2, which is represented as in Equation 3-6. The BCF rate law is similar to the form of Equation 3-6 with a reaction order of 1 or 2.

However, Zhang found that calcite growth from supersaturation solution is not purely surface controlled reaction but a mixture of diffusional and surface reactions [75]. The kinetics growth rate of individual calcite crystals in a dynamic flow system was developed by Zhang and Dawe [76] who discovered that the overall rate constant as a function of temperature, ionic strength and over the range of $[Mg^{2+}]/[Ca^{2+}]$ ratio of 0.1 and 0.5 could be expressed in terms of

$$\log k_p = 0.1257(IS)^{0.5} - 2400/(T + 273) - 2.11 \quad \text{Equation 3-8}$$

where IS is the ionic strength in mol/kg, T is the temperature in°C.

During crystal growth process, the crystal growth rate is influenced by two reactions, the mass transport and surface reactions. Hence, a control index q_d is introduced to determine which mechanism controls precipitation and is expressed as in Equation 3-9

$$q_d = \frac{R}{R_D}$$ Equation 3-9

where R is the measured crystal growth rate and R_D is the calculated diffusion – controlled growth rate. When $q_d \leq 0.1$, the crystal growth is surface reaction controlled. If $q_d \geq 0.9$, diffusion dominates the growth process, but if $0.9 > q_d > 0.1$ both surface and diffusion-controlled mechanisms affect the growth process.

Plummer *et al.* [74] established a model which attempts to describe calcite dissolution and precipitation at any pH and P_{CO_2} (partial pressure CO2). The overall dissolution model is given as

$$R_c = k_1 + k_2 a_{H^+,s} + k_3 a_{H_2CO_3,s} - k_4 a_{Ca^{2+},s}.a_{CO_3^{2-},s}$$ Equation 3-10

where k_1, k_2 and k_3 were given by Plummer *et al.* [74] as 0.051, $3.45X10^{-5}$ and $1.19X10^{-7}$ cm/sec at 25 ºC. When the pH >8 and P_{CO_2} is low, the solution pH at the calcite surface is lower than bulk solution.

3.4 Crystal Dissolution

During crystal dissolution, the reaction between the solid and solution is observable by the change of solution composition and mass of the solid. The solubility of mineral scale depends on the concentration and temperature of the system. For example, the solubility of $BaSO_4$ in 0.5 M NaCl is 7 ppm at room temperature and 30 ppm at 80°C [77]. For the same temperature conditions at a higher concentration of 1 M NaCl, the solubility of $BaSO_4$ is about 23 ppm and 42 ppm respectively [77]. In reality, it is impossible to obtain the absolute precipitation and dissolution rates of crystal, hence usually the net change (the difference between the opposed directions) is measured. Although most of the literature concentrates on the crystal growth rather than crystals dissolution, the basic concept is applicable to both processes. The general calcium carbonate mineral dissolution rate is described as [78]

$$R = -\frac{dm}{dt} = (\frac{A}{V}k)(1-\Omega)^n$$ Equation 3-11

where R is the rate of dissolution in $\mu molm^{-2}h^{-1}$ and m is the number of moles of calcite, t is the time, A is the total surface area of the solid, V is the volume of the solution, k is the rate constant and n is a positive constant known as the order of the reaction.

Generally, the precipitation and dissolution rates of calcium carbonate in a $H_2O - CO_2 - CaCO_3$ system are controlled by three rate-determined processes;

i.) The kinetics at the mineral surface;

ii.) The slow reaction of $H_2O + CO_2 \leftrightarrow H + HCO_3^-$;

iii.) Mass transport of the reacting species away from or towards the mineral surface by molecular diffusion.

The calcite dissolution has been characterised in terms of three pH regimes, at low pH, a transition and high pH regime [70, 74] as shown in Figure 3-7. At low pH (<4), the dissolution rate is under mass transfer and is directly proportional to the H^+ concentration. In the transition regime, between 4<pH<5.5 the dissolution is dependent of the H^+ concentration where the kinetics of the surface reaction begins to influence the mass transfer controlled. At high pH regime, pH <5.5 the dissolution rate is mixed kinetics (mass transfer and kinetics of the heterogeneous reaction on the carbonate surface) and is independent of H^+ concentration.

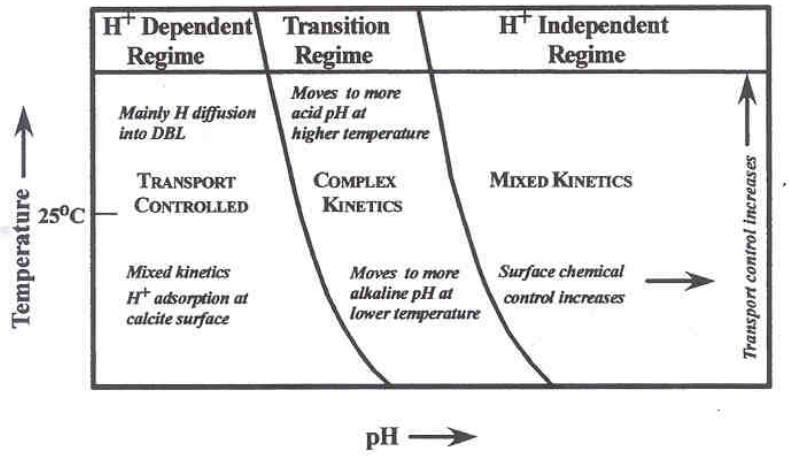

Figure 3-7 Schematic representation of the rate-controlling mechanisms of calcite dissolution as a function of pH and temperature [79]

A number of investigations claimed that the dissolution kinetics of calcite approximately below pH 4-5 is a mass transfer-controlled at ambient temperature [70, 74, 80]. Plummer *et al.* [74] used the pH-stat technique (A device for continuously sensing the pH of a solution and automatically adding acid or alkali to maintain the pH constant) to investigate the dissolution kinetics of calcite as a function of pH, P_{CO_2} and

temperature. The overall reaction of calcite dissolution in aqueous solution can be described as follows:

$$CaCO_3 \xrightarrow{k_1} Ca^{2+} + CO_3^{2-}$$ Equation 3-12

$$CaCO_3 + H^+ \xrightarrow{k_2} Ca^{2+} + HCO_3^-$$ Equation 3-13

$$CaCO_3 + H_2CO_3^* \xrightarrow{k_3} Ca^{2+} + 2HCO_3^-$$ Equation 3-14

where $H_2CO_3^* = CO_{2(aq)} + H_2CO_3$. According to Plummer, the overall rate of dissolution R_c is defined as the net difference in the forward and backward rates. Hence, the equation is described in Equation 3-10.

Where k_4 is the backward reaction for Equation 3-12. The result of calcite dissolution as a function of pH is shown in Figure 3-8. Plummer *et al.* [74] concluded that at very low acidic conditions calcite dissolution reaction rate is sufficient to be described as

$$R=k[H^+]_s^n$$ Equation 3-15

where R represents the calcite dissolution in mol $cm^{-2}s^{-1}$, k is the rate of constant $cm\ s^{-1}$, $[H^+]_s$ is the surface concentration of hydrogen ions and n is the order of reaction. Plummer reported k has a value of 0.05 $cm\ s^{-1}$ and n is equal to 1. Rickard obtained a k value of 0.03 $cm\ s^{-1}$ with a reaction order of 0.9. Campton *et al.* [80] found that at very acidic conditions at pH<4, the order reaction is equal to 1 and the rate constant has a value of 0.043 ± 0.015 $cm\ s^{-1}$. The variation of these values can be explained by the differences of diffusion boundary layer (DBL) thickness that has a great influence on the diffusion of H^+ across the DBL. The faster the rotational speed the thinner the DBL, hence the diffusion of H^+ across the layer increases. Chou *et al.* [81] reported a linear dependence of the magnitude solution flux on a_{H^+} in the range 2<pH<5 at 25 º C (i.e. n=1) and with no prediction for a weaker acid (n<1) where the pH level was below pH 2.

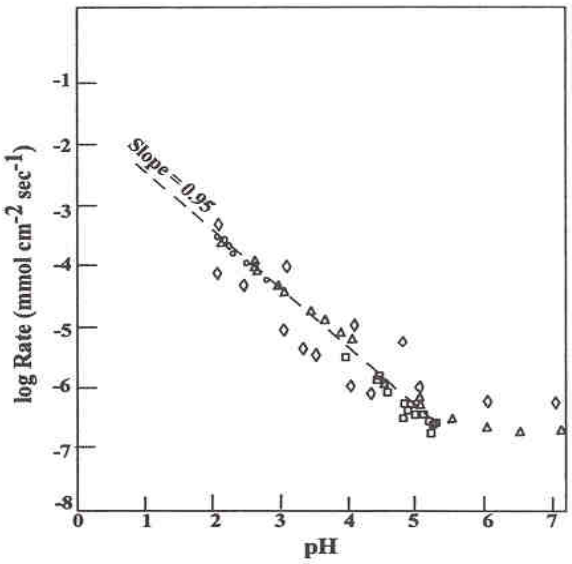

Figure 3-8 Calcite dissolution rate vs. pH [82]

The diffusion-controlled rate in low acidic conditions is unaffected by the change of P_{CO_2} [78]. This is because as pH decreases, the P_{CO_2} must increase as a result of calcite dissolution by releasing the CO_2. Over the diffusion range, the P_{CO_2} is very high and eventually exceeds 1 atmosphere [83]. The P_{CO_2} in the bulk solution and surface is equal if the P_{CO_2} is relatively high (>0.03 atmosphere), hence the rate is independent of the diffusion of CO_2 and $H_2CO_3^*$.

Rickard and Sjoberg [79] illustrated an intermediate behaviour between a strong dependence and independence of hydrodynamic condition that influences the calcite dissolution. At the transition regime, calcite dissolution can be represented as

$$k = \frac{k_C k_T}{k_C + k_T} \qquad \text{Equation 3-16}$$

where k_T is the transport controlled rate constant and k_c is the chemically controlled rate constant. The dissolution is chemically controlled if the $k_T >> k_c$ while if $k_c >> k_T$, the dissolution is mass transport controlled.

Different reactive surface sites on the calcite and surface morphology can influence calcite dissolution [84]. This may be related to the presences of defect in the crystal such as dislocations, the point defects, kinks and microfracture. Schott *et al.* [85] observed that for a strained calcite with defect densities of 10^{-7} to 10^{-8} cm^3, the calcite

dissolution rate is 2-3 times more compared to a defect-free calcite. There are many types of defects in crystal, however point defects and dislocations are the highest dissolution rates compared to others such as kinks and grain boundaries. The schematic diagram summaries the types of defects and relative dissolution rates of calcite, as shown in Figure 3-9.

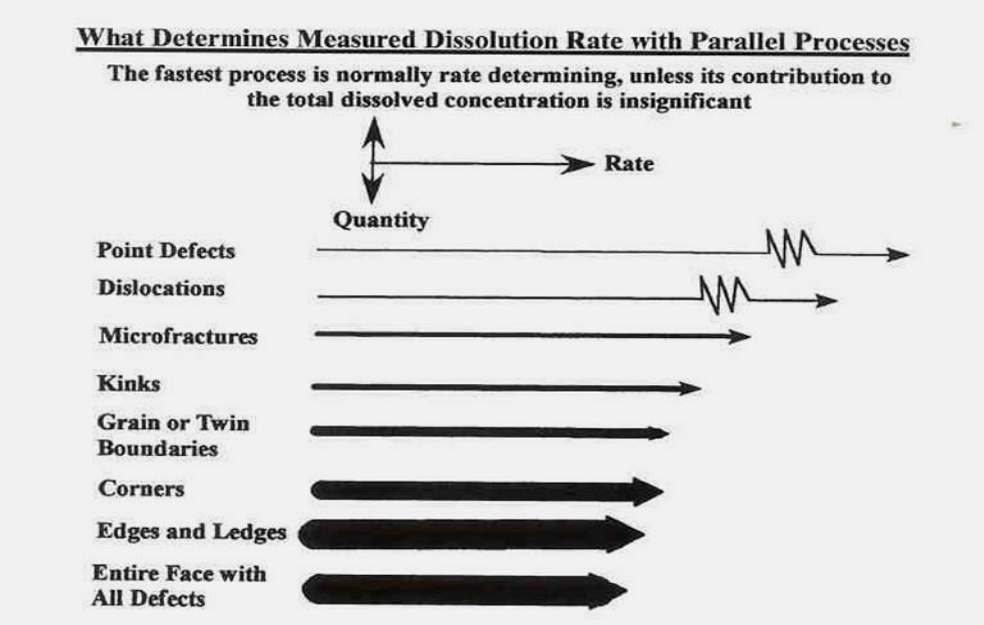

Figure 3-9 Schematic diagram for process involved in dissolution. Horizontal length of arrows is relative to rate and the thickness represents the quantity of material dissolved [85]

Recently Van Cappellen [86] developed a surface complexation theory to investigate and analyse the dissolution kinetics of calcium carbonate. The speciation of surface sites is strongly influenced by the solution chemistry rather than saturation state. This model is based on the surface coordination theory where there are two primary hydration sites $> MeOH^0$ (Me =Mg, Ca) and $> CO_3H^0$. The dissolution is promoted by the protonation of the surface carbonate groups ($> CO_3H^0$) when the pH is less than 5.

3.4.1 Industry Cleaning/ Scale Removal

In acid dosing plants, sulphuric acid is usually used to remove mineral scale especially alkaline scale such as calcium carbonate, since this is normally the cheapest acid available. Only a small amount of acid is needed (5 to 10 ppm) to maintain a system at a pH of 7.2 to 7.5 and to slow down scale deposition. In the power industry, in any

event a decrease in plant efficiency is recorded, the cleaning process is carried out using pH 4 for a period of 2-4 hours and occasionally pH 2.5 is used for a more vigorous acid cleaning. If the pH is too low, potential problems associated with corrosion can be encountered, therefore precaution must be taken in order to avoid the promotion of general corrosion. Milder organic acids such as citric acid can be used to overcome this problem. However, this can be expensive approached as higher volume of acid may be required [87] for the removal of same amount of mineral scale.

Some scales can be removed easily by acid applications, while other scales may require special chemicals for scale removal. Basically, calcium carbonate (calcite) is by far the most common carbonate scale that is acid soluble. Others such as iron carbonate also known as siderite $FeCO_3$, iron sulphides (pyrite FeS, FeS_2) and iron oxide of various types such as $Fe(OH)_2, Fe_2O_3, Fe_3O_4$ can also be removed by acid cleaning. Barium sulphate $BaSO_4$, strontium sulphate $SrSO_4$, calcium sulphate (>110º C anhydrite $CaSO_4$, <110º C gypsum $CaSO_4.2H_2O$) are the acid insoluble scale, hence these type of scales require special chemicals in order to be dissolved or removed. Calcium or barium sulphate does not react with acid since it is a relatively insoluble salt. For example, one litre dissolves 2 g at 30 ºC. Hence, this type of scale can usually be removed using a high-pressure water jet system (5000-10,000 psi). However, this is more successful for gypsum and hemihydrates scale rather than for anhydrite scale. In this case, mechanical cleaning like drilling is required to remove anhydrite scale. Out of all the techniques, the most effective way to remove calcium sulphate is to use chelating agents such as EDTA to form soluble complexes with calcium. Chelating agents react similarly with other divalent ions like iron, copper and some trivalent ions [87].

3.4.2 Scale Control

Scale precipitation and deposition on internal walls of equipment often causes major problems in many industries. These problems include scaling across perforations, flow assurance problems and the scaling of surface treating equipment. There are several mechanisms by which scale formation can be eliminated. These methods include treatment with acidulants, chelating agents and scale inhibitors [88, 89]. Acidulants function as scale inhibitors by reducing the proportion of carbonate ions present in a system through shifting the system equilibrium. However, acidulant does not reduce

the total concentration of carbon dioxide species present, it only alters the relative concentrations of each.

The most common method to control scale deposition is to use scale inhibitors. The mechanism by which a scale inhibitor acts is not fully understood. Scale inhibitors actually form an integral part of the scale crystal. When a scale crystal begins to form, the scale inhibitor is absorbed into the crystal. It is this absorption that prevents the crystal from growing larger. Some of the scale inhibitors slow the kinetics of crystal growth [90]. Other inhibits the crystal nucleation rather than crystal growth. Examples of scale inhibitors are polyphosphates and polyacrylates. Polyphosphates have been used extensively as scale inhibitors in the water industry, whereas polyacrylates are used extensively in the oilfield as scale inhibitors [91].

Chelating agents function by coordinating to the metal ion in a cage structure with coordination number 6. These materials surround the metal ion preventing the formation of the scaling species. Typical chelating agents include ethylene diamine tetra-acetic acid (EDTA) and nitrolotriacetic acid (NTA). Chelating agents are excellent scale inhibitors, unfortunately, their use is cost prohibitive.

3.5 Review of Surface Scaling

Energy interaction on the surface such as the adhesion step in a fouling process has been described in literature in terms of DLVO theory (Derjaguin-Landau-Verwey-Overbeek) [92, 93]. The theory describes the force between surfaces interacting through a liquid medium. It combines the effects of the Van der Waals attraction and repulsion due to the so-called doubled layer of counter-ions. The principle attractive forces between colloidal particles are due to London-Van der Waals interactions. However when the particles are immersed in a liquid medium, electrostatic double layers generally lead to repulsive force development.

3.5.1 London-Van der Waals Forces

Van der Waals forces are dependent on the geometry and the physical and chemical properties of the interacting bodies. London-Van der Waals forces arise from the interaction of fluctuating dipole moments generated by the motion of electrons around

the nuclei of neutral atoms in close proximity to each other. For particle diameters less than 100μm, Van der Waals forces dominate over the effect of gravity [94].

3.5.2 Electrostatic Double-layer Force

When solid bodies are immersed in a liquid medium, especially in the water, they generally show a tendency to acquire an electrical surface charge due to preferential adsorption of ions by dissociation of the surface groups or by isomorphic substitutions in the lattice [95]. The ions of opposite charge (counter-ions) will be attracted to the surface, whereas the ions of same sign (co-ions) will be repelled. This effect creates an electrical double layer near the surface. When two charged solid bodies of like sign approach each other, the interpenetration of the two double layers will lead to repulsion. The potential energy arising from the interpenetration of electrical double layers depends on the geometry of the interacting bodies and on the electrical behaviour during the interaction. Generally, it is assumed that the interactions may occur either at constant surface potential or at constant surface charge.

Interactions other than DVLO such as hydrophobic interactions and ion bridging can play important roles for adhesion. Hydrophobic interactions are based on electron donor-electron acceptor (Lewis acid-base) interactions in polar media (e.g., water), can surpass the DLVO forces by as much as two orders of magnitude. Positively charged ions (Ca^{2+} and Mg^{2+}) can act as bridging agents between two negatively charged surfaces. These ions can depress the monopolar electron donor parameter of the surface tension of the interacting bodies, as cited by Van Oss *et al.* [96] it is also able to depress the mutual repulsion and degree of hydration.

3.5.3 Characteristics of Surface Scaling

Extensive research about mineral scaling has been concentrated primarily on three main areas: kinetics of precipitation, prediction models, development of scale inhibitors and treatments. As a result, significant reliable knowledge and understanding of the mechanisms of precipitation under various conditions have been obtained. The studies of kinetics are primarily focused on homogeneous nucleation (bulk precipitation) of mineral scale in bulk solution. Bulk precipitation and surface scaling are two different processes. These processes have different mechanisms of crystal nucleation and growth. In bulk precipitation, the supersaturated brine gives rise to agglomeration of scale-

forming ions due to random collisions of the ions in the motion. The cluster of ions coalesces to form a crystal once it exceeds the critical precipitation size. Whereas, surface scaling is mainly caused by foreign bodies and surfaces which induce the precipitation process. Hence, surface scaling is susceptible to surface chemistry of the material, solution (supersaturation), the presence of impurities in the solution, pressure, pH and temperature.

Numerous methods and studies to detect and assess scale formation on pipeline surfaces in oil and gas industry and desalination industry have been reported by Hasson *et al.* [12] and Zhang [76]. Often significant anomalies exist between an actual adhesion rate and the rate estimated by some predictive models that are usually based on a bulk supersaturation scaling index. Hasson *et al.* [12] demonstrated that there are discrepancies between the actual scale deposition and that estimated by the prediction models. Results of the static bottle tests and TSMR (Thickness Shear Mode Resonator) conducted by Emmons *et al.* [38] showed a discrepancy between surface scaling and bulk precipitation. This could be explained by static bottle tests that measure both dispersed scale and adherent scale while TSMR measured only scale adhered to the sensor surface. Harris and Marshall [97] demonstrated that there are wide anomalies between actual deposition on component surfaces and the scaling rates estimated by the predictive models. Sohnel and Garside [98] reported that the induction time for mineral scale formed on the metal surface is less than the precipitated scale formed in the bulk solution. This confirms that heterogeneous crystal nucleation is easier than homogenous crystal nucleation. The average size of the scale crystals formed on the metal surface is larger than the precipitation crystals formed in the bulk solution, which implies that heterogeneous scale formation conditions promotes crystal growth compared to homogenous conditions.

Calcareous scaling of calcium carbonate was investigated by Abdel-Aal *et al.* [99] using the QCM (Quartz Crystal Microbalance) technique as means of ion concentration measurement (bulk solution). In this experiment, the electrode was not subjected to external forces such as electrochemical potential. Hence, the precipitation and growth were governed by the supersaturation factor. The adhesion rate and the morphology of $CaCO_3$ on the surface were predominantly controlled by bulk solution supersaturation. The authors claimed the adhesion process produces direct growth of calcite on gold surfaces when the supersaturation is high.

3.5.4 Electrochemically Accelerated Scaling Tests

Recently, research work is shifting the focus on to surface scaling investigation, investigating the mineral scale formation on metal surfaces rather than bulk precipitation. Metallic surfaces have been used as the foreign solid for the deposit formation in contrast to other studies which use seeded crystals like calcite crystals, sand particles and glass particles [98, 100, 101]. A few common techniques such as TSMR, QCM and RDE are often linked and used to study the surface scaling. Among these techniques, an electrochemical technique, in conjunction with a rotating disc electrode, submerged impinging jet or impedance technique has been widely used to study surface scaling, as well as crystal morphology.

Chronoamperometry is one of the electrochemical techniques that has been used to investigate the electrochemically accelerated scaling process. The current against time is recorded during the carbonate scaling process when the electrode is being polarised. The progressive blocking of the active electrode surface by $CaCO_3$ can be detected by the decrease of the current with time. A parameter referred to as scaling time, can be obtained from I =f (t). Scaling time is defined as the time needed when the current attains a very low and stable value (residual current), which usually corresponds to the current plateau.

The chronoamperometry technique is more or less similar to cathodic protection. When cathodic protection is imposed either in natural seawater or in an electrolyte consisting of Mg^{2+} and Ca^{2+}, magnesium and calcium-containing deposits, known as calcareous are formed. The rate of calcareous deposition as well as the morphology of the film can be altered by changing the physical or chemical variation of the environment, such as applied potential, flow characteristic, pH, salinity, temperature, surface finish and chemical composition of the seawater. The calcareous deposit provides a physical barrier to reduce the oxygen-reduction on the metal surface, consequently lowering the cathodic current [102-104].

This methodology is often used as an accelerated test for $CaCO_3$ crystallisation by polarising a metallic electrode at a sufficiently negative range to promote cathodic reduction of dissolved oxygen. The oxygen reduction process causes formation of calcareous deposits on a metallic surface due to

i.) an increase of interfacial pH at the metal/electrolyte interface;

ii.) enhanced carbonate ion concentration at the interface by altering the inorganic carbon equilibria;

iii.) precipitation of inorganic compounds whose product solubility exceeds SR.

The oxygen reduction reaction occurs according to

$$O_2 + 2H_2O + 4e^- \rightarrow 4OH^-$$ Equation 3-17

The production of OH^- (hydroxyl ions) in the vincity of the electrode as a result of this reaction (above) increases the pH and forces a solid crystalline phase of calcium carbonate to precipitate on the metal surface according to a two-step chemical reaction

$$HCO_3^- + OH^- \rightarrow CO_3^{2-} + H_2O$$ Equation 3-18

$$Ca^{2+} + CO_3^{2-} \rightarrow CaCO_3 \downarrow$$ Equation 3-19

This gives the overall equation

$$Ca^{2+} + HCO_3^- + OH^- \rightarrow CaCO_3 + H_2O$$ Equation 3-20

The interfacial pH or amount of OH^- is a function of the applied potential. At an applied potential of –0.5V/(SCE), the interfacial pH is close to 9.3 and to 9.6 for –1.0 V/(SCE) [102]. The controlling factor of the oxygen reduction in an aerated solution is the O_2 supply to the metal surface. This process is under convective diffusion control and is represented by a diffusion plateau on the cathodic polarisation plot.

Under the high pH condition (pH~9.5) and presence of Mg^{2+} in a system, magnesium hydroxide precipitation has been reported by Kobayashi [105]. He also reported that pH reaches a value of 10.5 on stainless steel surfaces in 3.5% sodium chloride at a potential of –0.8V. Magnesium hydroxide is known to provide a gel-like film and hinder the transport of ionic and non-ionic species, which is similar to $Zn(OH)_2$. Magnesium hydroxide precipitates in the form of brucite that consists of hexagonal platelets. However, under an electrochemical technique, $Mg(OH)_2$ tends to aggregate as palettes and it is hard to observe a well-defined crystal [103].

This surface scaling acceleration test is susceptible to the surface chemistry of the material, solution (supersaturation), the presence of impurities in solution, the pH,

temperature and flow rates etc. Therefore, the following sections review the factors affecting scaling during electrochemical processes.

3.5.4.1 Applied Potential

Under cathodic protection, the oxygen-reduction reaction can be split into two elementary steps as below and the reduction of water leading to evolution of hydrogen. The steps involve is depend on the applied potential [15].

$$O_2 + 2H_2O + 2e^- \rightarrow H_2O_2 + 2OH^- \quad \text{Equation 3-21}$$

$$H_2O_2 + 2e^- \rightarrow 2OH^- \quad \text{Equation 3-22}$$

When a metal is immersed in a neutral or alkaline aerated solution, the two main cathodic reactions at potential E_{corr} (free corrosion) are the reduction of oxygen and hydrogen evolution. The contribution of cathodic current due to hydrogen evolution is less significant under this condition. It becomes more significant when is more negative than $E_{2H_2O+2e^- \rightarrow H_2+2OH^-}$. However, if the potential electrode is forced to a more negative potential (cathodic protection) from E_{corr} to E_1, the diffusion of dissolved oxygen species becomes the slowest step in the oxygen reduction reaction. Under these conditions, the process is known as diffusion controlled. As a result, the current reaches a limiting value, known as the limiting current under this condition. The total current that contributes to the cathodic reaction is mainly from the oxygen reduction reaction until hydrogen evolution becomes the main cathodic reaction when the potential is more negative $E_{2H_2O+2e^- \rightarrow H_2+2OH^-}$.

In general, calcareous deposits consist of a uniform thin layer of an Mg-rich inner layer, presumably magnesium hydroxide and a thicker overlapped layer of aragonite needles. However, the deposit would be expected to have lower $CaCO_3$ ratio to $Mg(OH)_2$ when the specimen is polarised to a potential that is more negative. This is because at a more negative potential, the higher pH favours the formation of magnesium hydroxide at the metal surfaces. However, the calcareous composition and morphology may be varied with the applied potential. The kinetics of calcareous deposition in an artificial seawater has been analysed by chronoamperometry and EHD (electrohydrodynamical impedance technique) techniques. It was found that at 20 ˚C, calcareous deposits were composed of aragonite when the applied potential was –0.9 to -1.1V/ (SCE), $Mg(OH)_2$ brucite and

aragonite when the applied potential was –1.2V/(SCE) and only brucite for applied potentials of <-1.3V/(SCE) [104].

In the absence of Ca (II), a porous layer containing Mg (II) could form even at potential values where $Mg(OH)_2$ brucite could not be deposited. $Mg(OH)_2$ is porous and amorphous and does not play a significant blocking role [103]. In any event where the cathodic protection is interrupted (a reduction of current for the CP as scale formed), $Mg(OH)_2$ will be dissolved into electrolyte since it has higher solubility than $CaCO_3$ and this leads to the formation of a less protective layer with poor coating properties [102]. However, in the absence of Mg (II), calcium carbonate deposited under the electrochemical process will be composed of two defined crystalline forms; calcite and aragonite.

3.5.4.2 Surface Material or Substrate

The study of calcium carbonate deposition is strongly influenced by the surface substrate. The surface of a substrate can simulate crystal particles and promotes heterogeneous nucleation to take place at low free energy. Gabrielli *et al.* started to study precipitation of calcium carbonate on a range of insulating materials [28, 63]. The insulating materials were covered with a platinum wire gauze. The sample is polarised by an electrochemical technique to promote oxygen-reduction and subsequently the local pH increases. Precipitation reactions take place at the non-metallic surfaces as a result of high localised pH. The author compared the density of nuclei sites formed on the surfaces of insulating materials. PTFE (polytetrafluoroethylene) had the least nuclei sites (about 400 mm^{-2}), followed by PVC (polyvinyl chloride) (about 3500 mm^{-2}) and Plexiglas (polymethy methacrylate) (4500 mm^{-2}). The scaling susceptibility of PTFE is approximately ten times lower than other insulating materials. In this experiment, it is also shown that the surface chemistry of material has an effect on the formation of different types of crystal structure. On PVC surfaces, nuclei are aligned along the polished grooves, which act as active sites promoting nucleation.

Calcite polymorph morphology was observed simultaneously with various ill-formations of vaterite, such as lentil and gypsum flowers. The majority of scale was calcite and a few hexagonal vaterite crystals were found on Plexiglas surfaces. PTFE showed mostly vaterite and exhibited gypsum flowers on the surfaces. Hort *et al.* [106] also claimed that heterogeneous processes are governed by scaling and its rates are

smaller on copper than on other insulating materials. This is mainly because the scaling process on polymeric materials is being initiated by the formation of colloidal $CaCO_3$ aggregates due to electrostatic attraction by the surface charge of the wall. There are other explanations suggesting that it is due to the presence of chemical groups at the polymer surface, however the actual mechanism is unclear.

3.5.4.3 Effect of Rotation Speed or Flow Rate On Electrochemical Measurement and pH Buffering

Electrochemical reactions are influenced by the flow rate from the impinging jet and also rotating speed from the rotating disc electrode. The higher the rotation speed the thinner the diffusion layer and hence a higher transfer rate of oxygen to the metal surfaces is possible. Consequently, this increases the oxygen reduction processes and the pH on the electrode surface. In such conditions, a higher current density is also anticipated as the rotation speed increases. However, this is not the case for the pH at the electrode surface, as a higher rotational speed also promotes OH^- ions that are diffused back into the bulk solution (from the electrode surface to bulk solution). As a result, a higher rotation speed makes little contribution to the formation of calcareous deposits, even though the total current density increases considerably [107]. Flow rate not only has an effect on current density but also on crystal morphologies. A thinner, compact layer was reported at a high flow rate compared to a lower flow rate. However, if the flow rate is too high, it will impede the nucleation and growth rate of the calcareous deposition [17].

3.5.4.4 Effect of Temperature

The thermodynamics and kinetics of the precipitation may also depend upon the temperature. In spite of the increase of dissolved oxygen in the bulk solution at lower temperatures, no significant increase of the mass transfer of oxygen is found in these conditions as a lower oxygen diffusion coefficient is expected. At 0˚C, $CaCO_3$ deposition is limited by the rate of diffusion of Ca^{2+} and $CaCO_3^{2-}$ ions to the metal surface. The surface coverage of $CaCO_3$ is also less because of a smaller reaction constant $k_{sp_{CaCO_3}}$ and a reaction order is expected. Hence, the kinetics are the rate-controlling factors in low temperature conditions despite the higher solubility constant of $CaCO_3$ [107]. The calcareous, consisting of Mg^{2+}, forms a rich film in cold water that indicates high porosity and poor protection. Kunjapur *et al.* [98] found that mineral

scale deposited under 3 ˚C had the micro-porous structure of the Mg rich deposits as well as semi-conductive properties.

3.5.4.5 Effect of Salinity on Electrochemical Measurement

The concentration of oxygen reduces as salinity increase; hence, a lower initial current density is observed when a metal is polarised. However, the concentration of the reactive ions such as Ca^{2+}, Mg^{2+} and CO_3^{2-} increases as the salinity increases. Since the transfer of species from the bulk solution to electrode surface is mass transfer controlled, the concentration of species on the electrode surface is dependent on bulk concentration. As a result of high supersaturation, the formation rates of $CaCO_3$ and $Mg(OH)_2$ are slightly increased [107]. The presence of magnesium ions in a solution favours the formation of aragonite and inhibits calcite formation. In addition, it also decreases the oxygen-reduction rate by forming a film to prevent oxygen reduction.

3.5.4.6 Effect of Divalent Cations and Organic Additives on Crystal Morphologies

Magnesium exerts a significant influence on calcium carbonate precipitation. In the presence of Mg^{2+}, calcium carbonate precipitation usually favours aragonite rather than the thermodynamically favoured, calcite. However, the presence of malic and citric acids tend to stabilise calcite, with respect to aragonite, in the presence of Mg-containing solutions. The magnesium ions can either be incorporated within the calcite lattice when the Mg:Ca ratio is low or induce aragonite precipitation when the magnesium concentration is sufficiently high. The Mg^{2+} ion is more strongly hydrated than Ca^{2+} and is strongly adsorbed on to the surface of growing calcite crystals. Dehydration of the Mg^{2+} when it is incorporated in the calcite lattice creates a barrier to the growth of calcite nuclei.

A wide range of calcite morphologies was observed in the presence of Mg^{2+}. A change of morphology from calcite (rhombohedral) to a continuous thin Mg rich film as the Mg:Ca ratio increases was reported [108]. This suggests that the presence of Mg^{2+} binds specifically to certain crystal planes during calcite growth, thereby modifying the morphology. Mg^{2+} interacts specifically with {011} faces of calcite, producing crystals elongated along the c-axis. Rounded surfaces or edges were found on calcite crystals contaminated with Mg^{2+}. Elongated single calcite crystals were often found when organic additives such as citric or malic acids are present in Mg-free solutions [109].

Impurities such as Mg^{2+}, Ni^{2+}, Co^{2+}, Fe^{2+}, Zn^{2+} and Cu^{2+} encourage aragonite formation whereas Mn^{2+}, Cd^{2+}, Ca^{2+}, Sr^{2+}, Pb^{2+} and Ba^{2+} favour calcite. In general, impurities with a small ionic radius and higher hydration energy than Ca^{2+} favour aragonite formation [71].

Chapter 4 Review and Development of a Submerged Impinging Jet as a Monitoring Sensor

4.1 Introduction

The formation and deposition of mineral scale on process equipment surfaces continuously incur massive costs as well as flow assurance problems. Any new developments capable of monitoring mineral scale precipitation and deposition would be beneficial to industry. It is clearly indicated that there are various techniques already in existence, which can be used to investigate and monitor mineral scaling in a system as described in Chapter 2. However, some of these techniques are complicated in terms of equipment set up and data interpretation; such exhibited by the ultrasonic technique and electrochemical impedance technique. Other techniques are expensive such as the Gamma Ray Attenuation that was developed by Schlumberger Oilfield Services [39]. Any new technology development should be not only robust and reliable to succeed in detection and monitoring of mineral scale, but also needs to be simple to use to allow easy interpretation of results.

This led to the development of a rotating disc electrode (RDE) [22]. The main benefit of this technique is the flow hydrodynamics that could be easily manipulated for the electrochemical study. In addition, this system is relatively inexpensive and easily set up compared to other techniques. The use of RDE to investigate and quantify mineral scale formed on component surface was extensively studied by Morizot [15] as presented in Chapter 2. However, one of the main drawbacks of using this technique is the sealing issue especially at the rotating part of the system when operating at higher pressure conditions. Though further development and laboratory trial tests are still required, the challenge of sealing may hinder the future development of this technique to be transformed into a viable technology especially at higher pressure conditions. The evolution of a rotating disc electrode to a submerged impinging jet has addressed the sealing issue. Some of the benefits of using submerged impinging jet in conjunction with electrochemical technique comparing to other techniques are:

i.) Relatively cheap and easy to set up;
ii.) Less complexity in term of data interpretation;
iii.) Capable of generating a wide range of hydrodynamic flow patterns from laminar to turbulent flow regimes. This is true especially for the laminar

flow condition for studying an electrochemical process where the electrode is uniformly accessible with respect to mass transfer;

iv.) The SIJ has the advantage that there is no mechanical movement as in the rotating disc electrode (RDE) system, hence it can easily be adapted as a monitoring technique in a high pressure system without having sealing problems;

v.) For sophisticated investigations such as an electrochemical noise analysis, or system involving complicated electrical connections, the rotating electrical contacts may cause some problems. Using SIJ will not foresee such an issue.

Figure 4-1 represents the route map of this research work. The main objective of this chapter is to investigate and explore the feasibility of using a SIJ (submerged impinging jet). An understanding of the background behind the SIJ and the development of the SIJ as a sensor, are essential in order to develop the technology. Hence, in this chapter, background and theory of the application of the SIJ technique and electrochemical measurement are reviewed. Furthermore, the hypothesis of this technique to measure the scaling tendency of brine is also presented. SIJ was deployed as a means of delivering the flow and electrochemical control to access the extent of scale on the specimen surface. It was also used to assess the scaling tendency of a system. This chapter can be divided into the sections that follow:

i.) Review of the electrochemical and submerged impinging jet technique (SIJ) as a means to study mineral scaling;

ii.) Background of SIJ and electrochemical technique to detect the mineral scale by measuring the extent of mineral scale deposited on component surfaces;

iii.) Background of the same technique to measure and monitor the saturation ratio of brine system;

iv.) Finally, the reliability and reproducibility were verified through extensive calibrations by using the SIJ equipment setup in combination of electrochemical measurement.

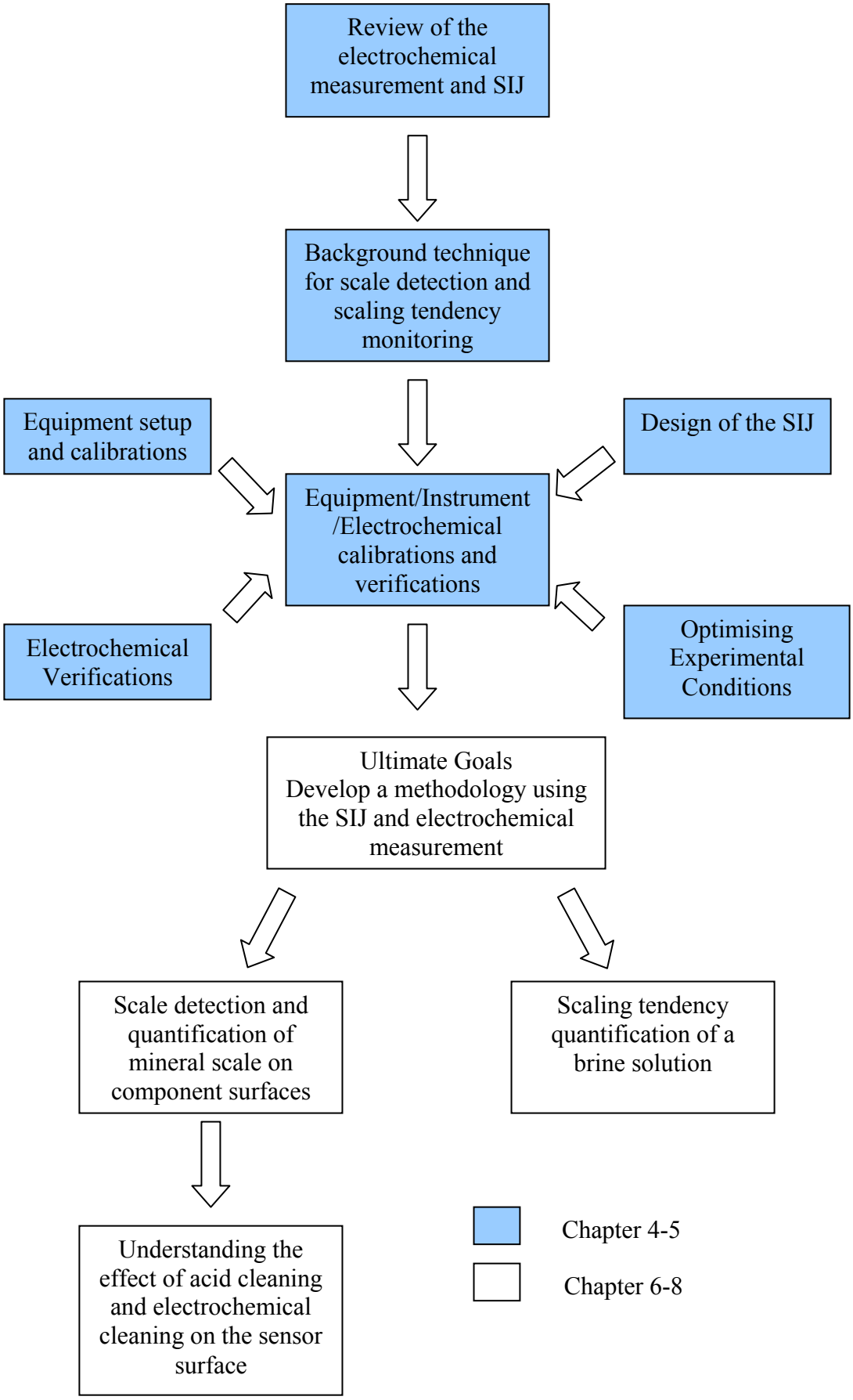

Figure 4-1 Schematic diagram represents the road map of this research work

4.2 Review of the Electrochemical Measurement

In this section, the application of the SIJ to dictate the hydrodynamics of a system over a wide range of flow patterns to study the electrochemical measurement is addressed. The electrochemical measurement and flow parameters are described in order to provide basic knowledge of this technique. The electrochemical technique uses dissolved oxygen as a tracer. When a potential in a cathodic regime is applied, the oxygen-reduction reaction takes place at the specimen surface. The rate and kinetics of the oxygen-reduction reaction are controlled by the diffusion of oxygen from the bulk solution to the specimen surface. This reaction is under the mass transfer control when the diffusion of oxygen becomes the slowest step in the reaction and is limited, hence a well-defined plateau region in the potential log current (E log I) is obtained. At this region, the current remains constant, with respect to the potential, and this current is known as the limiting current.

In an electrochemical measurement, the current responses to flow must be expressed in terms of geometry-independent fluid flow parameters instead of its velocity as the primary parameter in hydrodynamic systems. The purpose is to enable the application of laboratory test data to the field operation. There are several dimensionless parameters, which are used in the fluid flow analysis. One of these parameters is the dimensionless Reynolds number (Re). It is used to predict the transition from the laminar to turbulent flow and is represented by the dimensionless ratio as in Equation 4-1.

$$\mathrm{Re} = \frac{ud}{\nu} \qquad \text{Equation 4-1}$$

where u is the mean velocity of the flow (ms^{-1}), d is the characteristic specimen length (m) and ν is the kinematics viscosity (m^2s^{-1}).

For turbulent flow, there will still be a thin laminar layer near the metal surfaces as a result of viscous drag. The relationship between the thickness of diffusion boundary layer (δd) and the laminar layer (δh) is governed by the dimensionless Schmidt number (Sc)

$$Sc = \frac{\nu}{D} \qquad \text{Equation 4-2}$$

where D is the diffusivity of the relevant species. The higher the value of Sc, the thinner the diffusion layer will be. The mathematical development of δh/δd leading to the Schmidt values of $Sc^{1/3}$. The mass transfer rates can also be expressed in a non-dimensionless group as shown in Equation 4-3

$$Sh = \frac{kd}{D} \qquad \text{Equation 4-3}$$

where Sh is the Sherwood number. The Sherwood number is proportional to the limiting current, i_L following the definition

$$Sh = \frac{i_L d}{nFACD} \qquad \text{Equation 4-4}$$

i_L = limiting current, mA
n = number of electrons
F = Faraday constant, $C.mol^{-1}$
C = concentration of electroactive species, $mol.dm^{-3}$
D = diffusion coefficient, $cm^2.s^{-1}$
d = nozzle diameter, cm
A = area of the electrode, cm^2

4.3 Review of a Submerged Impinging Jet (SIJ)

Many applications of the impinging jet have been found in heat and mass transfer, especially in turbine blade cooling, paper drying and electronic packaging due to their effective transport capabilities [110]. Impinging jets are frequently used when high heat and mass transfer rates are required. Inefficiency or non-uniformity of heating or cooling has been regarded as a major source of malfunctioning of equipment (hot spots, noise level etc). Therefore, the jet impingement is widely used for rapid cooling/heating applications. Convective cooling/heating is very efficient when jets of cold/hot air are directed onto the object to be cooled /heated. Some of the SIJ applications can be found in electronics cooling (miniaturization of high power chips), heat processing of ceramics, metals, cooling of internal combustion engines and cooling of aircraft blades and stationary gas turbines, etc. Recently, the SIJ has appeared as an alternative method of studying electrochemical and erosion-corrosion processes at the laboratory stage, since the hydrodynamics flow pattern at the vincity of the electrode surface can be carefully controlled for the electrochemical measurements. The SIJ also provides an unique electrochemical method to evaluate of chemical inhibitors film persistency [111].

The Submerged Impinging Jet (SIJ) consists of a jet that may either be in the form of a slot or circular orifice. If the jet fluid is the same as the stagnant fluid (same medium) then the jet system is referred as a submerged jet. The jets are said to be confined, if the exit flow pattern is confined as a result of other walls present in addition to the impingement surface. In the present study, a single circular nozzle was immersed in the electrolyte and the flow of the electrolyte was perpendicular (normal) to a disc electrode. Two flow regimes can be obtained near the electrode as the electrolyte strikes its surface. These are the stagnation and wall-jet regions. In the stagnation region, the electrode is subjected to laminar flow if $r < r_{nozzle}$. In the wall-jet region, the flow is turbulent. This occurs when the radial position is $r > 2.5r_{nozzle}$. A transition of flow occurs when $r_{nozzle} < r < 2.5r_{nozzle}$. A properly designed submerged impinging jet can avoid turbulent flow in the stagnation region and generates a laminar flow where the electrode surface presents a uniformly accessible surface. Laminar flow is most used in the practical applications of SIJ because the equations of mass transfer are well defined under this regime. In contrast, the transport under turbulent flow is difficult to model, despite the increase in mass transfer rate occurring with turbulent flow. This characteristic of SIJ makes it very useful for studying electrochemical processes where electrons and mass transfer take place at uniform regions (laminar flow) near an electrolyte/solid interface. Hence, a constant surface concentration can be maintained throughout the electrode surface, which makes it a useful tool for electroanalytical studies [112].

In SIJ, the flow can be separated into four regions as shown in Figure 4-2. The diameter of the nozzle is denoted as d. The flat surface where the incident electrolyte strikes is known as the impingement surface. H is referred to the distance or height to the impingement surface. H/d is the ratio of the nozzle distance to plate to the nozzle diameter and r/d is the radial position from the stagnation point.

i.) Region I is known as the potential core region and has a conical potential core. The velocity profile changes from a pipe flow to a free jet flow in this region. Fluid properties and velocity are relatively constant. Core length varies from 4.7~7.7 nozzle diameters, which is dependent on the nozzle geometry;

ii.) Region II, in this region, the velocity profile is well developed. The centre velocity (magnitude) is inversely proportional to the distance from the nozzle exit and becomes zero at the stagnation region. It usually has a length

of 1.6-2.2 height of nozzle, between an apex of potential core and the flat plate;

iii.) Region III is known as the stagnation region, the flow regime in this region has a thickness of 1.6-2.2 nozzle diameters and radius of 0.6-1.4 nozzle diameters. The flow changes from axial to radial direction in this region. The thickness and boundary layer is relatively independent of radial position near the stagnation point. It consists of axial velocity v=-2az and radial velocity u=ar, where a= hydrodynamic constant that depends on the volume flow rate and nozzle geometry and can be obtained theoretically or empirically;

iv.) Region IV is called the wall jet region. Radial velocity starts to decay and the thickness of the boundary layer increases with radial positions. This flow region can be divided into 2 sub-layers; an inner and outer layer. The flow at the inner layer is influenced by the wall, whereas the outer layer flow is influenced by the surrounding fluid. Maximum velocity occurs at the boundary of the two sub-layers and its magnitude is inversely proportional to radial distance.

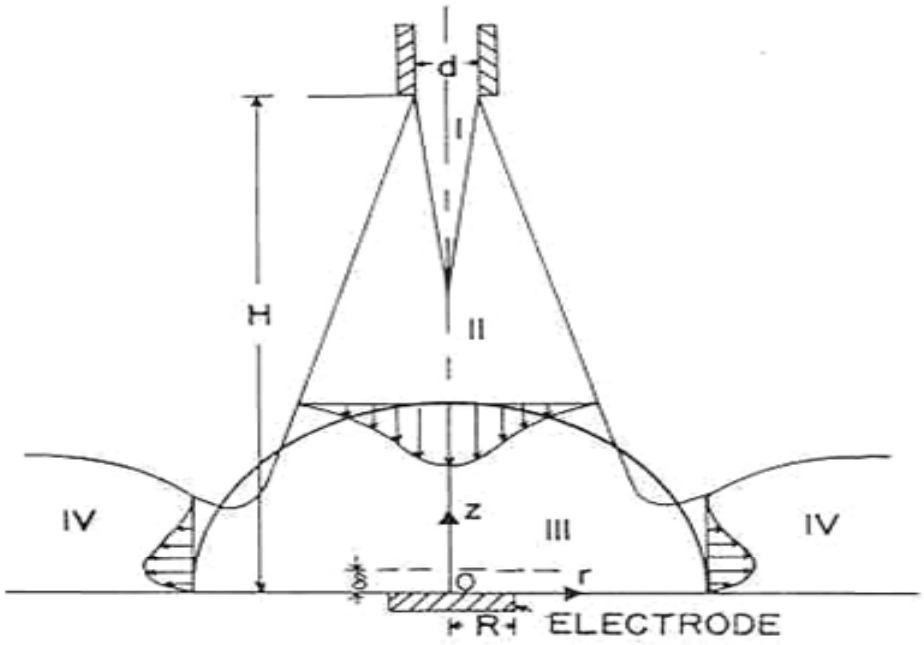

Figure 4-2 Schematic diagram represents different flow regions of an impinging jet [112]

In a SIJ system, it is found that for r/d <0.5 the flow is a laminar and has similar properties to a rotating disc where the mass transfer rate is independent of the radial position in the laminar flow. In addition, the flow in the stagnation region of the

impinging jet is axisymmetric, thus it has close similarities to the flow near a rotating disc electrode (RDE) [112]. Bouet *et al.* [113] reported that the SIJ electrode surface is uniformly accessible for mass transfer as for the RDE. They found for a SIJ system under laminar jet condition (Re=560) with an electrode r/d=0.78 and $i=1/2i_{L,}$ an identical matching of the impedance diagram plot to a RDE at 600 rpm.

The local mass transfer rate at a flat plate in the SIJ system is dependent on the nozzle Reynolds number of the fluid, Schmidt number of diffusion species, geometric parameters such as the relative nozzle-to-plate distance (H/d) and relative radial position, (r/d). In the uniformly accessible region, the mass transfer rate is proportional to Re and decreases by increasing the relative nozzle-to-plate distance (H/d).

Extensive theoretical and experimental work related to mass transfer were studied in details by Chin and Tsang [112]. The SIJ setup was developed and deployed to investigate different experimental conditions that influence mass transfer, such as the nozzle flow rate, the arrangement of geometry parameters r/d and H/d. In this experiment, a circular nickel disc electrode was located within the stagnation region and subjected to electrolyte impingement by the SIJ. The limiting current corresponding to the cathodic reduction of ferricyanide ions was measured. Chin and Tsang [112] claimed the electrode possesses a property of uniform accessibility to the diffusing species for a turbulent flow nozzle and laminar flow nozzle where r/d is within 0.1-1.0 and 0.1-0.5 respectively. The wall jet region starts at approximately r/d=4. A general semi-empirical solution of convective diffusion model [112] was derived through this study as stated below

$$Sh = \alpha.\mathrm{Re}^{1/2}.Sc^{1/3}.g(Sc).f(H/d) \qquad \text{Equation 4-5}$$

where α is a constant coefficient depending on the nozzle geometry, on the laminar and turbulent character of the jet and difference for low or high Schmidt numbers, Re is Reynolds number, Sc is the Schmidt number. Both g(Sc) and f(H/d) are the function of Sc and relative nozzle-to-plate distance respectively. The function of g(Sc) is equal to unity at large Sc values

The mass transfer rate in the wall jet region is proportional to the Reynolds number, raised to the power 0.75 and inversely proportional to the dimensionless radial position (r/d). In the stagnation region, the mass transfer rate depends on $\mathrm{Re}^{1/2}$ and is independent of the radial position. These findings were reported through the

examination of the evaporation of naphthalene to an air jet and dissolution of trans-cinnamic acid to a water jet.

The below equations are empirical relation derived from a least squares curve fitting of the experimental results of the reduction ferricyanide from Equation 4-5. These equations are valid for $0.2 \leq H/d \leq 6$.

Laminar jet: $Sh = 1.51 \mathrm{Re}^{0.5} Sc^{0.33} (\frac{H}{d})^{-0.054}$ Equation 4-6

(if Re <2000, 0.1<r/d< 0.5)

Turbulent jet: $Sh = 1.12 \mathrm{Re}^{0.5} Sc^{0.33} (\frac{H}{d})^{-0.057}$ Equation 4-7

(if 4000<Re< 16,000, 0.1<r/d< 1)

For laminar flow substitute Equation 4-4 into Equation 4-5 gives the limiting current, i_L as below

$$i_L = 1.51 \mathrm{Re}^{0.5} Sc^{0.33} (\frac{H}{d})^{-0.054} g(Sc) \frac{nAFCD}{d}$$ Equation 4-8

where α is a constant coefficient, Re is Reynolds number, Sc is the Schmidt number, i_L is the limiting current (mA), n is the number of electrons, A is the active area (cm^2), F is the Faraday constant ($Cmol^{-1}$) , H is the height of nozzle to electrode (cm), d is the diameter of the nozzle (cm), C is the concentration and D is the diffusion coefficient (cm^2s^{-1}).

Coeuret reported that the stagnation flow is approximately r/d=1.4 for a tubular circular jet [114]. Similar investigations were performed by Bouet *et al.* [113] using the electrochemical impedance in conjunction with a SIJ where the setting of d=4 mm, H/d=3, r/d=0.57. In the laminar flow region, a straight line passing through the origin was obtained from the limiting current versus square root of Re plot. Arkam *et al.* [13] claimed that the electrode is uniformly accessible to mass transfer within the stagnation region for r <0.8d of a laminar flow. The distance H has no effect on the current if the ratio H/d is maintained between 0.5-3.

4.4 Background Technique of Scale Detection

In this section, a brief explanation of the principle of the SIJ technique as a scale detection sensor is to be presented. This technique is capable of measuring the extent of scale formed on the sensor surface. The electrochemical measurement is carried out in conjunction with the SIJ as a scale detection technique. SIJ is used as a means of getting the flow regime in the stagnation regime, which is generated by laminar flow. The background of the technique is shown in Figure 4-3. Before scale forms on the active surface area for a bare specimen, it has a value A_1 allowing the oxygen-reduction reaction to occur. A_2 is defined as an active surface area, which is not covered with mineral scale on the electrode after scale deposition process. The initial value A_1 of the bare electrode, changes to a lower value A_2 where the active surface area becomes less due to scale formation on its surface. All the parameters (the concentration of oxygen, diffusion coefficient and viscosity of the electrolyte) in the Equation 4-9 are assumed constant at ambient temperature and atmospheric pressure. The only parameter, which may vary is the active surface area or partially blocked surface area of the electrode. The change of area initial value A_1 (bare electrode) to A_2 (scaled electrode) causes a lower slope value of limiting current versus square root of Reynolds' number (i_L versus $Re^{1/2}$). The extent of scale coverage on the surfaces electrode can be calculated by plotting i_L versus $Re^{1/2}$, which can be used to determine the slope value before and after scale deposition. The change of the slope values, initial slope, K_i to final slope, K_f indicates the coverage of scale or the extent of scale deposited on the specimen surface as shown in Equation 4-11. The summary of this technique is shown in Figure 4-3. The entire plot is performed using the equation below

$$i_L = 1.51 \mathrm{Re}^{0.5}\, Sc^{0.33} \left(\frac{H}{d}\right)^{-0.054} g(Sc) \frac{nAFCD}{d} \qquad \text{Equation 4-9}$$

$$i_L = K \mathrm{Re}^{1/2} \qquad \text{Equation 4-10}$$

$$Scale\ Coverage = \frac{Initial\ Slope - Final\ Slope}{Initial\ Slope} = \frac{K_i - K_f}{K_i} \qquad \text{Equation 4-11}$$

i_L = limiting current, mA

n = number of electrons

F = Faraday constant, $C.mol^{-1}$

C = concentration of electroactive species, $mol.dm^{-3}$

D = diffusion coefficient, $cm^2.s^{-1}$

Re = Reynolds number

Sc = Schmidt number

d = nozzle diameter, cm

H = height of the nozzle to electrode

A = area of the electrode, cm^2

K = constant or slope value

K value can be determined from experimental by plotting the i_L versus $Re^{1/2}$.

There are a few assumptions made for the analysis:

i.) Deposition of the mineral scale acts as a complete barrier and the mineral lattice does not allow oxygen to diffuse through;

ii.) The rate of oxygen-reduction reaction and oxygen diffusion coefficient are constant for a bare and scaled electrode;

iii.) The corrosion reaction at metallic surfaces is small and has negligible effect.

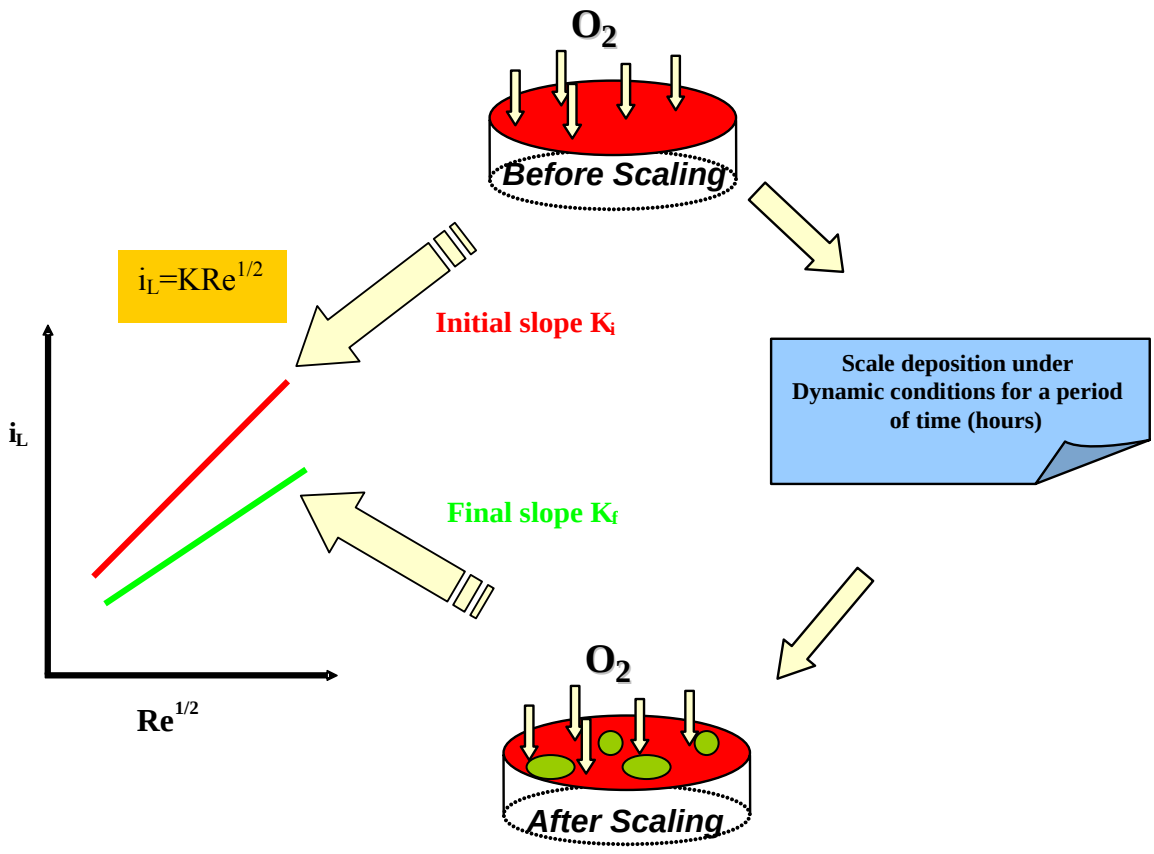

Figure 4-3 Schematic diagram representation of this technique as a means to determine the scale coverage on a specimen surface

4.5 Background Technique of Scaling Tendency

In this section, a brief explanation of the principle of this technique as a scaling potential sensor is presented. Scaling tendency is related to how easy a specimen surface is to be scaled when using an electrochemical driving force. The scaling tendency can be determined through an electrochemical measurement by utilising the slope value obtained from current versus time when a specimen is cathodically polarised under the laminar flow pattern that is delivered and controlled by the SIJ. The hypothesis is the current density will drop linearly against time and form a slope value (current vs. time). This slope value, is anticipated rise with increases of the brine saturation ratio.

Again, all parameters such as the concentration of oxygen, diffusion coefficient and viscosity of the electrolyte indicated in Equation 4-9 are assumed to be constant at ambient temperature and atmospheric pressure. The only parameter, which may vary, is the active surface area of the electrode exposing to the electrolyte. The oxygen-reduction reaction takes place when the specimen is cathodically polarised to -0.8 V. As a result of high pH generation at the electrode surface, this promotes calcium carbonate deposition. The surface of the electrode is blocked by calcium carbonate that causes the decrease of an active area for the oxygen reduction reaction. This technique is only suitable for calcium carbonate mineral scale. This is mainly because the deposition of calcium carbonate is influenced by the pH and this is described more details in Chapter 7.

Before scale deposits on the active surface area, it has a value A_1 and all of the surface areas are available for oxygen-reduction to occur. Once scale is deposited onto the active surface area of the electrode, as a result of polarisation, the initial value A_1 of a bare electrode changes to a lower value A_2 where the active surface area becomes less due to the scale formation on its surfaces. As a result of area changes from an initial value A_1 (bare specimen) to a final value A_2 (scaled specimen), the limiting current decreases with time. Hence, a limiting current versus time (i_L versus t) graph can be obtained. It is expected that when a specimen is polarised to -0.8 V, the calcium carbonate deposition on the sensor surface is accelerated. Therefore, the extent of scaling tendency of brine can be determined by the slope value of limiting current versus time plot (i_L versus t).

The summary of this technique to determine the scaling tendency is shown in Figure 4-4. The change of the slope value (K) and scaling times correspond to the brine saturation ratio. The slope value K increases as the saturation ratio of the brine increases. As shown in Figure 4-4, K_1 is less than K_2 which is corresponds to the brine 1 with a saturation ratio value less than brine 2. The slope is determined using a linear regression technique, by extracting a portion of the data of i_L versus time. The higher supersaturation of brine causes an increase in the slope and a decrease in the scaling time. The changes of the scaling slope give or indicate the scaling tendency or water chemistry of the brine solution in a system. The entire plot is performed in the stagnation regime, which is generating laminar flow.

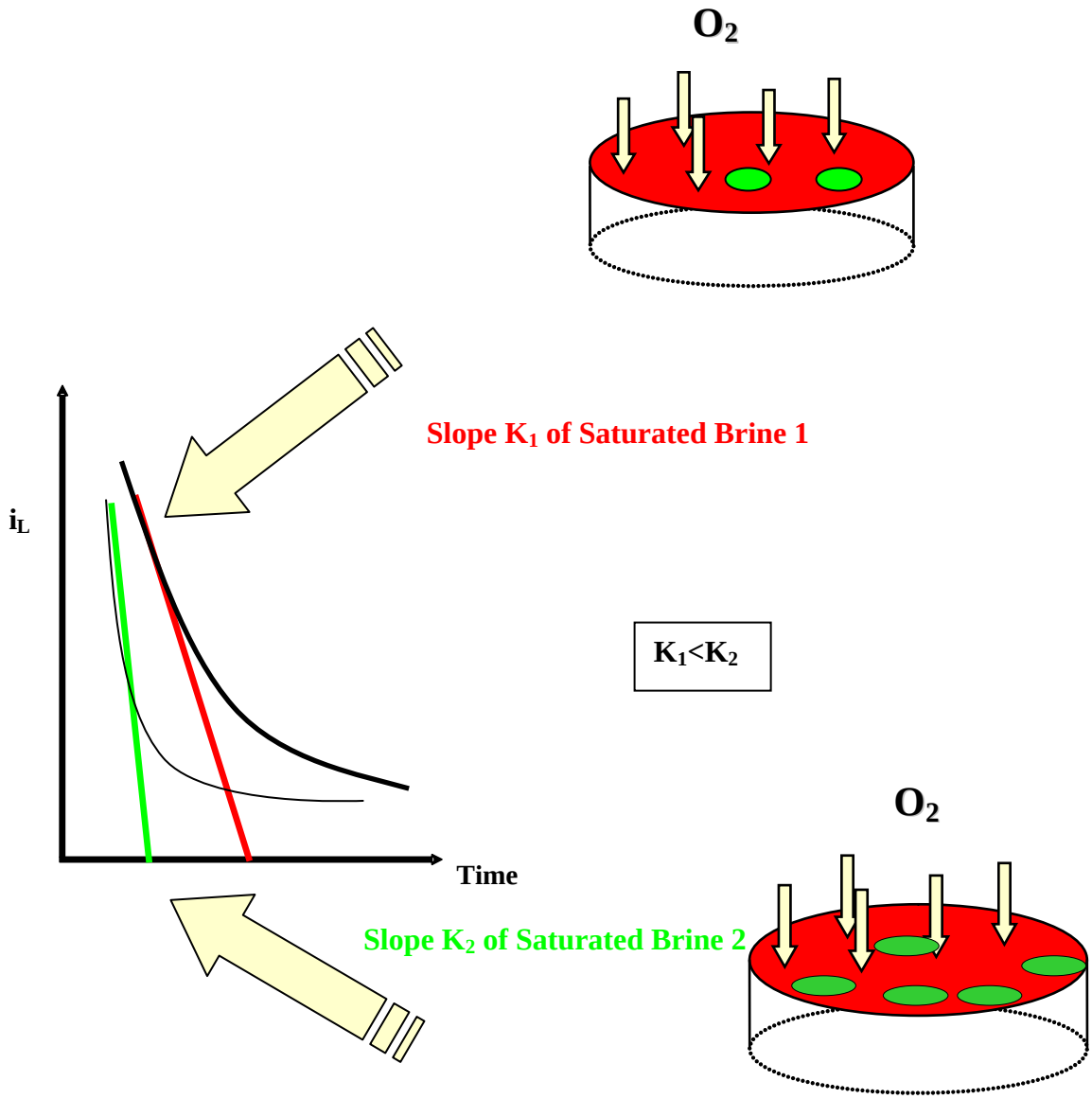

Figure 4-4 Schematic diagram representation of this technique as a means to determine the scaling tendency of brine solution consisting of a certain saturation ratio

4.6 Background of Scale Removal/Cleaning

The purpose of this section is to investigate the possible ways for mineral removal after mineral scale deposited on the component surface, using the non-destructive techniques. In order to perform the electrochemical measurement continuously without the replacement of new electrode surface cleaning is required. There are two types of cleaning processes a) electrochemical technique and b) acid cleaning. For the electrochemical technique, generated gas is used to remove any scale deposited on the specimen surface. Gas like hydrogen is generated at the specimen surface when the specimen is cathodically polarised to a specific potential. The contribution of a cathodic current due to the hydrogen-evolution is less significantly at free corrosion potential. It becomes more significant at a more negative potential (more negative than $E_{2H_2O+2e^- \rightarrow H_2+2OH^-}$).

For the possible cathodic reactions, the equilibrium electrode potential is worked out using Nernst Equation. Hydrogen evolution and the activity of hydrogen gas is unity. The potential calculated value is based on standard hydrogen electrode (SHE), (Ag/AgCl at E^0 = +0.2224 V vs. SHE)

$$E_{2H_2O+2e^- \rightarrow H_2+2OH^-} = E^0_{H_2O/H_2} + 2.3\frac{RT}{nF}\log\left[\frac{a_{H_2O}}{(a_{H^+})^2}\right] \qquad \text{Equation 4-12}$$

$$E_{2H_2O+2e^- \rightarrow H_2+2OH^-} = -0.826 + 2.3\frac{8.314*298}{2*96487}\log\left[\frac{1}{(10^{-4})^2}\right] \qquad \text{Equation 4-13}$$

$$= -0.590\,V\ (SHE)$$

The equilibrium potential for hydrogen-evolution in silver chloride scale is –0.590-0.2224=-0.8124 V Ag/AgCl. Therefore it is known that hydrogen-evolution occurs once the applied voltage reaches above –0.8V (Ag/AgCl) at pH 10. Scaled-specimen is cathodically polarised to a potential where hydrogen-evolution occurs as shown in Equation 4-14.

$$2H_2O + 2e^- \rightarrow H_2 + 2OH^- \qquad \text{Equation 4-14}$$

Acid cleaning is done by immersing the scaled specimen into a specific acid solution. This leads to the dissolution of calcium carbonate on the electrode surface according to Equation 4-15.

$$CaCO_3 + 2H^+ \rightarrow Ca^{2+} + CO_2 + H_2O \qquad \text{Equation 4-15}$$

Before scale forms on the active surface area, it has a value of A_1 and all of the surface areas are available for oxygen-reduction reaction to occur. As the scale deposits onto the active surface area of the electrode, the initial value A_1 of the bare electrode changes to a lower value A_2 where the active surface area becomes less, due to scale formation. Once the scale is removed, either by means of electrochemical or acid cleaning techniques, new active areas (A_3) will resume back to more or less same as the bare active surface area. The change of area initial value A_2 (scaled electrode) to A_3 (cleaned electrode) causes a higher slope value of i_L versus time. Therefore, the extent of scale removed can be calculated by plotting i_L versus time and by comparing the slope value of scale after scale deposition and the slope value after cleaning. Summary of this technique is shown in Figure 4-5.

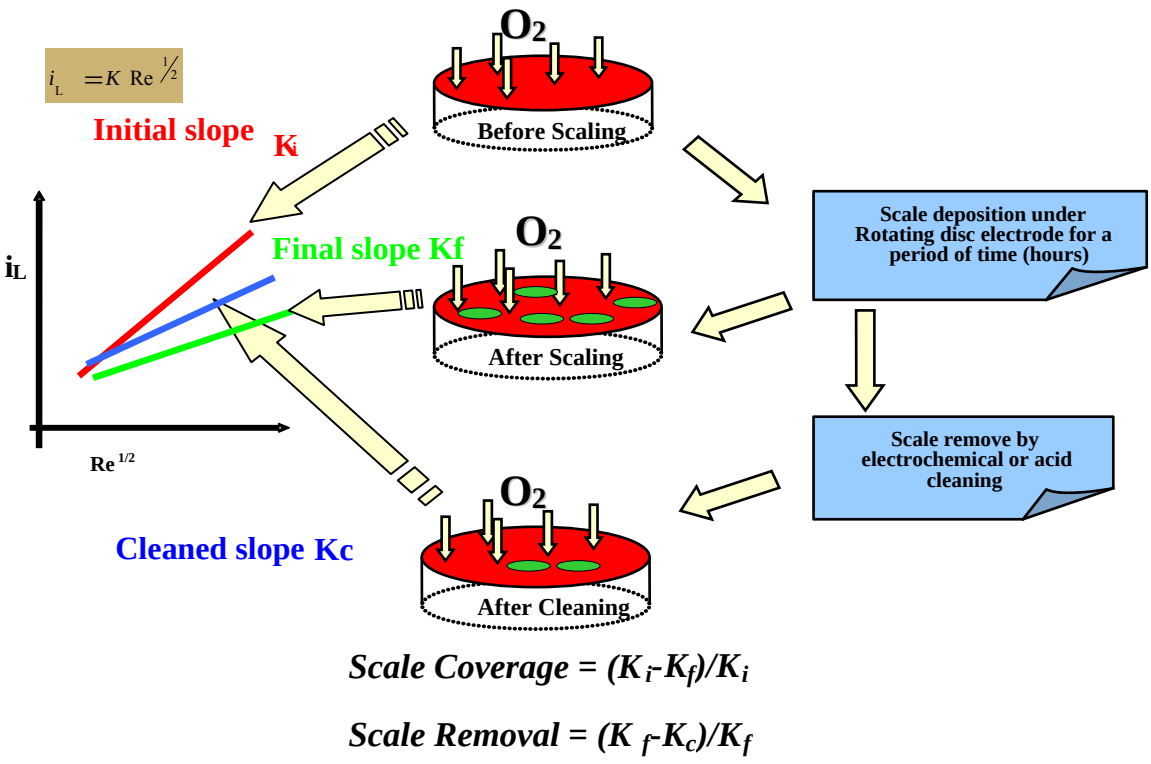

Figure 4-5 Schematic diagram represents summary of the steps involved in scale removal investigation

4.7 Design of the Submerged Impinging Jet (SIJ) and Equipment Set-up

The submerged impinging jet cell used in the present study is similar to the design by Chin and Tsang [112]. The SIJ cell is shown schematically in Figure 4-6. It consists of a cell rig, divided into a few parts, Perspex.

i.) Perspex top plate with a dimension of 20 x 20 x 12 cm and a mounted L shape top support plate with a dimension of 12 x 10 cm;
ii.) Perspex bottom plate with a dimension of 20 x 20 x 12 cm;
iii.) A bottom support plate having a diameter of 3.5 cm;
iv.) Perspex cell wall is a pipe of 14 cm inner diameter and 6.5 cm long;
v.) A nozzle tube glass with 0.8 cm outer diameter and 17.6 cm long.

The SIJ system also consists of some components that are attached to it. A long glass tube nozzle with an inner diameter 0.8 cm that is located at the central hole on the top plate. A cable gland connector being screwed onto the top plate and a nozzle supporter plate are used to hold the glass tube. A potentiometer mounted on the top support plate is used to measure the height of the nozzle. The principle and height measurement is covered more in section 5.5.1.2. Each individual part or component of the SIJ is illustrated in Figure 4-6. One of the cable glands screwed onto the top plate was used to hold the nozzle. Other the cable glands are used to accommodate a reference electrode, counter electrode and an additional glass tube. The purpose of an additional glass tube is to circulate any electrolyte exited from the cell rig. The remaining cable glad connector is used for other probe insertion such as a thermometer to measure the temperature of the electrolyte.

The SIJ flow loop is completed by the presence of a flow meter with a needle valve, a peristaltic pump and a solution tank, as shown in Figure 4-7. Electrolyte circulation between the cell rig and storage tank is controlled manually by adjusting the speed of gear or peristaltic pump or the needle valve. The flow rate reading is displayed as a percentage on the panel. A flow meter or a flow sensor is also installed to this flow loop for flow monitoring purpose. A personal computer is connected to the potentiostat to record the current or potential as a function of time via software known as Corrware. This depends on the experiment conducted, for the potentiostatic test, current as a function of time is recorded, whereas potential as a function of time for the potentiodynamic test.

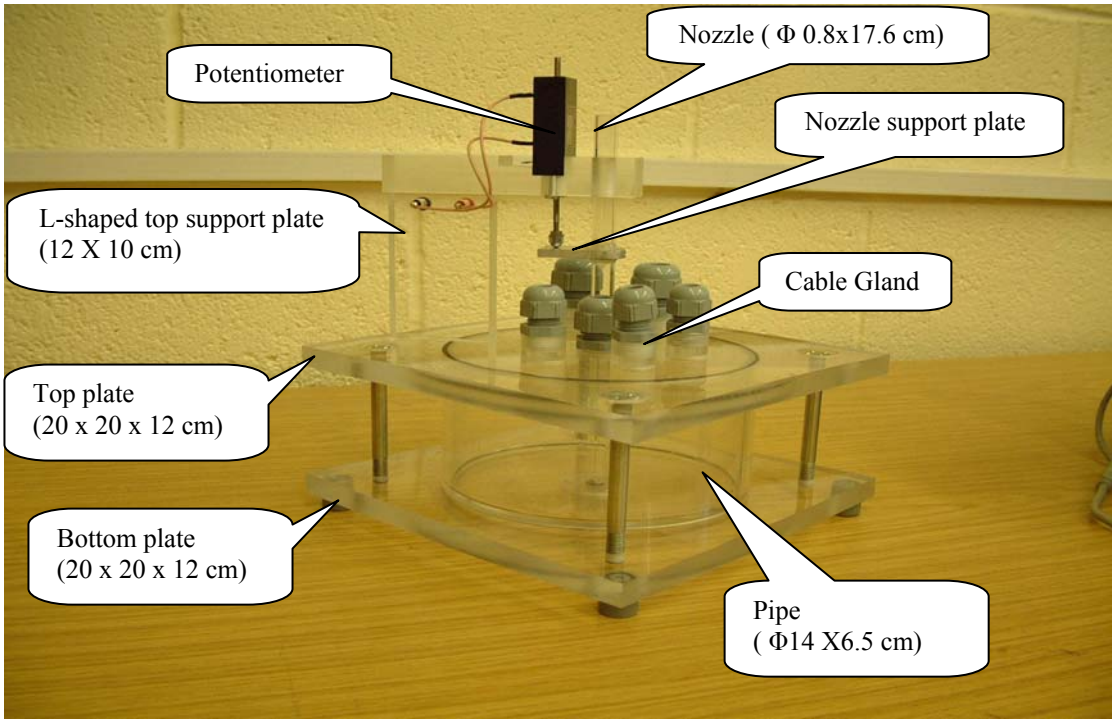

Figure 4-6 Prototype of the SIJ cell rig with some components attached onto the rig

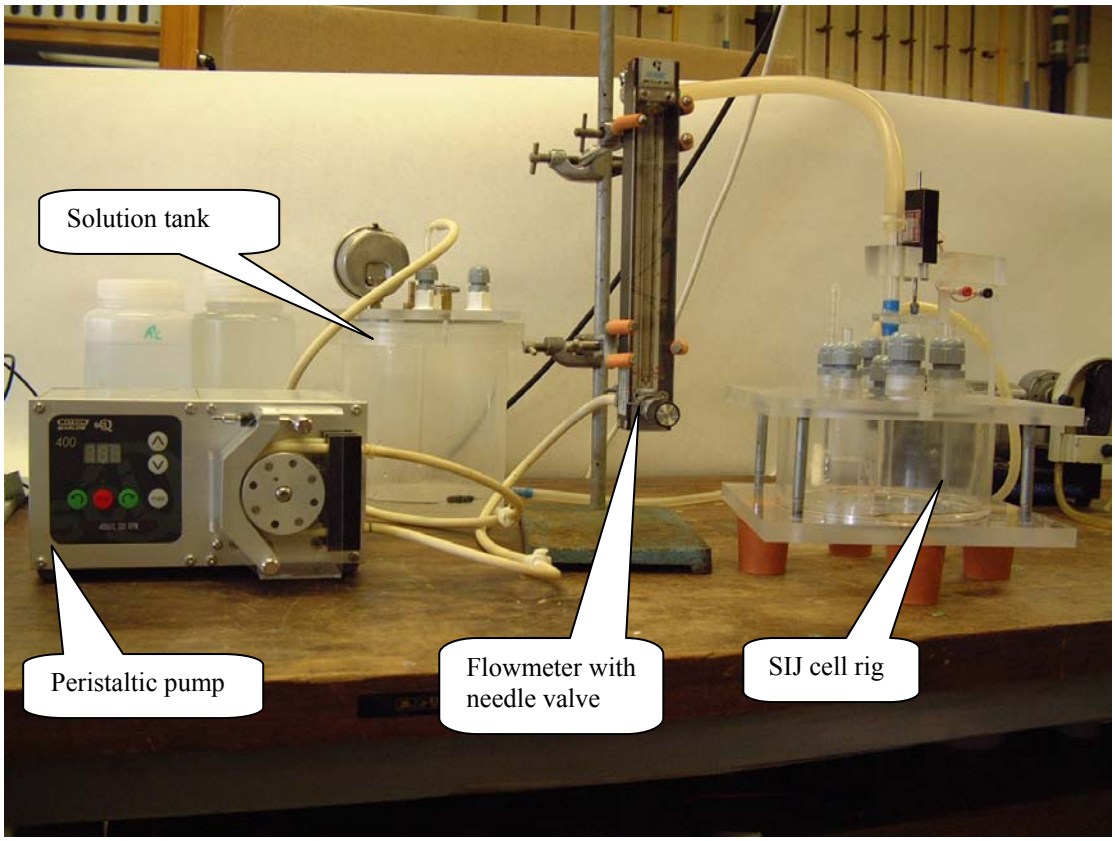

Figure 4-7 A complete set-up of SIJ flow loop system used to investigate scale detection and scaling tendency

Chapter 5 Experimental Procedures and Calibrations

5.1 Introduction

An electrochemical technique in conjunction with a submerged impinging jet (SIJ) setting was used to study mineral scaling. In this chapter, the experimental procedures and methods used to study mineral scaling are described. The experimental procedures are split into three main sections: 1) scale coverage 2) scaling tendency 3) cleaning (as shown in Figure 5-1). In the scale coverage section, steps or procedures used to assess or determine the amount of scale deposited on the specimen surface by the electrochemical technique are covered. In the scaling tendency section, steps required to determine when a system is likely to form mineral scale are described, and finally the experimental procedures involved in investigating the scale removal processes is presented.

A summary of the stages involved for scale coverage and scale cleaning section is shown in Figure 5-1. Generally, it can be subdivided into a few stages as follows:

i.) Sample preparation - to prepare the specimen/sensor;

Initial analysis - to obtain the electrochemical data of a bare specimen;

ii.) Scale deposition - to deposit mineral scale on specimen surface. This was carried out using RDE or magnetic stir. The purpose of this is to form an even distribution calcium carbonate crystals on specimen surface;

iii.) Final analysis - to obtain the electrochemical data of a scaled specimen;

iv.) Cleaning analysis-to obtained the electrochemical data of a specimen after subjected to cleaning (scale cleaning only);

v.) Post analysis - to determine the scale coverage/scale removed quantified by the electrochemical measurement. In addition, image analysis is used to quantify the amount of scale deposited on specimen surfaces.

For scaling tendency quantification, similar procedure involved for specimen preparation except scale deposition (scaling tendency measurement). The variation, detailing of each stage for each section of each stage is covered in the following section in this chapter.

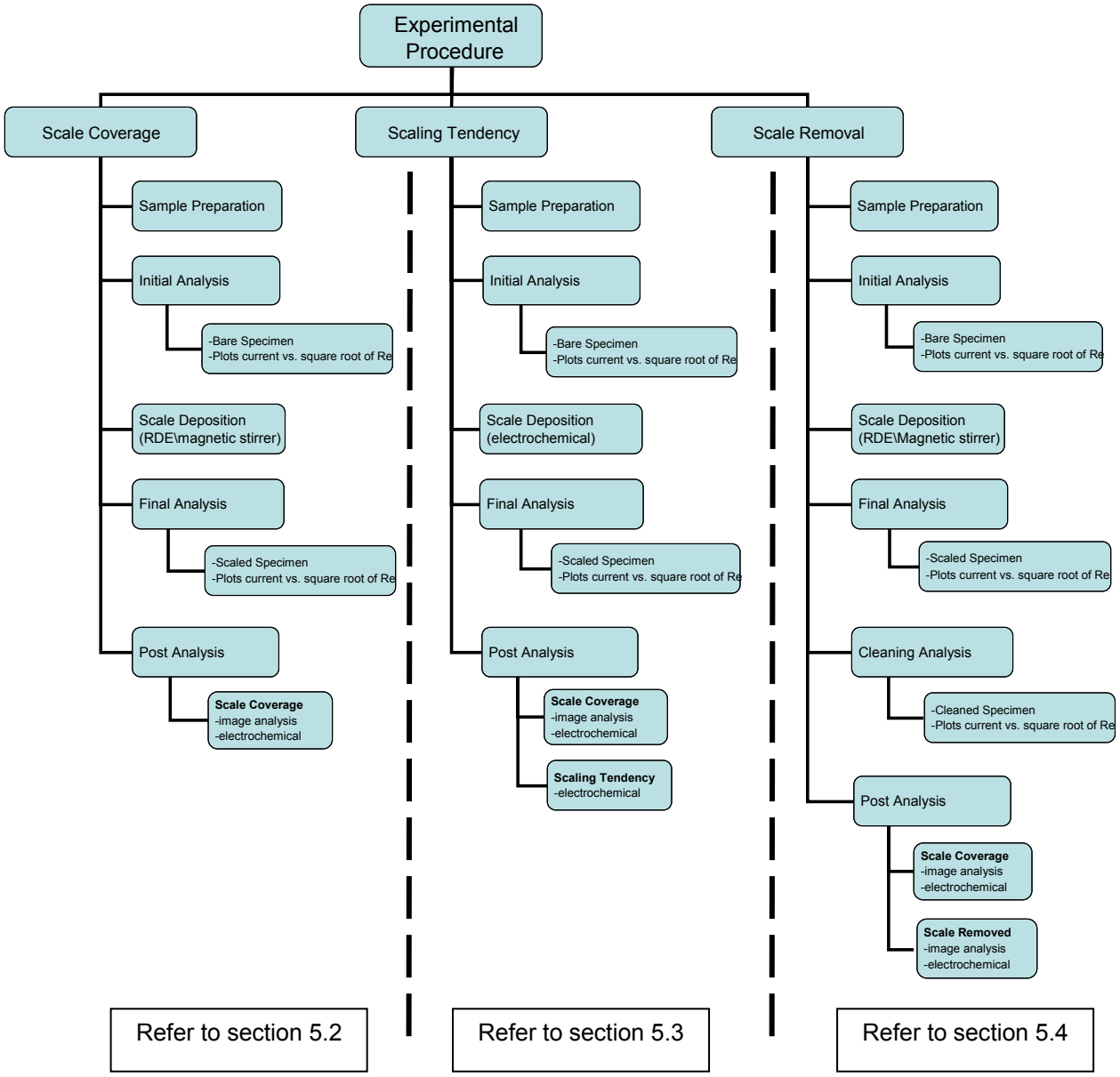

Figure 5-1 Represents the summary of the experimental procedures involved in the investigation of (a) scale detection on the component surface, (b) scaling tendency of a brine solution and (c) scale removal

5.2 Study and Investigation of Scale Coverage

Theory and background to the electrochemical technique, as a means of development of a scale detection sensor or monitoring technique can be found in Chapter 4. The study of scale coverage is divided into a few simple steps:

i.) Sample preparation;
ii.) Initial analysis;
iii.) Scale deposition;
iv.) Final analysis;
v.) Post analysis.

5.2.1 Sample Preparation and Mechanical Polishing

This is the first stage of the process to investigate scale coverage on metallic surfaces. The purpose of this step is to prepare a specimen that can then be used as a sensor to study scale coverage. Following is a brief description of the apparatus and materials required to prepare a specimen. The experimental procedures and methods used to prepare samples are also included. The specimen or sensor used was made of 316L stainless steel. This material is corrosion resistance alloys (CRA) and is selected to prevent any corrosion that will influence on electrochemical data. Other CRAs could be used as an electrode. Sometimes the sensor is referred to as a working electrode in a three-electrode cell system.

5.2.1.1 Experimental Procedure

All the stainless steel specimens were mechanically polished to obtain a good surface finish to provide reproducible results. Each specimen was mounted in resin (acrylic resin). The specimen was prepared from 316L stainless steel, 3 m long and 5 mm in diameter. First, the 316 stainless steel was cut into approximately 20 mm lengths from a 3 m steel rod. Then the specimen was knurled approximately into 5 mm lengths as shown in Figure 5-2 (a) to ensure that the steel could be held to the resin (acrylic resin) without falling off when the polishing process was carried out. Then the specimen (knurled-specimen with 20 mm long) was placed in a plastic mould and held by a holder to ensure it was mounted in the centre of the mount as shown in Figure 5-2 (b). This is to ensure the sensor surface was situated in line with the nozzle when it fitted in the submerged impinging jet rig.

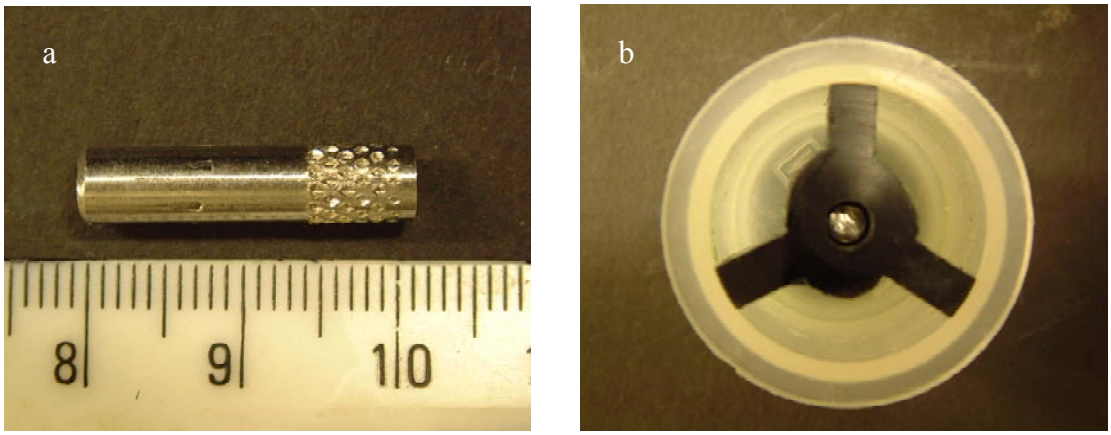

Figure 5-2 (a) Dimensions of a 316L stainless steel with knurl (knurled-specimen) before mounted with resin and (b) was held by a holder to ensure the pin was in centre of the plastic mould

The mould was then filled with epoxy resin that was prepared by mixing two substances (the hardening powder and hardening liquid) according to a ratio 2:1. Care was taken to avoid formation of bubbles when mixing both substances. Then the resin was poured into the plastic mould. The reason for using the resin is to ensure that only a diameter of 5 mm of the surface is electrochemically active as shown in Figure 5-3 (a). The resin was allowed to harden for a day. Once it was hardened, the specimen was machined to a diameter of 28 mm so it could be inserted into the submerged impinging jet (SIJ) rig. Figure 5-3 Pictures (a) plan view and (b) side view of 316 stainless steel embedded with resin and machined to the required diameter. Mechanical polishing was then carried out where the specimen was polished with SiC grade 600 and 1200 paper followed by diamond paste 6 μm to remove any resin that covering the specimen surfaces. The use of diamond paste also provides a flat surface finish. After polishing, the specimen was rinsed once more with distilled water followed by acetone. Finally, it was once more rinsed with distilled water and dried with a dryer. The mechanical polished specimen was stored in a desiccator to prevent or reduce surface oxidation by the atmosphere before proceeding to the next step (initial analysis).

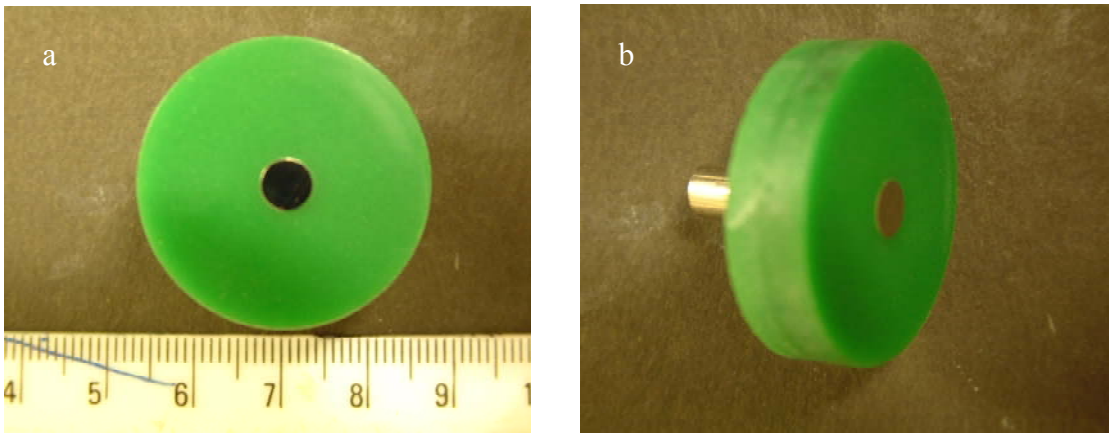

Figure 5-3 Pictures (a) plan view and (b) side view of 316 stainless steel embedded with resin and machined to the required diameter

5.2.2 Initial Analysis

The purpose of the initial analysis is to obtain electrochemical data and assess the surface condition of a sensor when it is clean, without any scale deposition. With the known surface condition, it acts as a reference or base line, which can be used to compare the surface coverage once mineral scale is deposited onto the specimen surface.

5.2.2.1 Experimental Procedures

The mechanical polished specimen obtained from the sample preparation stage was fitted onto the bottom plate of SIJ cell rig where the sensor surface was at the same level as the bottom plate surface. The nozzle, a long glass tube with an inner diameter of 0.8 cm, was inserted perpendicular through a centre hole on the top plate. The height of the nozzle-to-plate, H, was obtained through adjusting the nozzle, which was mounted on a nozzle support plate, by moving the tube up and down. It was held in place by a cable gland as shown in Figure 5-4. A digital depth gauge was mounted on the L-shaped top support plate, which was then used to measure the height. To provide a clear idea a picture of part of the SIJ cell rig is shown in Figure 5-4. More detail of the SIJ configuration and dimension are covered in Chapter 4, section 4.7.

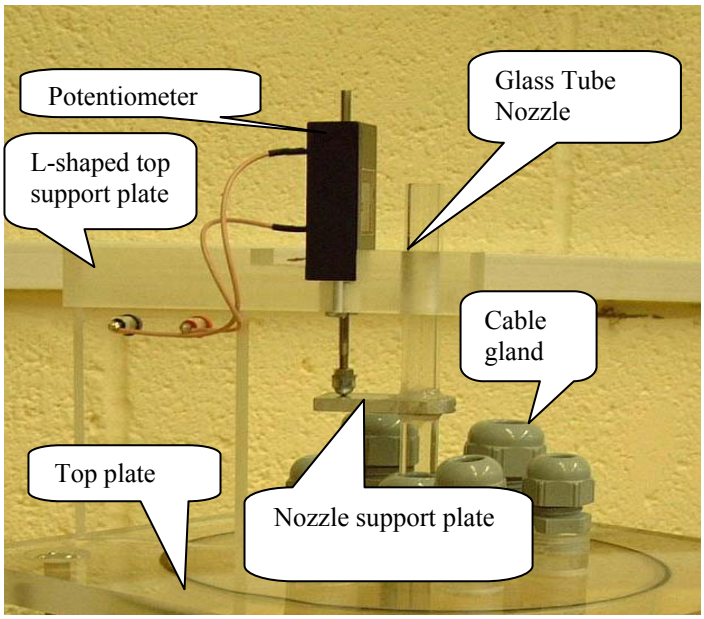

Figure 5-4 Represents the parts found in a SIJ cell rig

A freshly prepared sodium chloride solution with a concentration of 5 g/L known as the analysis solution was used for the electrochemical analysis. The pH of the solution was maintained at 10 throughout the experiment by addition of 0.1 M NaOH. All measurements were performed at ambient temperature and atmospheric pressure. Analysis solution was circulated between the cell rig and solution tank. The purpose of having the solution tank is to store the analysis solution. The electrolyte flow rate was controlled by a peristaltic pump and a needle valve. A flow meter or flow sensor was used to monitor the electrolyte flow rate.

Electrochemical measurement was carried out to record the limiting current, i_L responses flow rate (expressed in terms of Re, Reynolds number) of a bare specimen by

a potentiostat machine and PC. A three-electrode cell system that consists of a reference electrode (Ag/AgCl), a counter electrode (platinum wire) and a working electrode (316L stainless steel) was used for the electrochemical analysis in conjunction with the submerged impinging jet (SIJ). The electrodes were connected to a EG&G potentiostat machine and a potentiostatic test was performed where a constant potential was applied to the working electrode. The current versus the time was recorded and monitored through a PC. By end of the initial analysis, the i_L versus $Re^{1/2}$ of a bare specimen can be obtained and then be used at a later stage, post analysis, for data processing.

It is well established that the controlling factor of oxygen reduction in aerated solutions is mass-transfer and this can be indicated a diffusion plateau on the cathodic polarisation curve. In this region, the oxygen reduction current is limited by the rate of oxygen supply to the active surface. Therefore, it becomes under diffusion control, a limiting current, i_L is established as a result of this. The limiting current varies as the flow rate changes. A plot of i_L versus $Re^{1/2}$ was determined for a bare specimen. More detail regarding cathodic polarisation and diffusional control is explained in Chapter 4, section 4.2. The mechanically polished specimen was cathodically polarised into the diffusion plateau region, at a potential of –0.8 V (Ag/AgCl). A model EG&G potentiostat power supply was used to apply a constant voltage. This was a preliminary test of a deposition-free/ bare specimen (with no scale formation on the metallic surface) and was carried out in the analysis solution to determine the oxygen reduction kinetic reaction as a function of flow rate. After polarisation, the specimen was rinsed with distilled water then it was dried with a dryer. The specimen was then stored in desiccator to prevent surface oxidation from the atmosphere before it deposited with mineral scale at the next stage (scale deposition).

5.2.3 Scale Deposition (Normal Deposition)

The purpose of this stage is to deposit mineral scale, such as calcium carbonate onto the specimen surface. Precipitation and deposition of scale onto electrode surfaces were performed over varying times in the scaling solution. The scaling solution consists of scaling substance that precipitates calcium carbonate such as calcium ions and carbonate ions. This solution was used to deposit mineral scale on the specimen surface. It should be emphasised that the specimen scaling was carried out at flow dynamic

conditions e.g. continuously stirred using the RDE technique, at a rotating speed of 600 rpm at ambient conditions.

5.2.3.1 Experimental Procedures

The scaling solution was prepared from distilled water by adding analytical grade of chemicals from BDH Chemical. The composition and concentration of each substance to form a scale solution is presented in Table 5-1. This solution is graded as severe scaling solution as a result of high saturation ratio (SR) of 17.5. The SR is estimated by software that is written in Excel provided by Baker Petrolite.

The specimen from the initial analysis was immersed into a 500 ml beaker where precipitation and deposition of calcium carbonate takes place. Specimens were immersed at approximately 8 mm deep from the solution level at ambient temperature and atmospheric pressure. The surface scaling took place in a flow dynamic condition, generated by the RDE technique at 600 rpm. Initially, the pH of each brine solution was buffered to 6.7 by adding acetic acid or sodium hydroxide or both. The concentration of acetic acid and sodium hydroxide is 0.1 M respectively. The specimen was removed from the scaling solution after certain periods of deposition. Then it was cleaned with distilled water to remove any residual scaling solution and non-adherent crystals. After scale was deposited on the specimen, the specimen is known as scaled specimen. The scaled specimen was dried with a dryer and kept in a desiccator.

Ions	Brine 1 (mg/L)
Na^{+}	6873
Mg^{+}	0
Ca^{2+}	1440
K^{+}	0
Ba^{2+}	0
Sr^{2+}	0
Fe^{2+}/ Fe^{3+}	0
Cl^{-}	12136
SO_4^{2-}	0
HCO^{-3}	2193

Table 5-1 Brine composition of a scaling solution for calcium carbonate deposition

5.2.4 Final Analysis

The purpose of the final analysis is to record the limiting current, i_L responds to the flow rate (in term of Reynolds number, Re) of a scaled specimen when the electrochemical measurement is performed using a potentiostat machine and PC. The ultimate purpose of the final analysis is to obtain i_L versus $Re^{1/2}$ of a scaled specimen. Then the plot of i_L versus $Re^{1/2}$ of the scaled specimen is used in the later stage for the post analysis. This information can be used to compare information from the bare specimen analysis in the initial analysis.

5.2.4.1 Experimental Procedures

Mineral scale was deposited on the bare specimen in the scaling solution over a period of time. A scaled specimen was formed, which was placed into the analysis solution and electrochemical analysis was then carried out in accordance to the operational method as in the initial analysis. A three-electrode cell system (consisting of a reference electrode (Ag/AgCl), as well as platinum as a counter electrode and a scaled specimen as a working electrode) was connected to the potentiostat machine. A potentiostatic test was performed by applying a constant potential –0.8 V (Ag/AgCl) to the working electrode and the flow rate was varied from 98.74~336.6 cm^3/min (30-95 % rotating speed of the peristaltic pump). A potentiostatic experiment was performed in conjunction with SIJ to access the amount of scale deposited on the sensor. Current, i_L versus $Re^{1/2}$ of the scaled specimen was recorded and monitored through a PC. Then the specimen was cleaned with distilled water and dried with a dryer before storage in a desiccator.

5.2.5 Post Analysis of Scale Coverage

The purpose of post analysis for scale coverage is to determine the extent of calcium carbonate deposited on the sensor surface. The scale coverage was determined by two methods 1) electrochemical and 2) image analysis.

5.2.5.1 Electrochemical Technique

This section describes the steps or methods used to quantify scale coverage determined by the electrochemical technique. The electrochemical technique assessment is based on analysing the electrochemical data recorded of the initial and final analysis in order to access the extent amount of scale deposited on the sensor. The data recorded at those

stages were then processed or presented as a graph, i_L versus $Re^{1/2}$. Slope values were obtained from the i_L versus $Re^{1/2}$ plots. The slope value of i_L versus $Re^{1/2}$ obtained from the initial and final analyses are defined as initial-plot and final-plot respectively. With these slope values, scale coverage determined by the electrochemical technique could be defined. The coverage was determined or quantified by comparing the initial–plot (as reference) to the final-plot (scaled specimen). For the post analysis stage, a schematic diagram to illustrate steps comparing the initial-plot and final-plot is shown in Figure 5-5. Further background and theory to determine the scale coverage can be found in Chapter 4.

5.2.5.2 Image Analysis

The purpose of the image analysis is to quantify the amount deposited on the specimen's surface. It is also provided as an alternative technique to verify the accuracy of scale coverage determined by the electrochemical technique. In this section, scale coverage of a specimen surface was determined by analysing the mineral scale deposited on the specimen surface using an image analysis technique. Each scaled specimen from the final analysis was photographed under the light microscope or SEM (Scanning Electron Microscope). Image analysis software was then used to determine the percentage of calcium carbonate covered on the scaled specimen surface. Images were taken by the light microscope or alternatively SEM could be used as additional information to analyse the morphology and characteristic of the mineral scale formed.

The procedures involved in investigation and determination of scale coverage is illustrated in a schematic diagram as shown in Figure 5-5. The process started at sample preparation and was continued until a mechanical polished specimen was in place. Then an initial analysis was carried out to obtain the initial-plot of a bare specimen. After the initial analysis, the next stage is the scale deposition where calcium carbonate was deposited onto a specimen's surface to form a scaled specimen. Then a final analysis was performed to obtain the final-plot of a scaled specimen. The final stage is the post analysis, where the extent of scale deposition is determined by the electrochemical and image analysis. Experimental conditions of each stage are written in the text box on the left side of the diagram. The right side of the diagram represents a brief explanation of each investigation stage.

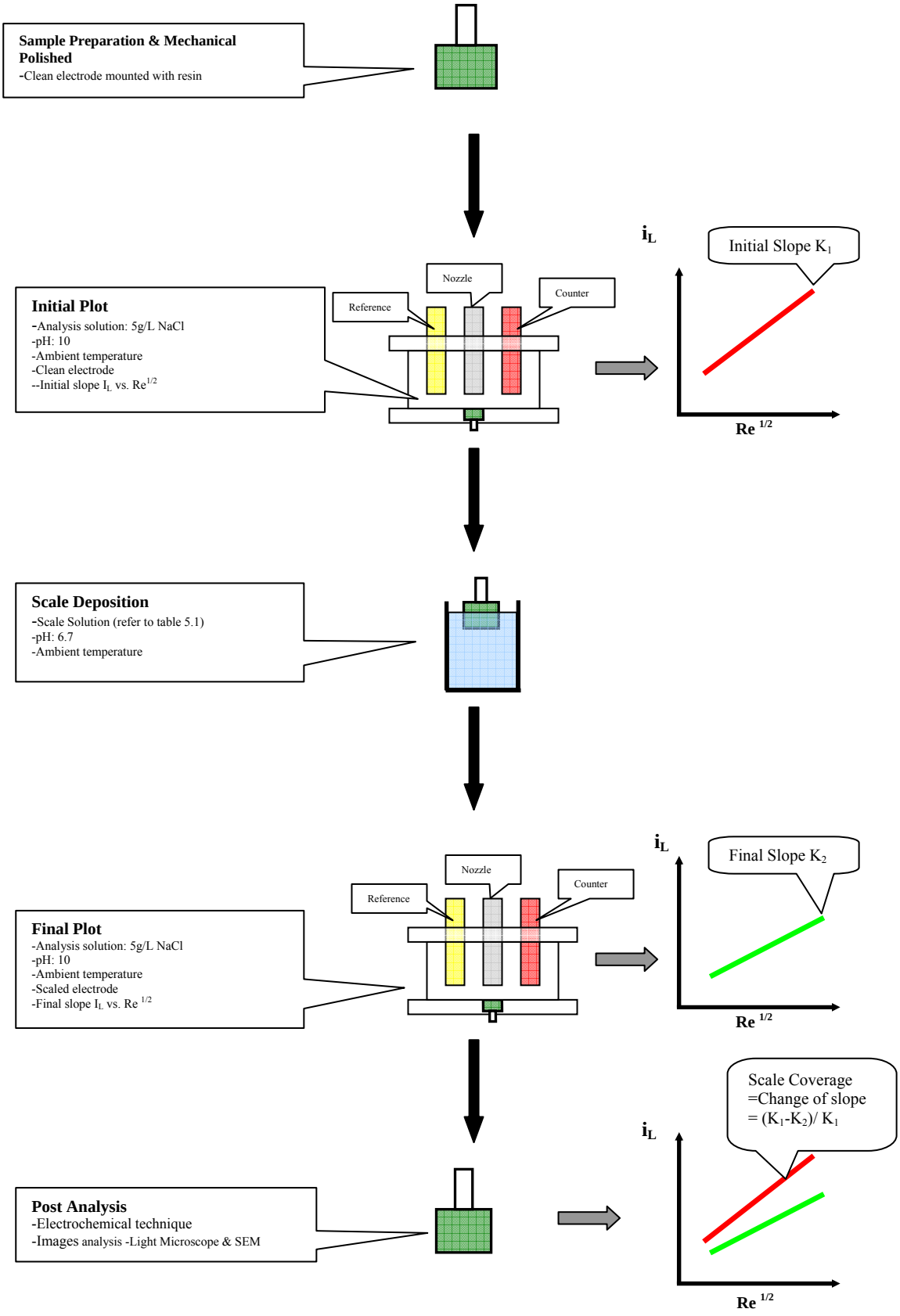

Figure 5-5 Schematic diagram and information of the stages involves in the study of scale detection

5.3 Study and Investigation of Scaling Tendency

Although scale detection enables the extent of scale onto metallic surfaces to be determined, it does not provide any information on when scaling is likely to occur. Therefore, the study and investigation of scaling tendency of a process system such as water or brine solution is important. This technique utilised high pH condition generated at electrode/electrolyte interface when the electrode is cathodically polarised to a negative potential where oxygen reduction takes place. The generation of hydroxide ions at electrode/electrolyte causes a local pH increment and favours the promotion of HCO_3 into CO_3^{2-} ions, which then reacts with Ca^{2+} ions to precipitate $CaCO_3$ as shown in the following steps:

$$O_2 + 2H_2O + 4e^- \rightarrow 4OH^-$$
$$HCO_3 + OH^- \rightarrow CO_3^{2-} + H_2O$$
$$Ca^{2+} + CO_3^{2-} \rightarrow CaCO_3$$

Hence, the current technique used to investigate the scaling tendency is only suitable for any inorganic scales that are strongly influenced by the pH especially calcium carbonate scale. Information regarding the water chemistry such as the scaling tendency of a system can be monitored through the scaling tendency.

Experimental procedures to monitor the scaling potential or tendency of water with a series of supersaturation are described in this section. The investigation of scaling tendency can be divided into 3 stages:

i.) Sample preparation (refers to section 5.2.1);
ii.) Scale deposition;
iii.) Post analysis to quantify scale formed on component surface under electrodeposition.

5.3.1 Scale Deposition (Electrochemical Deposition)

The purpose of this stage is to deposit mineral scale, such as calcium carbonate, onto the specimen surface. Calcium carbonate was deposited onto the electrode surface by an electrochemical technique. When the specimen was cathodically polarised using a potentiostat machine in a scaling solution, mineral scale was deposited, and known as electrochemical deposition. Electrochemical data such as current responses with times of certain flow rates and saturation ratios was recorded. This data was then used in the post analysis to obtain a scaling tendency slope. The theory and background of these

are referenced in Chapter 4. Different flow rates and saturation ratios of scaling solution were used to deposit calcium carbonate over a period.

5.3.1.1 Experimental Procedures

After performing the initial analysis, the bare specimen was fitted onto the bottom plate of the SIJ rig where its surface was at the same level as the bottom plate surface. The height of the nozzle-to-plate, H, was obtained by adjusting the nozzle tube up and down so H/d=1 could be obtained. A digital depth gauge was mounted on the top plate to measure this parameter.

A volume of 500 ml scale solution with a certain saturation ratio value was freshly prepared. These values were calculated using software provided by Baker Petrolite. The composition of each scale solution is shown in Table 5-2. The pH of the solution was maintained at 6.7. This was carried out by buffering each brine solution before mixing it together to form a scaling solution. Acetic acid or sodium hydroxide of 0.1 M was used to control or buffer the scaling solution. For each new experiment, a new bare specimen and scaling solution were prepared. Four different saturation ratios were used, 0.27, 1.09, 8.91 and 17.8, and all measurements were performed at atmospheric pressure and ambient temperature.

Electrochemical analysis was carried out using an EG&G potentiostat machine. The three-electrode cell system consists of a reference electrode (Ag/AgCl), a counter electrode (platinum wire) and working electrode (316L stainless steel) which were connected to the potentiostat machine. A potentiostatic test was performed by applying a constant potential to the working electrode. Current versus time was recorded and monitored through a PC. The specimen was cathodically polarised into the diffusion plateau region, at a potential of –0.8 V (Ag/AgCl) using EG&G machine under a potentiostatic test. The electrochemical data limiting current versus time of certain flow rate and saturation ratio was recorded. The data was then used at a later stage (post analysis) to obtain scaling tendency information. Four flow rates in the laminar flow condition were chosen, 40, 80 120 and 160 ml/min. Scaling solution was circulated between the cell rig and a storage tank. The circulation was controlled by a peristaltic pump and needle valve. The flow rate of the system was monitored by a flow meter.

After the specimen was deposited with calcium carbonate scale, it was cleaned with distilled water to remove any residual scaling solution and lose mineral scale on the specimen surface. Then scaled specimen was dried with a dryer and kept in a desiccator prior to proceeding to post analysis.

Ion	Brine 1 (mg/L)	Brine 2 (mg/L)	Brine 3 (mg/L)	Brine 4 (mg/L)
Na^+	6873	7285	7085	7085
Mg^+	91	91	91	91
Ca^{2+}	1440	1202	350	175
K^+	0	0	0	0
Ba^{2+}	0	0	0	0
Sr^{2+}	0	0	0	0
Fe^{2+}/ Fe^{3+}	0	0	0	0
Cl^-	12136	12567	12136	12136
SO_4^{2-}	0	0	0	0
HCO^{-3}	2193	1289	533.75	266
Saturation ratio (SR)	17.8	8.91	1.09	0.27

Table 5-2 Brine compositions of a scaling solution of different saturation ratio

5.3.2 Post Analysis of Scaling Tendency

In this section, the two main purposes of post analysis are to determine the extent of scale deposited by the electrochemical technique and to obtain scaling tendency. The amount of scale covered on the specimen surface when scale is deposited by the electrochemical technique can be quantified by two methods, 1) electrochemical technique and 2) image analysis. Further details of these two methods can be found by reference to section 5.2.5 Post Analysis of Scale Coverage.

The slope of scaling tendency was obtained through an analysis of the electrochemical data recorded during sample polarisation. A portion of the electrochemical data, i_L versus time or $Re^{1/2}$ was extracted and processed to obtain a scaling tendency slope. Information about the scaling tendency of brine can be determined through this method. Further details of the background and theory to determine the scale tendency is covered in Chapter 4. Figure 5-6 represents the stages used to investigate and determine the scaling tendency of a brine solution. Starting with the first stage for sample preparation, the specimen was mechanically polished to produce a bare specimen. The next step is

the scale deposition stage where calcium carbonate was deposited on the specimen surface to form a scaled specimen. An electrochemical deposition process was used for deposition at this stage. The last stage is post analysis where the extent of scale deposition was determined by electrochemical and image analysis. Scaling tendency was also determined at this stage. Experimental conditions for each stage are written in the text box on the left side of the diagram. The right hand side of the diagram represents the information, which can be obtained from each stage involved in the scaling tendency investigation.

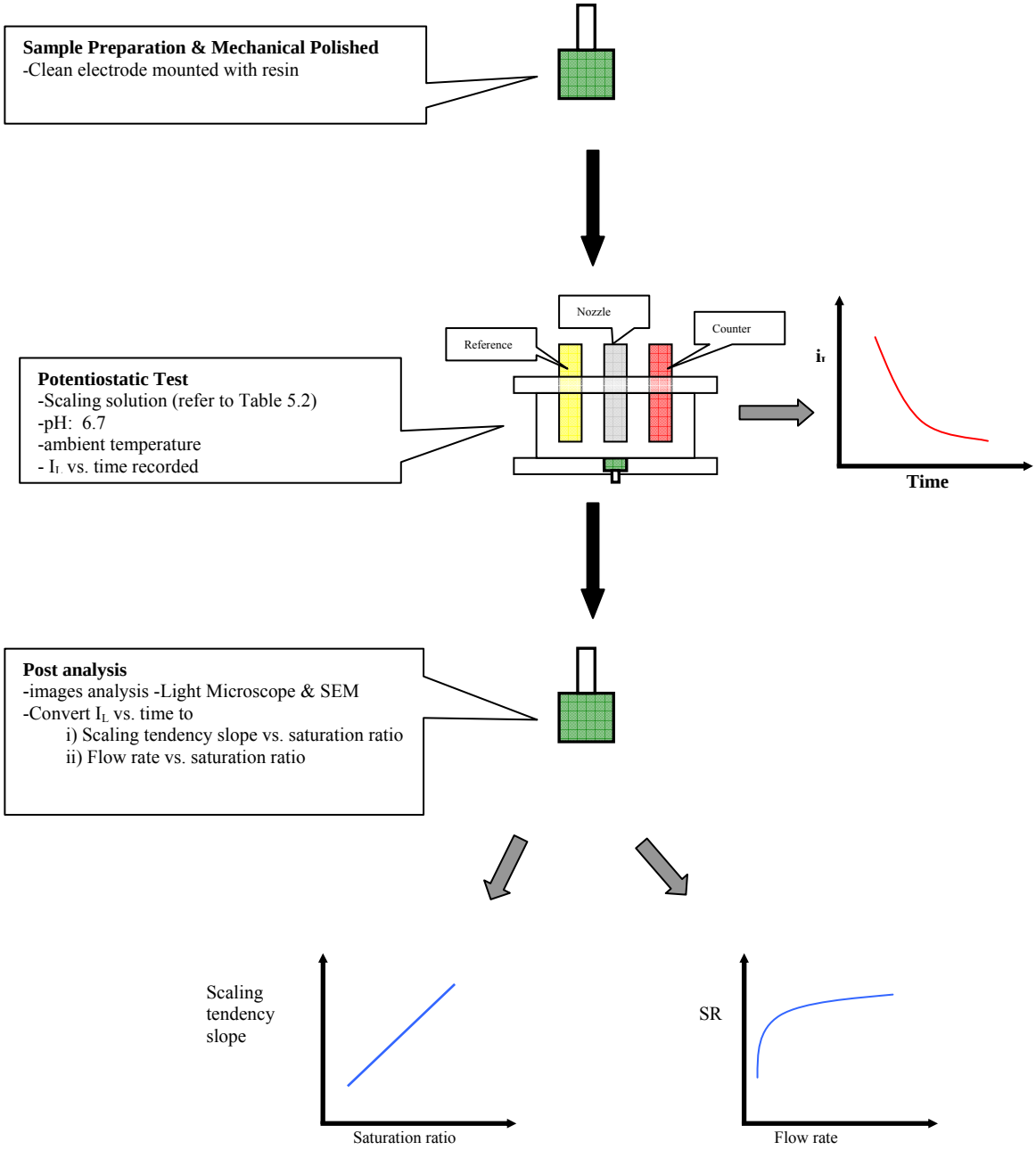

Figure 5-6 Schematic diagram represents the procedure and information which can be obtained from each stage of the scaling tendency study

5.4 Study and Investigation of Scale Removal/Cleaning

Although scale detection enables the extent of scale on metallic surfaces to be determined, once the active surface of the electrode is completely blocked off by the scale it will not provide any information. Therefore, the purpose of this study is to examine the feasibility of the cleaning process by removal of any mineral scale deposited on sensor surfaces. Experimental procedures and conditions to remove mineral scale or cleaning of the surface specimen are also included. The study and investigation of scale removal or cleaning are basically divided into 5 simple steps

i.) Sample preparation (refers to section 5.2.1);
ii.) Initial analysis (refers to section 5.2.2);
iii.) Scale deposition;
iv.) Final analysis (refers to section 5.2.4);
v.) Cleaning analysis;
vi.) Post analysis.

5.4.1 Initial Analysis

Initial analysis is a preliminary test on precipitate-free/bare-specimens (without scale on metallic surfaces). The purpose of initial analysis is to obtain an initial-plot (slope value) of i_L versus $Re^{1/2}$ of a bare-specimen. By the end of the initial analysis, this data can then be used in the later stage for post analysis. For further information and experimental procedures, refer to sections 5.2.2 and 5.2.2.1.

5.4.2 Scale Deposition (Not Electrochemical Deposition)

Mineral scale was deposited onto electrode surfaces by immersion into a scaling solution using a range of immersion times. The experimental procedure is the same as specified in section 5.2.3.1, the only difference is that the mineral scale was deposited using a rotating disc electrode technique (RDE) for 3 hours under a rotating speed of 600 rpm at ambient temperature in a scaling solution with a supersaturation ratio of 17.5.

5.4.3 Final Analysis

The purpose of the analysis is to record and obtain the electrochemical data in the forms of limiting current i_L versus $Re^{1/2}$. This experiment was carried out using scaled specimens (with scale on specimen surfaces) in the same analysis solution as in the

initial analysis. The outcome of this analysis is the recorded electrochemical data of i_L versus $Re^{1/2}$ of the scaled specimen. This data is then used in later stage (post analysis). For further information and experimental procedures can found in sections 5.2.4 and 5.2.4.1

5.4.4 Cleaning Analysis

The purpose of this experiment is to obtain a cleaned specimen after cleaning/removing scale from a scaled specimen. The ultimate goal is to obtain a plot of i_L versus $Re^{1/2}$ that can then be used in post analysis.

5.4.4.1 Experimental Procedures

This is a general experimental procedure for cleaning the electrode. Further details of experiment can be found in section 5.4. Two types of cleaning or scale removal were studied

i.) Electrochemical technique;

ii.) Acid cleaning-hydrochloric acid (HCl) and acetic acid (CH_3COOH).

In an electrochemical technique, the scaled specimen was polarised to a potential where hydrogen evolution occurs at surface of electrode for a known period. It is based on the assumption that the generation of hydrogen will blow off the scale on electrode surfaces. For the acid cleaning test, the scaled specimen was immersed in a beaker containing a specific acid with a known concentration for a certain period to remove calcium carbonate scale on electrode surfaces. As mentioned previously, once the cleaning process is completed, the specimen is known as the cleaned specimen.

After cleaning process, an electrochemical measurement was carried out to access the amount of scale remained on sensor surfaces. Potentiostatic experiments in conjunction with SIJ were performed for a clean-specimen. The cleaned specimen was fitted onto the bottom plate, where the specimen's surface was at the same level as the bottom plate of the SIJ cell rig. The analysis solution (the same solution from the initial analysis) was used to perform the electrochemical measurement. Sodium chloride having a concentration of 5 g/L is known as analysis solution was used as an electrolyte. The pH of the solution was maintained at 10 throughout the experiment by addition of 0.1 M NaOH. All measurements were carried out at ambient temperature and at atmospheric

pressure. The current was measured as a function of flow rate or Reynolds number. Analysis solution was circulated between the cell rig and storage tank. It was controlled by a peristaltic pump or a needle valve. The flow rate of the system was monitored by a flow meter.

The specimen was polarised cathodically into the diffusion plateau region, at a potential of –0.8 V (Ag/AgCl) using EG&G machine. This was a test on a cleaned specimen and was carried out in the analysis solution to determine the oxygen reduction reaction kinetic as a function of flow rate. As a result of the polarisation, a limiting current, i_L was established for various flow rates. Hence, a plot of i_L versus $Re^{1/2}$ could be determined for a cleaned specimen. After this, the specimen was rinsed with distilled water and dried with a dryer. The specimens were then stored in desiccators before proceeding to the final stage.

5.4.5 Post Analysis

The purpose of post analysis is to determine the extent of calcium carbonate scale deposition on sensor surface before cleaning and after cleaning. Coverage before and after cleaning can be quantified in two ways 1) electrochemical measurement and 2) image analysis.

The post analysis of electrochemical analysis is determined by comparing the slope value of the slope value of scale deposited (after deposition process) and the slope value of the scale removed (after cleaning process). For image analysis, scale deposition and scale removal were determined using the image analysis technique. Images were taken by SEM or light microscope is quantified using image analysis software. This technique not only gives an estimation of scale coverage but also information such as morphology and characteristic of the scale formed onto the electrode surfaces.

5.4.5.1 Electrochemical Technique

Electrochemical data recorded during the initial, final and cleaning-analyses were presented as i_L versus $Re^{1/2}$ graph, which were then process to obtain slope values. The slope value of i_L versus $Re^{1/2}$ for initial analysis and final analysis are known as initial-plot and final-plot respectively. The slope value of i_L versus $Re^{1/2}$ of clean analysis is known as cleaned-plot.

Scale coverage before cleaning was determined using the electrochemical technique by comparing the initial-plot and final-plot. By comparing the initial-plot and cleaned-plot, the scale coverage after cleaning could be defined (extent of scale on sensor surfaces after cleaning was carried out). The amount of scale removed was obtained as scale coverage before cleaning deducts scale coverage after cleaning. Scale removed is defined as

Scale Removed=Scale coverage before cleaning – Scale coverage after cleaning

5.4.5.2 Image Analysis

Scale covered on specimen surface is determined by analysing the mineral scale deposited on the specimen surfaces through image analysis. Each scaled specimen from the final analysis and cleaned specimen from the cleaned analysis were photographed with light microscope and SEM (Scanning Electron Microscope). Image analysis software was used to determine the percentage of calcium carbonate cover on the scaled specimen surfaces as well as the cleaned specimen. In addition, light microscope or SEM images were used to analyse the morphology and characteristic type of calcium carbonate formed.

Figure 5-7 indicates the procedures or steps involve in scale removal study. The first stage of the process is sample preparation. The specimen was mechanically polished to a good surface finish to obtain reproducible results. Then an initial analysis was carried out to obtain an initial-plot of the bare-specimen. After initial analysis, the next stage is scale deposition stage where calcium carbonate was deposited on specimen surfaces to produce a scaled specimen. Mineral scale was deposited using the RDE technique. Final analysis was conducted after scale deposition, in this stage, the final-plot of scaled specimen was obtained. After this, a cleaned analysis was carried out to obtain a cleaned-plot of cleaned specimen. The last stage was post analysis where the extent of scale deposition and scale removal as determined by the electrochemical and image analysis techniques. Experimental condition for each stage is written in the text box on the left hand side of the diagram. The right hand side of the diagram represents the information obtained from each individual stage of the investigation.

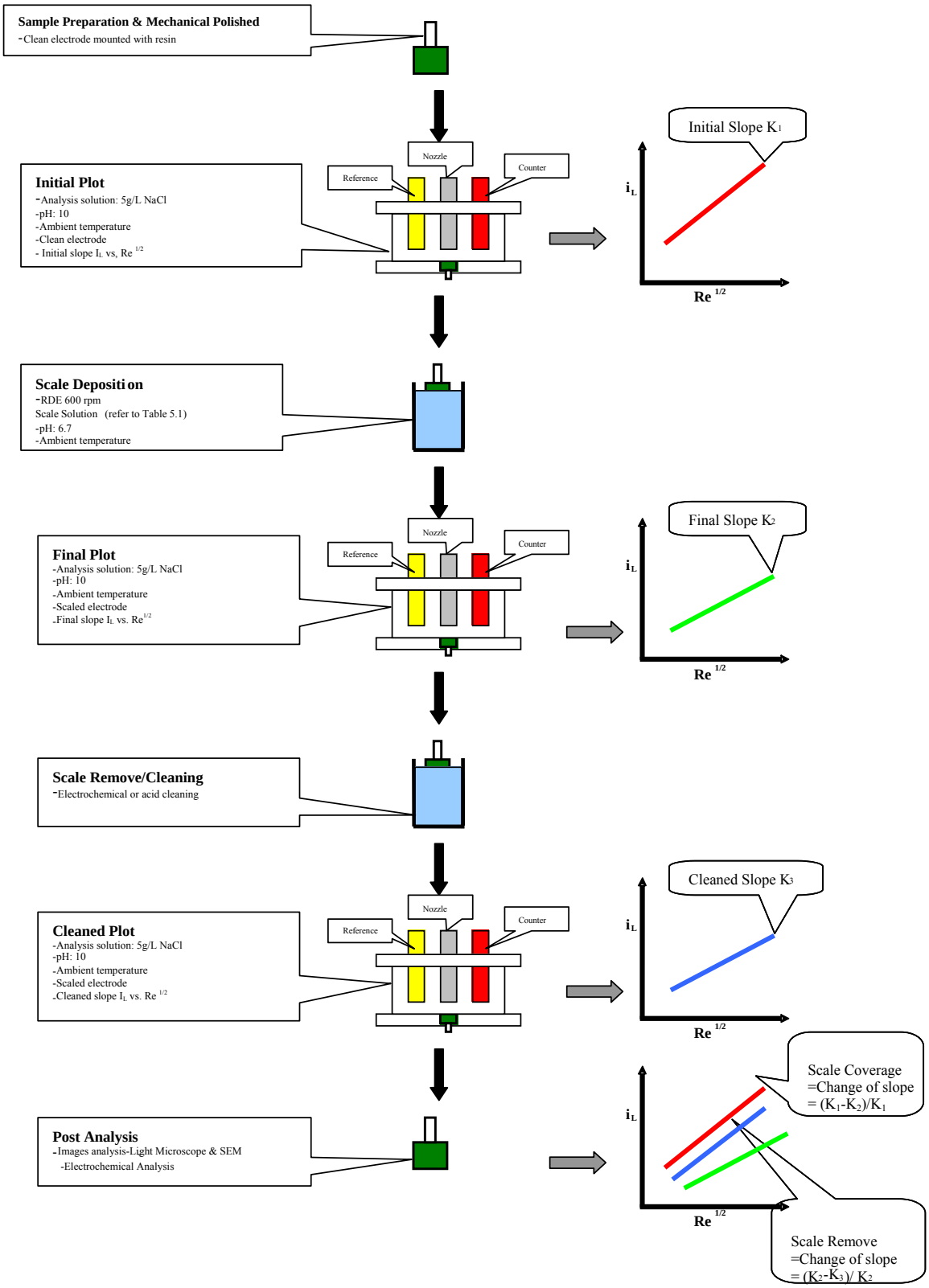

Figure 5-7 Schematic diagram of the stages involved in the study of scale removal and the information that can be extracted from each stage

5.5 Calibration of the System Parameters and Technique for Electrochemical Measurement

The SIJ system and the electrochemical technique were evaluated to ensure the reliability, as well as the reproducibility throughout the studies. The following section briefly describes the calibration as below:

i.) Calibrations of the SIJ set-up and its associated equipment;

ii.) Optimising the experimental conditions;

iii.) Calibrations of the electrochemical technique.

Calibration is to verify the use of SIJ and electrochemical technique as monitoring sensor. This also ensures accurate data and any experiment errors due to SIJ equipment set up are be avoided or minimised.

5.5.1 Calibration of the SIJ Set-up and Its Associated Equipment

For the SIJ set-up, the height setting of a nozzle to the specimen surface and the flow rate delivered by the pump are critical factors to generate a laminar flow regime that is necessary for the electrochemical measurement. Therefore, the consistency of flow delivery from the peristaltic pump is a crucial factor. Verification and calibration of the nozzle geometry and flow rate were examined.

5.5.1.1 Calibration of the Flow rate

Experimental data was collected to determine the flow rate of the actual system delivered by the pump. This is to verify if the value corresponds to the flow meter reading without any variation. The flow rate of the system was calibrated by measuring the volume of electrolyte collected over a certain period. The electrolyte was delivered to the nozzle from the solution tank by a peristaltic pump. It passed through a needle valve and flow meter before reaching the glass nozzle. The volume exit of electrolyte from the nozzle was collected in a beaker for 1 minute. Two measurements were carried out to determine the actual flow rate and its average value. The flow rate of the electrolyte was changed manually, either by controlling the needle valve or the peristaltic pump. The volume of the analysis solution was collected and compared to the flow rate reading value provided by the manufacturer. Figure 5-8 shows that the delivered flow rate corresponds perfectly to the manufactures value, which was obtained by directly reading the flow rate value on the flow meter.

As shown in Figure 5-8, a good correlation between the actual measured flow rate and the theoretical flow rate was found. The actual flow rate was proportional to the flow meter reading. A linear relationship was established from both plots. Both of the plots were perfectly matched showing the slope values of 3.756 and 3.672 for the theoretical and the actual flow rate respectively with R^2 above 0.99. The error between both slopes was less than 3 %.

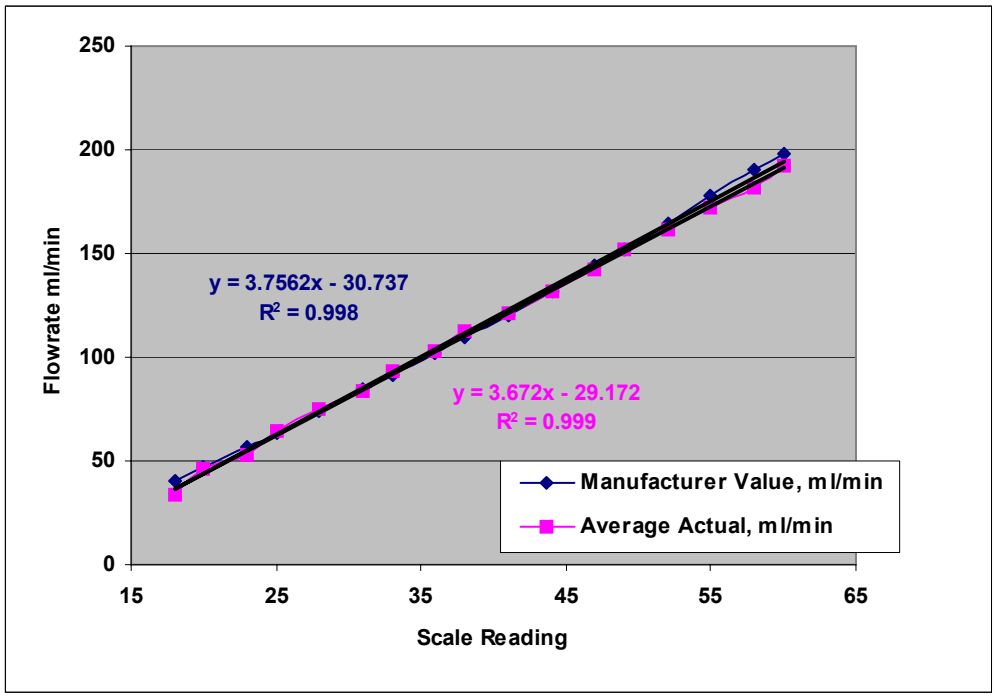

Figure 5-8 Represents the flow rate between the actual flow rate and the theoretical value (reading on the flowmeter scale)

This clearly indicates that the actual flow rate of the system is in agreement with the actual flow rate. This also confirms the system is in the right flow rate without any correction factor is needed for the actual flow rate.

5.5.1.2 Nozzle Height Determination Using a Potentiometer

The potentiometer used to measure the height of nozzle from the specimen surface was examined in this section. The main purpose of this experiment was to establish the relationship between the resistivity reading of the potentiometer and the height/length of the nozzle movement. With the established information, the height of the glass nozzle to the specimen surface could be easily measured. The basic principle of the potentiometer functioning is based on the resistivity changes in response to movement of the nozzle tip to a height/length. A potentiometer was connected to a multi-meter. This was used to measure the length of the nozzle movement from the specimen surface

by indicating the resistance reading on the multi-meter. The potentiometer was mounted on the L-shaped top support plate and its tip was set in a normal position to the nozzle support plate, which was attached to the nozzle as shown in Figure 5-4.

The height/length between the nozzle support plate and the top of the support plate was adjusted by moving the nozzle tube. The actual length of movement is measured by a verneir gauge that was corresponded to the resistance reading displayed on the multi-meter. The results of resistance change, as a consequence of height/length change between the nozzle support plate and the top support plate is presented in Figure 5-9. A linear correlation was found between the resistance and the height/length.

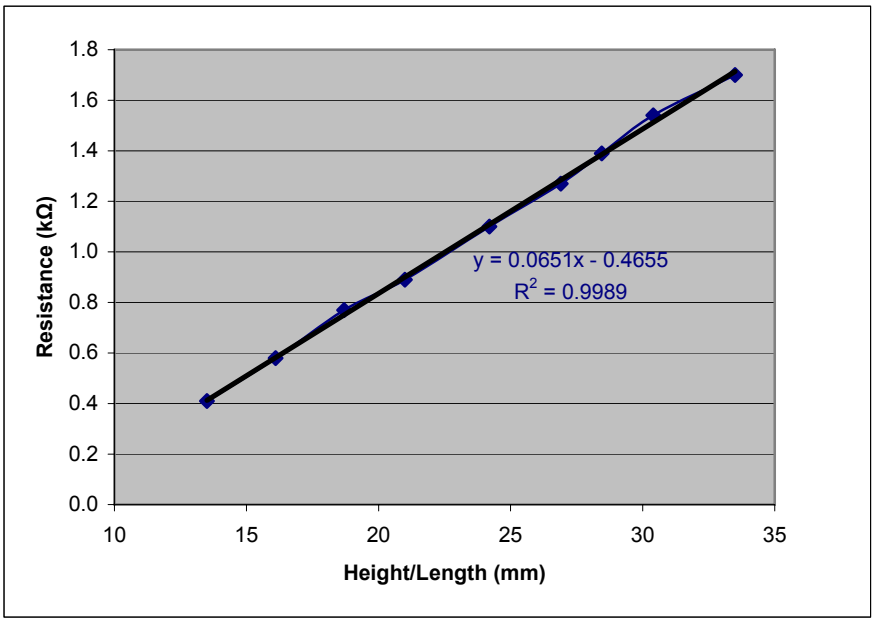

Figure 5-9 Correlation between resistance and height/length for a potentiometer

A linear correlation with an equation Y=0.0651X-0.4655 that related between the resistance and the length was established as shown in Figure 5-9. The result shows the resistance was proportional to the length with the value R^2 of 0.9989. The slope of the curve is 0.0651 kΩ/mm. This implies that for every 1 mm change in height/length, the resistance reading should indicate 0.0651 kΩ. For a nozzle diameter of 8 mm, the resistance was calculated as 0.0651(8 mm) =0.50208 kΩ.

A simple formula to determine the nozzle high measurement was created through this investigation where the setting resistance was determined using the Equation 5-1.

Setting resistance = Reference resistance-(0.0651xH) Equation 5-1

In order to achieve H/d=1, an average of 5 readings were taken as a reference resistance when the nozzle in contact with the bottom plate and setting resistance was calculated using the equation above. Therefore, the setting resistance was set by adjusting the nozzle up or down until the reading of the multi-meter displayed the same reading as the setting resistance.

5.5.2 Optimising the Experimental Conditions

Although the electrochemical measurement in a SIJ cell rig conducted at ambient conditions, the influence of other parameters such as applied potential, pH solution, oxygen concentration cannot be ignored. In this section, preliminary experiments to determine the optimum operating conditions were addressed. Optimum conditions such as the applied potential, pH of the analysis solution were examined to ensure reproducible results could be achieved.

The concentration has an effect on the electrochemical measurement as this developed methodology uses oxygen as a tracer. There are a few initial assumptions made for the oxygen concentration

i.) In an aerated condition with respect to the brine salinity, the oxygen concentration is assumed to be 8 ppm (as the normal concentration of oxygen at standard temperature and pressure conditions);

ii.) The concentration of oxygen remains constant before, during and after the electrochemical measurement.

No investigation was carried out to determine the oxygen concentration but it is believed the oxygen concentration is not a major issue. This is mainly because 2L of electrolyte was used for circulation purpose and the oxygen concentration in the electrolyte was more than sufficient for any electrochemical measurement that only last for 10- 15 minutes. Even though the specimen was catholically polarised for two hours, there was not any sign of oxygen depletion in the solution. This finding is supported by the scaling tendency investigation result and is covered more details in Chapter 7.

5.5.2.1 Verification and Confirmation of the Applied Potential

Oxygen-reduction occurs on the sensor surfaces when the sensor is cathodic polarised to a potential of –0.8 V (SCE) has been reported throughout the literature. The rate of

oxygen-reduction rate is mainly controlled by the diffusion of oxygen. Consequently, under the mass transfer reaction, a well-defined plateau region is achieved where the current remains constant with respect to the potential for the E-log I curve. Hence, the main objective of this section was to verify and confirm the selected cathodic potential so cathodic reaction takes place at the plateau regime. In addition, to ensure the oxygen reduction remains under diffusion controlled with respect to the selected flow rate.

Experiments were conducted to define the potential range corresponds to the diffusion plateau region for various flow conditions. A potentiodynamic experiment was performed to record the potential (E) versus current. Analysis solution was used as the electrolyte and its pH was buffered to 10 by NaOH solution.

The results presented in Figure 5-10 show the influence of Reynolds number (Re) on the polarisation curve. It found that when the specimen was polarised from a free corrosion potential towards the cathodic direction, the recorded current were divided into 3 regions as shown in Figure 5-10. In the first region, the current increases slowly, as the potential increases until -0.7 V. Region 2 indicated a constant current at the potential between -0.7 V and -1.2 V. Above -1.2 V a faster current increase was observed. As the Re increases, the curve tends to shift to higher limiting current. The limiting current increment was less, especially at higher flow rate with Re at 368.8 and 473.7. When the flow rate or Re increases, the limiting current curve tends to shift higher, but the plateau region remains the same. The higher Re leads to the formation of a thinner diffusion layer and the rate of dissolved oxygen diffused to the metal surface increases. Therefore, a higher limiting current was obtained as shown in Figure 5-10.

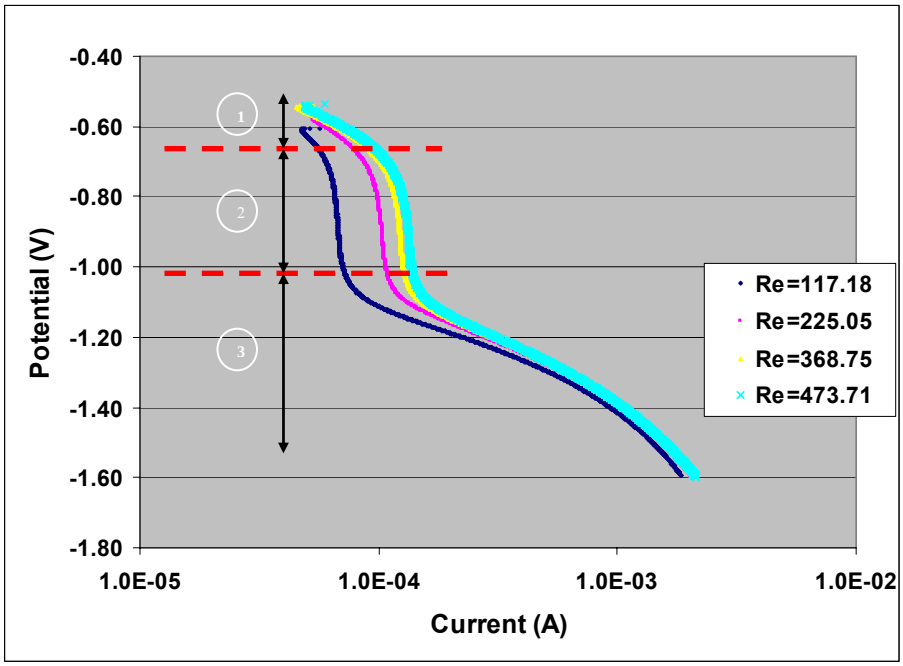

Figure 5-10 Potentiodynamic test of the cathodic polarisation curves of 316 stainless steel for various flow rates expressed in terms of Re i) 117.18 ii) 225.05 iii) 368.75 iv) 473.31 in the analysis solution 5 g/L NaCl and at pH 10

Under cathodic polarisation, two main cathodic reactions contribute to the cathodic current in most aerated solutions; the hydrogen-evolution and oxygen-reduction. The domination of the reaction depends on the applied potential. As shown in Figure 5-10, the cathodic polarisation was divided into 3 regions (1, 2 and 3). A range of potentials from –0.7 to -1 V/ (Ag/AgCl) indicated a plateau region where the oxygen-reduction reaction occurs under mass transfer control for a range of flow rate or Re. This finding is in agreement with Morizot [15] and Tao Chen [115]. The cathodic current recorded in region 3 is attributed to hydrogen evolution. In regions 1 and 2, the overall cathodic current is mainly a cause of the oxygen reduction process. However, in region 1, the oxygen reaction is mainly governed by the kinetics factors, whilst in region 2 it is diffusional controlled by diffusion.

Hence, this verifies the selected potential -0.8V (Ag/AgCl) with respective to the Re (117 to 473) is under the mass transfer controlled. This value is also in between the investigated potential -0.7 to -1 V which also shown at the regime the oxygen reduction is under mass transfer controlled.

5.5.2.2 Determination of the Reynolds Number and Nozzle Geometry

In electrochemical technique measurements, as explained previously, the limiting current is the function of the oxygen-reduction rate on the metal surfaces. This process is mainly diffusionally controlled and is under mass transfer control. Consequently, constant surface concentration throughout the electrode surfaces must be required and maintained. This can only be achieved by having a laminar flow on a metal surface with a uniformly accessible region. A special SIJ arrangement especially on the nozzle geometry is required for achieving uniform accessibility for the oxygen reduction process.

Therefore, the purpose of this experiment was to determine the Reynolds' number of the system under the laminar flow regime. The experimental procedures of the specimen preparation and initial analysis used in this investigation are described previously in section 5.2.1 and 5.2.1.1. The limiting current was recorded as a function of $Re^{½}$ for H/d =1.0. The experiment investigating the effect of the height of the nozzle to the specimen surface (H/d) for the same range of $Re^{½}$ was examined to provide a better understanding of the flow regimes. The height of the nozzle was set by adjusting the nozzle tube as described in section 5.5.1.2. For this study, three ratios of H/d were used, H/d=0.5, 1.0 and 3.1. Four measurements were used to define the flow regimes of H/d=1.0. The specimens used in this experiment were not mounted in resin. The limiting current versus various flow rates were recorded and the results are presented as in Figure 5-11.

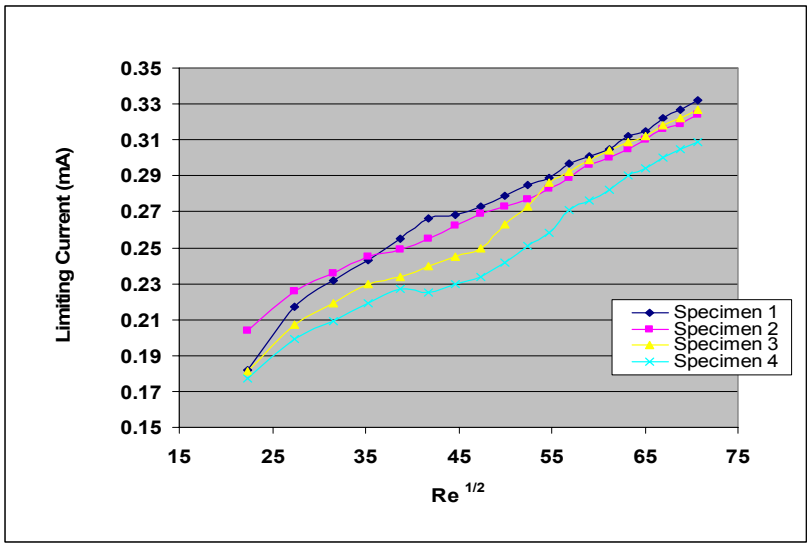

Figure 5-11 Represents the i_L versus $Re^{½}$ of four specimens without resin mounting at H/d=1

Figure 5-11 shows the inconsistency and poor reproducibility of the i_L versus $Re^{1/2}$ for the four measurements. When the electrolyte impinged on the surface of the specimen, which was fitted at the bottom plate, instability flow streams were generated around the surface, especially at the edge of the electrode. This is illustrated with a simple diagram shown in Figure 5-12. Hence, it is believed that the non-reproducible result was mainly due to small vortex or turbulent flows at the edge that causing an uniform flow along the surface of the specimen. An improved experiment was conducted, using a resin-mounted specimen to avoid the turbulent flow at the edge. As the electrolyte impinged on the specimen surface, a continuous or laminar flow stream flowed along the specimen's surface without causing any disruption as illustrated in Figure 5-13 Having resin mounted around the electrode, more reproducible results were achieved. This was supported by the consistency of i_L versus $Re^{1/2}$ result as shown in Figure 5-14.

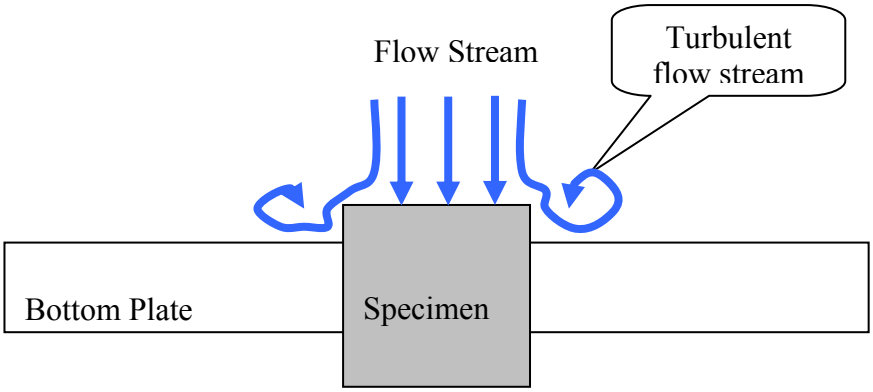

Figure 5-12 Turbulent flow stream was generated at the edge of the electrode surface

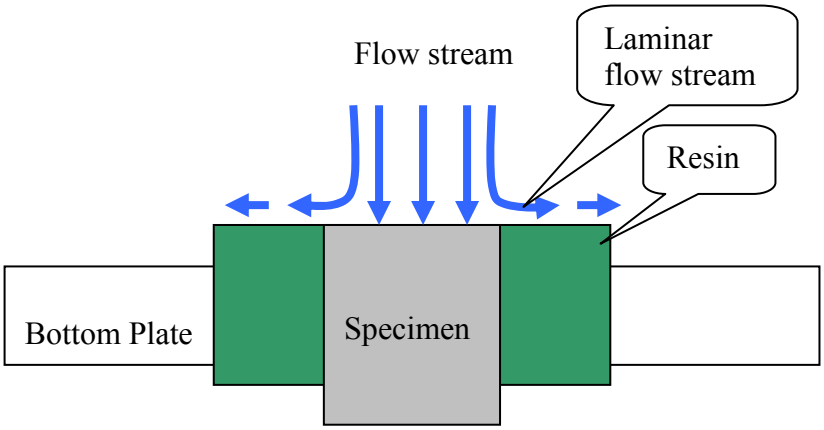

Figure 5-13 Laminar flow stream along the specimen surface is generated for a specimen mounted with resin

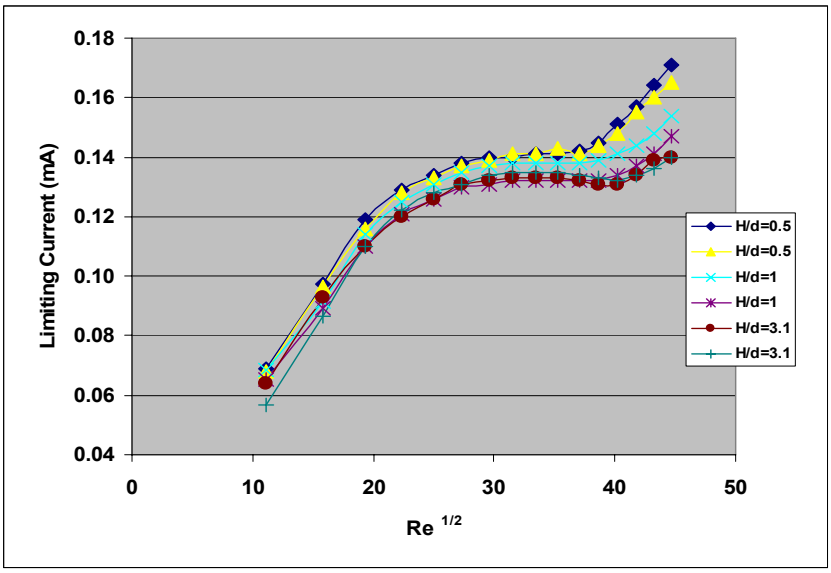

Figure 5-14 Two measurements of i_L versus $Re^{½}$ for each H/d setting, H/d=0.5, H/d=1.0 and H/d=3.1

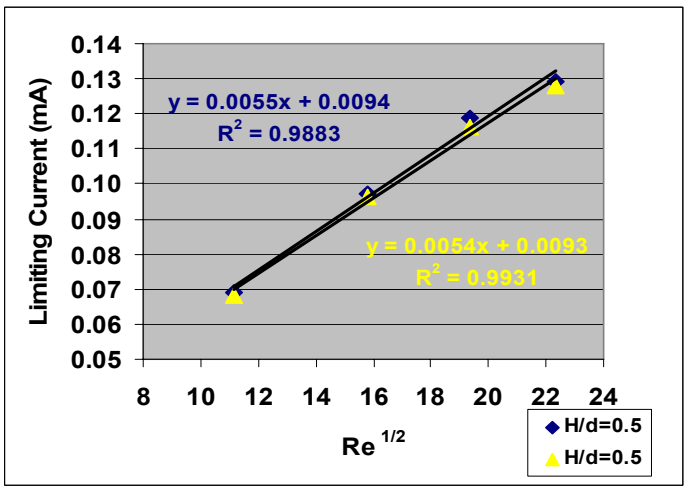

Figure 5-15 i_L versus $Re^{½}$ within the laminar flow regime for H/d=0.5

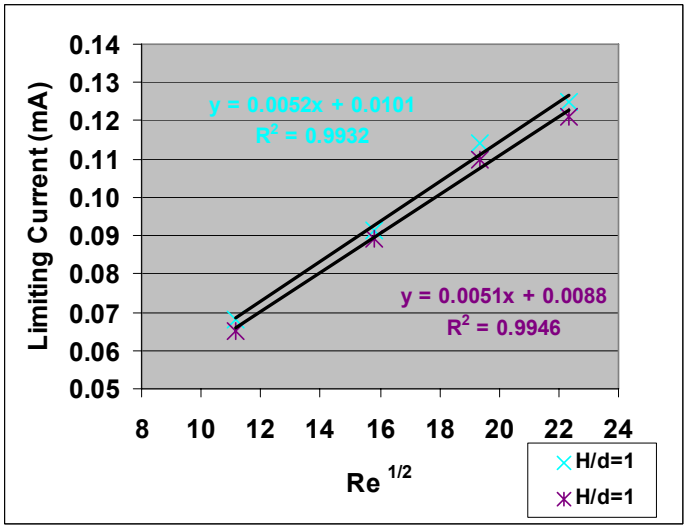

Figure 5-16 i_L versus $Re^{½}$ within the laminar flow regime for H/d=1.0

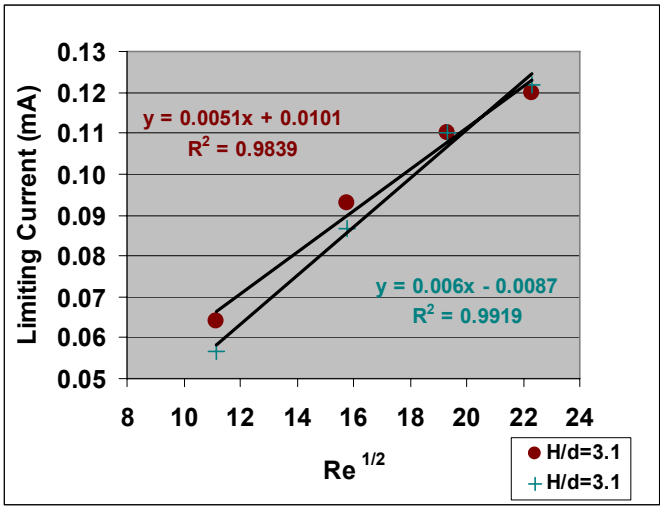

Figure 5-17 i_L versus $Re^{½}$ within the laminar flow regime for H/d=3.1

The effect of the height of nozzle to the diameter of electrode (H/d) on the limiting current was also investigated. Three ratios of H/d were examined 0.5, 1.0 and 3.1. Data obtained in Figure 5-14 was used to plot the i_L versus $Re^{½}$ within the laminar flow regime for these three different H/d values. The curves are shown in Figure 5-15 for H/d=0.5, Figure 5-16 for H/d=1.0 and Figure 5-17 for H/d=3.1. There was only small a dependence of the transport limiting current with respect to H/d. This observation is in agreement with Arkam that distance H has no effect on the current if the ratio H/d is maintained between 0.5-3 [13].

All of these H/d showed a correlation coefficient of above R^2 =0.98 for i_L versus $Re^{½}$. Although the graph consists of limited data (four points), more data to plot i_L versus $Re^{½}$ was carried out and a similar R^2=0.98 was achieved as presented in section 5.7. The entire slope of all these H/d has a value of 0.05 ± 5 %. The variation of the slope may be explained due to the different H/d and specimen surface finished but the effect is not significant.

It could be noticed with respect to H/d setting, the value of the limiting current at Re=0 is not zero predicted by using Equation 5-5. The extrapolated straight line from i_L versus $Re^{½}$ did not pass exactly through the origin. This may be explained by the existence of convection in the system and not solely by the diffusion-convection process. A similar finding was discussed for RDE in literature and according to Filinnosvly *et al.*, [116] the current versus $\omega^{1/2}$ is not zero but a finite value for RDE technique using Levich's equation.

The result shown in Figure 5-14 indicated that for any specimens mounted in the resin subjected to the $Re^{1/2}$ ranges from 11 to 48, three distinctive well-defined flow regimes were obtained; the laminar flow, the transition flow and the turbulent flow. Any flow disruptions around the electrode surfaces were prevented by using a mounted specimen. Laminar flow was generated near the electrode surface for $Re^{1/2} < 22$. As the flow rate increases, the flow becomes turbulent, this occurred once the $Re^{1/2}$ was above 40. In between these two flow regimes was the transition flow regime where the value of $Re^{1/2}$ was between 22~40.

In general, the limiting current as a function of Reynolds' number plot shows that the limiting current increases with increasing fluid velocity. The plot also shows that there was a noticeable discontinuity of linearity in the limiting current when the velocity of the fluid was around 6.6 cm/s (Re 498) comparing to the value reported by Deslouis (Re 625) [23], Bouet (Re 225) [113]. At this value, the laminar flow becomes unstable and transitions of flow forms (from laminar to transition flow). The variation is believed to be attributed to the length to diameter ratio that used to determine the flow profiles (flat or parabolic flow profiles) generated in the nozzle tube. Using the laminar flow development criterion $L/d = 0.05\ Re$, the maximum laminar Reynolds number possible while still achieving fully developed flow can be determined. This flat velocity profile contains smaller amounts of momentum and kinetic energy for the same mass flux compared with that fully developed parabolic profile (higher shear stress). Deslouis [23] reported the maximum laminar flow regimes could be achieved with a 50 tube diameters. Bouet *et al*. [113] claimed that the length-to-diameter ratio of 19 was corresponding to the transition value (Re 225). In this study, the nozzle used was not long enough (length-to-diameter ratio of 22) to achieve fully developed a jet with a parabolic velocity profile but the jet velocity profile is having a flatter velocity. Though the narrowness of the laminar regime occurred at lower Re (<498), the momentum and kinetic energy is enough to be distributed uniformly over the cross-section of the electrode where the mass transport controlled with a uniform current density can be achieved for an electrochemical measurement.

The exact point of departure from uniform mass transfer is of some dispute (transitions of flow regime from laminar to transition). The critical Reynolds number corresponding to the laminar and turbulent flow are Re =1369 and Re_T=3364 respectively was reported. The laminar flow regime in agreement with the finds less

than the Re = 2000 reported by Chin *et al.* [117] and Alkire *et al*. [118] for a similar system.

5.5.2.3 Selection of the Solution pH

Choosing a suitable pH is important as this can minimise the dissolution of $CaCO_3$ deposited at low pH solution and minimise the possible of hydrogen generation that could cause any mineral scale removed from the electrode surface. At high pH, the hydrogen-evolution reaction is thermodynamically favourable at more negative potential than at neutral pH. Hence, the pH has significant influence on the cathodic potential. A pH value at 10 was selected and the possible cathodic reaction was theoretically determined by using the Nernst Equation. At two possible cathodic reactions, the equilibrium electrode potential was calculated using the Nernst Equation. The equilibrium potential of oxygen reduction reaction in the alkaline media pH=10 at temperature 25 °C and concentration of dissolved oxygen in solution is assumed to be 8 ppm, hence

$$E_{O_2+2H_2O+4e^- \rightarrow 4OH^-} = E^0_{O_2/OH^-} + 2.3\frac{RT}{nF}\log\left[\frac{a_{O_2}}{(a_{OH^-})^2}\right] \qquad \text{Equation 5-2}$$

$$E_{O_2+2H_2O+4e^- \rightarrow 4OH^-} = 0.401 + 2.3\frac{8.314*298}{4*96487}\log\left[\frac{2.5x10^{-7}}{(10^{-4})^4}\right] \qquad \text{Equation 5-3}$$
$$= 0.5397\,V\ (SHE)$$

The potential value calculated was based on a standard hydrogen electrode (SHE) scale, therefore for the value on silver chloride (Ag/AgCl) scale, the potential was 0.539-0.2224 = 0.3166 V (Ag/AgCl at E_0 = +0.2224 V vs. SHE). A similar calculation was applied for hydrogen evolution and the activity of hydrogen gas is unity.

$$E_{2H_2O+2e^- \rightarrow H_2+2OH^-} = -0.826 + 2.3\frac{8.314*298}{2*96487}\log\left[\frac{1}{(10^{-4})^2}\right] \qquad \text{Equation 5-4}$$
$$= -0.590\,V\ (SHE)$$

Hence the equilibrium potential for hydrogen evolution in silver chloride scale is –0.590 – 0.2224= –0.8124 V (Ag/AgCl) at pH =10. Hydrogen-evolution reaction is thermodynamically feasible only when the potential of the electrode is more negative than the potential of –0.8124 at pH 10. At pH=8, the potential (E) is –0.472 V (SHE) or −0.6944 V (Ag/AgCl) where there is a possible to generation of hydrogen. Hydrogen

evolution began at potential –0.95 V (Ag/AgCl) on the steel substrate, which was reported in literature [15].

Furthermore, most of these experiments were performed at an applied potential of –0.8 V (Ag/AgCl) for the oxygen-reduction process to take place on the working electrode. The polarisation process took 10-15 minutes for each sample. Therefore, it is believed that polarisation under the cathodic region has no effect on the electrochemical activity of the solution, and that the surfaces of the electrode are not affected after polarisation.

5.5.3 Calibrations of the Electrochemical Technique

The focus of this section briefly demonstrates the reliability of the application of SIJ as a means of electrochemical measurement to detect and estimate the scale coverage at metal surfaces as well as the scaling tendency of a system. This can be divided into four parts:

i.) The response of the electrochemical on various active area of the electrode;
ii.) Calculation of the oxygen diffusion coefficient;
iii.) Accuracy of the electrochemical measurements using SIJ;
iv.) Sample Model- Lacomit.

5.5.3.1 The Effect of Active Surface Area on the Electrochemical Measurement

Throughout the experiment, it is assumed that the entire active surface of the electrode before scale deposited is $(0.25)^2$ л =0.196 cm^2. As the scale deposited, the active area change formed an initial value of a bare electrode A_1 to the final value A_2 of scale deposited electrode. A calibration experiment was conducted to demonstrate how the electrochemical technique responds to the active surface area. In this experiment, two different diameter electrodes were used to analyse the electrochemical responses on the active surface areas. Both analyses were carried out in the same analysis solution, so the solution chemistry and properties remain unchanged throughout the experiment. The sample preparation and experimental procedures were described in section 5.2.1.

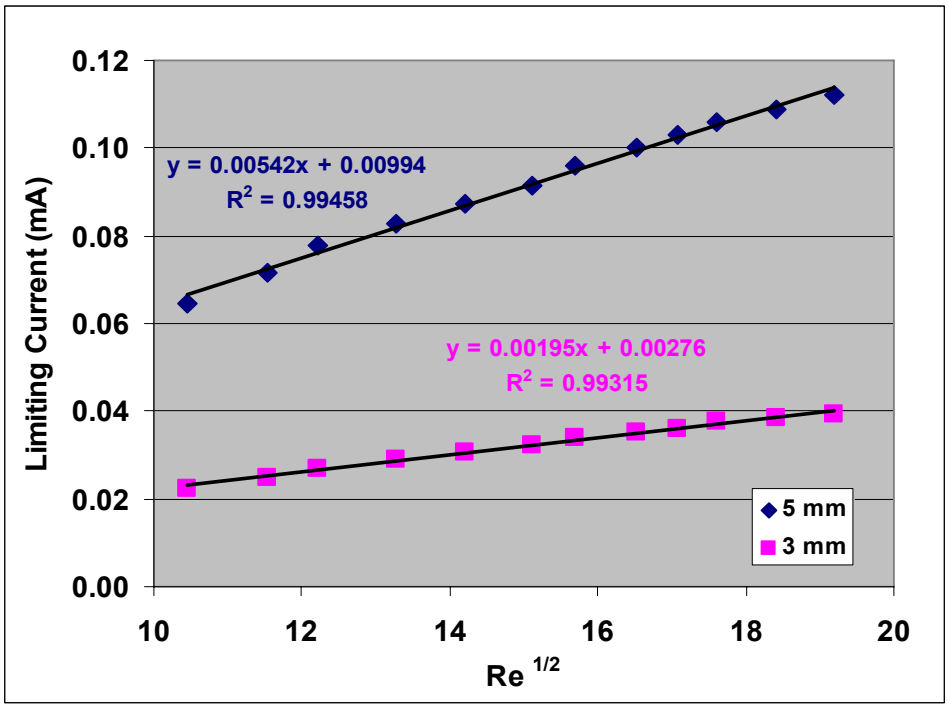

Figure 5-18 Represents the slope value of i_L versus $Re^{½}$ for two different diameters electrode, 3 mm and 5 mm

From the i_L versus $Re^{½}$ plot in Figure 5-18, results showed the slopes of the plot for 3 mm and 5 mm diameter electrodes were 0.00542 and 0.00195 respectively. According to Equation 5-5, limiting current depends solely on the active surface area since other parameters are assumed constant as described in Chapter 4, section 4.4. When the active area decreases, limiting current decreases, hence a lower value of slope is obtained as a result of this.

In this experiment, it is clearly proven that the response of electrochemical measurement is governed by the change of active area. This was confirmed by varied diameter sizes of clean electrodes, as the i_L measured was proportional to the active surface. From the calculation obtained, as shown below, an excellent correlation was found between the slope ratio of the experiment value and the area ratio of the two electrodes. The calculation of slope ratio of electrode and area ratio of the electrodes was given as follow:

$$\text{Slope ratio of the electrodes} = \frac{(\text{slope of 5mm electrode})}{(\text{slope of 3mm electrode})}$$

$$= \frac{0.00542}{0.00195} = 2.7794$$

$$\text{Area ratio of the electrodes} = \frac{(\text{Electrode area for 5mm diameter})}{(\text{Electrode area for 3mm diameter})}$$
$$= \frac{\pi 2.5^2}{\pi 1.5^2} = 2.7777$$

Consequently, the ratio of the slope is theoretically identical to the ratio of the surface area of both electrodes. This validates the notion that the active area surface can be accurately described by the electrochemical measurements.

5.5.3.2 Verification of Oxygen Diffusion Coefficient

In order to ensure Equation 5-5 was correctly applied, validation of the equation was examined using data obtained from the electrochemical measurements. The slope of i_L versus $Re^{½}$ plot obtained from the initial analysis was used to determine the oxygen diffusion coefficient by assuming all the parameters in Equation 5-5 remained constant. The oxygen coefficient was determined by substituting all parameters and slope values into the following equation:

$$i_L = 1.51 \mathrm{Re}^{0.5} Sc^{0.33} \left(\frac{H}{d}\right)^{-0.054} g(Sc) \frac{nAFCD}{d} \qquad \text{Equation 5-5}$$

From Equation 5-5, the slope value for i_L versus $Re^{½}$ is represented in Equation 5-6

$$k = 1.51 \nu^{0.33} \left(\frac{H}{d}\right)^{-0.054} g(Sc) \frac{nAFC}{d} \qquad \text{Equation 5-6}$$

A list of constants obtained from literature was used to determine diffusion coefficient of oxygen

i_L = limiting current, mA
n = 4 (number of electron)
F = 96500 (Faraday constant, $Cmol^{-1}$)
C = 2.5×10^{-4} (concentration of electroactive species, $mol.dm^{-3}$)
$\nu = 1 \times 10^{-2}$ (kinematic viscosity, $cm^2.s^{-1}$)
Re = Reynolds number
g(Sc) = 1 (Schmidt number)
d = 0.8 (nozzle diameter, cm)
$\frac{H}{d} = 1$ (ratio height of the nozzle to electrode)
A = 0.1963 (area of electrode, cm^2)

By rearranging and substituting the constant values into Equation 5-6 this gives

$$D^{0.666} = \frac{i_L}{k\,\mathrm{Re}^{0.5}} \qquad \text{Equation 5-7}$$

where $i_L / \mathrm{Re}^{0.5}$ is equal to the slope of i_L versus $Re^{½}$

From Figure 5-18, a slope of 0.00542 from i_L versus $Re^{½}$ was obtained from a 5 mm diameter electrode. Substituting this slope value and other parameters obtained from the literature into Equation 5-7 to calculate the oxygen diffusion coefficient D, gives

$D = 1.81X10^{-5}\ cm^2 s^{-1}$

The value obtained from oxygen diffusion coefficient is close to the value reported by Deslouis et al. [23] (1.63x10-5 cm^2s^{-1} at 25 °C), Babic et. al [119] (1.73x10-5 cm^2s^{-1} at 20 °C) and Morizot [15] (1.72x10-5 cm^2s^{-1} at 20 °C). The differences between these values may be associated with the experimental techniques applied and the parameter values used in the calculation. Furthermore, different experiment i.e. RDE, pipeline flow may lead to differing ionic species absorption onto surfaces. However, the value obtained through SIJ is within 10 %. This is discussed in the following section on the accuracy of this technique.

Based on the diffusion coefficient of oxygen obtained from, the oxygen diffusion coefficient is approximately of $D = 1.8X10^{-5} cm^2 s^{-1}$. This is based on a four electrons path oxygen reduction. However, calculation for two electrons path had a value of $D = 5.12X10^{-5} cm^2 s^{-1}$ and it is far from the theoretical value $D = 2.0X10^{-5} cm^2 s^{-1}$. Therefore, it can confirm that the oxygen reduction reaction occurs through a four electrons path instead of through a two electrons path.

5.5.3.3 Accuracy of the Electrochemical Measurement Using SIJ

The purpose of this section is to determine the experimental error of this technique (SIJ in conjunction with the electrochemical technique) by measuring the slope value of i_L versus $Re^{½}$ plot. A bare specimen was used to determine the error. Further details of the sample/specimen preparation, can be referred to in 5.2.1. The experimental conditions and procedures used in this investigation were the same as the initial analysis previously described in section 5.2.2. In order to determine the error of this technique, 36 experiments were examined and the slope value of i_L versus $Re^{½}$ and least square fits,

R2 the for each test was determined. These values are presented in Table 5-3 and the result of the slope value versus number of experiment is shown in Figure 5-19.

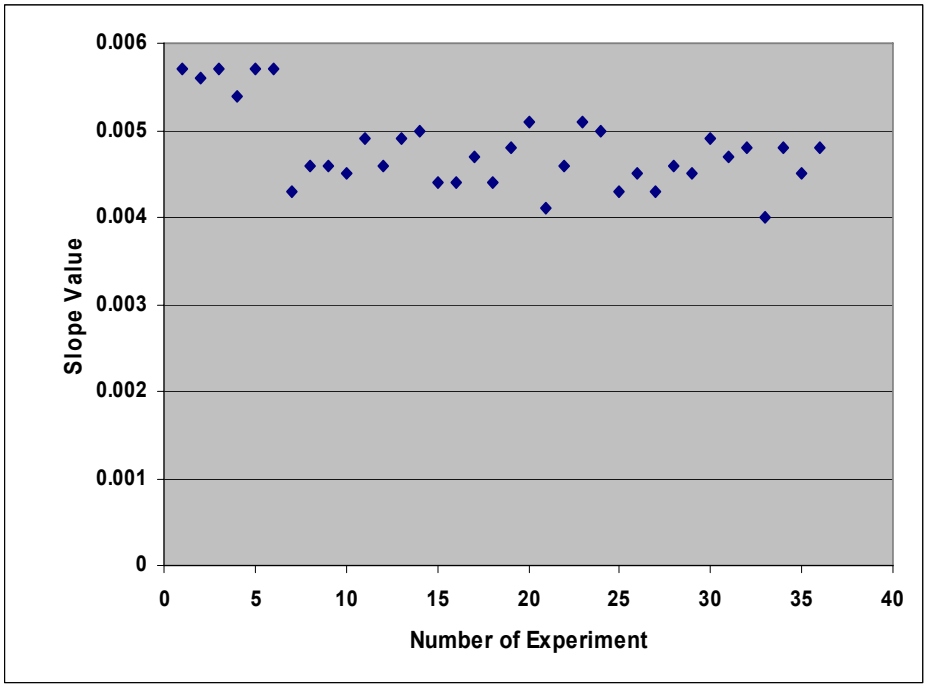

Figure 5-19 Slope value of i_L versus $Re^{1/2}$ was determined from the initial analysis for 36 experiments

It found that the slope value obtained from i_L versus $Re^{1/2}$ is in the range of 0.0041 to 0.0057. Result indicated an average slope value of 0.00479 with a standard deviation of 0.00046. Therefore, the error margin of this technique to measure the slope was approximately 10 %. The deviation of the gradient was less than 0.5 %. A good correlation from an outweighed least square fits of the data is always obtained around 0.9968.

Number of Experiment	Slope of i_L vs. $Re^{1/2}$	R^2
1	0.0057	0.9993
2	0.0056	0.9988
3	0.0057	0.9994
4	0.0054	0.9981
5	0.0057	0.9992
6	0.0057	0.9985
7	0.0043	0.9952
8	0.0046	0.9955
9	0.0046	0.9945
10	0.0045	0.9962
11	0.0049	0.9944
12	0.0046	0.9957

Number of Experiment	Slope of i_L vs. $Re^{1/2}$	R^2
13	0.0049	0.9936
14	0.0050	0.9931
15	0.0044	0.9913
16	0.0044	0.9921
17	0.0047	0.9913
18	0.0044	0.9942
19	0.0048	0.9997
20	0.0051	0.9992
21	0.0041	0.9987
22	0.0046	0.9997
23	0.0051	0.9971
24	0.0050	0.9994
25	0.0043	0.9970
26	0.0045	0.9980
27	0.0043	0.9985
28	0.0046	0.9982
29	0.0045	0.9991
30	0.0049	0.9978
31	0.0047	0.9982
32	0.0048	0.9984
33	0.0040	0.9974
34	0.0048	0.9982
35	0.0045	0.9981
36	0.0048	0.9931
Average	**0.00479**	**0.9968**
Standard Deviation	**0.00046**	**0.0025**
% Error	**9.6**	**0.3**

Table 5-3 Represents the error of the electrochemical measurement using SIJ

5.5.3.4 Model Samples of Different Levels of Lacomit Coverage

The purpose of this section was to create some samples where the levels of coverage can be easily quantified by the image analysis as well as the electrochemical technique. The generation of sample models can simulate as homogenous scale coverage on the surface of the electrode. In this section, the sensor surface was blocked by Lacomit varnish coverage. Three levels of Lacomit coverage; modest, medium and severe coverage were generated. This is analogous to the random scale distribution on metallic surfaces. Basically, the experiment procedure is the same as the study scale coverage, except after the initial analysis, specimens were coated with Lacomit instead of immersed specimen into the scaling solution to deposit mineral scale. A control experiment (bare specimen) was also performed where no Lacomit was coated on the sensor surface.

Post-analysis was performed to calculate the Lacomit coverage through electrochemical technique by comparing the slope of the initial and final plot of i_L versus $Re^{½}$. Images were taken by a light microscope and the Lacomit coverage was then determined by using Aquinto a4i Docu software.

Figure 5-20 shows the initial and final analysis of i_L versus $Re^{½}$. Again, it demonstrated the good reproducibility of this technique for four non-scaled/ bare specimens (initial plot) which were subjected to the analysis solution at normal pressure and ambient temperature. The surface coverage was then determined by assessing the change in the slope of the i_L versus $Re^{½}$ relationship. To develop controlled samples with certain coverage, Lacomit was randomly coated onto the three electrode surfaces to simulate scale covering the surface on 3 levels, which could be referred to as modest, medium and severe. Each of the conditions is shown in Figure 5-21 and the final analysis was performed after it was coated with Lacomit. For each specimen, 20 images were taken through a light microscope to determine the coverage and an average value was obtained for the Lacomit coverage.

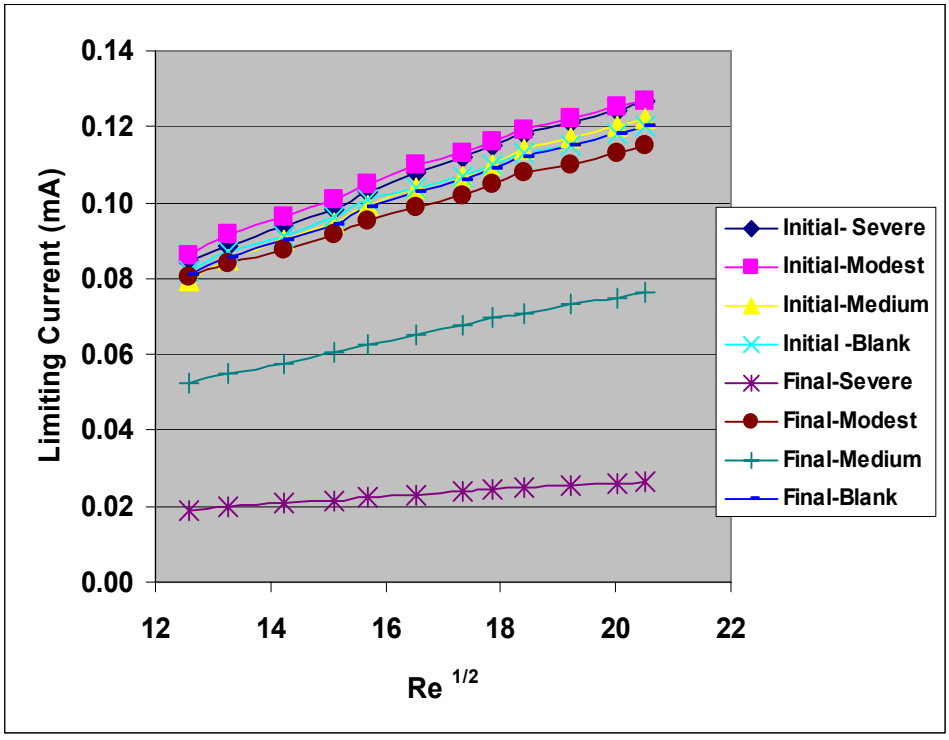

Figure 5-20 Result of i_L versus $Re^{½}$ of the initial and final analyses for various Lacomit covering the electrodes

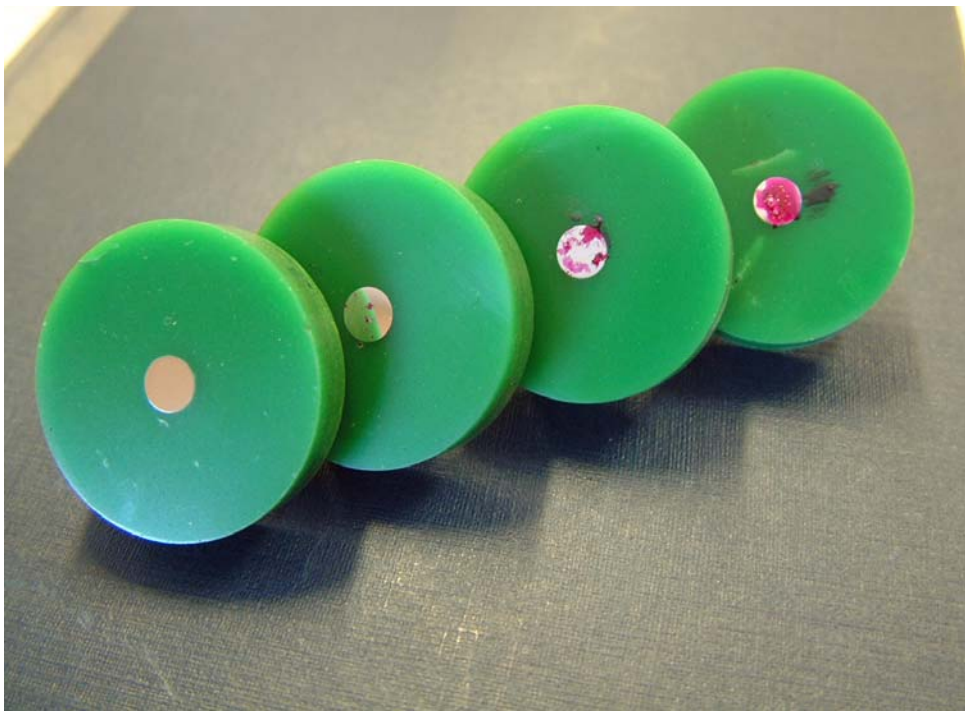

Figure 5-21 Different levels of Lacomit coverage on electrode surfaces starting from the left: Blank (clean), Modest, Medium and Severe.

Each condition and level of Lacomit deposited on the specimen is shown in Figure 5-22 to Figure 5-25. The current i_L versus $Re^{½}$ of the initial analysis for the bare specimen before covered with Lacomit and the final analysis of same specimen after it was covered with Lacomit were used to determined the plot values. For the blank specimen experiment, the initial and final analyses for the specimen (without any Lacomit) were carried. The modest level of Lacomit on specimen is shown as in Figure 5-23. The medium and severe levels of Lacomit coverage are represented as shown in Figure 5-24 and Figure 5-25 respectively. The initial and final analyses of each level of coverage Lacomit were then used to obtain initial and final plots for post analysis to determine the percentage of coverage on the specimen's surface. Lacomit coverage was determined by comparing the initial and final plot example for the medium coverage of Lacomit on specimen surfaces which had an initial value of 0.0053 and final plot of 0.0030. Hence, the coverage is given as

Lacomit Coverage

$$= \frac{Initial\ \ plot - Final\ \ plot}{Initial\ \ plot}$$

$$= \frac{0.0053 - 0.0030}{0.0053}$$

$$= 43.39\ \%$$

Results of the initial and final plots as presented in Table 5-4. The percentage of Lacomit coverage result quantified by the electrochemical and image analysis techniques are also presented as in Figure 5-26. The same process was used to determine the percentage of scale coverage on the specimen that covered with Lacomit. The percentage determination is said to be based on electrochemical methods because the initial and final plots were obtained through electrochemical measurement. Hence, the percentage of Lacomit coverage determined by electrochemical for blank, modest, medium and severe conditions indicated the coverage of -4 %, 14 %, 41 % and 83 %. The coverage determined through image analysis technique, 0 %, 7 %, 50 % and 89 % correspond to the blank, modest, medium and severe conditions respectively. A sample model of image taken by the light microscope is presented in Figure 5-27 where image (a) represents the Lacomit coverage on the surface electrode and image (b) represents the amount of Lacomit covered determined by image analysis software. The image analysis is able to detect all the Lacomit coverage on the surface even with small sizes. Hence, the coverage result showed good correlation for both technique and scale coverage increase as the coverage of Lacomit on the specimen's surface increases as shown in Figure 5-26.

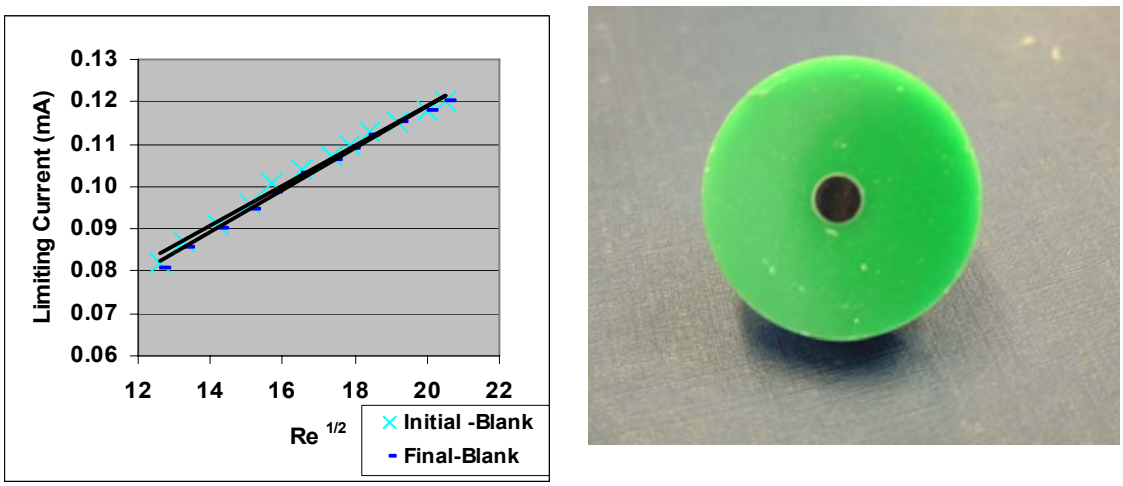

Figure 5-22 The initial and final plots of blank (clean) Lacomit specimen. The image on the right represents the sensor condition

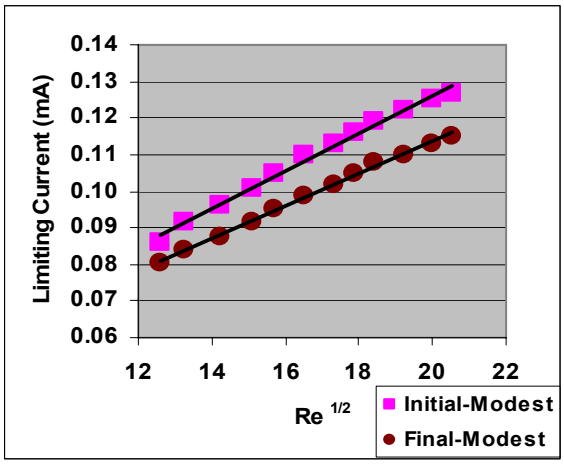

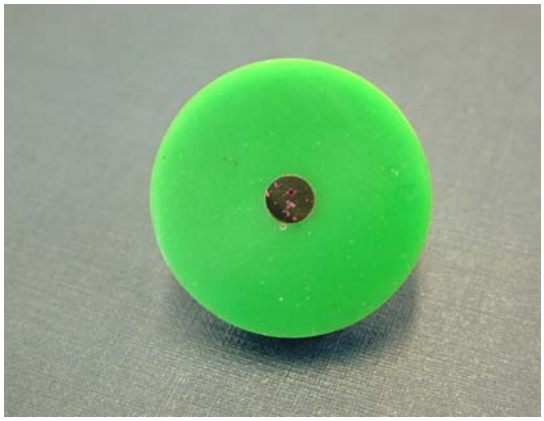

Figure 5-23 The initial and final plots of modest Lacomit specimen. The image on the right represents the sensor condition

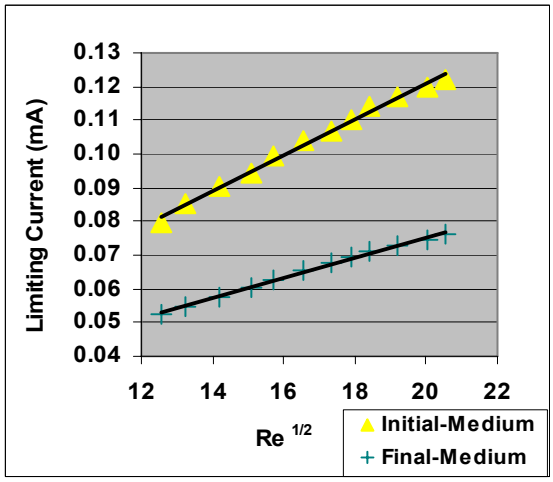

Figure 5-24 The initial and final plots of medium Lacomit specimen. The image on the right represents the sensor condition

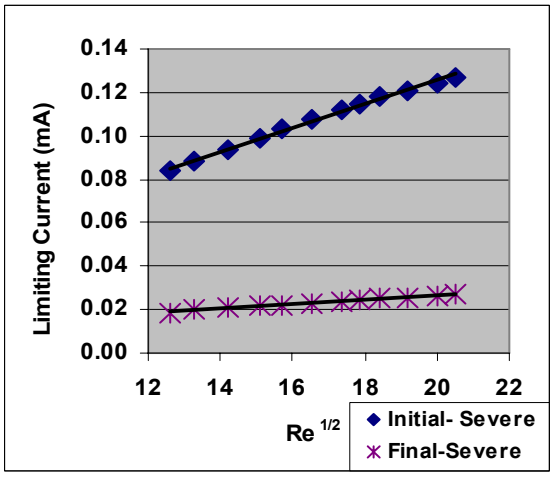

Figure 5-25 The initial and final plots of severe Lacomit specimen. The image on the right represents the sensor condition

Specimen	Initial plot	Final plot	Percentage of Coverage (Electrochemical)	Percentage of Coverage (Light Microscope)
Blank	0.0047	0.0049	-4.3	0.0
Modest	0.0051	0.0044	13.7	6.9
Medium	0.0053	0.0030	43.4	49.9
Severe	0.0054	0.0010	81.5	88.9

Table 5-4 Result of the plot values and scale coverage after being coated with Lacomit in various conditions, determined by the electrochemical technique and image analysis technique

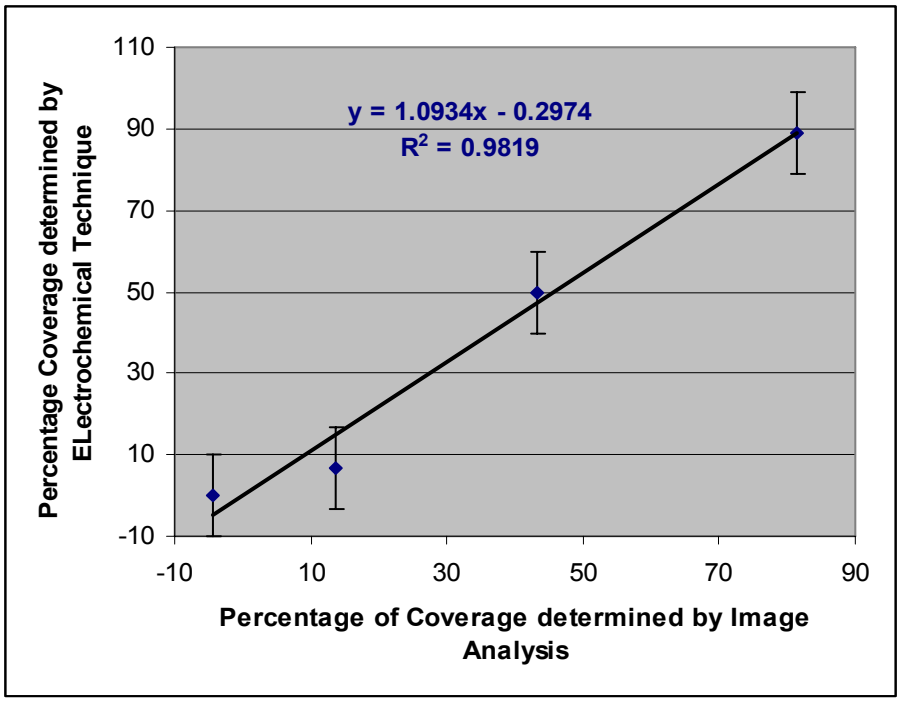

Figure 5-26 Percentage of Lacomit coverage in various surface conditions determined by electrochemical and microscope techniques

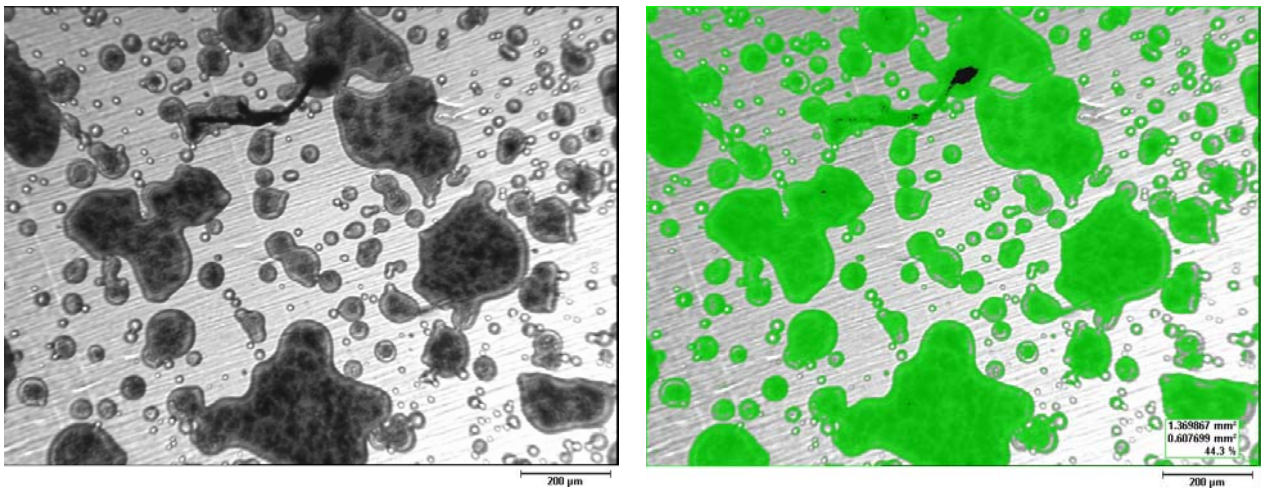

Figure 5-27 Image of sample electrode model covered with Lacomit (medium condition) and the surface coverage by image analysis technique

Results in Table 5-4 clearly indicate that as the Lacomit coverage increases, the final-plot value decreases. It confirms that the active areas are mainly responsible for the decrease of the limiting current and slope values. When the electrode surfaces are covered with Lacomit, a lower limiting current is obtained as less active area is available for oxygen-reduction reaction. Therefore, a lower slope value of a final-plot is achieved for specimens covered with Lacomit compared to the initial-plot (specimens without Lacomit).

This also further verifies the calibrations and SIJ cell rig development such as nozzle geometry arrangement, selected flow regimes and other parameters, which enables an electrochemical measurement to be used for scale detection study.

The scale coverage results estimated by the electrochemical technique are in agreement with the scale coverage obtained using the image analysis technique as shown in Figure 5-26. There is a slight variation of scale coverage between these two techniques, however it is less than 7 % difference for both techniques. Hence a good correlation between the electrochemical analysis and the images analysis is obtained and it is a reliable technique to detect the scale coverage for electrochemical and image analysis to quantify the extent of scale deposited on electrode surfaces.

5.5.3.5 Conclusion of Sample Models-Lacomit

Results of the Lacomit sample models clearly indicate both techniques used for coverage quantification, the electrochemical and the image analysis techniques are

correlated. There is no discrepancy surface coverage between the quantification methods used.

5.6 Conclusions of the Development and Verifications of the Electrochemical Measurement Using a SIJ Cell Rig

The study has verified the use of the use of submerged impinging jet (SIJ) equipment setup for the electrochemical measurement. In order to perform an electrochemical measurement using oxygen as a tracer for the oxygen reduction process on the surface of the electrode, a well-defined laminar flow is necessary. This was established using the SIJ cell rig. The concept of uniform accessibility for mass transfer were testified using the nozzle geometry arranged for H/d=1 and r/d=0.3125.

The calibrations and verifications presented in this chapter, further strengthen the potential of this methodology to be used as a mean to investigate mineral scaling

- Surface simulation by using different sizes of electrode to represent different active surface areas has shown that the electrochemical measurement (limiting current) is solely responsible for the oxygen reduction process on the active surface areas of an electrode. A decrease of limiting current is corresponded to a smaller electrode size (less active areas) being used;
- The oxygen reduction coefficient ($D = 1.81X10^{-5}\ cm^2 s^{-1}$) obtained is in agreement with the values reported in literature where using various technique such as RDE ($1.72\ X\ 10^{-5}\ cm^2 s^{-1}$) [15].
- Model sample of Lacomit also demonstrated that a good correlation of scale quantified by the electrochemical technique and scale determined by image analysis technique. Image analysis also validated the electrochemical technique used to quantify the surface coverage.

The electrochemical measurement results clearly demonstrate that the SIJ cell rig set-up can be used to detect calcium carbonate deposition on the electrode surface by plotting the limiting current versus square root of the Reynolds' number. This methodology shows an accuracy of approximately 10%. An excellent correlation coefficient (R^2 =0.99) obtained for the initial analyse on unscaled electrode confirmed the validity of the following equation [112].

$$i_{\lim} = 1.51\mathrm{Re}^{0.5}(\frac{\nu}{D})^{0.33}(\frac{H}{d})^{-0.054} g(Sc)\frac{nAFCD}{d}$$

Chapter 6 An Investigation of SIJ as A Means of Detecting Mineral Scaling

6.1 Introduction

The development of a robust technique that is able to monitor and investigate mineral scaling on component surfaces has remained a major issue for the oil and gas industry. Any new technology development that capable of detecting or monitoring mineral scale deposition is benefit to industry.

Currently various techniques are available to detect and investigate mineral scale deposited on a component surface. Some common techniques like RDE [120], EIS [19], EQMB [17] and AFM [121] have widely been used in the laboratory stage to investigate the early stage of mineral scaling, whereas techniques such as Ultrasonic [31], acoustic emission techniques [122], Attenuation Total Reflectance [42] and Dual/Triple Gamma Ray Attenuation [20] have been involved at the commercial level or field trails. However, the accuracy of all these techniques is strongly influenced by the thickness layer of scale formed on a component surfaces, from a very initial stage of crystal nucleation to a multiple crystal layer formation. Usually electrochemical techniques are capable of detecting the thickness of a layer of mineral scale in μm to mm. Pressure monitoring and ultrasonic techniques require a certain thickness of mineral scale (cm range) and when there is significant scale built up in a system.

For this thesis, the research work is concentrated on the scale detection at the early stage of crystals growth. One of the main benefits of this is the pre-emptive actions that can be taken to prevent the further growth of the scale that will eventually cause the pipeline blockage. Hence, an electrochemical technique is selected to study and investigate scale deposition as presented in Figure 6-1. This technique is also superior to other prediction techniques such as using pressure monitoring method that often detects scale in later stage once the scale build up to a certain level. This is the crucial factor for avoiding an unscheduled production shut down which would cause significant financial losses in the oil and gas production.

Most of the scale detection technologies primarily focus on a laboratory research work to study and investigate early stage of mineral scaling. The transformation of laboratory techniques to a potential commercially viable technology remains a challenge for the industry. The use of an electrochemical technique like RDE has shown potential of transformation as compared to other electrochemical techniques. This technique is less complicated in terms of data interpretation as well as setup as in EIS, ultrasonic, attenuation technique. Most importantly, this technique can detect scale at the early stage of scaling process with an accuracy of 5 % which makes RDE potentially viable for development into a monitoring technique [15]. However, the application is restricted to being used in a high-pressure condition where sealing can be a potential issue at for a rotating part. The use of this technique is restricted to a deep-water environment especially for the new field in West Africa and Gulf of Mexico where high pressure is expected. Hence, an alternative novel approach using a submerged impinging jet (SIJ) system in conjunction with an electrochemical technique is developed to overcome issues with mechanically rotating parts. Some other features may be beneficial to the submerged impinging jet over other techniques are as below

- Easy equipment set up with a simple configuration compared to an Atomic Force Microscope (AFM);
- Data interpretation is less complicated compare to ultrasonic, electrochemical impedance spectroscopy;
- Less expensive compare to dual/triple gamma ray attenuation and AFM.

A summary of the existing techniques found in laboratory research and field trials stage as well as the current research work that concentrate on the development of the submerged impinging jet technique used to study mineral scaling is presented in Figure 6-1. The selected technique SIJ as a means of a reliable scale detection technique focuses at the early stage of scale growth. The background /understanding and validity of this technique were described in Chapter 4 and Chapter 5 respectively.

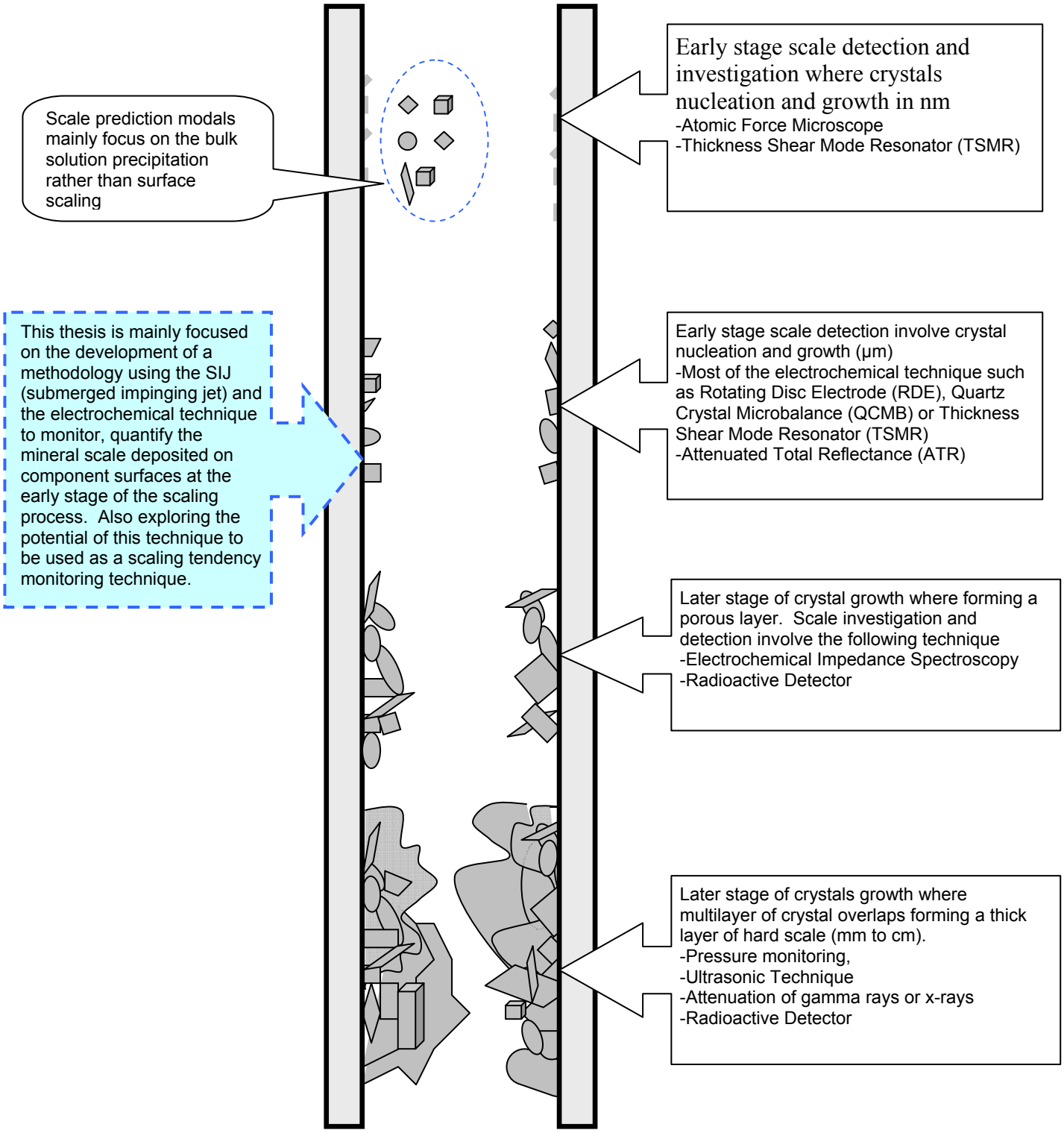

Figure 6-1 Representation of the new developed methodology fit into the overall scale detection

6.2 An Introduction of Scale Coverage Investigation

The novelty of this technique is its capability of detecting mineral scaling on sensor surfaces using an electrochemical technique and an SIJ cell rig. The flow field is controlled by the submerged impinging jet (SIJ). In addition to detection, the amount of mineral scale deposited on the sensor surfaces can be quantified through this technique. The main purpose of this chapter is to present the results of this technique where this technique was being examined and accessed under various conditions.

The results are divided into two main sections. First, the accuracy and capability of this technique as a means of detection were testified by using calcium carbonate in the presence and absence of magnesium ions. The influence of divalent ions such as Mg^{2+}, Ni^{2+}, Mn^{2+} etc on calcium carbonate precipitation and morphologies was reported by many researchers. Morizot reported that a continuous thin Mg rich film formation is favourable as the Mg:Ca ratio increases [15]. Therefore, an Mg^{2+} containing solution was used to investigate scale detection and coverage for this study.

Secondly, the response of the sensor to different levels of mineral scale deposited on the sensor surfaces was investigated and presented. Different levels of mineral scale were deposited onto the surfaces of the specimen by immersing the specimens in the scaling solution for different durations. Subsequently analysis of morphology was conducted to give a better understanding of the effect crystal characteristics on the coverage measurements.

A control specimen (bare specimen) was used for every experiment to factor the error of this technique or the scale deposition processes. The error could be varied but generally, the maximum error of the electrochemical measurement using the SIJ configuration is about ± 10 %. This has been presented in Chapter 4 “Review and Development of a Submerged Impinging Jet as a Monitoring Sensor”.

6.3 The Use of SIJ to Detect Calcium Carbonate

The purpose of this experiment was to investigate and access the electrochemical measurements for calcium carbonate detection using a submerged impinging jet configuration. The principle of the surface coverage quantification is based on the surface changes on the electrode. It is assumed that the active areas changed from an

initial value of a bare electrode A_1 to the final value A_2 after calcium carbonate scale is deposited on electrode surfaces. The electrochemical reaction (oxygen reduction reaction) is assumed only to take place on the active surface areas. The change of the slope values, initial slope, K_i to final slope, K_f indicates the coverage of scale or the extent of scale deposited on the specimen surface as using equation below

$$Scale\ Coverage = \frac{Initial\ Slope - Final\ Slope}{Initial\ Slope} = \frac{K_i - K_f}{K_i}$$

Both K values are obtained by plotting i_L versus $Re^{½}$ for a bare and scale deposited specimen respectively. The study of scale deposition or scale detection on sensor surfaces was divided into four steps:

i.) Initial analysis to assess the bare specimen surface;
ii.) Deposition of calcium carbonate on the specimen surface;
iii.) Final analysis to assess the scaled specimen surface;
iv.) Post analysis to carry out an imaging and the electrochemical scale quantification.

Further details of each step or analysis can be found by referring to Chapter 5. Two identical tests were carried out to determine the scale covered on the specimen surface to ensure that reproducible results could be obtained. Calcium carbonate was deposited on the specimen surfaces by immersion in the scaling solution over different periods of time.

6.3.1 Calcium Carbonate with the Presence of Magnesium Ions

The study of calcium carbonate scale precipitation and deposition on specimen/ electrode surfaces involved four steps, as mentioned in previous section 6.3. Again, details of the procedures can be found in Chapter 5. The only difference is in step (ii), deposition process where calcium carbonate scale was deposited from the scaling solution consisting of magnesium ions using the RDE technique at 600 rpm. The specimen was immersed four different times (1, 4, 10 and 24 hours). For the control / blank-specimen, the initial and final analyses were performed without any scale deposited onto the specimen surfaces.

Microscopy and electrochemical measurement were two methods used to quantify the surface deposition. The result of coverage determined by both techniques for different

immersion times is presented as in Table 6-1. A general trend of scale coverage expected that coverage would increase as the immersion or deposition times increases. The average scale coverage value of the two identical experiments determined by the electrochemical technique showed coverage of 3 %, 40 %, 69 % and 77 %, which corresponded to the deposition time of 1, 4, 10 and 24 hours. The scale coverage determined by the image analysis indicated average values of 0.1 %, 24 %, 40 % and 52 % for the same deposition times as the electrochemical technique.

Deposition Time (hrs)	Scale Coverage (Electrochemical)				Scale Coverage (Image Analysis)			
	Test 1	Test 2	Average Coverage	Standard Deviation	Test 1	Test 2	Average Coverage	Standard Deviation
1	2.3	3.5	2.9	0.9	0.2	0.0	0.1	0.1
4	38.5	42.1	40.3	2.5	20.6	28.1	24.3	5.3
10	64.5	72.6	68.5	5.7	35.2	43.8	39.5	6.1
24	75.0	78.1	76.6	2.1	47.9	55.9	51.9	5.7
Control	-3.9	8.5	2.3	8.7	0	0	0.0	0.0

Table 6-1 Percentage of scale coverage quantified by the electrochemical and image analysis of which scale was deposited in the presence of magnesium ions for various deposition times

The amount of calcium carbonate scale covering specimen surfaces increases with time as shown in Figure 6-2. This result matched the finding of scale coverage determined by image analysis that also showed an increase of crystal density and coverage on specimen surfaces with an increase of times. Both techniques showed a good correlation as scale coverage increases with the deposition times. However, the percentage of scale coverage quantified by both methods was not perfectly matched. There was a discrepancy of coverage between the scale coverage determined by the electrochemical and the scale coverage determined by the image analysis as shown in Figure 6-2. This was especially obvious with deposition over 1 hour where there was a significant difference in coverage.

Scale coverage quantified by the electrochemical technique indicated a higher coverage (> 15 %) compared to the image analysis technique. Further investigations were carried out to investigate the discrepancy which including the effect of brine solution on surface modifications, scale detection using Rotating Disc Electrode and the accuracy of the image analysis technique to quantify calcium carbonate. Details and explanation regarding this discrepancy is presented in the following section 6.4.5. However result from further investigation concluded that the discrepancy is mainly attributed to the

limitation of the light microscope to detect small mineral crystals on the specimen surface during the image analysis as well as the error of this technique.

Scale coverage estimated by the electrochemical technique showed less than 10 % for 1 hour's deposition time compared to other deposition times. This gives an inaccurate means of determining scale coverage for any mineral scale covering less than 10 % of the specimen surface. No mineral scale was detected by the electrochemical technique and the image analysis during the first hour of deposition. This could be attributed to no crystals formed on the specimen surface. It has been reported that the presence of magnesium ions increases the induction time of crystal formation [71, 123]. This result corresponds to the light microscope images where no scale was detected, as in Figure 6-3. A similar experiment was carried out by Tao Chen [124] using the RDE to deposit crystals using the same chemical composition, but with a higher rotating speed of 1500 rpm. Tao Chen reported that the induction time is approximately 1 hour in a magnesium-free solution and, the induction increases to 4.5 hours in 400 ppm magnesium ions. However, for deposition times over 4 hours, scale coverage determined by the electrochemical technique can be quantified as an accurate technique to detect calcium carbonate scale.

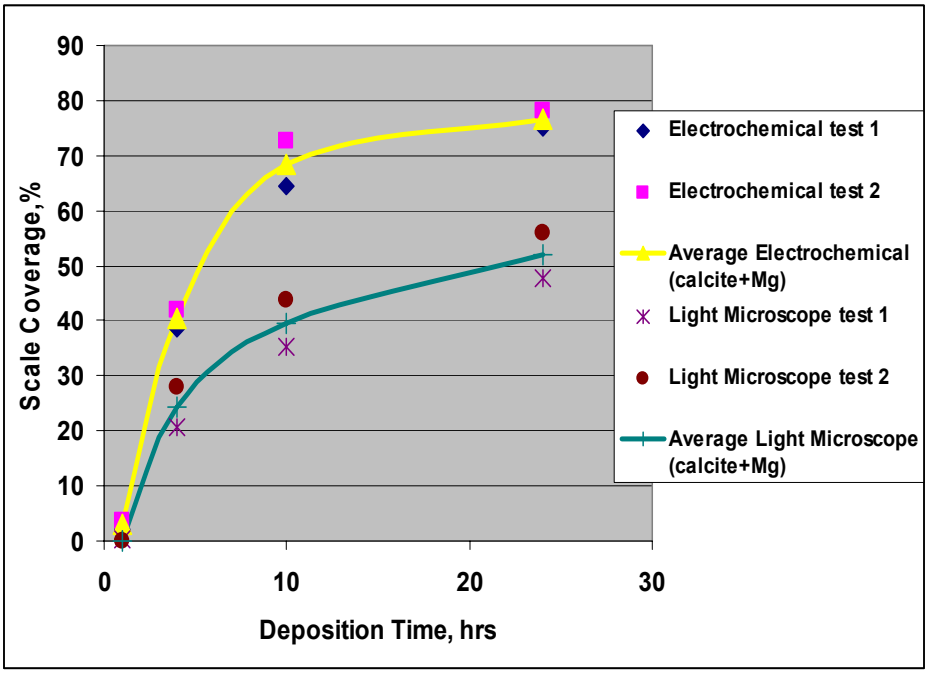

Figure 6-2 Percentage of scale coverage determined by the electrochemical and image analysis techniques which the specimen were deposited with calcium carbonate scale in the presence of magnesium ions for various deposition times

6.3.1.1 Image Analysis Examination

The crystal morphology such as the shapes and types of the crystals deposited can affect the scale coverage results since different crystal shapes may have different coverage on the surface. Part of the post analysis was to analyse the image and quantify calcium carbonate scale deposited on the specimen surface. All images used to analyse the crystal morphologies of calcium carbonate deposited on specimen surfaces were taken by a light microscope. The images were then used to quantify the amount of scale covered on specimen surfaces using an image analysis software. Further details of the procedures can be found by referring to Chapter 5 "Experimental Procedures and Calibrations".

The images of the two identical tests showed a more or less similar percentage of mineral coverage on the specimen surfaces, with approximately ± 6 % difference between the two experiments. However, only test 2 images are presented where calcium carbonate was being deposited on the specimen surface in a magnesium ions solution for 1, 4, 10, and 24 hours. The scale coverage determined by the image analysis indicated the average values of 0.1 %, 24 %, 40 % and 52 % for 1, 4, 10 and 24 hours of deposition. After an hour of scale deposition, no crystals were found on specimen surfaces as is clearly shown in Figure 6-3 (a) to Figure 6-3 (b) which represents the surface of a specimen after 1 hour of scale deposition. However, under the light microscope, crystals could be easily seen on the specimen surfaces only after more than 4 hours of scale deposition. The crystal's size increases as immersion time increases. This is strongly supported by the images shown in Figure 6-4, an increase in crystal sizes as the scale deposition time increases for 4, 10 and 24 hours.

Mixtures of vaterite and calcite crystals were deposited on the specimen surface as shown in Figure 6-5 (a) and (b) respectively. Vaterite was presented as "apricot" like crystals as in Figure 6-5 (a) or round spherulitic shapes as in Figure 6-5 (b). Both edge-sharp and edge-rounded rhombohedra calcite were also found on specimen surfaces as shown in Figure 6-5 (a). Most of the calcite crystals are different sizes and randomly orientated. This suggested that it formed aggregated micro-crystals rather than layer-by-layer on the surfaces. The orientation of the crystals in respect to substrate was found to be random and uniform across the surfaces.

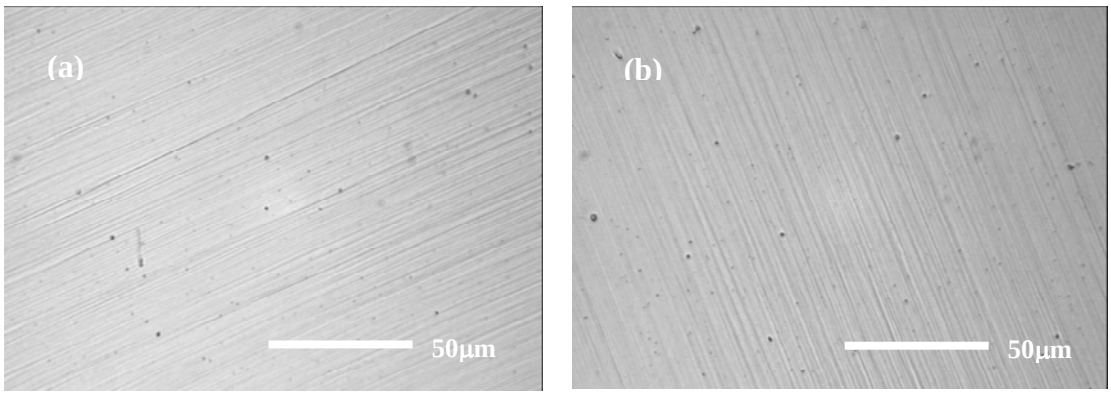

Figure 6-3 Surface conditions of the specimen (a) before scale deposition and (b) after deposited with scale $CaCO_3 + Mg^{2+}$ for 1 hour

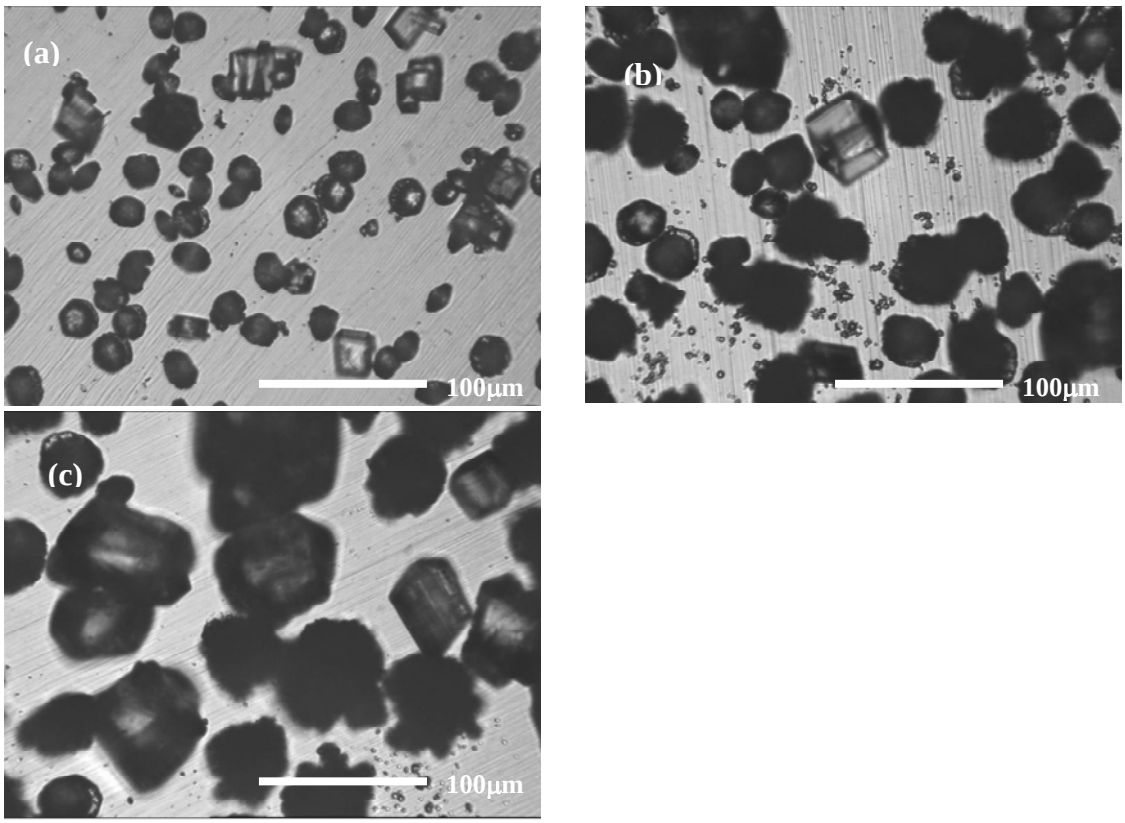

Figure 6-4 Surface conditions of the specimen after being deposited with scale $CaCO_3 + Mg^{2+}$ for (a) 4, (b) 10 and (c) 24 hours

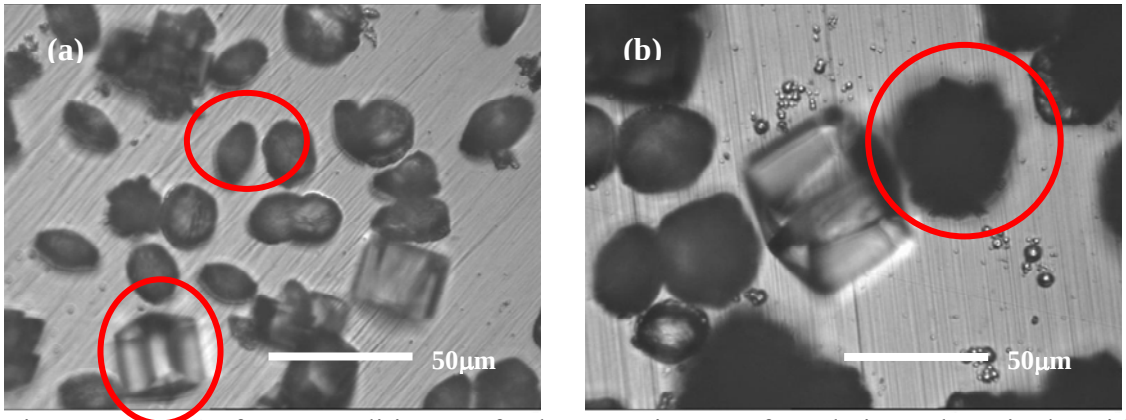

Figure 6-5 Surface conditions of the specimen after being deposited with $CaCO_3 + Mg^{2+}$ scale for (a) 4 hours, (b) 10 hours. Circle in image (a) apricot and (b) spherulitic shape of vaterite

There was a slight variation of calcium carbonate coverage in two identical tests for the same deposition time, as shown in Table 6-1. After 4 hours of scale deposition, the specimen surface coverage quantified by the electrochemical technique showed 39 % and 42 % for test 1 and test 2 respectively. While for the same deposition times, scale coverage quantified by the image analysis showed 21 % and 28 % for test 1 and test 2 respectively. This could be explained by the crystals density on the specimen surface. A higher and smaller size (an average 25 µm) was found in test 2 compared to test 1, which produced less crystals of a bigger size (an average 45 µm) on the specimen surfaces as shown in Figure 6-6. Therefore, a higher coverage was obtained for scale coverage quantified by both techniques for test 2 compare to test 1. In addition, the variations of these two tests may be due to the influence of surface conditions such as the surface finish of the specimen as well as variation in the alloy composition of the specimen, which could affect the scale deposition. The error of calcium carbonate scale surface deposition is about ± 25 % for each deposition process. However, this would not affect the application of SIJ as an electrochemical technique as a mean to detect the mineral scale on the sensor surfaces.

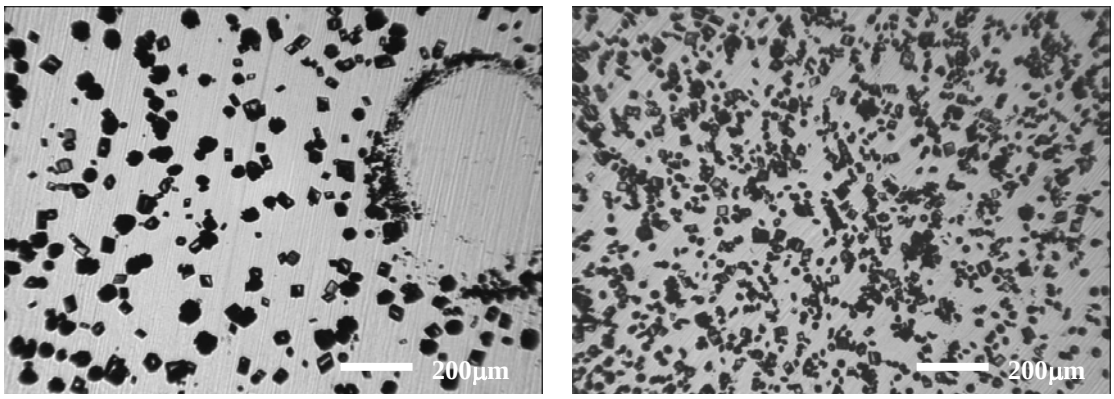

Figure 6-6 Surface conditions of the specimen after being deposited with scale $CaCO_3 + Mg^{2+}$ for test 1 (left) and test 2 (right)

6.3.1.2 Remarks of Calcium Carbonate Detection In The Presence of Magnesium Ions

Though there is significant difference in scale coverage determined by the electrochemical technique versus image analysis, both techniques show the capability of detecting different level of scale deposited on the electrode surface. The discrepancy of coverage determined by both techniques is mainly attributed by the presence of small scale and the limitation of the image analysis software to detect small amounts of mineral scale on the electrode's surface. The supporting evidence is presented in section 6.4.5. In addition, the use of SIJ as a means for electrochemical measurement has an accuracy of 10 %.

6.3.2 Calcium Carbonate with the Absence of Magnesium Ions

Generally, the experimental conditions and procedures to investigate the deposition of calcium carbonate without magnesium ions are the same as in section 6.3.1. The only difference is that calcium carbonate was deposited from a saturated scaling solution in the absence of magnesium ions. Again, two identical tests were carried out (tests 1 and 2) to quantify the scale coverage. The electrochemical and the image analysis techniques were used to quantify scale coverage as mentioned in the post analysis section found in Chapter 5, section 5.2.5. The percentage of calcium carbonate coverage (without magnesium ions) graph and the result data for both methods is presented in Figure 6-7 and Table 6-2 respectively. The percentage of scale coverage curve of calcium carbonate scale without magnesium ions shows a similar trend of curve as the calcium carbonate scale deposited in the presences of magnesium ions.

The scale coverage determined by the electrochemical and the image analysis technique showed significant discrepancy between these two techniques as shown in Figure 6-7. Average scale coverage determined by the electrochemical technique indicated a higher coverage value compared to the image analysis with respect to deposition times as shown in Table 6-2. However, both techniques showed increases of scale coverage as the deposition time increases. For example after 4 hours of scale deposition, calcium carbonate covered 32 % and 15 % on the specimen surfaces when the deposition was quantified by the electrochemical technique and the image analysis respectively as shown in Figure 6-7. Again scale deposited in the absence of magnesium ions showed similar results as previous section where significant discrepancy of coverage quantify between the image analysis and the electrochemical measurement. A difference of more than 15 % coverage is found for between both techniques. This suggested the discrepancy is not caused by the presence of magnesium ions. Further investigations were carried out and included in the late stage of the investigation.

Deposition Time (hrs)	Scale Coverage (Electrochemical)				Scale Coverage (Image Analysis)			
	Test 1	Test 2	Average Coverage	Standard Deviation	Test 1	Test 2	Average Coverage	Standard Deviation
1	3.0	-5.5	-1.3	5.9	0.1	0.5	0.3	0.3
4	34.9	29.7	32.3	3.7	22.9	15.6	19.2	5.2
10	59.1	52.8	56.0	4.5	33.0	30.8	31.9	1.5
24	61.7	64.9	63.3	2.2	40.8	50.0	42.4	2.2
Control	-2.7	-8.4	-5.5	4.1	0.0	0.0	0.0	0.0

Table 6-2 Percentage of scale coverage quantified by the electrochemical and image analysis of which scale is deposited in the absence of magnesium ions over various deposition times

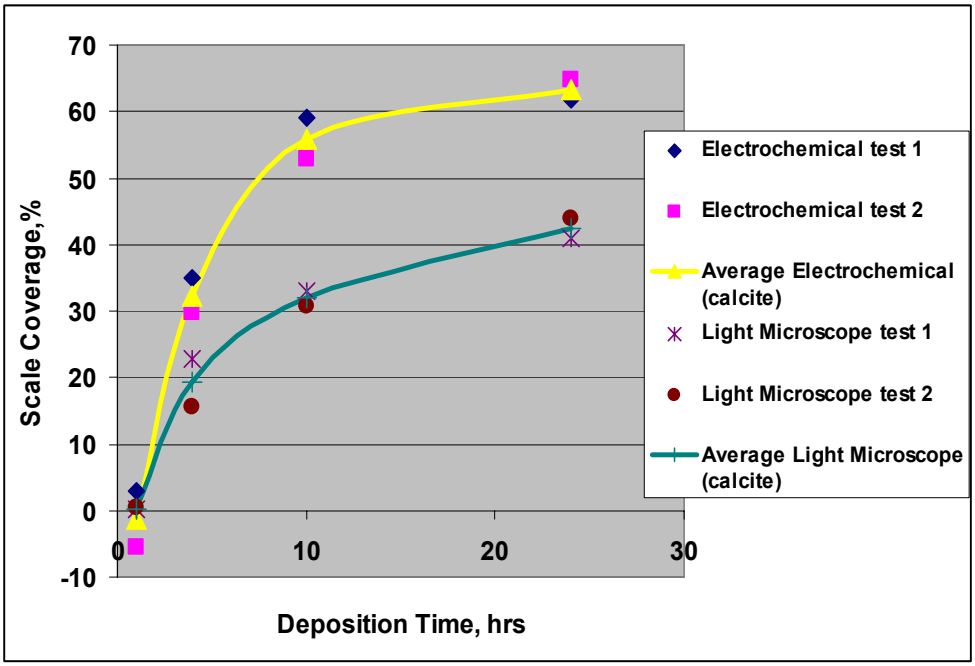

Figure 6-7 Scale coverage is determined by the electrochemical and the image analysis technique for calcium carbonate scale in the absence of magnesium ions

Table 6-2 represents the percentage of scale coverage quantified by electrochemical analysis. The average of scale coverage determined by the electrochemical technique showed coverage of -1 %, 32 %, 56 % and 63 % for deposition times 1, 4, 10 and 24 hours. For the same deposition times, the percentage of scale coverage quantified by the image analysis technique showed 0.3 %, 19 %, 32 % and 42 %. Results of two identical tests are presented in Table 6-2. For the control experiment, scale coverage quantified by the electrochemical technique indicated coverage of -3 % and -8 % for test 1 and test 2 respectively. The negative values could be explained as the inaccuracy of the SIJ technique to detect the calcium carbonate. However, for deposition times over 4 hours, scale coverage determined by the electrochemical technique could be quantified as an accurate technique to detect calcium carbonate scale.

6.3.2.1 Crystal Morphology of Calcium Carbonate

Only light microscope images from Test 2 are displayed where calcium carbonate in the absence of magnesium ions was deposited on specimen surfaces for deposition times of 1, 4, 10, and 24 hours. For an hour immersion time, no calcium carbonate scale was deposited on specimen surfaces as presented in Figure 6-8. As the deposition time exceeds 4 hours, small calcite crystals were found and the crystal density increases when the deposition time increases as shown in Figure 6-9 after (a) 4, (b) 10 and (c) 24 hours of deposition. Observation of the crystal size was increased as times increases.

Crystal size of ~ 48 μm over 4 hour scale deposition increase to ~ 57 μm after 10 hours of deposition and finally after 24 hours of scale deposition, the crystal size was about 75 μm. The crystal morphology of calcium carbonate, without magnesium ions mainly composed of calcite and vaterite, are found on the specimen surfaces for all deposition times. Calcite exists as perfect sharp-edged rhombohedra and cubic crystals, as shown in Figure 6-10. Vaterite presents as a spherulitic shape as in Figure 6-11.

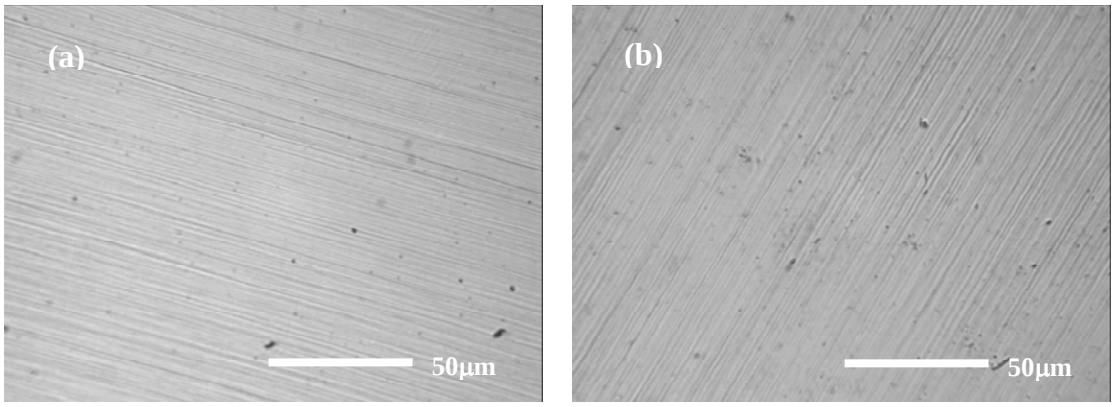

Figure 6-8 Representation of the surface conditions (a) before scale is deposited on specimen (b) after 1 hour of ($CaCO_3$) scale deposition on specimen surfaces

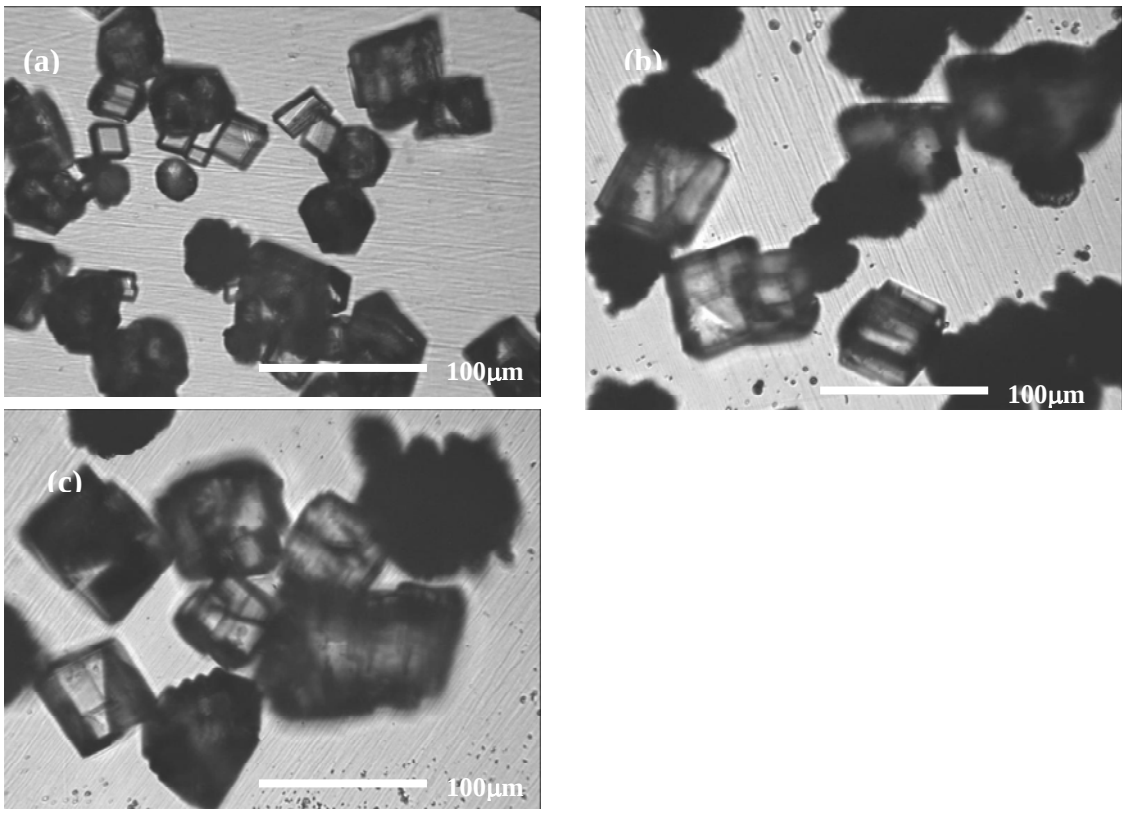

Figure 6-9 Surface of specimen after 4, 10 and 24 hours of $CaCO_3$ deposition

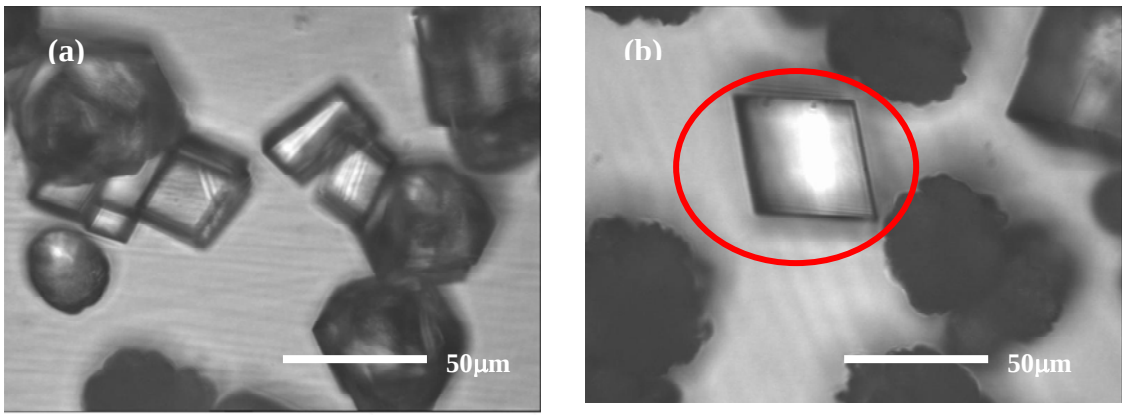

Figure 6-10 (a) Cubic and (b) rhombohedral shape of calcite after 4 hours and 10 hours of $CaCO_3$ scale deposition respectively

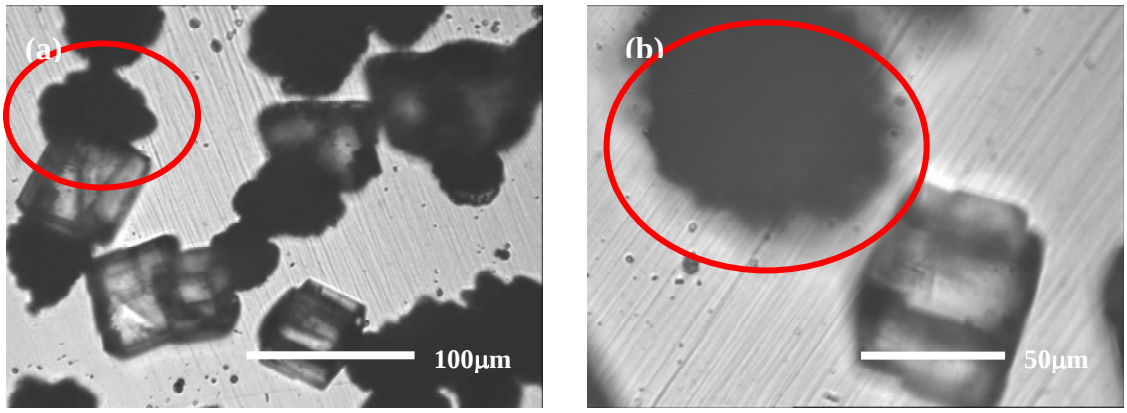

Figure 6-11 Spherulitic shape of vaterite found on the specimen surfaces after (a) 10 and (b) 24 hours of $CaCO_3$ scale deposition respectively

6.3.3 The Effect of Magnesium Ions on Scale Coverage Quantification

The presence of magnesium ions has an effect on the crystal morphology deposited on the surface of an electrode. Depending of the morphology of the crystals, as well as the crystal structure (calcite, vaterite or aragonite structure), these parameters can have significantly influence on the electrochemical technique used to quantify the amount of calcium carbonate deposited on electrode surface. This is because the crystalline structure and the morphology of the $CaCO_3$ crystals deposited may have different blocking effect on the electrode surface.

Two kinds of polymorph could be seen on the specimen's surface, calcite and vaterite having a structure of perfect or rounded-edge rhombohedra and spherulite respectively. The predominant crystals are calcite with rhombohedral crystals irrespective to absence

and presence of magnesium ions. However, with the presence of magnesium ions the calcite becomes a mixture of cubic and rounded calcite. Evidence of the retardant or inhibitory effect of magnesium ion on the growth of calcite crystals can be seen, as a smaller crystal size compared to calcite deposited in the absence of magnesium ions as shown in Figure 6-12. This result is in agreement with literature where calcite growth is inhibited by magnesium ions [125, 126]. Various explanations exist for the change of morphology in the calcite crystals in the presence of the magnesium ions in the electrolyte exist, using the seeded-growth method have shown that divalent cations, especially magnesium ion inhibit the growth of calcite [126-128]. The magnesium ion acts as an inhibitor on calcite surfaces where it preferably adsorbs and incorporates into the calcite crystal lattice [78, 129]. This modifies and suppresses the growth rate of crystals in certain directions. Ion substitution mechanism is proposed by Reddy [127] that calcium ion is substituted by magnesium ion in the lattice of calcite and causes dehydration of magnesium ion at the growth site reducing the overall growth rate. As a result of ion substitution, there is a faster dissolution rate of magnesium-calcite than pure calcite. Berner [130] reported that the solubility of calcite increases two fold due to magnesium inclusion into calcite lattice. The incorporation of magnesium ion causes strain in the lattice that leads to faster dissolution [127].

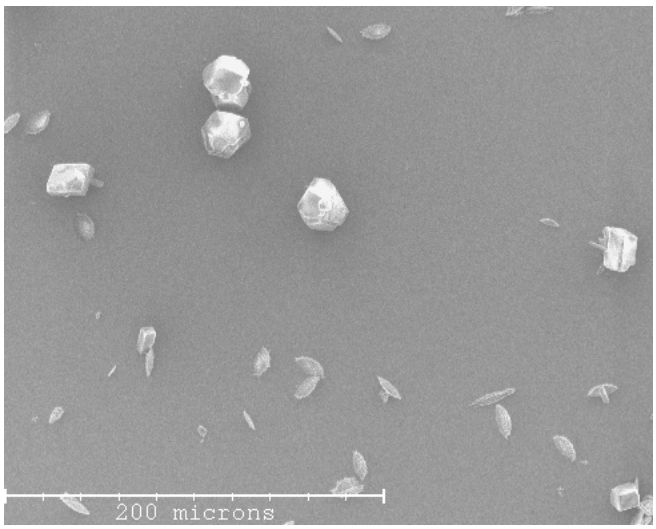

Figure 6-12 The effect of magnesium ion on calcite crystal causing rounded edge

There have been many reports on the effect of magnesium ions in the acceleration of the crystallisation of aragonite [59, 127, 131-133]. Aragonite crystals are usually stable at high temperature conditions and typically crystallize in preference to the thermodynamically stable calcite, when the Mg concentration is sufficiently high (2400 ppm [124] and 993 ppm [63]). However, in this work no aragonite was found on the

electrode surface the presence of magnesium ions. In the existing study, the Mg ions concentration was 91 ppm, which is well below the reported level in literature [124, 129].

The presence of Mg ions in this study is too low to cause any crystal modification or crystal morphology. It is difficult to quantify the scale coverage based purely on the crystal morphology through the electrochemical or image analysis techniques because most of the crystals found on the specimen are more or less the same for the experiment presence and absence of magnesium ions (calcite and vaterite). However, scale deposited with the presence of magnesium in the scaling solution shows a higher coverage compared to the scaling solution containing no magnesium as shown in Figure 6-13. Crystals formed in the presence of magnesium show a smaller crystal size but a higher density compared to those formed in the absence of magnesium, where crystals are bigger and less dense for all the deposition time. The presence of magnesium ions in the solution inhibits the growth of the calcite; therefore a magnesium-free solution has a faster growth rate and produces a bigger crystal size. Hence the scale coverage quantified by both techniques; the electrochemical and image analysis shows a higher coverage for calcium carbonate scale deposited with the magnesium ions.

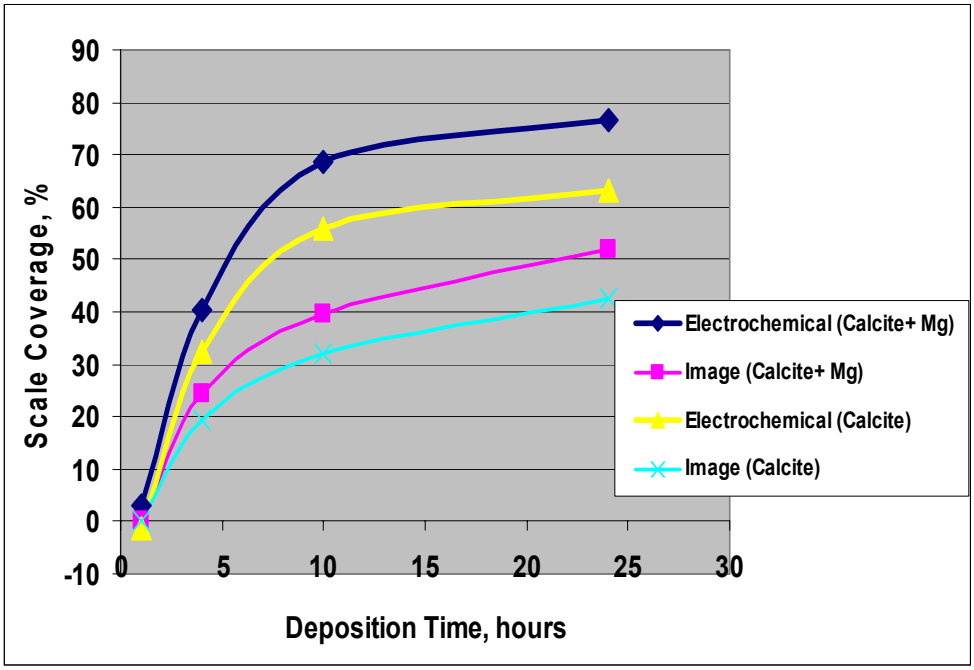

Figure 6-13 Percentage of scale coverage determined by the electrochemical and image analysis techniques which the specimen are deposited by calcium carbonate scale in the absence and presence of magnesium ions for various deposition times

In order to compare the mineral scale covering where a specimen was deposited with and without the presence of magnesium ions, a ratio is introduced. The electrochemical technique is capable of differentiating calcium carbonate in the presence and absence of magnesium ions covered on the surface through the ratio quantification, approximately 1.2 times higher of scale coverage for calcium carbonate deposited in the absence of magnesium ions comparing to calcium carbonate deposited with the presence of magnesium ions. Evidence of a consistency of coverage ratio of 1.2 determined with respect to deposition time for the electrochemical technique and image analysis is presented in Table 6-3 and Table 6-4 respectively. The concentration or the ratio of magnesium to calcium ($^{[Mg]}/_{[Ca]}$) used throughout this experiment was 0.104 irrespective to deposition time. The consistence of coverage ratio may be related to magnesium. It is believed that the scale coverage in the presence of magnesium ion was mainly due to sub-micro crystals which unable to be detected by the light microscope. As this has been reported in Tao Chen [124], Morizot [15], they concluded deposition in the presence of magnesium ions, submicron crystals were discovered on the electrode surface.

Scale Deposition Time, Hrs	Average scale coverage of Electrochemical Technique		Coverage Ratio of Electrochemical
	$CaCO_3 + Mg^{2+}$	$CaCO_3$	$\frac{CaCO_3 + Mg^{2+}}{CaCO_3}$
4	**40.3**	**32.3**	**1.3**
10	**68.5**	**56.0**	**1.2**
24	**76.6**	**63.3**	**1.2**

Table 6-3 Average coverage for two identical tests and ratio coverage determined the electrochemical technique

Scale Deposition Time, Hrs	Average scale coverage of Image Technique		Coverage Ratio of Image
	$CaCO_3 + Mg^{2+}$	$CaCO_3$	$\frac{CaCO_3 + Mg^{2+}}{CaCO_3}$
4	**24.3**	**19.2**	**1.3**
10	**39.5**	**31.9**	**1.2**
24	**51.9**	**42.4**	**1.2**

Table 6-4 Average coverage for two identical tests and ratio coverage determined the image analysis technique

The scale coverage ratio of calcium carbonate coverage estimated by the image analysis technique to scale coverage determined the electrochemical technique showed a consistency ratio of 1.2 irrespective to magnesium ions. This implies the limitation of the use of image analysis software to detect small crystals formed on the surfaces. Therefore, the electrochemical technique gives a better accuracy to detect crystals mineral scale on specimen surface than the image analysis by the light microscope.

6.3.3.1 Conclusion of Scale Detection and Coverage Quantification

It is clearly demonstrated that scale can be detected and quantified by using this developed methodology, a methodology that uses the electrochemical technique and submerged impinging jet. This methodology is able to detect and quantify the amount of scale deposition especially the calcium carbonate scale especially for calcium carbonate formed in the absence or presence of magnesium ions. Calcium carbonate formed in the presence of magnesium ions is 1.6 times higher than in the absence of magnesium ions.

In this study, it is believed that scale coverage determined by the electrochemical technique represents the amount of crystals on the specimen surface quantitatively. A correction factor of 1.65 is needed when using image analysis to give good surface quantification accuracy under normal deposition process.

6.4 Further Investigation of Scale Coverage Discrepancy between the Image Analysis and Electrochemical Technique

Post analysis results from previous sections (to measure the extent of calcium carbonate scale or scale coverage) indicated that there was a discrepancy of percentage coverage of the amount calcium carbonate scale quantified by the electrochemical technique and the image analysis technique. Further investigations were carried out to investigate the discrepancy between these two techniques. It can be divided into four main parts:

i.) The effect of brine solution on surface modifications;
ii.) Scale detection using Rotating Disc Electrode (RDE) compared to the Submerged Impinging Jet (SIJ);
iii.) The influence of mineral deposition on electrochemical measurement;
iv.) The accuracy of the image analysis technique to quantify calcium carbonate.

6.4.1 The Effect of Brine Solution on Surface Coverage

The purpose of this experiment was to investigate the effect brine solution has on electrode surfaces after immersion into a brine solution. Throughout the experiment, it is assumed that the active area is changed from the initial value of the bare electrode A_1 to the final value A_2 as if any element deposited (mineral scale, corrosion scale). Any surface modifications on the electrode surface may affect the electrochemical measurement data that can lead to inaccurate of this technique. Therefore, an investigation was carried out to determine whether if any surface modification could be caused by any other chemical elements in the brine solution as a result of immersion during mineral deposition process. Different brine solutions and immersion times were used for this investigation. The steps involved in this investigation (the effect of brine on surface electrode) can be divided thus:

i.) Initial analysis;
ii.) Immersion of specimen into brine over various times;
iii.) Final analysis;
iv.) Post analysis.

The experimental procedures of the initial, final and post analysis can be referred to in Chapter 5. An experiment for control purposes was also included to ensure the experimental error such as a change of the analysis solution (especially oxygen content) used in the initial and final analysis is within the error limit. It also ensures the equipment set-up is in optimal condition for the electrochemical measurement. For the control experiment, the specimen was not immersed in the brine solution but only initial and final analyses were performed. The experiment condition for the immersion was the same as the calcium carbonate scale deposition processes, the only difference being the chemical composition of scaling solution used. Three brine solutions with different chemical elements were used and are shown as below:

i.) Brine solution consisting of $CaCl_2$ and $NaCl$;
ii.) Brine solution consisting of $NaHCO_3$ and $NaCl$;
iii.) Brine solution consisting of $MgCl_2$, $CaCl_2$ and $NaCl$.

Table 6-5 is the brine chemical compositions used to prepare the brine solutions. Deposition was performed at room temperature and atmospheric pressure. The brine solution was buffered at pH 6.7 near neutral condition to ensure the pH solution is not to acidic to dissolve mineral scale and too high to cause crystals precipitation. Procedures

involved in the post analysis to determine the scale coverage after immersion into the brine solution by the electrochemical and the image analysis can be found in Chapter 5.

Ion	Brine (i) (mg/l)	Brine (ii) (mg/l)	Brine (iii) (mg/l)
Na^+	6047	6873	4683
Mg^+	0	0	91
Ca^{2+}	1440	0	1440
Cl^-	11871	9323	12136
HCO^{-3}	0	930	0

Table 6-5 Represents the chemical compositions of three different brine solutions

This section describes how scale coverage was determined by the electrochemical technique from the post analysis. Scale coverage determined by the image analysis is not shown as no mineral scale was found on the specimen surfaces with respect to immersion times. Results of initial-plot, final-plot obtained from i_L versus $Re^{1/2}$ of the initial and final analyses respectively are presented in table format. The change of the initial-plot and final-plot of the curve indicates the coverage value or the extent amount of scale covered on specimen surfaces.

6.4.1.1 The effect of $CaCl_2$ and $NaCl$ Brine Solution

Specimens were immersed in the brine solution consisting of $CaCl_2$ and $NaCl$ for 1.5, 3, 6, 12 and 24 hours. Figure 6-14 shows the limiting current versus the square root of Reynolds number of the initial and final analyses for each deposition time. After immersion, the current density of the final analysis showed that the current density is more or less same as the current density obtained from the initial analysis (before immersion). Results of the initial-plot, final-plot and percentage of coverage for each immersion time are presented, as shown in Figure 6-14. The first part of the legend represents the type of analysis carried out and the second part of the legend represents the experiment conditions performed. The experiment can be the immersion time/deposition time. Example Legend Initial-6 Hrs as shown in Figure 6-14 indicates for the first part of legend the Initial is represented as an initial analysis and the second part of the legend, 6 hrs, is represented as the specimen was immersed for 6 hours.

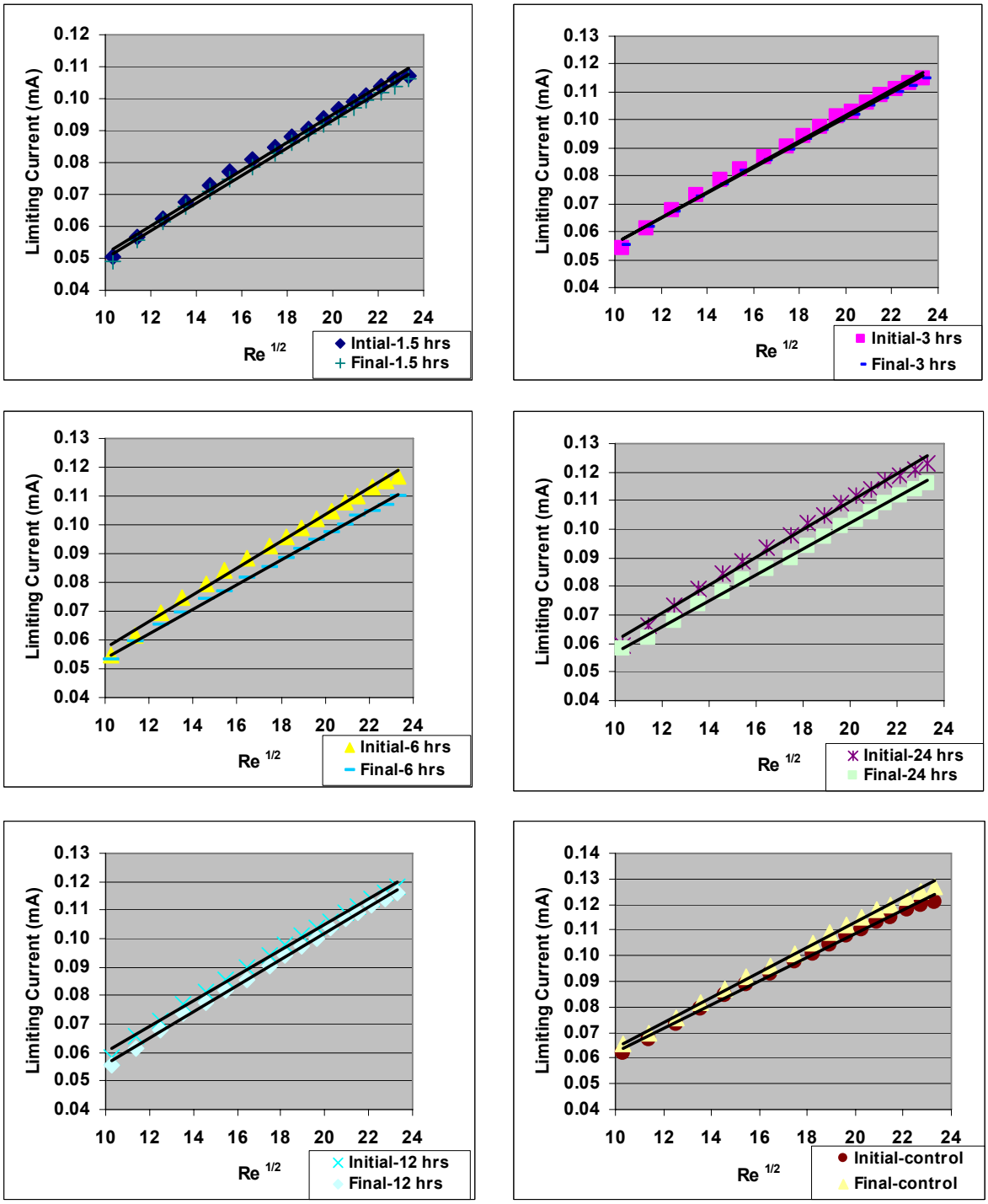

Figure 6-14 Representation of i_L versus $Re^{1/2}$ of the initial and final analyses of specimen before and after have been immersed for 1.5, 3, 6, 12, 24 hours, control specimen in a brine solution (i) respectively

The initial-plot and final-plot (slope value of i_L versus $Re^{1/2}$) shows similar results, which is in the range of 0.0043-0.0049 for the specimen before immersion and after immersion into the brine solution. Some negative values of coverage -2.2 and -6.5 were found for 12 hours of immersion and the control specimen respectively, this could be explained as mainly being due to the experimental error of this technique. Scale

coverage determined by the electrochemical technique showed within the error of the SIJ technique, within 10 % for all immersion times as shown in Table 6-6

Immersion Time, Hrs	Initial-plot	Final-plot	Percentage of Coverage
1.5	0.0043	0.0043	0.0
3	0.0046	0.0045	2.2
6	0.0046	0.0043	6.5
12	0.0045	0.0046	-2.2
24	0.0049	0.0045	8.2
Control/blank	0.0046	0.0049	-6.5

Table 6-6 Percentage of coverage determined from initial and final plots for different immersion times in the brine solution (i)

Image analysis was carried out to investigate the surface conditions of the electrode after immersed for 24 hours and no chemical element (mineral crystals) was deposited on the surface as shown in Figure 6-15. These results correspond to the electrochemical measurement data with no significant of coverage indicated. It is believed the electrochemical technique can provide a better method to detect any surface modifications comparing to the image analysis as it was hardly visible any surface modification using the light microscope.

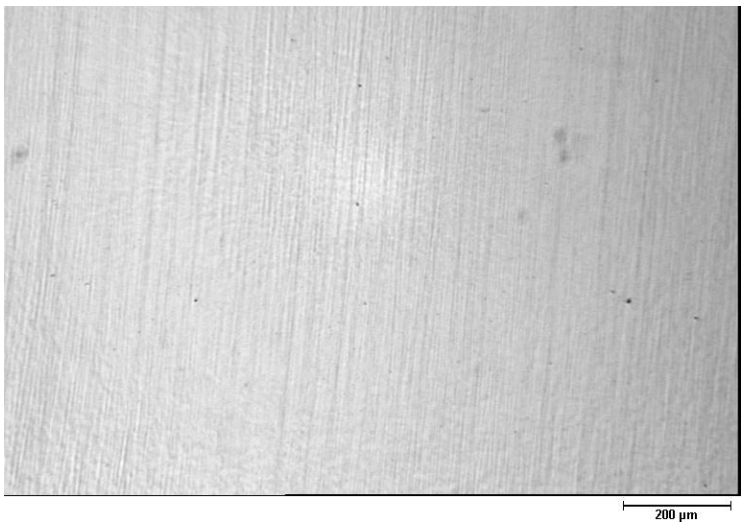

Figure 6-15 Represents the surface conditions of an electrode after 24 hours of immersion test

6.4.1.2 The Effect of $NaHCO_3$ and $NaCl$ Brine Solution

In this section, a brine solution consists of $NaHCO_3$ and $NaCl$ was used to study the brine effect on the specimen surfaces. Four immersion times were used in this experiment, 1, 3, 6, 12 and 24 hours. Figure 6-16 represents i_L versus $Re^{1/2}$ of the initial analysis (before immersion) and final analysis after specimens were immersed in the scaling solution for 1, 4, 12, 24 hours. The limiting current of final analysis is found to be lower than the initial analysis with respect to immersion times. Values of the initial-plot and final-plot were obtained from i_L versus $Re^{1/2}$ and are presented in Table 6-7. Scale coverage determined by the electrochemical technique found all specimens indicate surface coverage < 10 % after the specimen is immersed into brine (ii) but within the limit of this technique when revealed under a light microscope no scale can be found on the specimen's surface. Various immersion times and its coverage value are presented as in Table 6-7.

Immersion Time (Hrs)	Initial plot	Final plot	Percentage of Coverage
1	0.0053	0.0049	7.6
3	0.0054	0.0051	5.6
12	0.0053	0.0048	9.4
24	0.0056	0.0051	8.9
Control/ blank	0.0054	0.0051	5.6

Table 6-7 Percentage of coverage determined from initial and final plots for different immersion times in brine solution (ii)

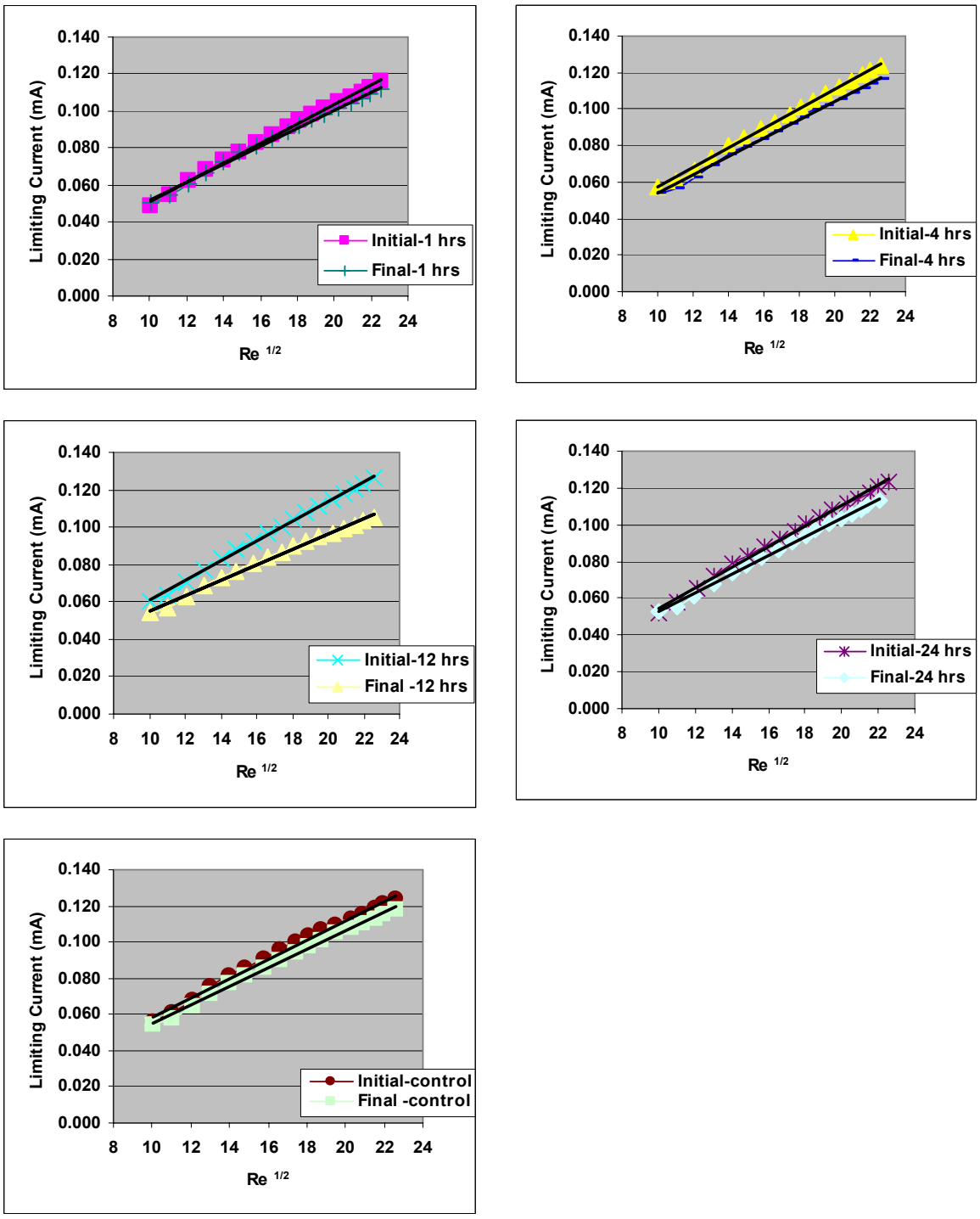

Figure 6-16 Representation of i_L vs. $Re^{½}$ of the initial and final analyses of specimen before and after immersed at 1, 4, 12, 24 hours, control specimen in a brine solution (ii) respectively.

Again similar results as using the brine solution consisting of $CaCl_2$ and $NaCl$ were found. It is also clearly indicated that the surface conditions of the electrode was not affected by polarisation process as there was not significantly changed in coverage for the control sample. Furthermore, the polarisation was performed under short period of

time (less than 10 minutes), hence it is believed surface modification as a result of polarisation is insignificant to contribute any surface coverage. As the result presented shows no sign of coverage on the electrode surface when brine solution consisting of $CaCl_2$ and $NaCl$ is used. Hence, it can conclude this brine solution does not contribute any surface modification or coverage on the electrode.

6.4.1.3 The Effect of $MgCl_2$, $CaCl_2$ and $NaCl$ Brine Solution

The effect of electrode/specimen surface condition was investigated by immersing specimens for 1, 4, 10 and 24 hours in the brine solution consisting of $MgCl_2$, $CaCl_2$ and $NaCl$. Figure 6-17 shows the current versus the square root of the Reynolds number of the initial and final analyses. The current density of the final analysis was less than the current density obtained from the initial analysis with respect to immersion times. Table 6-8 shows the slope value of the initial and final plots of each immersion time. These values were obtained from the current versus the square root of the Reynolds number. The percentage of scale coverage quantified by the electrochemical technique is also presented as in Table 6-8. Although, there was a decrease of current density of the final analysis compared to initial analysis, the final-plot value remained more or less the same as the initial-plot. The coverage of the specimen are approximately 4 %, 5 %, 5 %, 9 % and 9 %, these correspond to immersion times of 1, 4, 10, 24 hours and control.

Immersion Time, (Hrs)	Initial Slope	Final Slope	Percentage of Coverage
Control/blank	0.0054	0.0049	9.3
1.0	0.0056	0.0054	3.6
4.0	0.0057	0.0054	5.3
10.0	0.0056	0.0053	5.4
24.0	0.0056	0.0051	8.9

Table 6-8 Percentage of coverage is determined from the initial and final plots of different immersion time in a brine solution (iii)

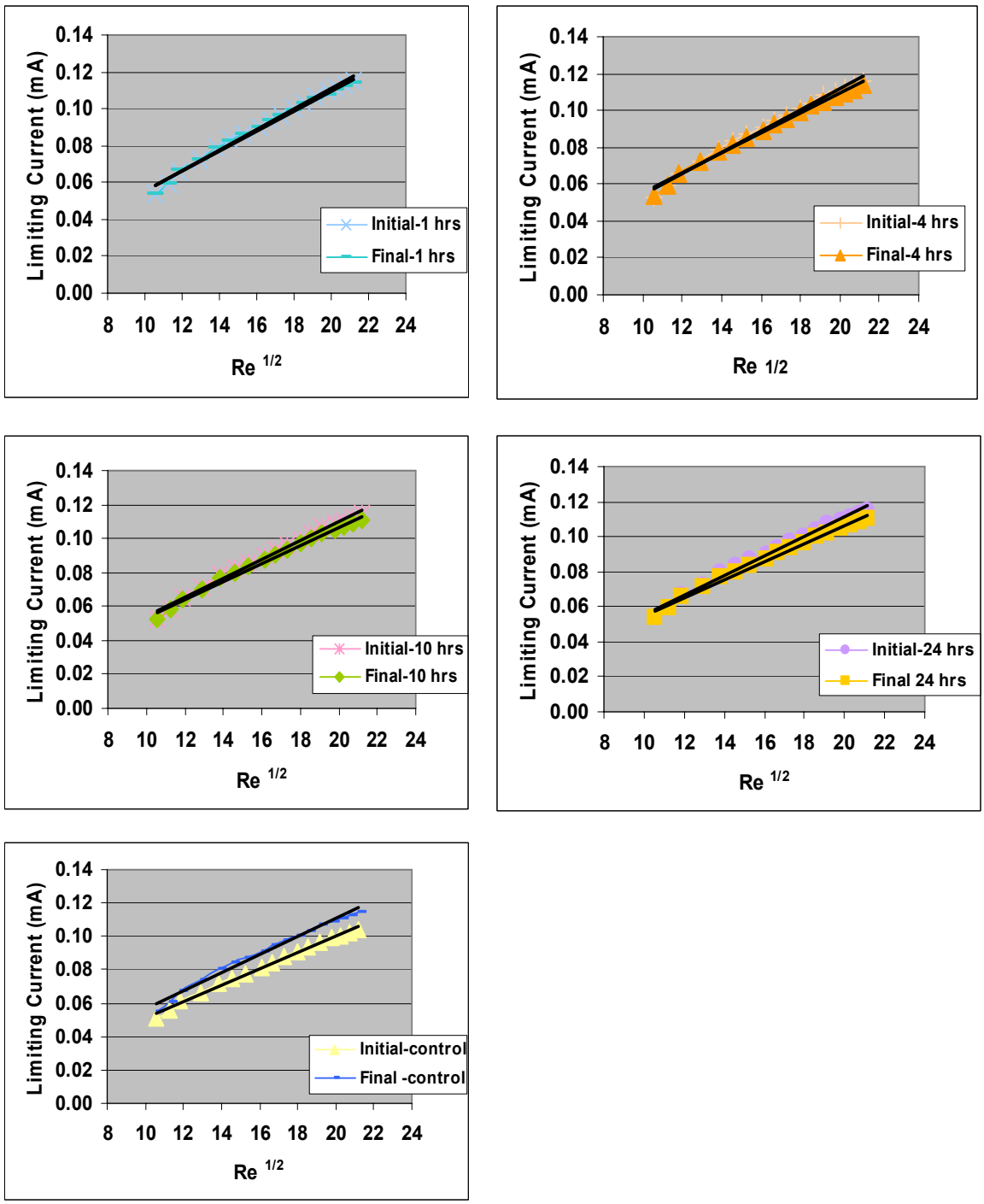

Figure 6-17 Representation of i_L versus $Re^{1/2}$ of initial and final analysis of specimen before immersion and after immersion over 1, 4, 10, 24 hours, control specimen in a brine solution (iii) respectively.

6.4.2 Overall Effect of the Brine Composition on Scale Coverage

The electrochemical measurement in a SIJ cell rig has demonstrated that oxygen reduction process can be easily quantified using a bare electrode. However, when it comes to scale quantification and detection of the scaled electrode, the influence of

scale deposited and surface modification could have a significant impact on the accuracy of this technique. The surface coverage may not be truly represented by the amount of mineral scale deposited on the specimen surfaces as a result of possibility surface modifications during the deposition or brine immersion processes. Often the surface modification is linked to surface corrosion related problems, passive layer film formation or complex film formation contributes to the surface modifications. Hence, a slightly higher percentage of scale coverage is estimated by the electrochemical technique for any complex film deposition and passive film formation.

The high corrosion resistance of the 316L stainless steel is attributable to the presence of a passive film [134]. This film is stable, invisible, thin, durable and extremely adherent and self-repairing. Although 316L stainless steel shows a very high corrosion resistance, there have been some failures of this material in many aggressive environments. This steel can suffer pitting corrosion in chloride environments [135]. It is well known that Cl^- ions are aggressive enough to attack steel and initiate pitting [136-139]. However, in this existing study, the risk of pitting corrosion is considered to be low as the pH solution is about neutral and it is in a flowing condition (600 rpm). Despite this, no pitting can be seen on all the specimens after immersing in for various times. Despite of no pitting corrosion, the possibility of chloride or bicarbonate ions adsorbed on the surface electrode cannot be excluded. The passive film formed on stainless steel depends on the solution being exposed. Generally, 316L in sodium chloride solutions containing bicarbonate ions consists of Fe_2O_3, Cr_2O_3, $(Fe,Cr)CO_3$ film and FeCl layer. Among the species, FeCl layer and $(Fe,Cr)CO_3$ is formed by Cl^- ion and HCO_3^- ion adsorptions [140]. However, with increasing HCO_3^- ion concentration in NaCl solutions, the formation of insoluble $(Fe,Cr)CO_3$ by HCO_3^- ions dominated over formation of the FeCl layer by Cl^- ions in the oxide film on type 316L stainless steel.

Many studies reported that the formation of $Mg(OH)_2$ on the surface only occurrs when an interfacial pH of an electrode is sufficient high. However, in the normal deposition process, the bulk pH of all test solution was about 6.7. Though no pH measurement were performed at the at the electrode/electrolyte interface, it is believed this pH and the concentration of magnesium ions are insufficient to promote the $Mg(OH)_2$ formations. An interfacial pH above 9.3 [103] is required to promote $Mg(OH)_2$ formation. Even the interfacial pH achieving pH 9.3 by means of cathodic polarisation, the low level of

magnesium ions is insufficient to promote the $Mg(OH)_2$ formation. The calculation of the solubility of $Mg(OH)_2$ is shown in section 7.3.1.2.

Experiment results showed the specimen's surface condition remained the same as the bare–specimen, even after a longer period 24 hours of normal immersion for all the brine solution including $NaHCO_3$ ($NaCl$, $NaHCO_3$ and $NaCl$) or $MgCl_2$ ($MgCl_2$, $CaCl_2$ and $NaCl$). This is covered in Chapter 8. The surface quantification is within the limit range and the electrochemical measurement is not affected.

6.4.2.1 Conclusions of Brine Solutions on Scale Coverage

It has been demonstrated that with respect of brine solutions and immersion times, the percentage of coverage determined by the electrochemical technique indicated no significant change on coverage percentage, results showed all the surface coverage on the electrodes are below 10 %. This is within the error limit of this technique as presented in section 5.5.3.3. Hence, the following findings can be made

- With respective of brine solution and immersion time, the potential of surface modifications on the electrode which may contribute to the surface coverage quantification measurement is insignificant and can be ignored. Even for the longest immersion test of 24 hours, the surface of the electrode remains unchanged;
- The electrochemical measurement used to quantify the percentage coverage is not affected by any of these brine solutions;
- It is clearly showed that electrochemical measurement through polarisation process does not affected or modified the surface conditions of an electrode. Also, it should be emphasised all the polarisations used for surface quantification are performed in a short period of time (less than 5 minutes).

6.4.3 Comparison of Scale Coverage Quantified By the RDE to SIJ

The RDE technique was used to assess the discrepancy of coverage results between the surface scaling quantified by the electrochemical measurement and the image analysis, since the RDE technique has been reported as one of the accurate methods to detect mineral scales, with an accuracy rate of 4~5 % [141]. Scale coverage quantified by electrochemical technique using the SIJ set up was verified using RDE technique. This also can provide further confirmation regarding if the discrepancy of calcium carbonate

coverage between the electrochemical technique and the image analysis technique as described in section 6.3 is mainly due to inaccurate either technique. A brief description of RDE to study the scale deposition is covered in the following section. Basically, the steps involved in studying scale coverage on surface specimen can be divided into a few stages.

i.) Initial analysis to polarise the bare specimen to obtain i_L vs. $\omega^{0.5}$;
ii.) Deposition of calcium carbonate scale by immersion into a scaling solution for various times to form a scaled-specimen;
iii.) Final analysis to polarise the scaled-specimen to obtain i_L vs. $\omega^{0.5}$;
iv.) Post analysis to quantify the scale coverage by the electrochemical technique and image analysis technique.

The experimental procedures and conditions to investigate scale coverage using SIJ technique can be referred to in section 5.2. For the RDE technique, the experimental procedures and conditions are basically the same, instead of the SIJ technique, it was replaced with the RDE technique, where a rotating disc electrode of 5 mm in diameter was used. The electrode is made from 316L stainless steel. The only difference in the RDE technique compared to SIJ is

i.) RDE uses a rotating electrode;
ii.) The limiting current is controlled only by mass transfer and is given by Levich's equation;
iii.) The electrochemical measurements of the initial and final analyses are limiting current versus square root of angular velocity, i_L vs. $\omega^{0.5}$.

The specimen was polarised at potential -0.8 V (Ag/AgCl) that corresponds to a diffusion plateau of oxygen while it rotates. The polarisation test lasted for 2-3 minutes. The initial and final analyses were determined by the RDE technique at a range of rotating speed of 3 to $9\omega^{0.5}$. At this range, the flow is well defined as laminar flow. The limiting current response to various rotating speeds was recorded and presented as i_L versus $\omega^{0.5}$. The limiting current for an oxygen reduction reaction is given by Levich's equation

$$i_L = 0.62\, nFCD^{2/3} \nu^{-1/6} \omega^{1/2} \qquad \text{Equation 6-1}$$

i_L = Limiting current, mA
n = number of electrons
F = Faraday constant, $C.mol^{-1}$
C = concentration of electroactive species, $mol.dm^{-3}$
D = diffusion coefficient, $cm^2.s^{-1}$
ω = angular speed of RDE, $rads^{-1}$
A = area of the electrode, cm^2
ν = kinematics viscosity of the electrolyte, $cm^2 s^{-1}$

For both techniques, RDE and SIJ, specimens were deposited with $CaCO_3$ from a supersaturated solution. The saturation ratio of the supersaturated solution of $CaCO_3$ free of Mg^{2+} is 17.8. Specimens were immersed into a scale-solution and the pH of the solution is adjusted to 6.7. Then it was deposited for different periods 1, 7, and 12 hours under static conditions. All depositions were carried out at room temperature and atmospheric pressure.

The initial analysis of the bare specimens and the final analysis of specimens that were deposited with scale onto the specimen surfaces for 1, 7 and 12 hours are shown in Figure 6-18. The right-hand column shows the graphs of i_L versus $Re^{½}$ for the initial and final analyses of those performed by the SIJ technique. The left-hand column of Figure 6-18 represents the graphs'analysis, performed using the RDE technique where limiting current versus angular velocity, (i_L vs. $\omega^{0.5}$) are plotted. The results of the initial-plot and final-plot of each deposition time of the SIJ and RDE technique are shown in Table 6-9 and Table 6-10 respectively.

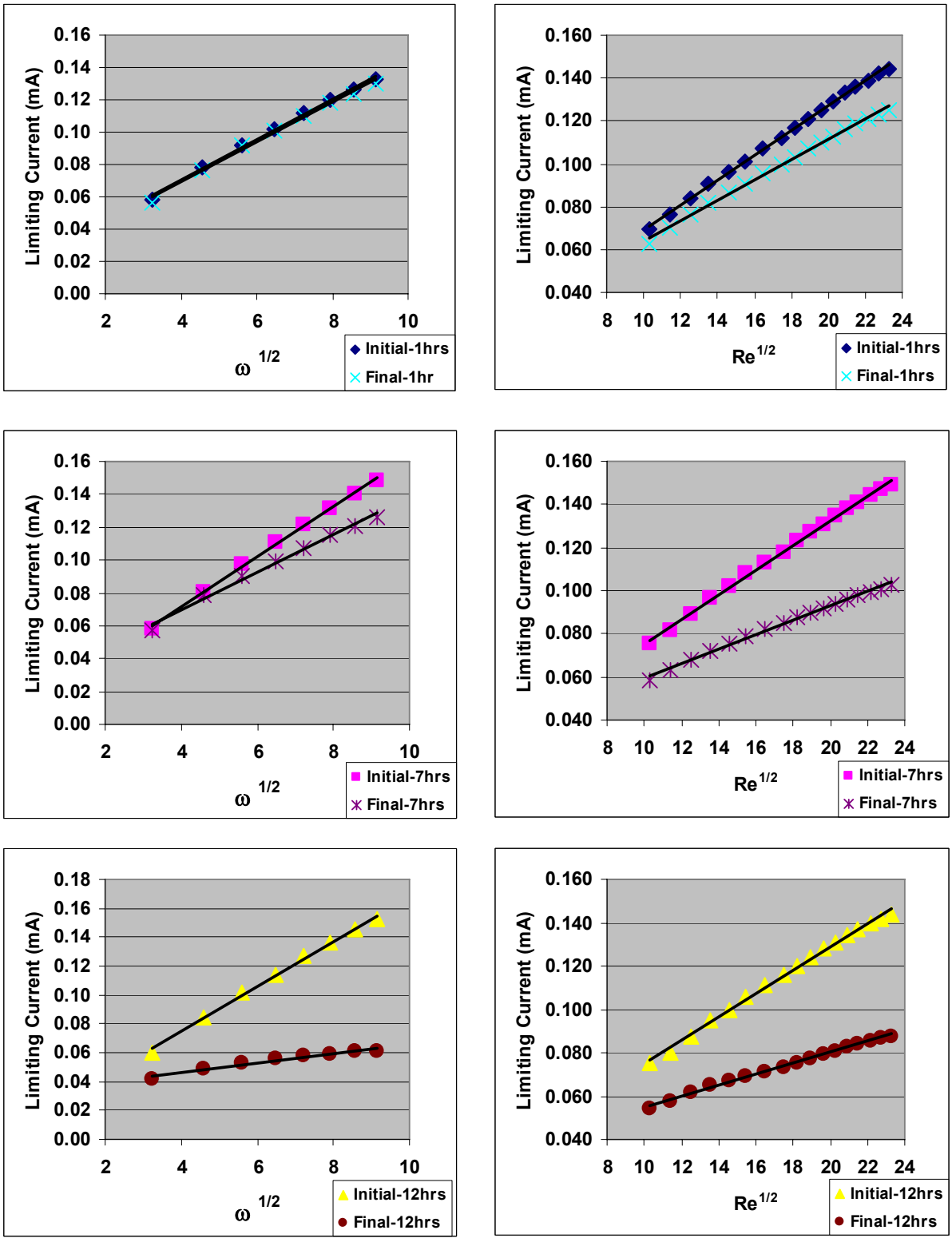

Figure 6-18 The initial and final plot of the slope of i_L versus $Re^{1/2}$ for the immersion time of 1, 7 and 12 hours. The left column for the RDE test and on the left column for the SIJ test

Post analysis was carried out to determine the scale coverage quantified by the electrochemical method by comparing the initial-plot and final-plot of (slope value) of the curve. In addition, images were taken from the light microscope were then analysed using image analysis software to determine the extent of scale covered on the specimen surfaces.

Figure 6-19 represents the quantified result of scale coverage determined by both methods (electrochemical and image analysis) using SIJ and RDE techniques. Scale coverage estimated by the RDE in conjunction with electrochemical technique showed 4 %, 29 % and 42 % that corresponds to deposition times of 1, 7 and 12 hours. For the same deposition times, image analysis obtained from this technique (RDE) showed 1 %, 3 % and 5 % as shown in Table 6-9. For the SIJ technique, scale coverage quantified using the electrochemical technique and image analysis are presented as shown in Table 6-10. The coverage determined by the electrochemical technique indicated 15 %, 42 % and 54 % and 2 %, 5 % and 8 % for scale quantified by the image analysis.

Scale coverage estimated using the SIJ technique showed coverage of mineral scale is about 15 % higher than RDE. The variation may be due to the characteristics and hydrodynamics of flow that are not exactly the same as the SIJ and RDE technique. Also, the assessment was performed using two different sets of specimen and there is some slight variation of the amount of scale deposited even in the same deposition conditions.

For both experiments, either scale coverage determined by electrochemical, or the light microscope analysis showed that scale coverage increases with deposition times as shown in Figure 6-19. However, it also found that there is discrepancy in percentage coverage (percentage of coverage is not matched) estimated by the electrochemical and scale coverage determined by the image analysis for the same deposition time using either SIJ or RDE techniques. SEM images also were carried out for the SIJ test to analyse the morphology of the crystals. Calcium carbonate in the crystal form of vaterite and calcite are found on specimen surfaces as shown in Figure 6-20. The average crystal size is 20 μm, however some crystals are smaller in size 1-2 μm are found on the specimen surfaces as shown in Figure 6-21.

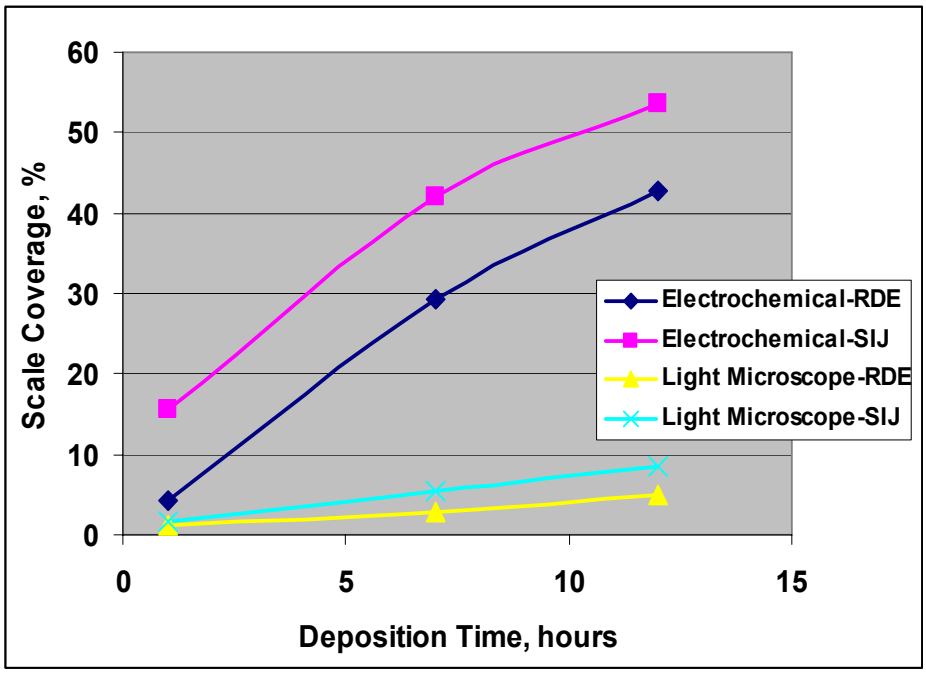

Figure 6-19 Post analysis to determine scale coverage using the electrochemical and image analysis (light microscope) for RDE and SIJ tests

Deposition Time (Hours)	Initial-plot	Final-plot	Scale Coverage , % (Electrochemical)	Scale Coverage , % (Image Analysis)
1	0.012	0.0115	4.2	1.3
7	0.015	0.0104	29.3	2.8
12	0.015	0.0086	42.7	4.9

Table 6-9 Result of the initial-plot, final-plot, the percentage of scale coverage determined by electrochemical and image analysis using the RDE method

Deposition Time (Hours)	Initial-plot	Final-plot	Scale Coverage, % (Electrochemical)	Scale Coverage, % (Image Analysis)
1	0.0058	0.0049	15.5	1.6
7	0.0057	0.0033	42.1	5.4
12	0.0054	0.0025	53.7	8.4

Table 6-10 Result of the initial-plot, final-plot, the percentage of scale coverage determined by electrochemical and image analysis using the SIJ method.

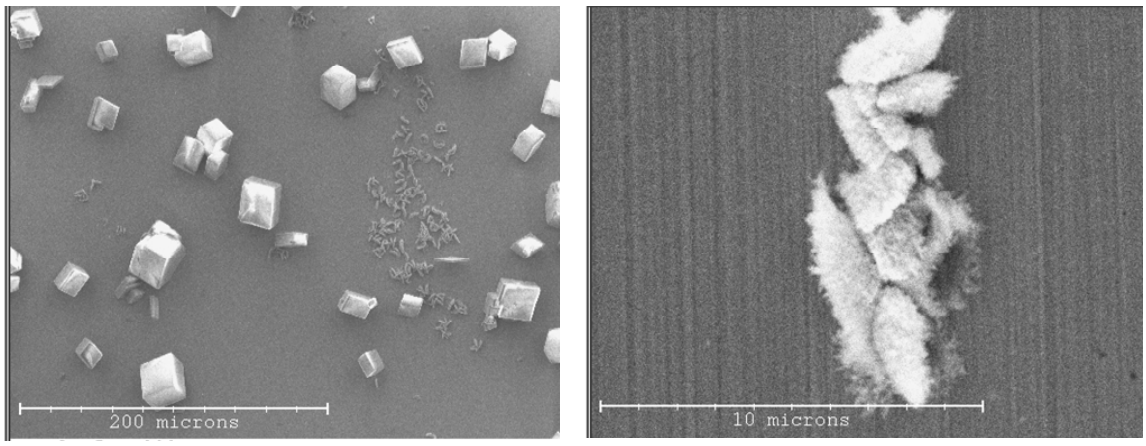

Figure 6-20 SEM images shows calcium carbonate exist as calcite (left) and vaterite (right)

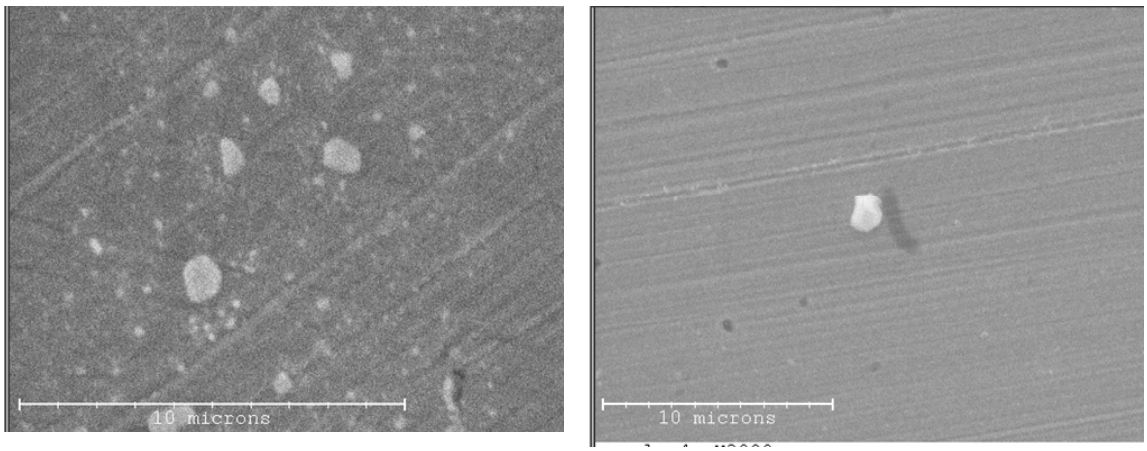

Figure 6-21 SEM images shows some small crystals deposited on the electrode surface

6.4.3.1 Conclusions of RDE Technique Comparing to the SIJ Technique

In the view of the results, the electrochemical technique used to assess the amount scale on the electrode surface for both RDE and SIJ technique indicated a similar trend of coverage. With respect to the techniques used (RDE or SIJ), the amount of scale covered on the electrode's surface quantified by the electrochemical measurement showed higher percentage of coverage compared to the scale quantified by the image analysis technique.

The combination of RDE and the electrochemical technique to enable comprehensive study of scale deposition has been reported by Morizot *et al*. [15, 22]. The authors claimed this technique has an accuracy rate of ± 5 % and is a good method to quantify scale deposition on specimen surfaces. This approach (RDE technique) was used to

validate the scale coverage discrepancy formed on specimen surface obtained by SIJ technique. Results from Figure 6-21 showed a RDE test highlighted a significant discrepancy of scale coverage between scale coverage quantified by an electrochemical technique and that determined by the image analysis using the RDE technique. This suggests the discrepancy scale coverage result between the image analysis and the electrochemical technique is not related to the application this methodology (the electrochemical measurement in a SIJ cell rig). This leads to the only possibility, the image analysis technique used to quantify the amount of scale on the electrode surface. The scale covered is being underestimated by the image analysis compared to the electrochemical technique. This is mainly due to two reasons limitation of the image analysis's software to analyse the scale and limitation to detect small crystal scales that will be presented in the following section 6.4.6. Hence, the actual coverage determined by the image analysis is less than the electrochemical technique. Also supporting evidence from SEM images indicated small calcium carbonate crystals found on the electrode surface.

6.4.4 The Influence of Crystal Deposited on Electrochemical Measurement

The surface finish of the electrode surface is considered to be extremely important in the electrochemical measurement. Roughness of the surface of the electrode has great influence on the current versus square root of the Reynolds' number. The current study has not investigated the surface conditions. However, it has demonstrated in section 5.5.3, all surface finishes with 6 μm diamond paste give good reproducible results. The surface finish quality of an electrode can be ensured by using the diamond paste.

The present of mineral crystals on the electrode surface were investigated. Two specimens, bare specimen and a scaled specimen were used to determine the i_L versus $Re^{½}$ as shown in Figure 6-22 (a) and (b) respectively. The scaled specimen was deposited with calcium carbonate scale for 24 hours with coverage of 75 %.

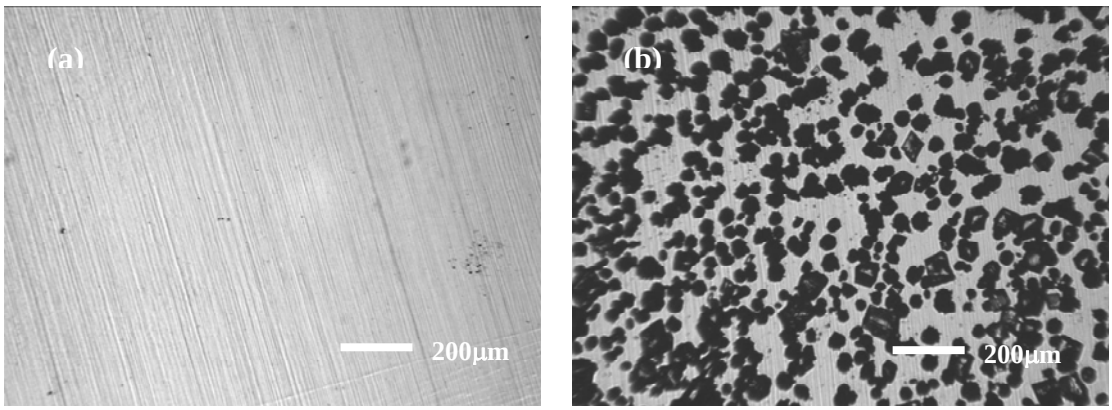

Figure 6-22 Surface condition of (a) bare specimen and (b) scaled specimen with 75 % of calcium carbonate coverage

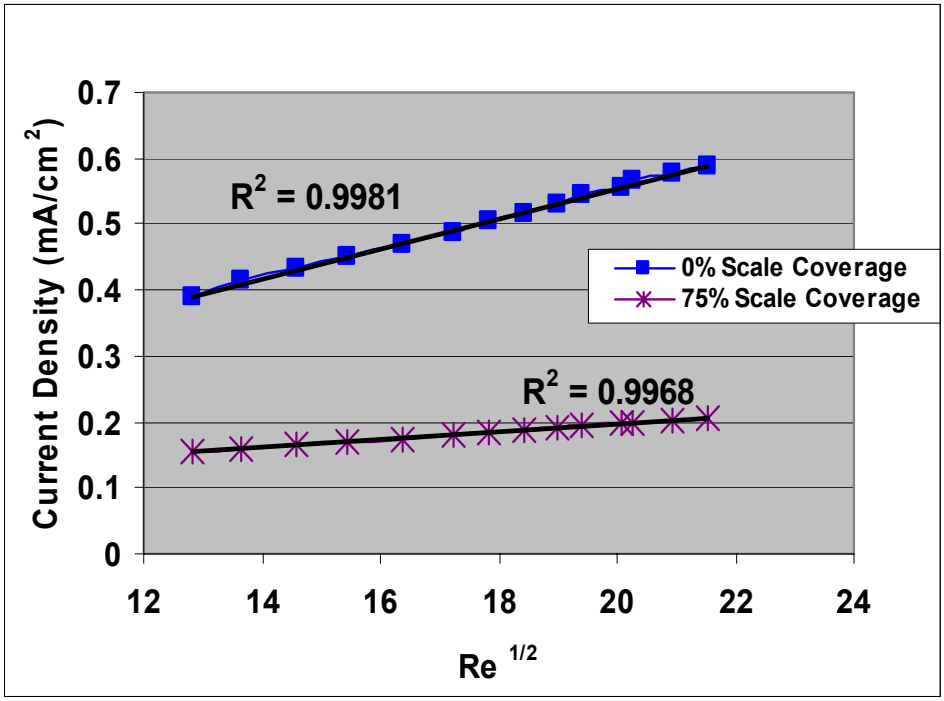

Figure 6-23 Represents the linearity of the best fit data of a bare specimen and a specimen 75% covered with calcium carbonate

The i_L versus $Re^{½}$ exhibited a small scattering and hence slight deviation from linearity not evident on the bare specimen as well as the scaled specimen as shown in Figure 6-23. A good correlation of the least square fits of the slope data is around 0.9968 ± 0.3 % which is within the limitation of this technique as demonstrated in section 5.5.3.3.

This technique relies on the entire surface being uniformly accessible for oxygen reduction. The presence of calcite or vaterite could induce local turbulence effects

which causing local turbulence and enhance the oxygen reduction process. This leads to an increase in the current density. No sign of increase in current density was observed for the scaled electrode. The presence of crystals on the surface specimen could generate some turbulence during the limiting current analysis and subsequently disturb locally the laminar flow induced by the impinging jet. However, this demonstrates that within the designated laminar flow regimes, the influence of calcium carbonate deposited is insignificant to provoke or destabilise the electrochemical current response as the regression fit of current versus square root of Reynolds' number achieved above 0.99. It is believed that local disturbance due to crystals only becomes significant when the crystal size exceeds the diffusion layer. Similar findings which use the rotating disc electrode to assess a scaled electrode were reported by Morizot [15].

The thickness of the diffusion layer generated by the SIJ is depend on the hydrodynamic flux as given below [142]

$$\delta_i = 1.6386 \times D_i^{1/3} \times \upsilon^{-1/3} \times \mathrm{Re}^{-1/2}$$

where δ_i is the thickness of the diffusion layer, υ is the kinematics viscosity, D_i is the diffusion coefficient and Re is the Reynolds Number. The maximum flow rate used in all the experiment was 200 ml/min (Re=530.32) and the thickness of the diffusion layer estimated is 145 μm ($D_{02} = 2 \times 10^{-5} cms^{-1}$, $\nu = 1 \times 10^{-2} cms^{-1}$). A similar value of diffusion thickness layer, 100 μm with twice the flow rate (400 ml/min) was reported by Devos *et al.* [143]. Majority of the deposited crystals are less than 100 μm and within the diffusional thickness layer and the electrochemical measurement is not affected by the local turbulence.

6.4.4.1 Conclusions of the Presence of Crystal on Electrochemical Measurement

The influence of surface roughness due to the presence of calcium carbonate scale deposited on the electrode surface is not significantly affected the electrochemical measurement as images of light microscope indicates that majority crystal size is < 100 μm which is within the estimated thickness value of the diffusion layer.

6.4.5 Investigations of Scale Coverage Discrepancy between the Electrochemical Versus the Image Analysis

The amount of calcium carbonate scale deposited on specimen surfaces was determined and quantified by the electrochemical and image analysis techniques. There was a discrepancy in scale coverage between the scale coverage determined by the electrochemical and scale coverage estimated by the image analysis for both experiments where calcium carbonate was deposited in the absence and presence of magnesium ions. This implies that the discrepancy of scale coverage determined by the electrochemical and the image analysis is not caused by the presence of magnesium ions. Although the presence of magnesium ions promotes formation of continuously Mg rich film formation and causing surface roughening has been reported in literature. The scale coverage estimated by the image analysis is less than the electrochemical technique is believed to be mainly due to two reasons,

i.) Limitation of the image analysis technique when the specimen is being analysed and quantified using the software. Figure 6-24 represents an image of calcium carbonate scale deposited on the specimen surface in the absence of magnesium ions for 12 hours. This is an image of specimen surface before scale coverage was estimated using image analysis software. The same image was used to estimate the amount of calcium carbonate scale covered on specimen surfaces by the image analysis software as shown in Figure 6-25 and Figure 6-26 respectively. Both figures indicate calcium carbonate coverage area was about 34 % and 44 % respectively. The scale coverage estimation determined by this software was based on the selection of the phase colour during the image analysis. Different sizes of crystal and orientation on specimen surfaces caused different contrasts or reflections when revealed under the light microscope. Therefore, there is a discrepancy of coverage estimated using the software. Ten measurements were carried out to determine the percentage of scale coverage by this technique. It indicated the error rate of scale coverage estimated by the image analysis is about ± 15 %;

ii.) Image analysis software used to analyse and estimate the mineral scale on specimen surface is unable to pick up small crystals. This is clearly indicated in Figure 6-25 and Figure 6-26 respectively, where small crystals were not encountered in the scale coverage analysis. The circle in Figure 6-25 represents small crystals (dark grey) which were not covered by the

analysis software. Hence, the actual scale coverage is less than it is supposed to be using this technique (image analysis) and it caused a discrepancy of coverage result.

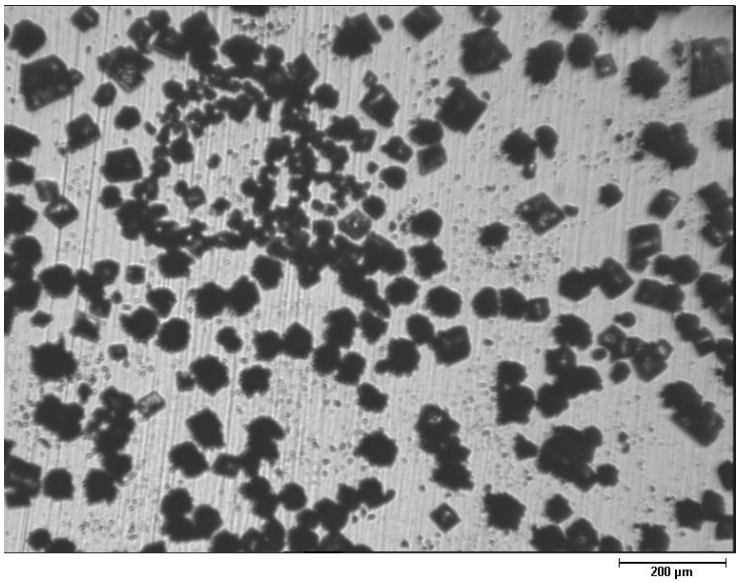

Figure 6-24 Image of calcium carbonate scales deposited on specimen surfaces after 12 hours of deposition in the absence of Mg

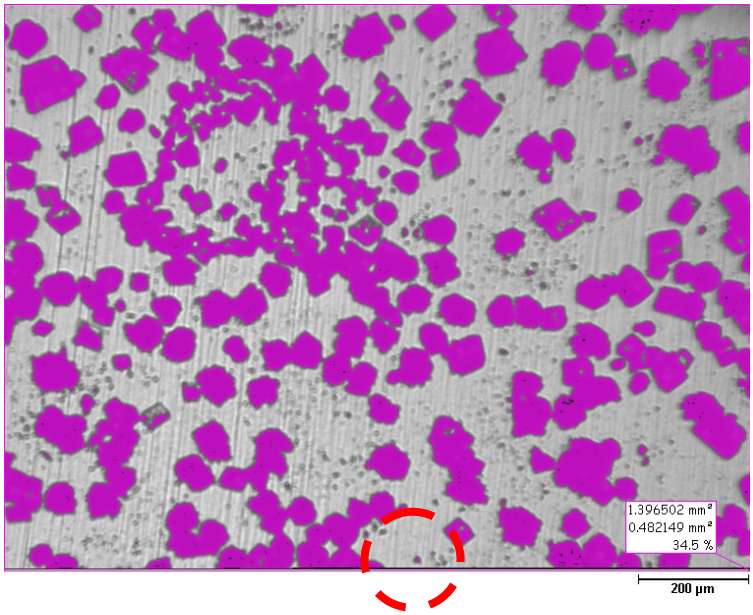

Figure 6-25 Purple colour represents the scale coverage estimated by the image analysis software and 34.5 % of coverage after 12 hours of deposition. The circle represents small crystals unable to be detected up by image analysis software

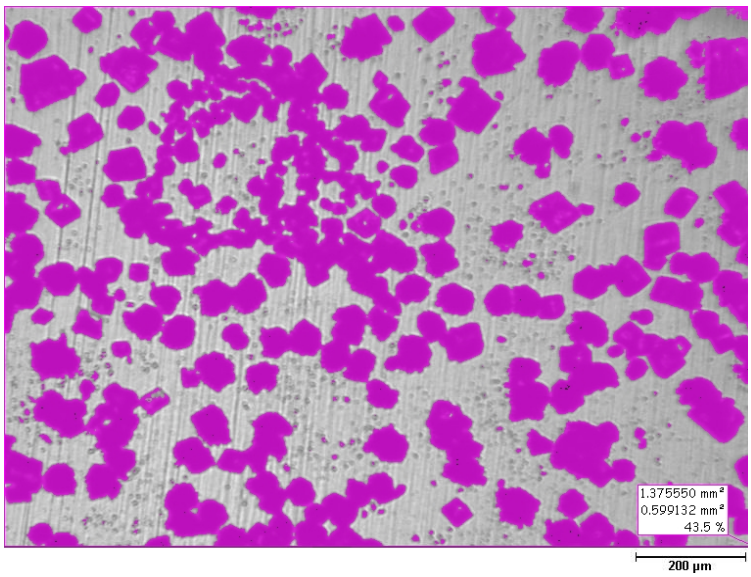

Figure 6-26 Scale coverage estimated by the image analysis software indicated 43.5 % of coverage after 12 hours of deposition

It is believed that scale coverage determined by the electrochemical technique represents the amount of crystals on the specimen surface quantitatively. It is expected that the higher scale coverage is quantified by the electrochemical measurement, the higher the surface area covered with mineral crystals. However, the scale coverage margin between each deposition time is small and a correction factor is required. Therefore, a correction factor or a ratio is needed when using image analysis to determine the extent of scale deposited on the specimen surface. A ratio of the scale coverage quantified by the electrochemical technique to the scale coverage quantified by the image analysis for various deposition times is presented as in Table 6-11. It is estimated an average correction factor of 1.6 for the image analysis with respect of calcium carbonate deposited in the presence or absence of magnesium ions as shown Table 6-11.

Deposition Time (hrs)	Scale Coverage Quantification for Calcite+Mg			Scale Coverage Quantification for Calcite		
	Electrochemical (calcite+Mg)	Light Microscope (calcite+Mg)	Ratio of Electrochemical to Image	Electrochemical (calcite)	Light Microscope (calcite)	Ratio of Electrochemical to Image
4	40.3	24.3	1.7	32.3	19.2	1.7
10	68.5	39.5	1.7	56.0	31.9	1.8
24	76.6	51.9	1.5	63.3	42.4	1.5
		AVERAGE	**1.62**		**AVERAGE**	**1.6**

Table 6-11 Ratio of percentage of scale coverage quantified by the electrochemical to the percentage of scale coverage quantified by the deposited in the presence and absence of magnesium ions for various deposition times

The scale coverage estimation determined by this software is based on the selection of the phase colour during the image analysis. Different sizes of crystal and orientation on specimen surfaces caused different contrasts or reflections when revealed under the light microscope. Therefore, there is a discrepancy in coverage when estimating using the software and it indicated the error rate of scale coverage estimated by the image analysis is about ± 15 %. Image analysis software used to analyse and estimate the mineral scale on specimen surface was unable to detect smaller crystals, approximately 1-2 um. Similar experiment conditions carried out by Tao Chen [115] also reported sub-micro of calcium carbonate scale found on specimen surface. Hence, the actual scale coverage is less than it is supposed to be using this technique (image analysis) and it caused a discrepancy in coverage result.

Based on these results, further confirmation of the significant difference of scale coverage between the electrochemical and the image analysis used for scale coverage determination is mainly due to other reasons and not the limitation of the SIJ technique as scale detection by the electrochemical technique.

6.4.6 Summary of Investigation of Scale Coverage Discrepancy between Electrochemical Technique and Image Analysis

The summary of experimental and findings for each investigation is presented as below: A summary of the experimental work and some of the main findings of the scale coverage discrepancy during the development of the submerged impinging jet technique used to study mineral scaling is presented in Figure 6-27. On the left hand section represents the experiment and on the right hand is the finding of the experiment.

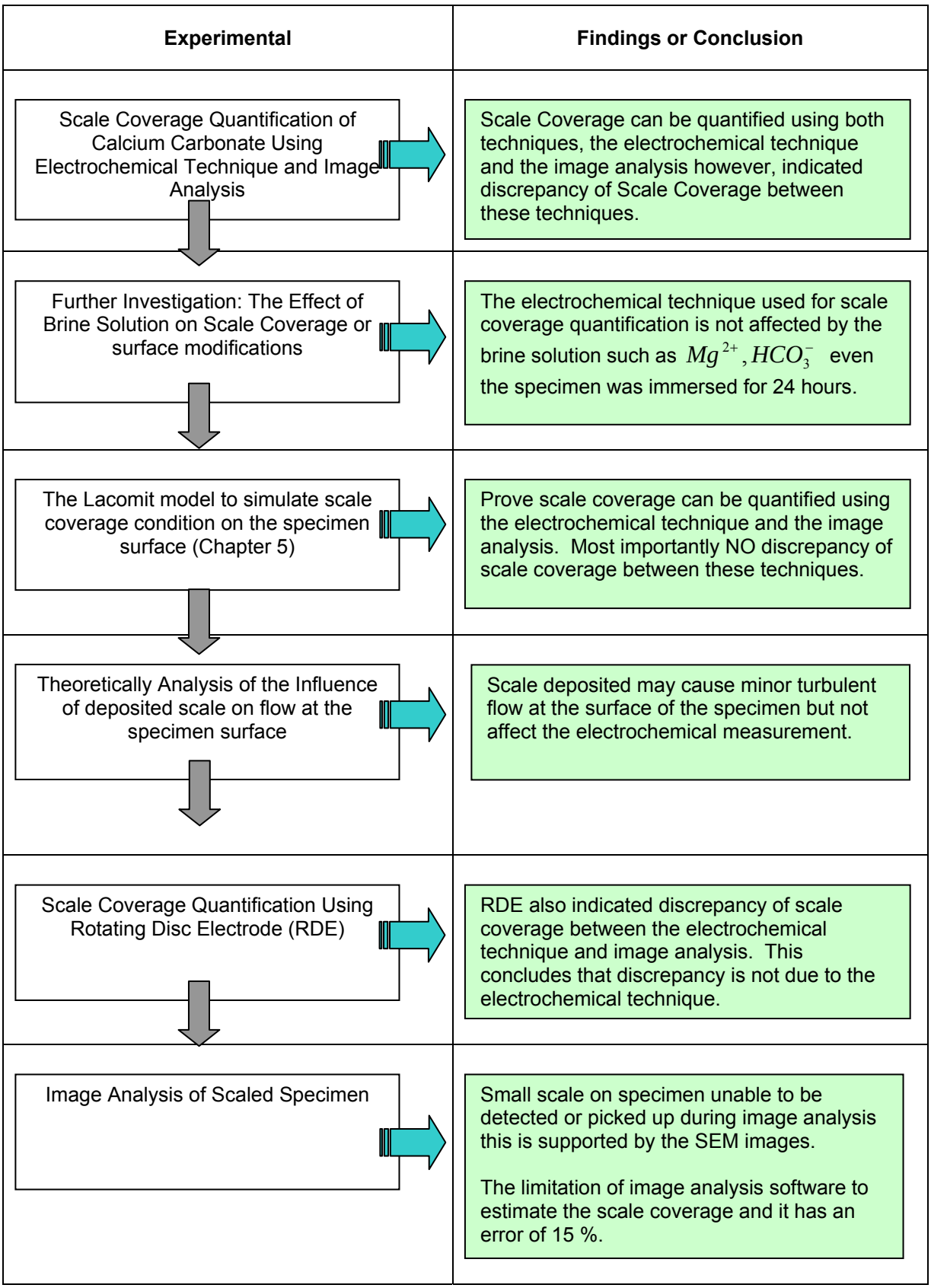

Figure 6-27 Summary of the experimental work to investigate the scale coverage discrepancy and findings

6.5 Concluding Remarks on Calcium Carbonate Detection

This technique has demonstrated the capability of an electrochemical measurement and SIJ configuration to detect mineral scale deposited on the electrode‘s surface. This technique not only detects the amount of scale deposited but is also capable of quantifying different levels of scale deposited on the electrode surface. However, calcium carbonate coverage quantified by the electrochemical technique using the SIJ technique shows a higher coverage comparing to scale quantified by the image analysis technique with respect to the deposition times. The discrepancy of coverage is mainly due to the limitation of the image analysis software and unable to detect small calcium carbonate deposited on the electrode’s surface.

Though the image analysis indicates less scale coverage quantified than the electrochemical technique, image analysis still can be used to quantify the amount of calcium carbonate deposited on an electrode surface by a correction factor of 1.6.

The presence of magnesium ions has influenced the crystal size and coverage on the surface where smaller crystal and less density of coverage. This is supported by the evidence of the light microscope images as well as scale coverage quantified by the electrochemical technique. Hence, this technique is also capable of differentiating calcium carbonate in the presence and absence of magnesium ions covered on the surface through the electrochemical quantification, approximately 1.2 times higher for scale coverage of calcium carbonate deposited in the absence of magnesium ions compared to calcium carbonate deposited with the presence of magnesium ions.

Chapter 7 An Investigation of Scaling Tendency

7.1 Introduction

Mineral scaling deposits often cause numerous technical and economical problems for industry processes. The issue of pipeline blockage leading to the decrease in production flow rate and reduction of the heat transfer efficiency in a heat exchanger are often the consequence of mineral scale deposition. Therefore, it is important to establish an appropriate method to study and monitor this phenomenon especially if the changes in water chemistry determine when a system is subjected to mineral scaling.

The potential for forming mineral scale for a brine/water system is often expressed as scaling tendency or scaling power. The higher the scaling tendency or scaling power, the more likely a system is to encounter mineral precipitation and deposition. The use of prediction models is one of the most common industry practices to determine the scaling tendency of a system. Usually the concentration of ions present in a brine system (e.g. barium or calcium ions concentration) is measured and used as a critical input data to predict the saturation ratio. During the previous decades, various electrochemical techniques focus on chronoamperometry, chronoelectrogravimetry and electrochemical impedance technique have been developed [13, 14, 18, 19]. These techniques are used as a means to study the nucleation and crystal growth process instead of scaling tendency. Each technique has its benefits and limitations as described in Chapter 2.

A saturation index or ratio has been used as the technique to estimate the scaling potential of a system, which often predicts the scaling in bulk solution rather than measuring the actual scaling conditions of a system. There is a lack of scaling tendency quantification research work found in the literature. Hence, this has led to the development of the current methodology (SIJ and electrochemical technique) which can be used to investigate and quantify the scaling potential. The main objective in this chapter is to study the feasibility of using the electrochemical measurement in a submerged impinging jet cell to determine and quantify a real life scaling formation process. The application of SIJ has overcome some of the issues such as monitoring the actual scaling tendency of a system rather than prediction or estimation as in most the prediction software.

7.2 A Brief Introduction of Background Technique of Scaling Tendency Measurement

The scaling power of water using the electrochemical precipitation of calcium carbonate was first proposed by Ledion [144]. The specimen is polarised at the potential corresponding to the reduction of the dissolved oxygen. The surface of an electrode is progressively covered by an insulating layer and the electrolysis current intensity decreases with time until it reaches zero. The characteristic of a decrease in current shape with time is related to the scaling power. The nucleation and growth kinetics of calcium carbonate by an electrochemical driving force has been studied in a more quantitative way by using an electrochemical quartz microbalance, which allows in situ measurements of the scale amount with respect to time to deduce the nucleation rate and the crystal growth rate [17, 145, 146]. To date no quantification and further assessment has been reported on the slope related to the saturation ratio of the water.

It is believed that scaling tendency can be determined through the electrochemical data. The SIJ cell equipment is used to control the flow in order to establish a laminar flow regime where the electrochemical measurement is performed. This methodology has been used as an accelerated test for $CaCO_3$ crystallisation by polarising a metallic electrode at a potential range sufficiently negative to promote the cathodic reduction of dissolved oxygen. The electrode is electrochemically polarised to a potential sufficiently negative (-0.8 V) where the reduction of the oxygen dissolved in the test water is given as

$$O_2 + 2H_2O + 4e^- \rightarrow 4OH^-$$

The generation of hydroxide ions at the vicinity of the electrode causes a local pH increment. As shown in the following steps, the local pH promotes the bicarbonate to turn into CO_3^{2-} that can be reacted with Ca^{2+} to form solid crystalline $CaCO_3$:

$$HCO_3 + OH^- \rightarrow CO_3^{2-} + H_2O$$

$$Ca^{2+} + CO_3^{2-} \rightarrow CaCO_3$$

The hypothesis is based on a reduction of limiting current being linear with the reduction of active area, as a result of progressive surface blockage by calcium carbonate. The limiting current is proportional to oxygen reduction reaction. It decreases as the active surface is progressively blocked by the growth of calcium

carbonate scale until it reaches a value close to zero when the surface is totally covered by the $CaCO_3$ insulating layer. It should be emphasised, all parameters such as the concentration of oxygen, diffusion coefficient and viscosity of the electrolyte are assumed to be constant at ambient temperature and atmospheric pressure except for the active areas. Therefore, the extent of scaling tendency of brine can be calculated and quantified by determining the slope value of limiting current versus time plot (i_L versus t). The details of the technique used to determine the scaling tendency was described in section 4.5. The changes of the scaling slope give or indicate the scaling tendency or water chemistry of the brine solution in a system.

The capability and sensitivity of the electrochemical technique to detect the changes of the scaling tendency of any brine in the system could be established through these tests. The scaling tendency investigation and quantification is only applied to calcium carbonate, as this mineral scale is pH sensitive as opposed to barium sulphate scale because neither barium ions nor sulphate ions are influenced by a change in pH.

In this chapter, the experiment results can be divided into three main sections as follows:

i.) Preliminary experiments-the influence of the brine composition on the scaling tendency measurement. The purpose of these experiments was to investigate the possible synergistic effects of the brine compositions on electrochemical measurement and also to understand the influence or the role of the element on scaling tendency measurement. Preliminary experiments were conducted to study the application of the SIJ as a means for the electrochemical measurements to detect and monitor the brine saturation ratio. Responses of the electrochemical data (current versus time) of different brine compositions were analysed and investigated;

ii.) Preliminary investigation of the scaling tendency determination using a brine solution consisting of calcium and carbonate ions. The purpose of this feasibility study was to establish and relate the electrochemical data to the scaling tendency of a brine solution;

iii.) Finally, different levels of brine saturation ratio were used to investigate or access the scaling tendency.

7.3 The Influence of Brine Compositions on Scaling Tendency

The scaling tendency measurement is based on the current responses of a polarised specimen in a solution contains calcium and carbonate ions. This measurement is strongly influenced by the operational parameters such as the brine chemistry, applied potential, surface finish of the electrode, flow conditions, temperature and pressure as previously described in Chapter 5. Any change of these parameters could impose a significant effect on the scaling tendency measurements. The study of the surface conditions and the flow effect on electrochemical measurement were demonstrated in calibrations and validations Chapter 5. Hence, the main purpose of the preliminary experiments was to examine the effect of various brine compositions on the scaling tendency measurements.

Four different brine solutions were used to investigate the current response of the electrochemical measurements. The specimen was polarised at -0.8 V (Ag/AgCl) for 2 hours and was subjected to the SIJ at a flow rate of 80 ml/min. Before starting the experiment, the brine pH was adjusted to 6.7 using acetic acid. When the specimen was polarised, the trend of current, as a function of time of the brine solution, was recorded and observed. Two experiments were conducted to ensure that reproducible results could be obtained. Different types of brine combinations were investigated and the chemical composition is listed in Chapter 5. The chemical elements are listed as below:

i.) $NaCl + CaCl_2$;

ii.) $NaCl + CaCl_2 + MgCl_2$;

iii.) $NaCl + NaHCO_3$;

iv.) $NaCl + NaHCO_3 + MgCl_2$.

Figure 7-1 (a) and (b) represents the current density as a function of time of brine i.) and ii.) respectively. Both brine solutions showed a slight increase in current density (towards a more negative direction). However, by comparing brine solution ii.) to brine solution i.), brine solution ii.) took longer to achieve a stable current. The only difference in both brines is the chemical composition, where brine ii.) consists of magnesium ions. Hence, a conclusion can be drawn from this observation that the presence of magnesium ions in the brine solution has caused a significant difference in current density response. A similar trend of curve could be observed for both brines consisting of $NaHCO_3$ (brine iii.) and (brine iv.), where a significant increase of current

density (towards a more negative current) at the initial stage (first 1500 s) and then a slower increase rate of the current density, as shown in Figure 7-2 (a) and (b) respectively.

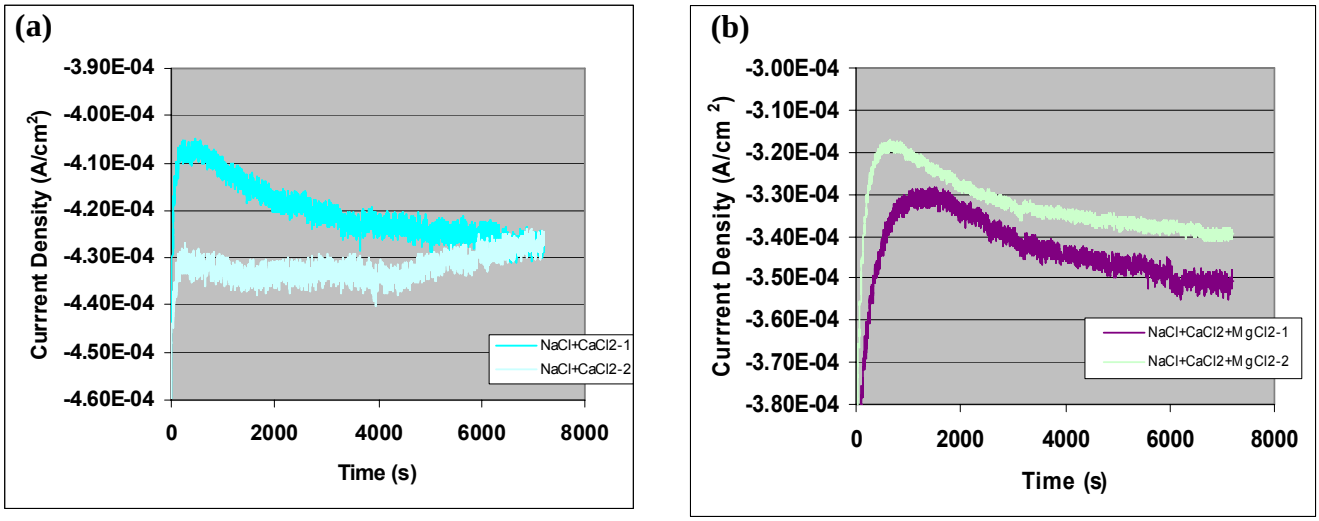

Figure 7-1 Current density versus time for two identical tests (1 and 2) that use the brine solution consisting of (a) NaCl and $CaCl_2$ and (b) NaCl, $CaCl_2$ and $MgCl_2$

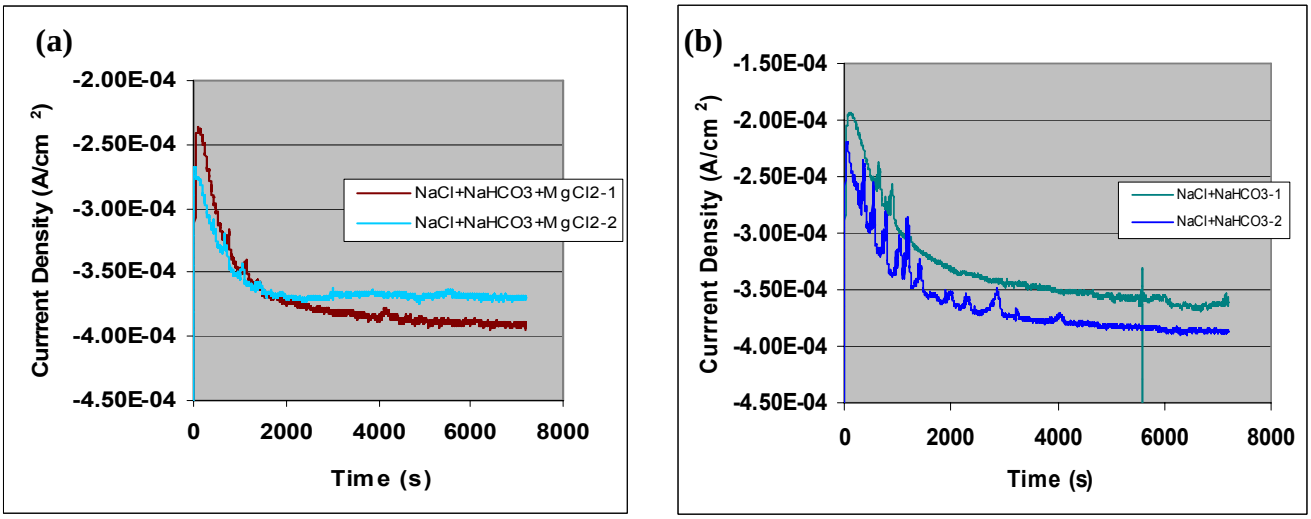

Figure 7-2 Current density versus time for two identical tests (1 and 2) that use the brine solution consisting of (a) NaCl, $NaHCO_3$ and $MgCl_2$ and (b) NaCl, $NaHCO_3$

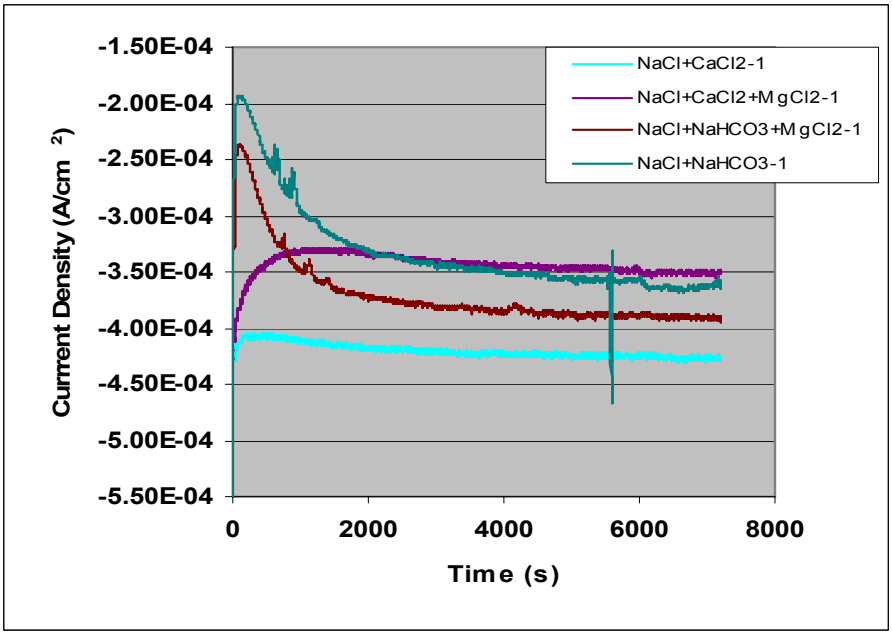

Figure 7-3 Result of current density versus time responses to different brine solutions for test 1

For comparison purposes, the current density versus time for four of the brine solutions of test 1 is presented as in Figure 7-3. The current density difference between the maximum value and minimum value of the current density in this graph for brine i.) and brine ii.) were approximately 2.0E-05 A/cm^2. Brine consisting $NaHCO_3$ (brine iii.) nd brine iv.)) indicated a different current density of 1.5E-04 A/cm^2 which was approximately 7 times higher. In addition, the brine solution consisting of magnesium ions and bicarbonate ions took a longer time to achieve stable current density approximately 1500 and 2000 seconds respectively as shown in Figure 7-3. Polarisation of the specimen using $NaHCO_3$ brine solution showed current density spiking. This suggests a film formation on the electrode surface. This film breakdown causes active area exposed to oxygen reduction and increase the current density.

Basically, the feature of the current response on each regime depends on two events performing in a synergetic way, reduction of the oxide film favouring the oxygen reduction current and calcium carbonate deposition decrease the oxygen reduction current. The oxide film reduction is supported by the current density curves findings as shown in Figure 7-3 where the current density increases (toward more negative) with time which various brine solutions. This phenomenon has been reported in literature [63, 147, 148]. Observation of lower limiting current suggests a formation of a film and surface modification on the surface of the specimen. The polarisation process

especially the current response is also affected by the brine composition being used. Two of the main chemical elements or ions, magnesium and bicarbonate have a significant influence on the polarisation process compared to using the brine solution consisting of NaCl and $CaCl_2$. When polarised a specimen in a brine solution consisting of magnesium ions, the surface is progressively blocked by forming the Mg-Ca rich compound that could not be detected by the visual inspection. The detail of magnesium influence on polarisation is discussed in more detail in the following section.

The iron content in the oxide film plays an important role for oxygen reduction (this is described more details in Chapter 8). Partial reduction of iron oxide is required in order for better oxygen reduction and the rate of oxygen reduction reaction is proportional to the amount of Fe (II) in iron oxide. This leads to the increase of current density toward more positive direction. Masaru Okuyama and Shiro Haruyama [148] discovered that in the potential range where oxygen-reduction occurs, part of the oxide film $\gamma - Fe_2O_3$ is reduced but Fe_3O_4 and Cr_2O_3 which are part of the oxide films remained on the surface. Reduction of mixed oxide film $Cr_2O_3 - Fe_2O_3$ in a neutral borate solution was investigated by XANES shows that cathodic polarisation leads to reduction of Fe^{3+} to Fe^{2+} and no reduction of Cr_2O_3 and dissolution of iron oxides (Fe^{3+}, Fe^{2+}). A similar result was reported with the addition of Cl^- ions into the solution [149].

If the depletion of oxygen in the solution is a limiting factor, a reduction of current density should be expected as polarisation time increases. This is because the oxygen reduction process at the surface electrode consumes the oxygen and the concentration of oxygen diminishes with time. However, this is not the case, the current density increase with time for all the test brine solutions. Hence, this concludes that the concentration oxygen in the solution is not the limiting factor and is sufficient polarisation.

7.3.1 The Effect of Bicarbonate Ions on Polarisation

In the case of HCO_3^- ions solution, not only surface modification due to the adsorption and incorporation of the HCO_3^- ions onto the oxide film at the initial stage of polarisation but also more time is required to achieve stable current approximately 1000 seconds. Stainless steel iron and chromium are the main alloying elements of 316L stainless steel. The external surface is constituted with $Cr(OH)_3$ in acidic medium [150]

and with Fe oxides and oxyhydroxides in alkaline medium [151-153]. Under the exiting study it is believed, the passive films contain less Cr oxide but a higher Fe oxides contents [154]. Macdonald *et al.* [151] have proposed a bilayer structure model for the passive film formed on Fe–Cr alloys: the inner part of the film consists mainly of anhydrous oxides containing Cr, the most oxidisable element [152, 153]. The outer layer is constituted of iron oxides and oxyhydroxides that can be subject to a high dissolution. Under the cathodic protection or polarisation, the dissolution of the iron oxides and oxyhydroxides is minimised and also the chromium rich film prevents the dissolution of the iron into the solution. However, during the oxide film reduction, it is not impossible for that the preferential adsorption of HCO_3^- ions at the oxide film and the possibility of forming a more complex film (Fe,Cr)CO_3. In sodium chloride solutions containing bicarbonate ions, the presence of oxide film consists of Fe_2O_3, Cr_2O_3, (Fe,Cr)CO_3 film and a FeCl layer has been reported. The sign of current spiking due to film breakdown during the polarisation suggests that the existence of a film on the surface electrode. The formation of complex film modifies surface condition towards the reactivity of oxygen reduction reaction. Evidence of the lower stable current density obtained when specimen is polarised HCO_3^- ions brine solution compared to others such as NaCl, $CaCl_2$ and $MgCl_2$ as shown in Figure 7-2.

7.3.2 The Effect of Magnesium Ions on Polarisation

In addition to the oxide film reduction, sample specimens are also subjected to scale deposition when polarised in the brine solution consisting of calcium ions, carbonate ions and magnesium ions. Scale deposition and oxide film reduction takes place simultaneously at the specimen surfaces. The oxygen reduction process increases the interfacial pH at the metal/electrolyte interface according to

$$O_2 + 2H_2O + 4e^- \rightarrow 4OH^- \qquad \text{Equation 7-1}$$

The production of OH^- (hydroxyl ions) increases the pH at the metal/electrolyte interface as shown in Equation 7-1 and forces the solid crystalline phase to be deposited on the electrode surfaces according to the chemical reactions as shown in Table 7-1.

Reaction	Solubility Product
$OH^- + Ca^{2+} + HCO_3^- = CaCO_3 + H_2O$	4.7-6.9 x 10^{-9} (mol^2/L^2)
$OH^- + Mg^{2+} + HCO_3^- = MgCO_3 + H_2O$	8.0 x 10^{-9} (mol^2/L^2)
$2OH^- + Mg^{2+} = Mg(OH)_2$	8.9 x 10^{-12} (mol^3/L^3)

Table 7-1 Chemical reaction and the solubility product of calcium carbonate, magnesium carbonate and magnesium hydroxide[155]

Cations (magnesium and calcium ions) compete for either OH^- and CO_3^- to form hydroxide and carbonate scale at metal interface can occur. In the literature, the formation of $Mg(OH)_2$ as an inner layer with a high degree of porosity has been reported when a specimen is cathodically polarised [103, 156]. In the case of brine solution, it only consists of magnesium ions. The possible of $Mg(OH)_2$ deposition is unlikely as this is demonstrated in below saturation calculation. Humble [157] reported that in deposits consisting of $CaCO_3$ and $Mg(OH)_2$, the ratio of $CaCO_3$ to $Mg(OH)_2$ is dependent on the water composition and velocity. Furthermore considering the solubility product data [155] as presented in Table 7-1, the formation of $Mg(OH)_2$ is favourable rather to deposit $CaCO_3$ and $MgCO_3$ since the solubility product of $Mg(OH)_2$ is the lowest compared to the solubility product of the carbonate scale. The deposition of $Mg(OH)_2$ is thermodynamically possible if the interfacial pH as high as 9.3 [103] which can be generated by polarisation.

Based on saturation ratio estimation for the existing study, a limited concentration of magnesium ions (0.00374 mol/l) is insufficient to trigger the precipitation of $Mg(OH)_2$ since the saturation ratio is less than 1 as calculated as below;

$$I_s = \frac{[Mg^{2+}][OH^-]^2}{K_{sp}}$$

$$I_s = \frac{[0.00374][10^{-4.7}]^2}{8.9X10^{-12}}$$

$$I_s = 0.16$$

This calculation is based on an ideal case (no ion pairing occurring and the activity is equal to the concentration) and assuming an interfacial pH is 9.3. The saturation is less than 1 where thermodynamically is impossible to precipitate $Mg(OH)_2$. The formation

of $MgCO_3$ over $CaCO_3$ is dependant on ratio Mg^{2+}/Ca^{2+} and 3:1 is needed in order to form $MgCO_3$ in seawater [158]. All the experiments were conducted where Mg^{2+}/Ca^{2+} was less than 1 so the formation of $MgCO_3$ is unlikely to happen.

The possibility of the formation of a magnesium-calcium rich compound at a very early stage of deposition has been reported [17, 103]. Magnesium is the main factor to promote and form a magnesium-calcium rich layer at the early stage of polarisation. Magnesium in the solution induces the deposition of a complex mixture of Ca and Mg carbonate and hydroxide deposit. The film formation may be the Mg-Ca rich compound on the specimen's surface as reported by Morizot [141]. Gradually $CaCO_3$ is incorporated into the deposit magnesium ions as the magnesium concentration decreases. Morizot has claimed that magnesium ions have a controlling influence in the deposition and a result in a significant of coverage of Mg-Ca rich layer deposited on the electrode surface as a result of a polarisation in a magnesium solution for 5 minutes. However, crystals on the specimen surfaces even after more than 1 day of polarisation are rarely observed and a magnesium rich thin layer that is only able to be determined by surface analysis, using the XPS technique was responsible for the electrode surface coverage was reported.

As suggested by Kunjapur and Hartt [156] the Mg-Ca rich compound has a less insulation resistivity than $Mg(OH)_2$ or $CaCO_3$. This compound consists of higher water content. Therefore, the formation of a magnesium-calcium rich compound could be responsible for the electrode's surface blockage rather than pure $CaCO_3$ and $MgCO_3$ crystals. Evidence of current density reduction and also blockage of the surface coverage on the electrode at the initial stage of polarisation are concurrent with the observation of polarising various brine solution experiment especially for the brine solution consist of calcium and bicarbonate ions; and the brine solution consists NaCl, $MgCl_2$ and $CaCl_2$ as shown in Figure 7-1 (b).

7.3.3 Conclusion of the Effect of Brine Solution Composition

The electrochemical measurement for the oxygen reduction is greatly influenced by various brine compositions. The presence of magnesium ions and bicarbonate ions has influenced the current density response especially at the initial stage of the polarisation.

It is believed that the unusual current response may be due to the formation of a magnesium-calcium rich compound and the change of carbonate adsorption the specimen's surface when the polarisation is conducted in the brine in the presence of $MgCl_2$ and $NaHCO_3$ respectively.

It should be emphasised that though the presence of these ions in the brine solutions have caused a significant difference in current density, the scaling tendency is not affected by the electrochemical measurement data (between 2000 to 3000 seconds) after scale deposition is the dominant and is described more details in the following section. The reduction of current density as a result of polarisation could be attributed to the oxygen depletion in solution. However, this is not the case as the presence of oxygen in the solution is more than enough for the entire polarisation process. The oxygen concentration in the solution is more than sufficient for two hours polarisation without any reduction or diminishment.

7.4 Feasibility Study and Investigation of Scaling Tendency

The main objective of this section was to investigate, explore and quantify the scaling tendency results obtained through the electrochemical measurements. Scaling tendency only provides partial information about the brine chemistry solution, additional information on surface scaling could contribute towards the understanding the surface scaling and the potential scaling of a system. Therefore, surface quantification using the electrochemical technique and the image analysis were carried out. It has been demonstrated in Chapter 5 that the electrochemical analysis gives a good estimation of the scale coverage on the specimen surfaces. The surface quantification was carried out to determine the surface coverage by obtaining the initial (prior to the scaling tendency measurement) and final plots (after the scaling tendency measurements). The investigation of scaling tendency could be divided into a few simple stages.

i.) Sample preparation (refer to section 5.2.1);
ii.) Initial analysis (refer to section 5.2.2);
iii.) Scale Deposition-scale was deposited by polarising the specimen and recording the current versus time. At the same time, the recorded electrochemical data was used to establish the scaling tendency;
iv.) Final analysis (refer to section 5.2.4);

v.) Post analysis-to determine and quantify the scale coverage using two methods; the electrochemical and the image analysis techniques. Furthermore, in this analysis, the scaling tendency information of the brine was also quantified using the electrochemical technique.

Further details of the experimental procedures can be found with reference to Chapter 5. In this section, experiments to investigate the scaling tendency of using the electrochemical technique in combination with the SIJ were conducted. All experiments were conducted by polarising the specimen for 2 hours in a specific saturation ratio scaling solution, to deposit scale as well as to obtain the electrochemical data of the scaling tendency. The specimen was subjected to an impinging jet at a certain flow rate while it was polarised to record the electrochemical data.

7.4.1 Understanding the Various Regimes of Current Response Prior to Scaling Tendency Quantification

The purpose of this section was to determine the potential scaling tendency regime through analysing and investigating the different regimes of a polarisation curve of a saturated brine. Scale was deposited on the specimen surface by polarisation process. The specimen was polarised to potential -0.8 V (Ag/AgCl) in the supersaturated brine consisting of magnesium ions with a saturation ratio of 17.8. Only this brine was selected for preliminary analysis as this is the worst case would be expected. Current versus time was monitored when the specimen was polarised for 2 hours and at the same time subjected to electrolyte impingement at flow rate 160 ml/min.

The current density versus time response of this saturated brine at 160 ml/min is presented in Figure 7-4. Basically, it was divided into a 4 regimes. In the first few seconds of polarisation, a decrease in current density could be seen and it followed by an increase of current density. Finally, there was a decrease in current density and it reached a plateau at the later stage of polarisation.

In order to understand the different regimes of the curve, experiments with different polarisation times were carried out. Four different polarisation times, 5 seconds, 300 seconds, 2500 seconds and 6120 seconds were selected for further investigation by quantifying the surface coverage using the electrochemical measurement and the image

analysis. Through this a better understanding and mechanism of scale deposited on the specimen on each stage of the polarisation can be gained by dividing the regime. The selected times correspond to the different regimes (regime 1, 2, 3 and 4) of current versus time as shown in Figure 7-4. For the first two regimes of the polarisation curve, it exhibited a similar trend of current response as in brine solution consisting of $MgCl_2$ and $NaHCO_3$ elements which was presented in Figure 7-1 and Figure 7-2. In addition, the influence of these elements to the electrochemical measurement, calcium carbonate also seen to be deposited on the specimen surface at the regime 2 as shown in Figure 7-8 (b). Regime 3, as polarisation time increases a reduction in current was expected as more calcium carbonate was deposited on the specimen surface consequently a reduction in active areas for oxygen reduction process took place. Above 4000 seconds, coalescence and overlapping of the calcium carbonate started to form a thick layer of scale as shown in Figure 7-8 (d).

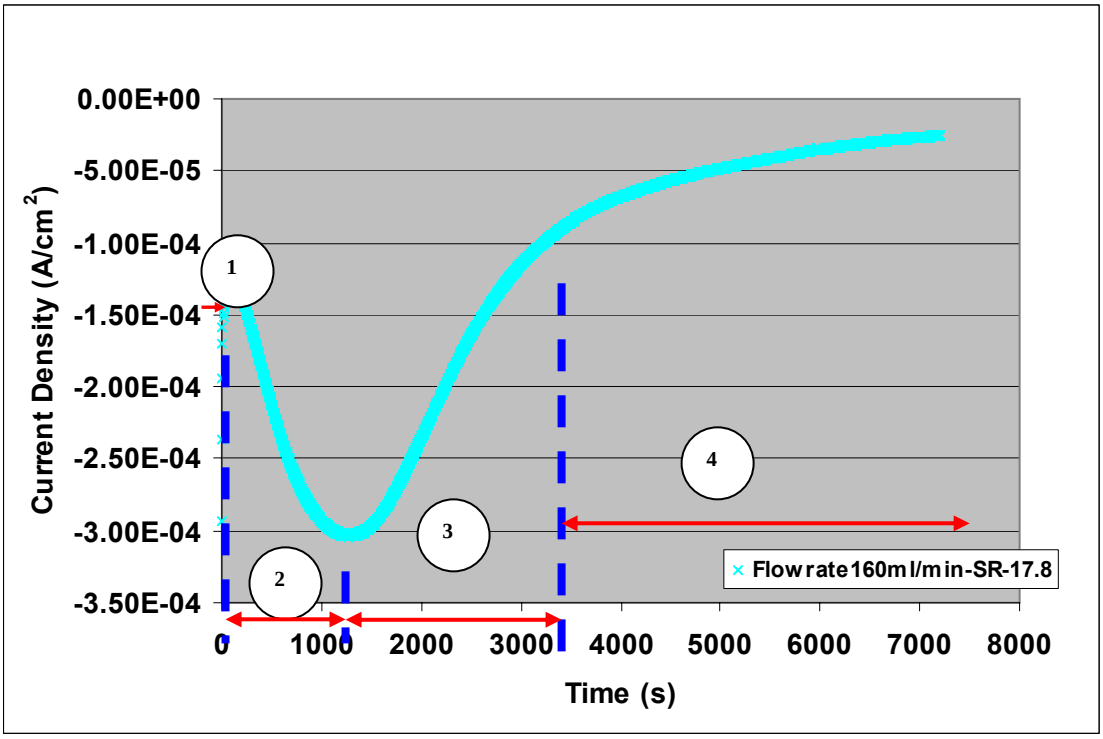

Figure 7-4 Different regimes of current responses to time of a specimen being polarised in a supersaturated brine of 17.8 for 2 hours at a flow rate of 160 ml/min

Figure 7-5 represents current density responses to different polarisation times at flow rate 160 ml/min in a saturated brine (SR=17.8) which corresponding to the various regimes as presented in Figure 7-4. Regime 1 is the representation of the specimen polarised for 5 seconds, a decrease in the current was observed, as shown in Figure 7-6.

The enlargement of Figure 7-5 that covering the current response of the first 10 seconds of polarisation is presented as Figure 7-6.

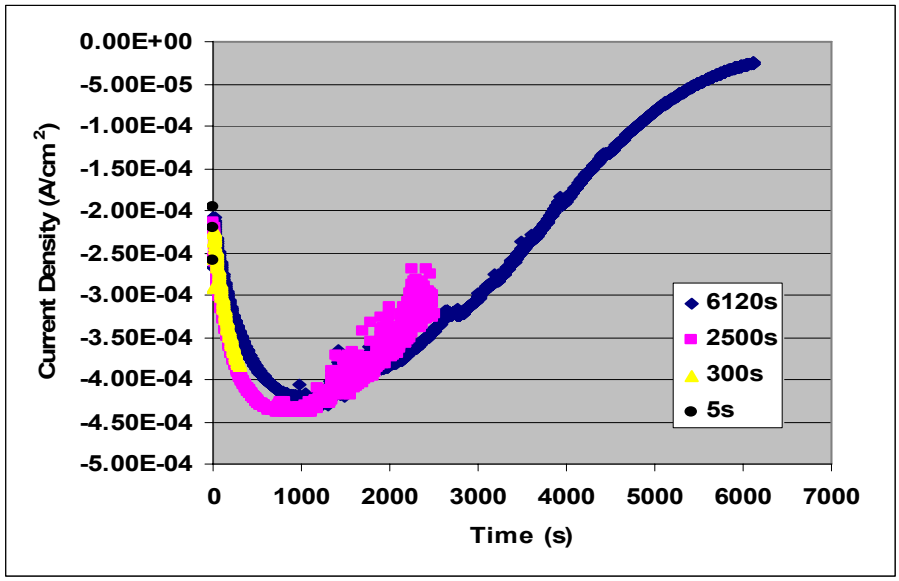

Figure 7-5 Current density responses to different polarisation time at flow rate 160 ml/min in saturated brine (SR=17.8)

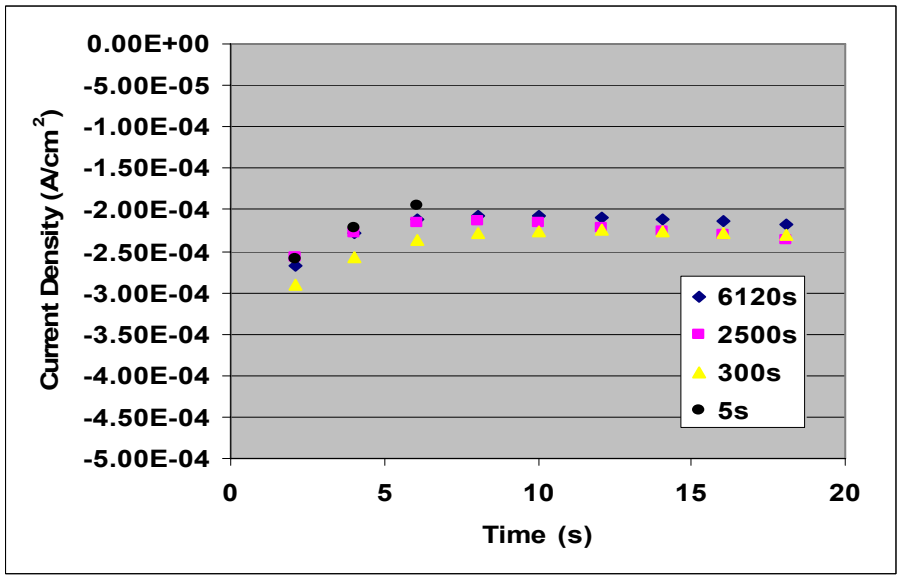

Figure 7-6 Enlargement of current density versus time for the first 10 seconds of polarisation at flow rate 160 ml/min for a saturated brine (SR=17.8). The specimen polarised for 5 seconds showed a decrease of current

The first regime is mainly attributed to the deposition of magnesium-calcium rich compounds. These compounds cause the blockage of the electrode and subsequently, a reduction in current density is obtained. The sign of current reduction suggested that blockage of the surface electrode by forming a magnesium–rich calcium film on the

specimen surface. It was only possible to quantify the coverage by the electrochemical technique where significant coverage was observed compared to the image analysis that shows 0 % coverage.

The specimen polarised for 300 seconds is represented as regime 2 where an increase of current density was also observed. As polarisation increases, the calcium carbonate scale starts to deposit on the electrode surfaces. Reduction of the oxide film and the influence of bicarbonate ions also took place simultaneously at the electrode surface (under acceleration process) [159]. However, oxide film reduction and the adsorption and incorporation of bicarbonate ions dominate the process in comparison to scale formation.

The formation of calcium carbonate increases with polarisation time, while oxide reduction decreases with time as a result of a less active area for oxide film reduction. The calcium carbonate scale acts as a physical barrier to prevent oxygen reduction reactions taking place. As a result, a decrease in current density was observed for 2500 seconds and it is represented at a later stage of the polarisation (Regime 3).

Finally, regime 4 represents a polarisation time of 6120 seconds whereby the current almost achieved plateau or zero. The current density decreases but did not reach zero and the residual current is observed. A layer of calcium carbonate was deposited and overlapping took place where small crystallites occur between the calcite and vaterite crystals leading to blockages of the surface electrode. However, it was not a completely compact layer and a partial block (porous layer) was formed. Hence, a residual current was observed at a later stage (regime 4). A similar finding has reported a porous layer of calcium carbonate scale is formed [160, 161].

7.4.1.1 Scale Coverage Quantification on Various Regimes

The scale coverage of each polarised specimen was carried out by the image analysis technique and the electrochemical technique. Figure 7-7 indicates two methods of scale coverage quantification; the electrochemical and the image analysis technique on each polarisation regime. The scale coverage determined by both techniques showed increases of coverage when the polarisation time increases as more scale was deposited. The percentage of coverage determined by the electrochemical technique and the image analysis are presented as in Table 7-2. There was a discrepancy in scale coverage

between these two methods especially at the initial stage of polarisation (5 and 300 seconds). Scale determined by the image analysis showed coverage of 0 % (Figure 7-8 (a)) and 4.8 % (Figure 7-8 (b)) for 5 and 300 seconds of polarisation respectively whereas scale coverage estimated by the electrochemical technique indicated coverage of 59 % and 89.5 % for the same polarisation time. For a polarisation time of 6120 seconds, no assessment had been carried out on the final-plot as the surface was totally covered by calcium carbonate scale. The current density was independent of the flow rates once the surface was completely covered with calcium carbonate. A control experiment was also carried out to ensure no variation in oxygen concentration as well as other experiment setup errors. The control specimen showed coverage of 9.17 % which is within an error limit of 10 % of this electrochemical technique.

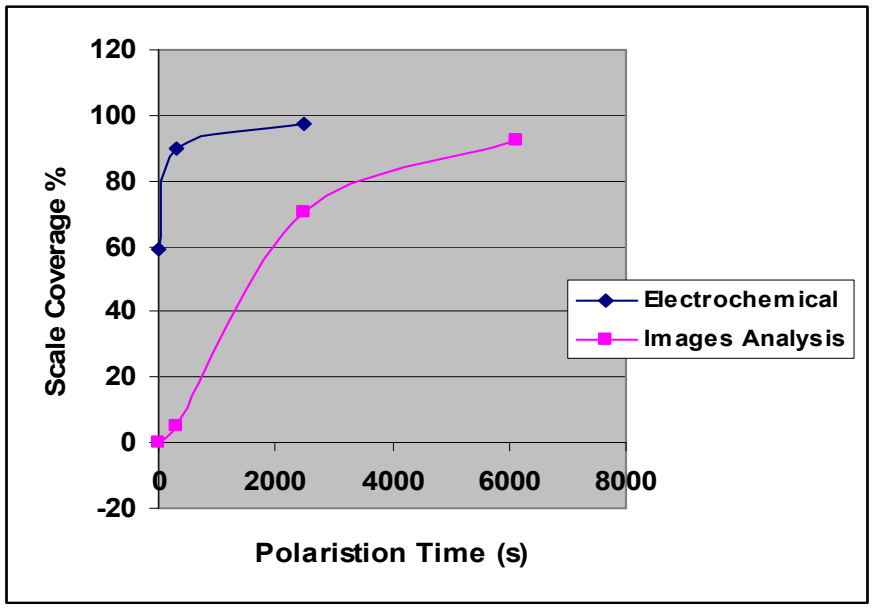

Figure 7-7 Percentage of scale coverage determined by the electrochemical technique and image analysis technique after the specimen electrodeposited for polarisation time at 5s, 300s, 2500s and 6120s

Polarisation time, seconds	Electrochemical			Coverage Images Analysis
	Initial plot	Final plot	Coverage	
5	0.0227	0.0093	59.03	0
300	0.0221	0.0023	89.59	4.86
2500	0.0207	0.0006	97.10	70.36
6120	0.0214	/	100	92.54
Control	0.024	0.0262	-9.17	/

Table 7-2 Result of the slope values and percentage of scale coverage after scale electrodeposited with various polarisation times, determined by the electrochemical technique and image analysis technique

Results of both quantification techniques seem to be in agreement with each other, scale deposition increases with polarisation times. However, there was a significant discrepancy in scale coverage determined by the electrochemical measurement and scale coverage determined by the image analysis. Scale coverage quantified by the electrochemical technique was significantly higher than scale coverage quantified by the image analysis technique. This was mainly attributed to the formation of a layer of Mg-Ca rich layer film on the electrode during the polarisation process that was hardly visible under the light microscope but was able to be detected by the electrochemical technique. This result is concurrent to the current response of 5 seconds of polarisation where a decrease of current could be seen as shown in Figure 7-5.

The scale coverage result quantified by the electrochemical technique should be in agreement with the current response of the 300 seconds polarisation, an increase in current density as shown in Figure 7-5. However, this was not the case as scale coverage determined by the electrochemical technique indicated approximately 90 %. This could be explained by the formation of an Mg-Ca rich film at the early stage of polarisation that did not fully cover the surface of the electrode, subsequently at a later stage the oxide film reduction and calcium carbonate deposition occur at deposit free areas. However, the oxide film reduction was the predominant process compared to the calcium carbonate deposition process. As this is strongly supported by analysing and comparing the current density of the bare specimen and the current density of same specimen after polarisation for 300 seconds where the film formed at early stage and subsequently oxide film reduction occurred. For the same flow rate (160 min/ml), the current density of the bare specimen was -5.17×10^{-4} A/cm^2 when compared to the highest current density recorded for the 300 seconds polarisation curve, -3.8×10^{-4} A/cm^2 as shown in Figure 7-5.

The longer the polarisation time, the more calcium carbonate was deposited. Scale coverage quantified by the electrochemical technique showed 70 % and 93 % of coverage for the specimen polarised for 2500 seconds and 6150 seconds respectively. These results were in agreement to the current response as shown in Figure 7-5 as the scale deposition process becomes dominate rather the oxide film reduction process; hence, a reduction of current was found due to the lack of active areas available for oxygen reduction process.

Figure 7-8 represents the images of specimen surface conditions after polarisation over various times. Figure 7-8 (a) and (b) represents the specimen's surface after 5 and 300 seconds of polarisation at a flow rate of 160 ml/min. Images in Figure 7-8 (c) and (d) represent the specimen surfaces after the specimen was polarised for 2500 and 6120 seconds respectively. As the polarisation time increased, more scale was deposited. Most of the scale deposited on the specimen surfaces was calcite with rhombohedra and cubic shapes. Vaterite, in a flower formation was also deposited but in a less amount than calcite. The crystal sizes increase with polarisation time. This finding is strongly supported by the crystal size growth 5, 10, 25 μm that correspond to 300, 2500 and 6120 seconds of polarisation times, as shown in Figure 7-8.

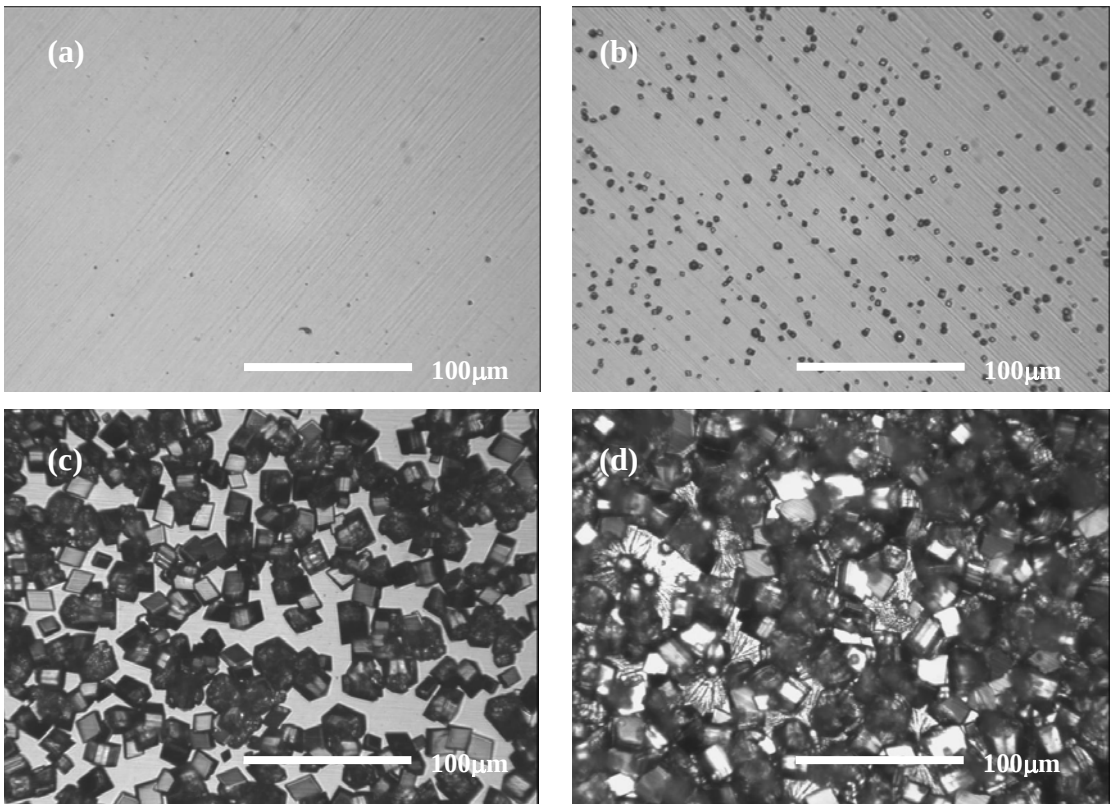

Figure 7-8 Surface of specimen after scale electrodeposited for (a) 5 seconds-Regime 1 (b) 300 seconds-Regime 2 (c) 2500 seconds-Regime 3 and (d) 6120 seconds-Regime 4 in a saturated brine of 17.8 at flow rate 160 ml/min

7.4.2 Summary of the Scaling Tendency Measurement Determination

A summary or conclusion can be drawn from the preliminary investigation, especially the physical and electrochemical representation of the current versus time curve. Among the 4 regimes, a suitable representation of scaling tendency can be established.

The most suitable regime used to quantify scaling tendency is regime 3, where mineral scale deposition takes place alongside a reduction in the active area. The rationale behind the selection of regime is solely based on the more stable and representative data as compared to other regimes. A schematic diagram summarises the possible scale formation as shown in Figure 7-9.

Generally, Regime 1 is too short for analysis (< 5 seconds), the electrochemical data from regime 2 exhibited a similar trend of current as the various brine solutions composition experiment as presented in 7.3. This concluded that not only surface deposition but also other factors affect the increase in current density. Oxide film reduction and the influence in the presence of $NaHCO_3$ are mainly contributed and represented by this regime. Regime 4 (above 3,500 seconds), coalescence and overlapping of the deposited crystals are too extensive to permit the characterisation of scale tendency measurement to be quantified. Hence, this leads to the selection of regime 3 for use in scaling tendency quantification. At regime 3, the oxide reduction and the scale deposition occur simultaneously. However, the dominant process is governed by the scale deposition. This is in agreement with the reduction of current response (above 2000 seconds) and the light microscope image of the surface electrode where calcium carbonate is deposited. A representative electrochemical data on regime 3 can be used for further investigation to quantify the scaling tendency measurement.

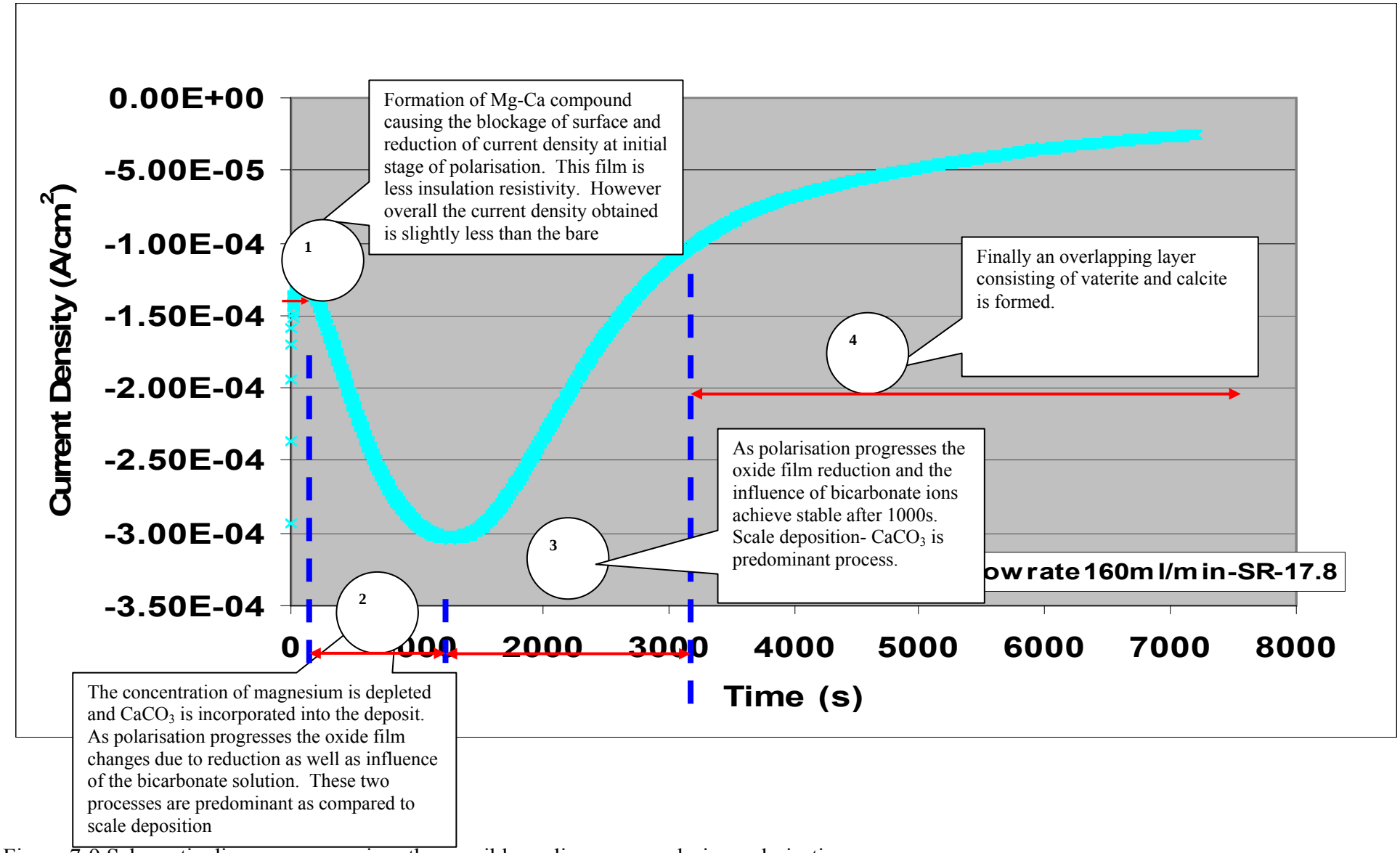

Figure 7-9 Schematic diagram summarizes the possible scaling process during polarisation

7.5 Scaling Tendency Quantification of Various Saturated Brine Solution (Different Saturation Ratio)

As demonstrated among the polarisation regime, only regime 3 is suitable and representative for scaling tendency measurements. In this section this regime was used for further investigation to quantify the scaling tendency measurement on various saturation brine and flow conditions. Scaling solutions of saturation ratios 0.27, 1.09 and 17.8 were selected for the experiment. Four flow rates 40, 80, 120 and 160 ml/min within laminar flow regimes were selected for each saturated-brine. Three identical tests were carried out for the same experiment to ensure the reproducibility of the result.

7.5.1 Saturated Brine Solutions

The scale tendency measurement was carried out by polarising the specimen to cathodic potential -0.8 V for saturated brine with saturation ratio of 1.09 and 17.8. The specimen was electrodeposited with calcium carbonate scale by polarising the specimen to cathodic potential at -0.8 V in a undersaturated brine. Only one set of results, test 1 is presented, since the rest of the results show similar trends of curve with respect of flow rates.

Post analysis was carried out to determine the scaling tendency, where the current density data between 2000-3000 seconds from current versus time was extracted to establish a slope value of the curve. This slope is known as the scaling tendency slope. Three identical tests were carried out.

7.5.1.1 Brine Solution with a Saturation Ratio of 1.09

Figure 7-11 represents the current density versus time of various flow rates of a saturated brine (SR=1.09). Current versus time curves indicated decreases of current density at the initial stage of polarisation, followed by increases of current density, eventually achieving a steady state at a later stage, at a flow rate of 40 ml/min. Other flow rates (80, 120 and 160 ml/min) exhibited a similar trend of curve as flow rate at 40 ml/min for the initial stage. However, at approximately 1200 seconds (later stage), decreases in current density rather then steady state of current were observed, as shown in Figure 7-11. Overall the current density increases with flow rate toward more negative direction. As the oxygen reduction process is under mass transfer process, increased flow rate decreases the diffusion layer thickness and more oxygen can be

transported to the electrode's surface. This increases the oxygen reduction and promotes a high local pH that can transform bicarbonate and subsequently calcium carbonate deposition. A higher current could be expected for a higher flow rate, therefore more scale was deposited on the specimen surface as shown in Figure 7-10.

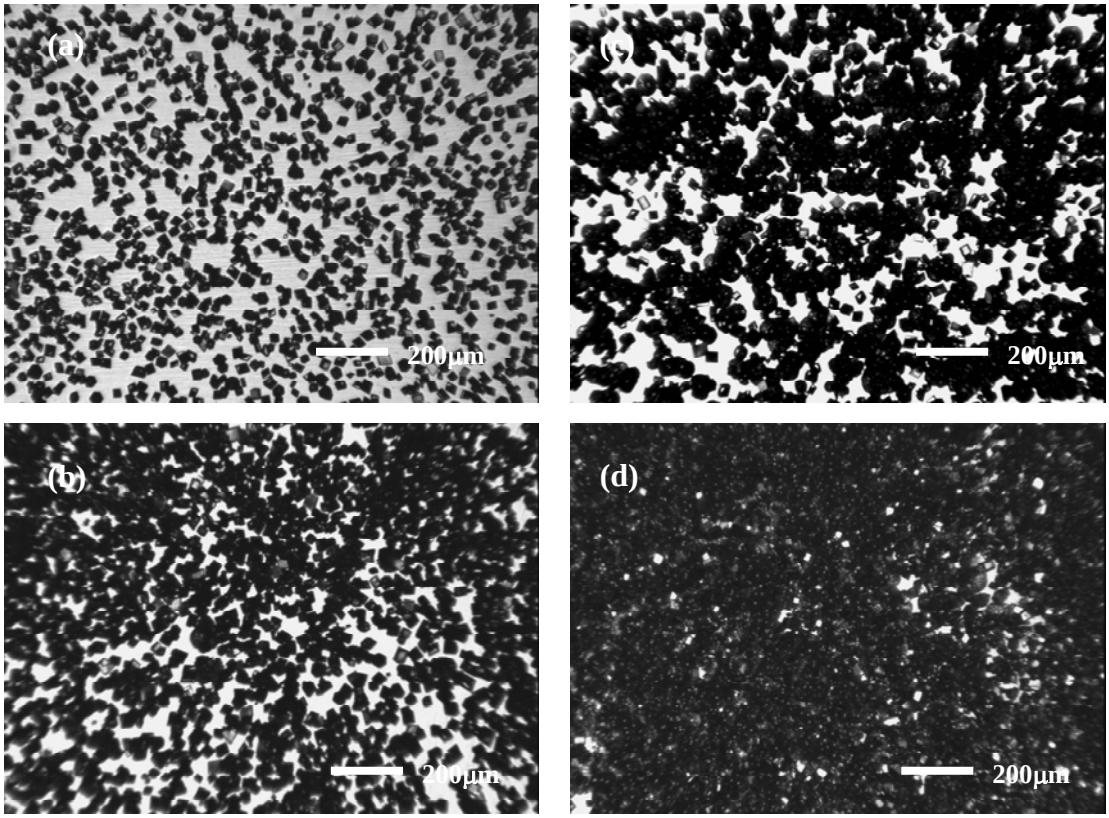

Figure 7-10 Representation of the crystal density on the specimen surfaces after electrodeposited in a saturated brine (SR=1.09) at flow rate (a) 40 ml/min, (b) 80 ml/min, (c) 120 ml/min and (d) 160 ml/min

The dashed line shown in Figure 7-11 was used to determine the scaling time of this brine solution. The scaling time is defined as the time where the slope crosses the X-axis. Details of the procedures to determine the scaling time can be found by reference to Chapter 5 Experimental Procedures and Calibrations. This is an additional parameter from the scaling tendency slope measurement which can be used to quantify the scaling tendency and is described in section 7.5.2. Again, the current density data between 2000-3000 seconds from current versus time was extracted to establish a slope value of the curve. Three identical tests were carried out and the average slope values of the supersaturated brine (saturation ratio 1.09) are presented in Table 7-3. The i_L versus time exhibited linearity, a good correlation of the least square fits of the slope data is

exceeded 0.90 irrespective to flow rate. In general, the scaling tendency slope increases as the flow rate of saturated brine increases as shown in Figure 7-12. The scaling tendency slope values showed a positive slope. The average slope values were 4.77, 12.5, 28.8 and 49.2 (x 10^{-09} A/cm^2/s) and correspond to a flow rate of 40, 80, 120 and 160 ml/min as presented in Table 7-3. A good correlation between the scaling tendency and the flow rate was plotted as shown in Figure 7-12.

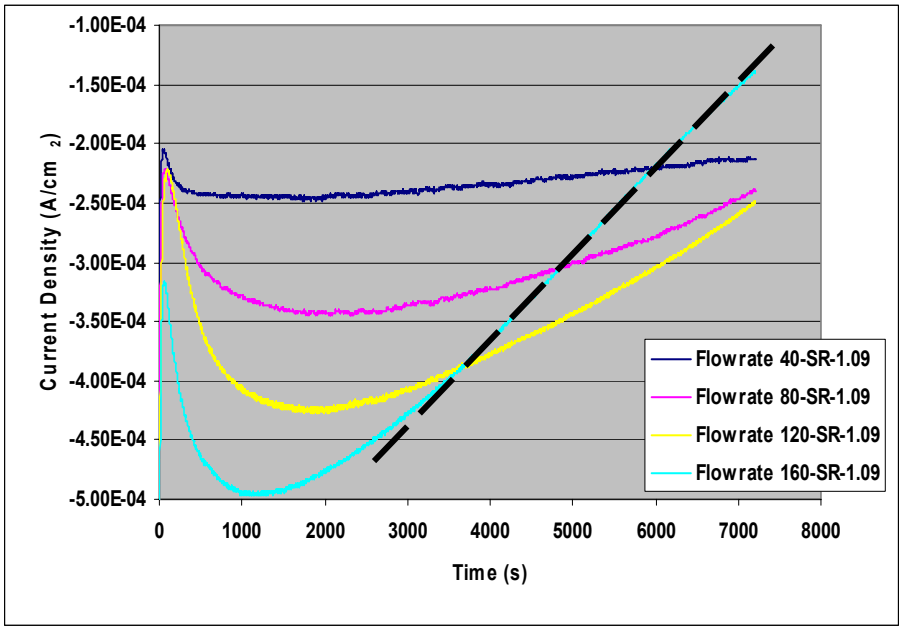

Figure 7-11 Current density versus time of different flow rates of saturated brine (SR=1.09) for test 1. The dashed line shows the method used to determine the scaling time where it crosses the X-axis (it is approximately 9000 seconds when the X-axis crosses at Y at O instead of -5E-04)

Flow rate (ml/min)	Test 1		Test 2		Test 3		Average Slope	Standard Deviation
	slope (A/cm^2/s)	R^2	Slope (A/cm^2/s)	R^2	Slope (A/cm^2/s)	R^2		
40	4.09E-09	0.964	5.60E-09	0.948	4.62E-09	0.961	4.77E-09	7.66E-10
80	9.67E-09	0.957	1.45E-08	0.963	1.34E-08	0.970	1.25E-08	2.53E-09
120	2.49E-08	0.925	3.01E-08	0.962	3.13E-08	0.981	2.88E-08	3.40E-09
160	4.83E-08	0.994	4.92E-08	0.993	5.00E-08	0.998	4.92E-08	8.50E-10

Table 7-3 Results of the scaling tendency slope measurement correspond to various flow rates at a saturation ratio of 1.09

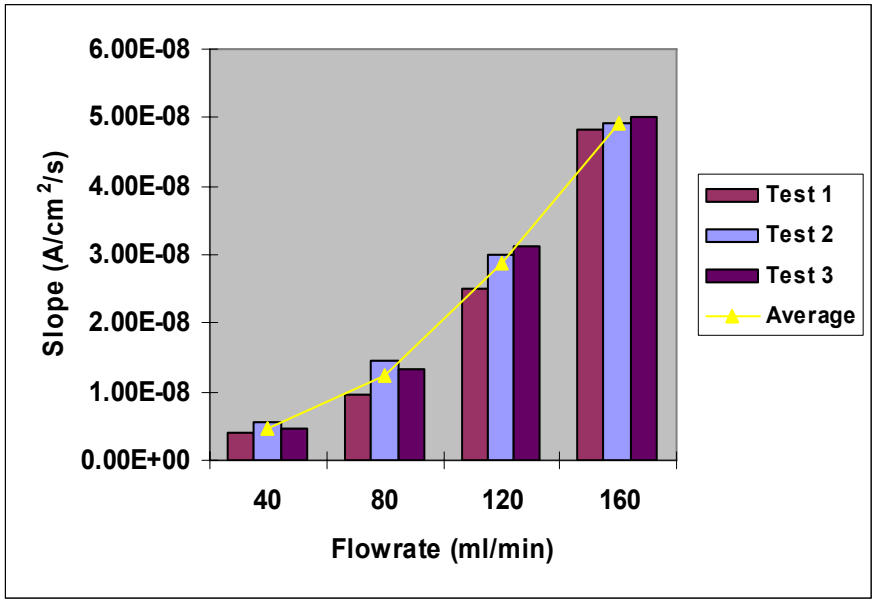

Figure 7-12 Representation of the scaling tendency slope values responses to various flow rates determined by polarising a specimen at –0.8V for 2 hours in a saturated brine (SR=1.09)

7.5.1.2 Brine Solution with a Saturation Ratio of 17.8

The current response of a specimen polarised in a brine solution consists of a saturation ratio of 17.8 was divided into a few stages with respect to the flow conditions, as shown in Figure 7-13. For the first 100 seconds of the polarisation, a decrease in current density was observed, followed by an increase in current density for approximately 1000 seconds. However, after 1000 seconds of polarisation, the current density reversed the direction by showing decreases and its rate was faster at 1000-5000 seconds. At a later stage of polarisation, current density decreased slowly and became almost constant. For this supersaturated brine, the scaling tendency slopes increased as the flow rates increase, as shown in Figure 7-14. The scaling tendency slope values were 14.6, 75.4, 84.3 and 134 (10^{-09} A/cm^2/s) which correspond to the flow rate of 40, 80, 120 and 160 ml/min as presented in Table 7-4. The scaling tendency slope values are found to be higher for this brine solution (SR=17.8) compared to the brine solution with a saturation ratio of 1.09. Basically, the higher thermodynamic driving force is expected as saturation ratio increases this leads to faster deposition.

Flow rate (ml/min)	Test 1		Test 2		Test 3		Average Slope	Standard Deviation
	slope ($A/cm^2/s$)	R^2	Slope ($A/cm^2/s$)	R^2	slope ($A/cm^2/s$)	R^2		
40	1.03E-08	0.931	1.27E-08	0.9602	1.22E-08	0.950	1.17E-08	1.29E-09
80	4.17E-08	0.996	5.79E-08	0.9807	5.13E-08	0.984	5.03E-08	8.14E-09
120	6.82E-08	0.981	8.85E-08	0.973	9.63E-08	0.989	8.43E-08	1.45E-08
160	1.57E-07	0.992	1.22E-07	0.9913	1.22E-07	0.991	1.34E-07	2.04E-08

Table 7-4 Results of the scaling tendency slope measurement correspond to various flow rates at a saturation ratio of 17.8

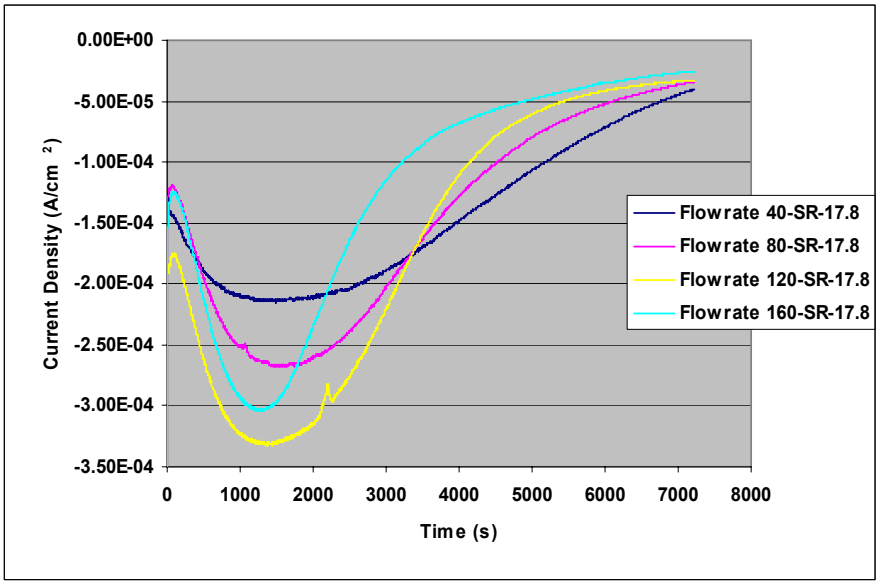

Figure 7-13 Current density versus time of different flow rates where the specimen is polarised in a supersaturated brine (SR=17.8)

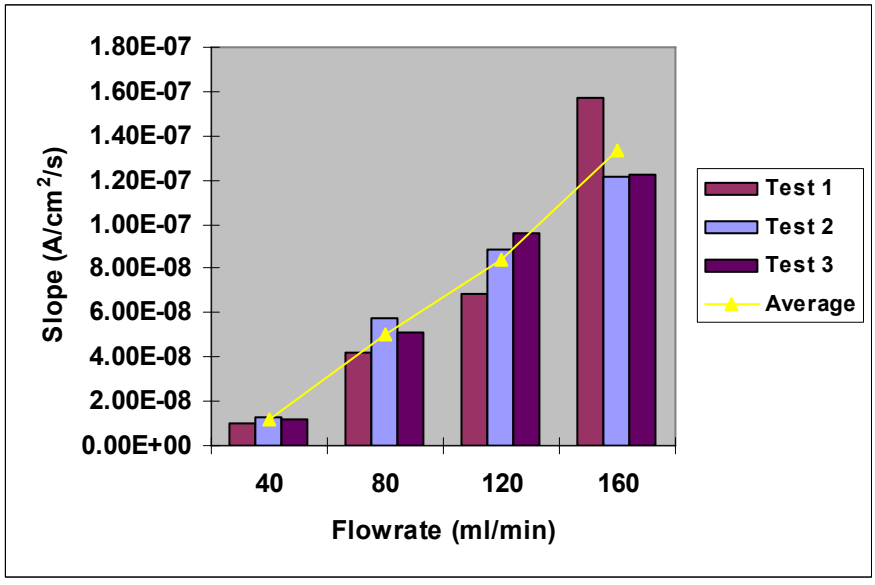

Figure 7-14 Representation of the scaling tendency slope values responses to various flow rates determined by polarising a specimen at –0.8V for 2 hours in an supersaturated brine (SR=17.8)

7.5.1.3 Concluding Remarks of Supersaturated Brine

The use of electrochemical measurement in a SIJ cell rig has demonstrated the capability to quantify the scaling tendency slope measurements of various flow rates. It is clearly shown the slope value responds to various supersaturated saturation ratio brine solution. This also confirms and verifies the electrochemical data from Regime 3 can be suitable used to quantify the scaling tendency slope measurement, a linear relationship between the current versus time can be established.

7.5.2 Undersaturated Brine (Saturation Ratio 0.27)

In this section, further investigation and quantification of the scaling tendency were carried out for the undersaturated brine with a saturation ratio of 0.27. The experimental conditions were the same as previous section. Again, the specimen was electrodeposited with calcium carbonate scale by polarising the specimen to cathodic potential at -0.8 V in an undersaturated brine. Current versus time curves indicated decreases of current density at the initial stage of polarisation, followed by increases of current density and until a steady state was achieved at a later stage, as shown in Figure 7-15.

The result of the three tests and the average scaling tendency slope value of various flow rates of undersaturated brine 0.27 is shown in Figure 7-16. This figure shows that negative scaling tendency slope values were obtained for the undersaturated brine as opposed to the saturated brine solution. When the flow rate increases, the slope value shifted towards a more negative direction. It is believed oxide film reduction modifies the surface condition of the electrode attributed to the increase in current density resulting in a negative slope value as discussed in section 7.3. The slope values were approximately -0.4, -4.38, -11.5 and -19.7 ($x10^{-09}$ $A/cm^2/s$) which correspond to flow rates of 40, 80, 120 and 160 ml/min as in Figure 7-16. The scaling time of the undersaturated brine is unable to be determined since the current density remained constant (40 ml/min) or increased slowly at times (80, 10 and 160 ml/min) as shown in Figure 7-15.

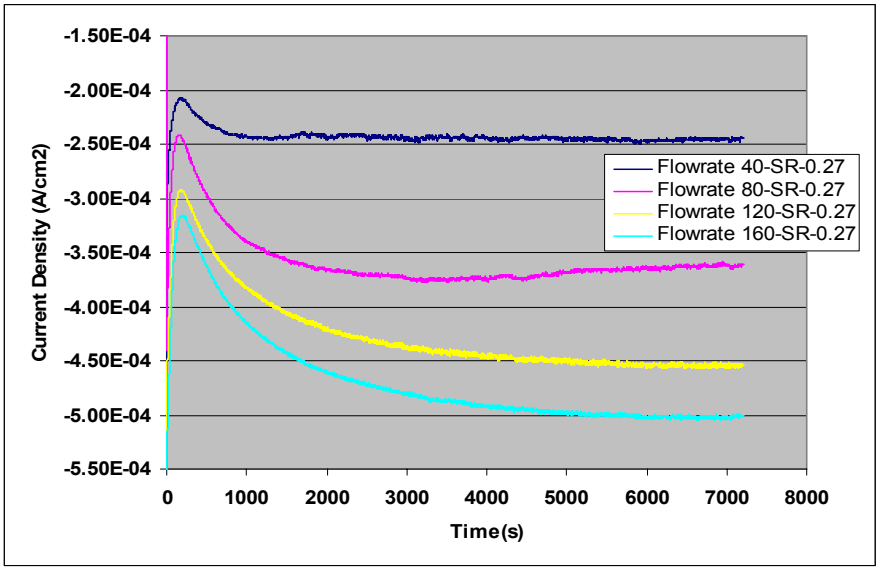

Figure 7-15 The effect of various flow rates on the current density versus time of an undersaturated brine (SR=0.27)

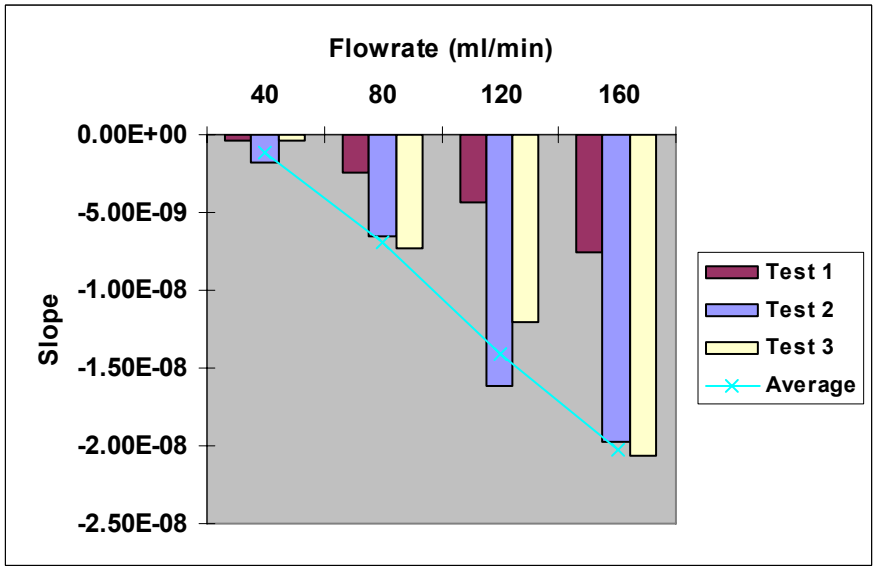

Figure 7-16 Representation of the scaling tendency slope values responses to various flow rates determined by polarising a specimen at –0.8V for 2 hours in an undersaturated brine (SR=0.27)

Flow rate (ml/min)	Test 1		Test 2		Test 3		Average Slope	Standard Deviation
	2000-3000s		2000-3000s		2000-3000s			
	slope ($A/cm^2/s$)	R2	slope ($A/cm^2/s$)	R2	slope ($A/cm^2/s$)	R2		
40	-1.81E-09	0.128	-3.81E-10	0.581	-4.48E-10	0.226	-8.80E-10	3.12E-01
80	-6.59E-09	0.829	-2.42E-09	0.6971	-7.26E-09	0.855	-5.42E-09	7.94E-01
120	-1.61E-08	0.939	-4.32E-09	0.8363	-1.20E-08	0.903	-1.08E-08	8.93E-01
160	-1.98E-08	0.977	-7.60E-09	0.915	-2.07E-08	0.979	-1.60E-08	9.57E-01

Table 7-5 Results of the scaling tendency slope measurement correspond to various flow rates at a saturation ratio of 0.27

7.5.2.1 Concluding Remarks of Undersaturated Brine

Modification of the surface conditions is mainly attributed to the reduction of the oxide film that takes place at the electrode surfaces during polarisation. This is in agreement with the current density curves as shown in Figure 7-3 where the current density increases with time for various brine solutions. All the current versus time curves indicated a gradual increase of current density (toward more negative) as time increased. The electrochemical measurement of an undersaturated brine also might be affected by the presence of magnesium ions. Hence, it is impossible to establish the relationship between the amount of scale covered on the surface quantified by either the electrochemical or the image analysis and the scaling tendency slope value ($A/cm^2/s$). However, a good correlation between the scaling tendency gradient /slope and the flow rate is established and the scaling tendency can be quantified for the brine.

Under cathodic polarisation, scale deposition is accelerated, even if a brine solution is undersaturated and deposition is where thermodynamically impossible under normal condition. This is because generation OH^- at the electrode/electrolyte interface as a result of oxygen reduction and causes the increase of the local saturation ratio. Results from section 7.5.1 and 7.5.2 show a negative scaling tendency slope value for undersaturated brine (SR=0.27) and a positive slope value for saturated brine (SR=1.09, 8.91 and 17.8) for all the flow rates. A negative scaling tendency slope of an undersaturated brine can mainly be explained by the reduction of the oxide film on the specimen surface.

The surface of the oxide film changes with time as polarisation takes place. It increases with the increase of flow rate. As this had been explained in an earlier section, the reduction of iron oxide is required in order to allow better oxygen reduction as the flow rate diffusion layer thickness decreases and oxygen diffuses faster to the electrode surface for oxygen reaction. Hence, a positive scaling tendency slope was obtained for all saturated brines. Scale deposition can thermodynamically occur without any additional external factors for supersaturated brine where the saturation ratio is above 1. A high interfacial pH was generated at the interface when polarisation was carried out. Therefore, scale deposition was accelerated and becomes the predominant process rather than oxide reduction. Hence, a positive slope value is observed for saturation ratio, SR >1. This is especially true for saturated brines with a saturation ratio of 1.09 and 17.8.

7.5.3 Crystal Morphology Formation by Polarisation Process

The images of scaled specimen under the influence of flow are presented as in Figure 7-17. Three magnifications of images were taken for each flow rate. Figure 7-17 represents scale deposited on the specimen surfaces of four flow rates, 40 ml/min, 80 ml/min, 120 ml/min and 160 ml/min. Images show the majority of crystals are metastable vaterite and with amount of calcite also deposited on the specimen surfaces. Different vaterite (ill-crystallised with different shapes) are also found on the specimen surfaces of crystal such as discs and lenses, as shown in Figure 7-17 (b).

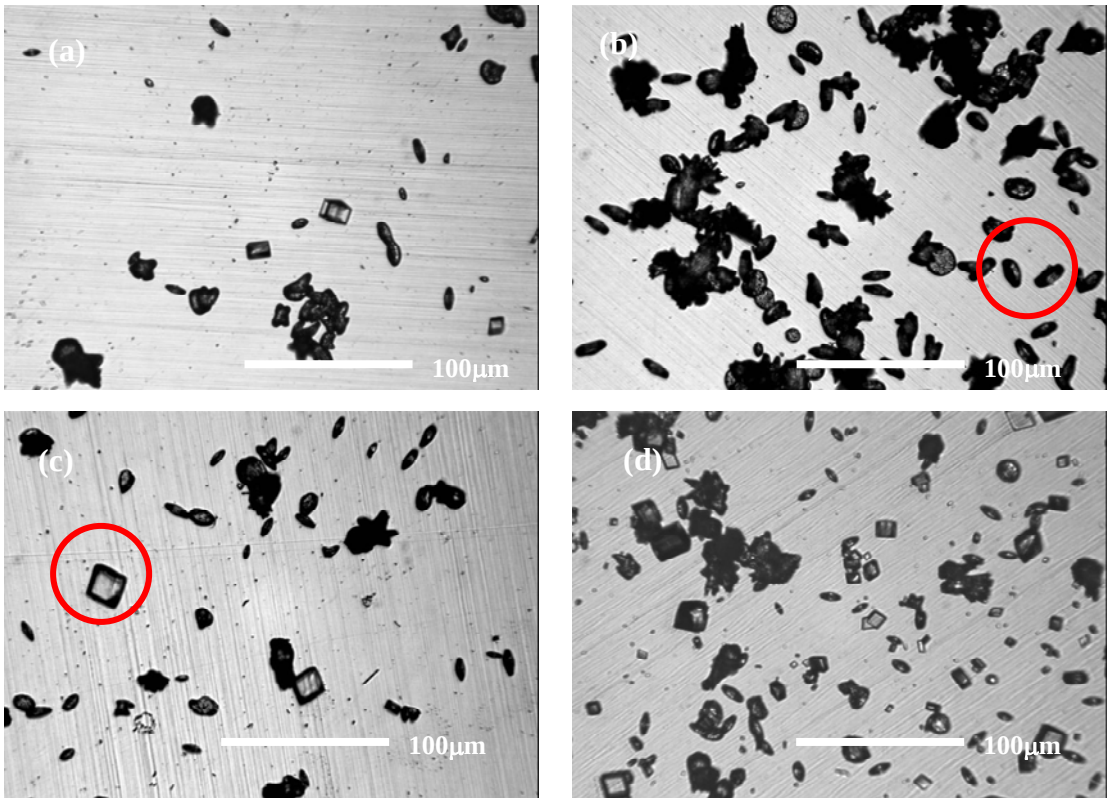

Figure 7-17 Surface conditions of the specimen after electrodeposition of scale under flow rate of (a) 40 ml/min (b) 80 ml/min (c) 120 ml/min and (d) 160 ml/min of in a saturated brine (SR=0.27). The circle indicates (c) rhombohedra calcite and other (b) vaterite

The crystals density on the specimen surfaces is found to be higher when the flow rates increased. This could be observed through comparing the images of scale on the specimen surfaces for flow rate 40, 80, 120 and 160 ml/min as shown in Figure 7-10 (a), (b), (c) and (d). Figure 7-18 represents the electrodeposition of calcium carbonate in the presence of magnesium ions on the specimen surfaces at flow rate (a) 40 and (b) 80, (c) 120 and (d) 160 ml/min. For saturated brine 1.09, different types of crystal shapes and

morphologies of calcium carbonate scale were deposited on the specimen surfaces. Most crystals were calcite, rhombohedra and cubic shapes, as shown in Figure 7-18 (a). The crystals appeared to be perfect-edged rhombohedra on the specimen surfaces. This is in contradiction to other findings where the presence of magnesium ions favours the formation of rounded-edge crystals. Only a small amount of vaterite found on the specimen surfaces as shown in Figure 7-18 (b) "flower" shape.

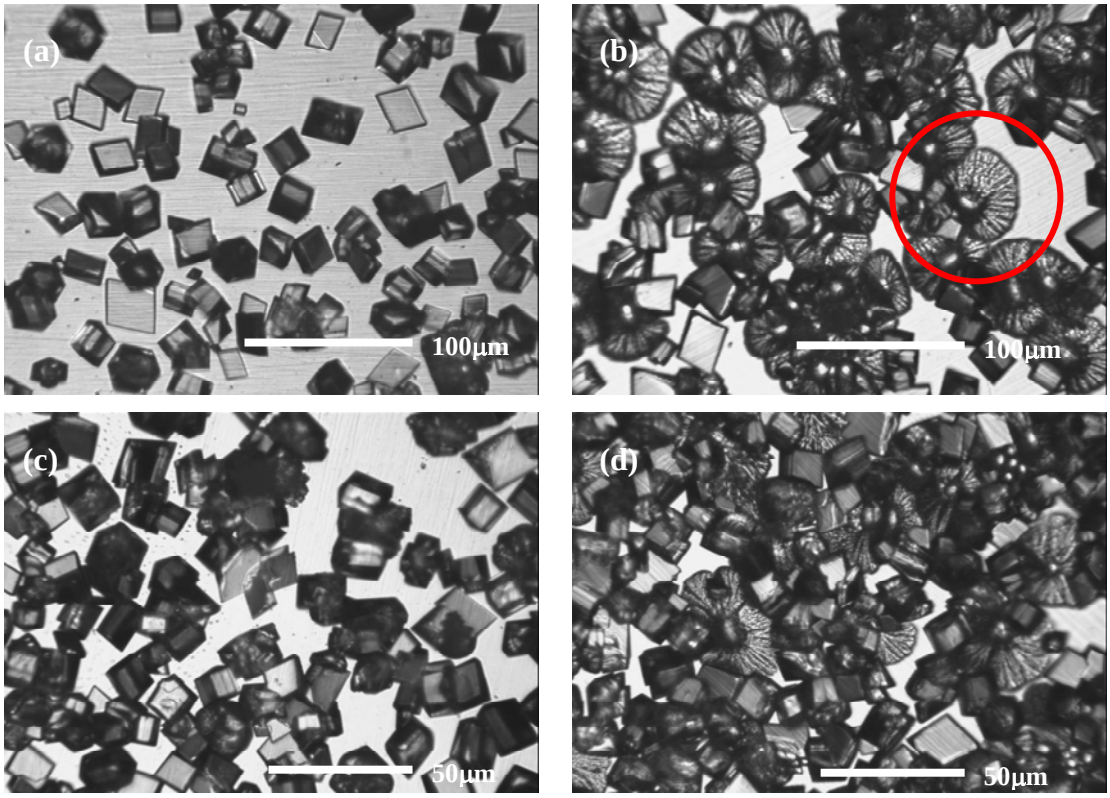

Figure 7-18 Surface conditions of the specimen after electrodeposition of scale under flow rate of (a) 40 ml/min (b) 80 ml/min (c) 120 ml/min and (d) 160 ml/min of in a saturated brine (SR=1.09)

All images show similar crystals coverage with respect to the flow rates, as the specimen surface was totally covered by mineral scale. Hence, only the image of flow rate 40 ml/min is chosen to be presented as shown in Figure 7-19 (a) and (b) for the saturated brine 17.8. Figure 7-19 (b) shows all active areas are covered by calcium carbonate scale with crystal morphology of calcite and vaterite. Images indicate no active area could be found as shown in Figure 7-19.

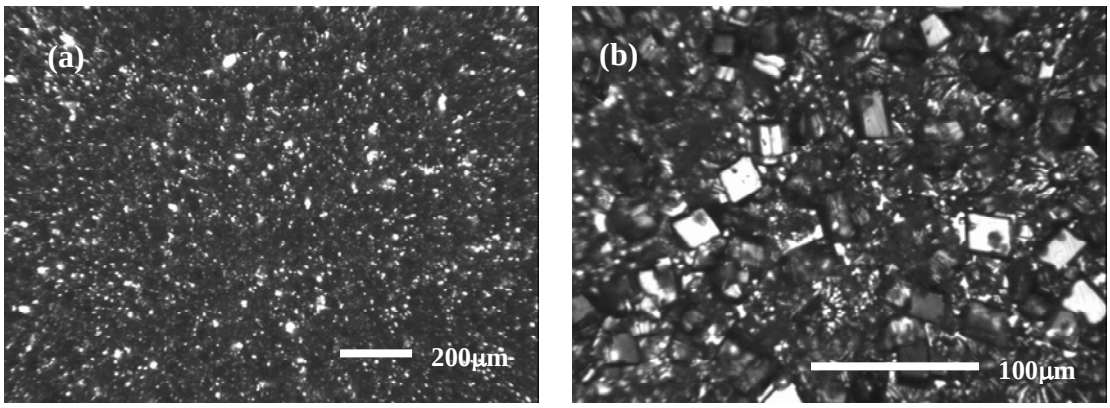

Figure 7-19 Represents an image of the specimen surface after electrodeposited with scale at a flow rate of 40 ml/min for saturated brine with a saturation ratio of 17.8.

Generally, the scale coverage quantification results of calcium carbonate deposited under cathodic polarisation are in agreement with the literature [162]. Polymorph, morphology and size of precipitated calcium carbonate are influenced by a number of parameters such as temperature, pH, degree of supersaturation, ion concentration and presence of additives [163-167]. In this study, the deposition conditions were similar except the brine hardness (saturation ratio) is being used for undersaturated and supersaturated brine. For all the experiments, the degree of supersaturation is sufficient for $CaCO_3$ crystallisation. The crystalline morphology is predominantly calcite and vaterite for the saturated brine solution and undersaturated brine solution respectively. As the experiments were carried out at room temperature, no aragonite could be observed.

The majority of the crystals formed in the undersaturated brine are the ill-defined vaterite. This is mainly related to the nucleation process. There is a strong correlation between the nucleation rate and the occurrence of type of crystal deposited as reported by Gabrielli *et al.* [16] and Euvard [162]. Kitano claimed a large percentage (40% at 10°C) of any precipitate from a carbonate solution is still calcite even in the presence of magnesium, except at high temperatures [168]. The degree of hardness is a major parameter governing the scaling power of the brine solution. Local supersaturation ratio is believed to be higher than bulk solution's saturation ratio, hence this condition favours sufficiently to allow nucleation of the vaterite and calcite. Although crystallisation occurs when specimen is polarised in undersaturated brine, types of scale found on the specimen's surface is different compared to saturated brine.

In a mild hardness solution (78 ppm and 357 ppm of Ca^{2+} and HCO_3^- respectively), vaterite is the predominant crystal where a low progressive nucleation is established. Conversely, supersaturated brine responded instantaneously to nucleation where the nucleation and growth of calcite and minor vaterite was promoted [63, 162]. Hence, a good correlation of the scaling tendency slope was established by the current versus the time for various saturation ratios and flow rates.

7.5.3.1 Concluding Remarks of Crystal Morphology

In summary, cathodic polarisation of a 316L stainless steel specimen at -0.8V (Ag/AgCl) in saturated brine solution at or above 1.09 favours calcite deposition whereas for undersaturated brine, 0.27 it favours vaterite deposition. Under the conditions of high pH, which can be generated at the electrode surface during electrodeposition and undersaturated brine solution, the formation of ill-vaterite is favourable.

7.5.4 The Effect of Flow rate on Scaling Tendency Slope Measurement

It is well recognised that velocity plays a major role on the scale formation and deposition processes. In general high velocities may reduce the scale formation due to scale removal and also impeded the nucleation rate [17]. However, this is not the case for this study, as the flow rate of the liquid is less than 200 ml/min that seem to be significant to cause any scale removed. Investigation of flow effect on various saturation ratios was carried out. The scaling tendency slope was slightly affected by the flow rate. Higher flow rate leads to more dissolved oxygen on the electrode surface hence generates a higher cathodic current density. The interfacial pH depends on the rate of diffusion of oxygen molecules toward the electrode, the rate of diffusion of OH^- ions toward the bulk solution, the rate of consumption of OH^- with bicarbonate and calcium to form calcium carbonate as below;

$$Ca^{2+} + HCO_3^- + OH^- \rightarrow CaCO_3 + H_2O$$

Within this flow range of 40-160 ml/min, the crystal growth rate is dependent on the flow for all the saturated brine. As the flow rate increases the growth and rate of the crystal increases for calcite and vaterite as can be observed on all the images. With an increase in the solution saturation ratio, a faster nucleation and growth of crystals is observed. High saturation brine provides a greater driving force for nucleation and growth process. These two effects also decrease the scaling time where the surface is

rapidly covered and blocked by calcium carbonate scale. An increase of the flow rate accelerates the scale deposition certainly via increase oxygen diffusion molecules as a result of a decrease in the thickness of the diffusion layer specimen/electrolyte interface. A faster mass transport process can occur, oxygen is transported towards the specimen's surface where oxygen reduction reaction takes place. This generates more OH^- and increases the local pH at the electrode surface. Hence, more scale is deposited more quickly on the specimen's surface and the steeper the scaling tendency slope value. This also confirms that under the scaling measurement it is under mass transport controlled. This also implies that in this flow range, the diffusion rate of OH^- to the bulk solution is less significant and the consumptions of OH^- with bicarbonate and calcium to form calcium carbonate does not decrease the interfacial pH generated. Devos [142] reported that the local pH increased with Re number, in particularly in a domain below 200 and for higher Re number, the pH at the electrode surface increase slightly to reach limiting value. Gabrielli [17] reported an increase of calcareous scaling as the flow rate is significantly increase between stagnation to a flow rate 300 ml/min, above this value only slight increase of scaling due to pH of the electrode surface due to diffusion backward of OH^-.

Deslouis [18] claimed that the observed current due to the diffusion-limited oxygen reduction largely underestimates the actual scale coverage when the electrode surface is partially blocked. The investigation is conducted using the EIS technique. It is noted that even though the use of impedance technique can considerably improves the understanding of the electrochemical scaling process, this approach is much too complicated and time consuming to be used in practical situations [17].

7.5.5 Scaling Time Quantification

A rough estimation of the potentiality of waters scaling has been reported and studied by determined the scaling time. The scaling time is defined as the intersection of the current curve and the time axis. This provides a rough estimation on scaling power of waters. The scaling time determined in this study is in concurrent with the Ledion [144], Leroy [169], Gabrielli [17] findings, that is scaling time decrease with increase the brine hardness. The shorter the scaling time, the more the brine solution is susceptible to scaling. The nucleation and growth kinetics of calcium carbonate by an electrochemical driving force has been studied on a more quantitative way by using an electrochemical

quartz microbalance. An approximation technique using the scaling time to define when likely a system is potentially subjected to mineral scale deposition was used in this study. This parameter, an additional to scaling tendency slope measurement was used as an in this investigation to determine the potential of scaling tendency of a brine solution as described in section 7.5.1.1. This section presents the results of scaling time of the supersaturated brine. For the undersaturated brine (SR=0.27), no scaling time could be determined as it was impossible to determine the intercept value on the X axis. The current density was almost parallel in time with respect to flow rate as shown in Figure 7-15.

Results of the scaling time obtained from the current density versus time data are presented in Figure 7-11 (section 7.5.1.1). The dashed line in this figure represents an example of the method to determine the scaling time. When the dashed line crosses the X-axis, the intercepted value on the axis gives the scaling time. The scaling time of each flow rate of the three identical tests are presented as in Table 7-6 and Table 7-7 for saturated brine 1.09 and 17.8 respectively.

Flow rate (ml/min)	Scaling Time, s			
	Test 1	Test 2	Test 3	Average
40	44000	38000	40000	40667
80	16800	11800	19000	15867
120	13800	14500	13500	13933
160	9000	7800	8500	8433

Table 7-6 Results of the scaling time for scale electrodeposited on the specimen surfaces under various flow rates in a supersaturated brine (SR=1.09) of three identical tests

For the lowest flow rate, 40 ml/min no scaling time could be determined since the slope value is out of the scale range and it is all most parallel to the X-axis. A shorter scaling time would be expected for a higher flow rate as shown in Table 7-6. This is consistent with the findings of steeper scaling tendency slope as saturation ratio increases. Table 7-7 represents determined scaling time of in a supersaturated brine (SR=17.8) for various flow rates. These results of scaling time also correspond to the flow rates, where less time was required to deposit scale on the specimen surfaces as flow rate increased as comparing to a less saturated brine solution (1.09). All the active areas of the specimen surfaces was covered with scale prior completion of the polarisation experiment as shown in Figure 7-13. Generally, the scaling time is at least twice as

faster for the all flow conditions for saturated brine with 17.8 saturation ratio. The scaling time obtained were 9 500, 5 600, 4 800, 3 933 seconds, that responds to 40, 80, 120 and 160 ml/min to cover >90% of the surface electrode.

Flow rate (ml/min)	Scaling Time(s)			
	Test 1	Test 2	Test 3	Average
40	9500	8000	11000	9500
80	4400	6200	6200	5600
120	5000	5000	4400	4800
160	3800	4000	4000	3933

Table 7-7 Results of the scaling time for scale electrodeposited on specimen under various flow rates in saturated brine (SR=17.8) of three identical tests

The scaling time of saturated brine (SR=8.91) is in-between the saturated ratio of 1.09 and 17.8. The scaling time decreases as the flow rates increase with respect to the saturation ratio as shown in Figure 7-20. It is at least 1.3 times longer than supersaturated brine with a saturation ratio of 17.8.

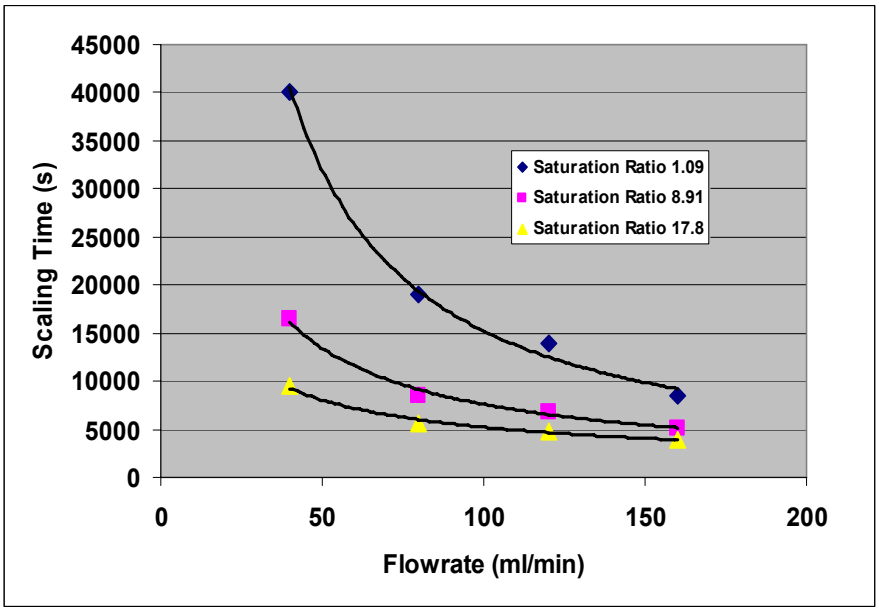

Figure 7-20 Representation of the scaling time as a function of flow rates for three saturated brines 1.09, 8.91 and 17.8

The scaling conditions of a brine solution can be monitored and quantified by the scaling time. The scaling time decreases as saturation ratio of brine solution increases. It is clearly demonstrated for the undersaturated brine solution (Saturation Ratio <1), no scaling time can be determined compared with saturated brine solution (saturation ratio >1). Scaling time determined for both saturated brine solution is in agreement with the

scaling tendency slope measurement. The higher the concentration of the saturated brine solution, the shorter of the time required for scale to be deposited on the electrode surface and also a steeper scaling tendency slope value is expected. This can be attributed to a higher thermodynamic driving force to promote faster mineral scaling. The ranking of scaling potential follows as: undersaturated brine with a SR=0.27 < saturated brine with a SR=1.09< saturated brine with a SR=17.8.

7.6 Verification of the Relationship of the Scaling Tendency Slope and the Saturation Ratio

The purpose of this section was to verify the relationship or the curve established between the scaling tendency slope and saturation ratio that under various flow rates. Additional saturated brine with a saturation ratio 8.91 was selected to determine the scaling tendency slope. The data (scaling tendency slope) was then refitted into the curve. Through this, the accuracy of the curve established in previous section could be assessed. Two identical experiments were carried out to ensure the reproducible result of this saturated brine for various flow rates 40, 80, 120 and 160 ml/min. For each of these flow rates, the scaling tendency slope was determined.

Electrochemical data of the current versus time was recorded for this saturated brine. A similar trend of current curve as in supersaturated brine 17.8 was obtained (as in previous section Figure 7-13). The scaling slope of saturation ratio 8.91 was determined from the post analysis which indicated that an increase of the slope values from 9.74×10^{-09} A/cm^2/s (40 ml/min) to 38.2×10^{-09} A/cm^2/s (80 ml/min) then 62.5×10^{-09} A/cm^2/s (120 ml/min) and finally a slope value of 88.6×10^{-09} A/cm^2/s as shown in Figure 7-21. The average value of the scaling tendency slope from this test was then fitted back into the scaling tendency slope versus the saturation ratio or flow rate, established from the previous section 7.4.1 and 7.5.1. The refit data of the scaling tendency slope of various flow rates for this saturation brine is shown in Figure 7-22. In this figure, the scaling tendency slope versus saturation ratio of all flow rates (40, 80, 120 and 160 ml/min) were established. It was done by fitting the additional data from 8.91. The example in Figure 7-22 flow rate 40-8.91 is represented as fitted data of the flow rate 40 ml/min of saturation ratio 8.91. A good correlation and well fitted data was found for the saturated brine with a saturation ratio 8.91 as shown in Figure 7-22 and Figure 7-23 respectively. As expected the data obtained from 8.91 is lies between 1.09

and 17.8 since the saturation ratio of 8.91 is more than 1.09 but less than 17.8. In addition, the concentration of calcium ions and bicarbonate ions are in-between those of the two brines.

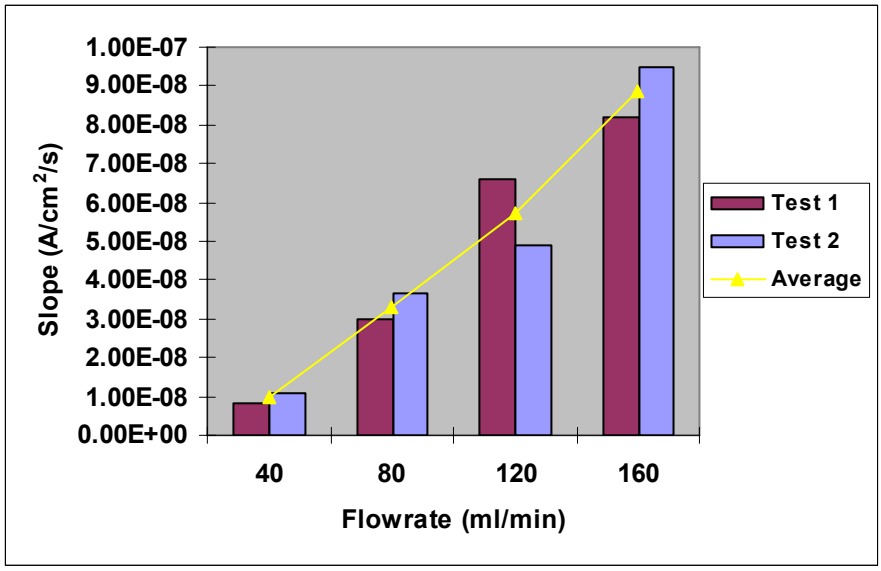

Figure 7-21 Representation of the scaling tendency slope values responses to various flow rates determined by polarised a specimen at –0.8V for 2 hours in an supersaturated brine (SR=8.9)

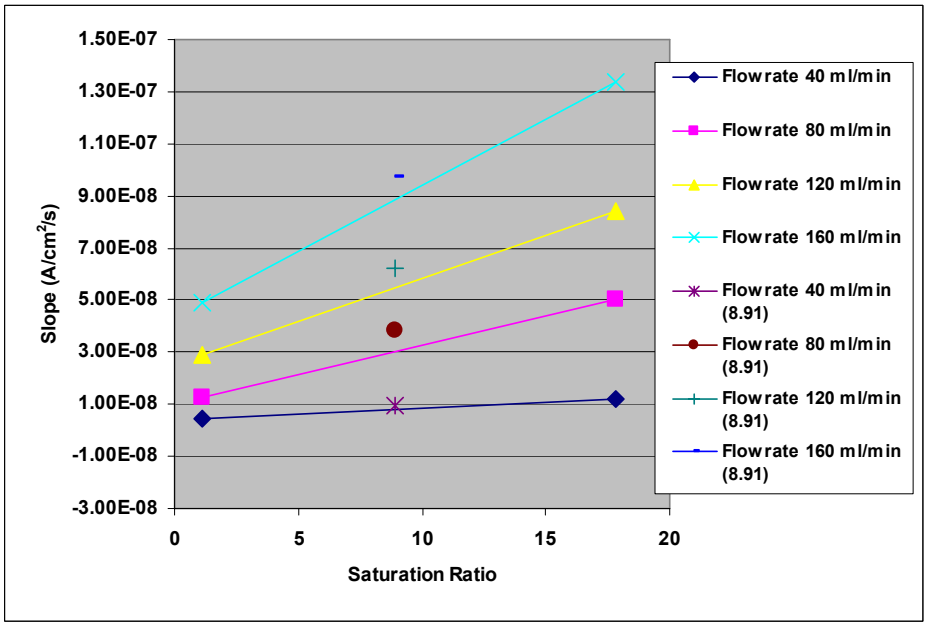

Figure 7-22 The refit data of the scaling tendency slope value of various flow rates for saturation ratio 8.91 into curve of slope versus the saturation ratio

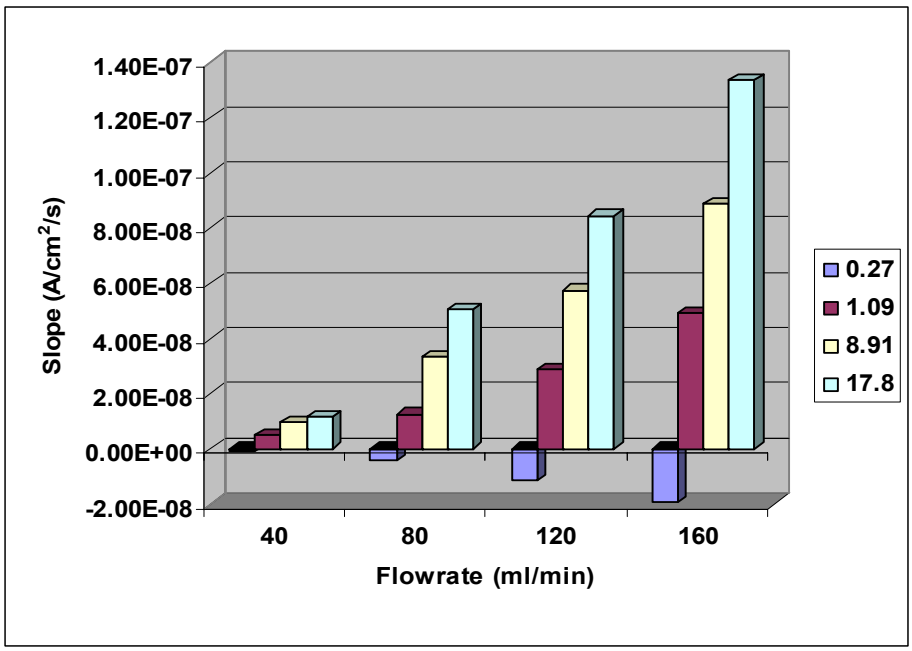

Figure 7-23 Representation of scaling tendency slope versus flow rates for the brine with different saturation ratios of 0.27, 1.09, 8.91 and 17.8

The existing study is mainly focused on understanding the electrochemical technique and the development of a methodology for scaling quantification. It is envisaged this methodology can be used to study the kinetics of calcium carbonate but a separate evaluation such as shape factor, number of nucleation sites has to be considered which has not been included in this study. There has been literature reporting that the current intensity greatly overestimated for a partially scaled or blocked electrode. This has been studied extensively using the EIS technique with an equivalent circuit to represent the scale deposited on the surface. The use of the electrochemical impedance spectroscopy has lead to a better understanding of the blocking process of the electrode by the insulating layer [19]. Various equivalent circuits for analysing EIS data have been proposed [14, 18, 25]. For qualitative assessment, a correction factor can be introduced into this methodology that could be determined by EIS in future work. However, the main objective of the existing study is to develop a methodology that can provide a good estimation and quantification on the amount of scale deposited as well as the scaling tendency of a system. This technique needs not only to be easy to use but also less complicated in terms of data interpretation compared to other techniques such as Electrochemical Impedance Spectroscopy (EIS).

A correlation between the calcium carbonate deposited and scaling tendency was demonstrated using this methodology. The hypothesis is based on the premise that the

reduction of limiting current is linear with the reduction of active area as a result of progressively surface blockage by calcium carbonate scale. The limiting current is proportional to the flow of oxygen moving by convective diffusion towards the electrode for oxygen reduction process. The limiting current decreases as the active surface is progressively blocked by the growth of calcium carbonate scale. The slope value of limiting current versus time (i_L versus t) plot can be used to establish the scaling tendency of a brine solution. Experimental results have demonstrated that a good correlation between the negative slope value ($A/cm^2/s$) of the limiting current density versus time. The changes of the scaling tendency slope give or indicate the scaling tendency or water chemistry of the brine solution in a system.

One of the findings from the scaling tendency quantification is a good correlation between the scaling tendency slope and the saturation index (log of saturation ratio) can be related with empirical equations for each flow conditions. The measured scaling slope value for the brine solution with a saturation index (SR =8.91) is close to the calculated value using the empirical equation that established between the scaling tendency slope and saturation ratio.

Experimental verification was performed using a submerged impinging jet cell, which ensured a quantitative hydrodynamic control. The negative scaling tendency slope increases with increase the saturation ratio and a set of empirical data was established through this study and is listed as below (saturation index is the logarithm of saturation ratio) as shown in Figure 7-24. The empirical relation of each flow rate is presented in Table 7-8.

Flow rate	$Re^{1/2}$	Empirical Relation	R^2
40	9.98	Y=-6.70E09X-3.55E-09	0.954
80	14.12	Y=-3.02E-08X-1.15E-08	0.969
120	17.29	Y=-4.98E-08X-2.09E-08	0.956
160	19.97	Y=-7.57E-08X-3.36E-08	0.938

Table 7-8 Summary of the empirical relation between the scaling tendency slope and saturation ration for various flow conditions

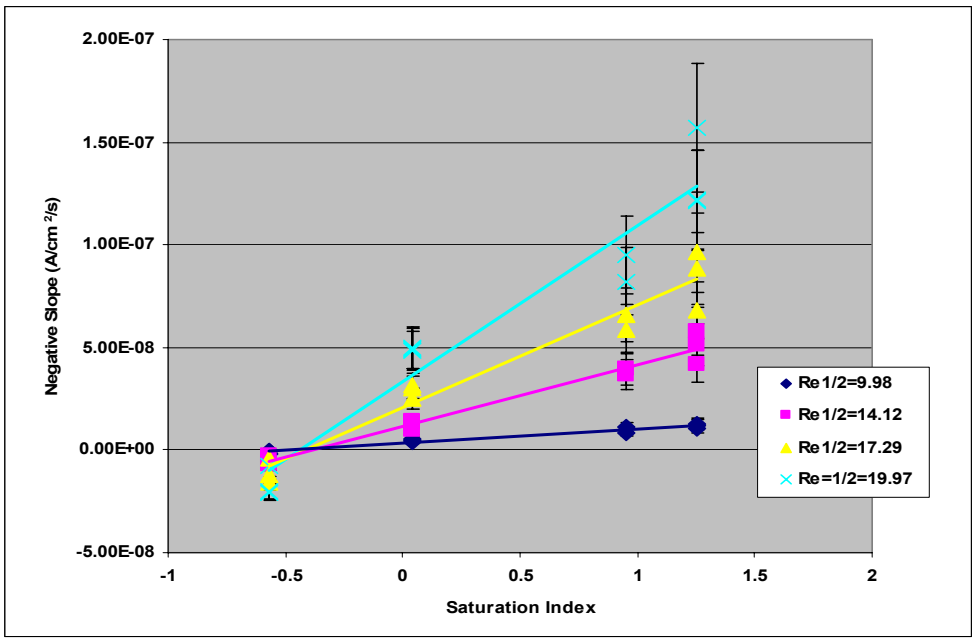

Figure 7-24 Scaling tendency slope versus saturation ratio for various Square root of Reynolds' Number

The accuracy of the scaling tendency slope measurement by the electrochemical technique in a SIJ cell is approximately 23 %. The significant error of the measured scaling tendency slope value could be explained as the synergistic effect among the oxide film reduction, the presence of bicarbonate and surface scaling during polarisation. The effect of each was discussed previously. Though scale tendency slope measurement is conducted at the predominantly at scale deposition process, these effect on electrochemical measurement cannot be completely ignored. Also for mineral scale deposition, it is the first layer of deposition which controls the further growth of the scale [170]. The formation of first layer Mg-Ca rich compound may have indirect influence on the subsequent calcium carbonate deposition as well as oxide film reduction. Despite the accuracy, the saturation index of various brine solutions can be clearly differentiated through using this methodology. The scaling tendency slope value is proportional to saturation index and flow rate. This also provides a better understanding of the use of technique toward electrochemical measurement especially surface scaling.

7.6.1 Conclusions of the Scaling Tendency Slope Measurement

A methodology has been developed to monitor and quantify the scaling tendency of brine solution. This is based on the electrochemical measurement in SIJ cell rig. Brine solutions consist of various saturation ratio can be quantified for various flow

conditions. Under the flow range 40-160 ml/min, a good correlation is established between the scaling tendency slope value and saturation ratio. It is clearly demonstrated that the slope value of the brine with saturation ratio 8.91 with various flow rates are well fitted into the establish relation. This verifies the established relation between saturation ratio and scaling tendency slope value.

7.7 The Practical Application of SIJ Technique

The research work is mainly concentrated on the development of a methodology to quantify the scaling conditions of a brine system. It started with a simple experiment and basic equipment set up. Hence, a less complicated condition such as absence of oil, inhibitors and sand, atmospheric pressure and temperature environments have been investigated. One of the main contributions and practical applications of this technique is for it to be used in the water industry, power industry to quantify the amount of scale deposited on equipment surface. The scaling tendency can be monitored through measuring the scaling tendency slope value then obtaining the saturation index from the empirical relationship as shown in Figure 7-24.

The results from this study will provide useful understanding and the direction for detecting carbonate scaling. Incorporation of this electrochemical technique in combination with SIJ to monitor the extent of scale deposit on the component's surface and the scaling tendency in a system can provide more information not only on potential scaling of a system but also mineral scale deposition.

The study of mineral crystal nucleation and growth using submerged impinging is concurrent with the electrochemical measurement has been reported with QCMB (Quartz Crystal Microbalance). This methodology developed though this study has demonstrated its capability to quantify the amount of scale deposited on the surface of an electrode. Hence, it is possible to use this technique to investigate the crystal growth process by establishing a relationship between the amount of scale deposited and the amount of Ca on the surface of electrode. The amount of mineral scale deposited can be quantified using this methodology whereas the amount of calcium ion can be determined by ICP.

Chapter 8 An Investigation of Surface Cleaning and Surface Sensivity

8.1 Introduction and Objective

Any monitoring device once installed in the production system, regular intervention may be necessary to replace the sensor in order to have a reliable, real time monitoring data. The sensor replacement process can take several days and may be a hugely costly operation if production shut down is required. This also has a significant safety implication involving monitoring or sensor retrieval. Therefore, any reduction of intervention for sensor replacement would be beneficial to the company in term of cost saving as well as safety issue.

Currently there are various cleaning techniques available for scale removal in industry such as a high-pressure jet systems, mechanical brushing or scrapping. However, this requires the setting up of additional equipment. Furthermore, in operational recovery, the usage of acids or chemicals is common especially during drilling or cleaning processes. Hence, in this study, the electrochemical and acid cleaning techniques were selected in this study. Most of all both methods are relatively cheap as compared to pressure jet system and mechanical brushing techniques. This is mainly because they do not cause any significant changes to the existing equipment setup. Scale cleaning and removal are an important issue for the development of this technique, not only to understand the effectiveness of cleaning but also the effect of acid or chemicals on the sensor/electrode surfaces. In this chapter, an essential preliminarily and feasibility investigation on the electrochemical cleaning and acid cleaning, also the effects of both cleaning techniques on the sensor surface were examined. Optimal conditions to remove scale deposited on the specimen surfaces such as cleaning time, dynamic or static flow conditions, concentration of the acid and intensity of the applied potential to generate hydrogen were investigated. Alternative approaches, such as using the SIJ and employing high corrosion resistance materials were also presented in this chapter.

8.2 Surface Sensivity after Scale Removal/Cleaning Technique

The main objective of this section and following subsections were to investigate the efficiency of two cleaning techniques and the effect on the sensor's surfaces after the cleaning processes. The two cleaning techniques carried out were a) an electrochemical technique and b) acid cleaning. The experimental procedures used to determine the coverage after the cleaning process is the same as described in Chapter 5. All specimens were scale deposited by the RDE at 600 rpm for 3 hours unless specifically specified.

Though the scale coverage determined by the image analysis often indicates less than the scale coverage determined by the electrochemical technique, this technique could be used as a means to quantify the amount of scale deposited/removed on the surface of the electrode and also a verification technique against electrochemical technique analysis. The previous chapter demonstrated that calcium carbonate deposited on the electrode's surface could be estimated by the image analysis with a correction factor of approximately 1.6 times. Hence, the image analysis was selected in addition to the electrochemical technique to quantify the amount of scale removed on the electrode surface.

8.2.1 Electrochemical-Cathodic Polarisation

In this section, the use of the hydrogen evolution process to remove mineral scale on the specimen surface was addressed. Hydrogen was generated on the specimen surface by applying a potential where hydrogen evolution occurs. All the electrochemical cleaning processes used to remove mineral scale were carried out using analysis solution (5 g/L sodium chloride) as a cleaning electrolyte. This electrolyte was also used in the initial analysis and the pH was adjusted to 10.

Up to now, all the experiments of scale coverage quantification had been conducted at a potential of -0.8 V where oxygen reduction takes place. No surface modification was noted for a short period of polarisation (within 5 minutes). For longer polarisation and more negative applied potential polarisation, the surface conditions of the electrode remain unknown. The cleaning processes are designed for a negative potential (above -0.8 V) and longer polarisation time. Hence, as part of the investigation, the cleaning and surface sensivity were assessed for different polarisation conditions in order to

establish a better understanding and the limitations of the sensor under various polarisation conditions might be expected in real working environment. In order to investigate an optimum cleaning condition, a few experiments were performed as follows:

i.) Electrochemical cleaning by applying different potentials to generate hydrogen gases on the sensor surfaces;

ii.) Application of submerged impinging jet to remove mineral scales.

8.2.1.1 Electrochemical Cleaning with Different Applied Potentials

When a specimen is polarised at potential -1 V (Ag/AgCl) the hydrogen evolution process takes place at the electrode/sensor surfaces. It is anticipated that the more negative an applied potential, the more hydrogen gases are generated. Therefore, the purpose of this experiment was to determine an optimum applied potential to remove mineral scale on the sensor surfaces at the same the effect of these optimum conditions on the surface sensivity. Throughout the experiment, a control experiment was setup where using a bare specimen (without mineral deposited on the sensor surface and no cleaning process). The rest of the electrodes were deposited with mineral scale using the RDE technique at 600 rpm for 3 hours and then surface coverage quantification was carried out using the electrochemical technique. All the cleaning processes were performed under static conditions by cathodically polarising the specimen to a potential where generation of the hydrogen gases to be expected. Two different applied potentials, -1.2 V and –1.8 V (Ag/AgCl) for 900 seconds were examined.

The percentage of scale removed is defined as the percentage of the scale coverage before cleaning deducts the percentage of scale coverage after cleaning as shown below

%Scale Removed=%Scale Coverage before Cleaning-%Scale Coverage after Cleaning

Figure 8-1 shows the percentage of scale removal quantified by the electrochemical technique. Preliminarily experiments showed the percentages of scale removed estimated by the electrochemical technique was 3 %, 8 % and 3% corresponding to the applied potential -1.2 V, -1.8 V and control experiment (without subject to electrochemical cleaning) respectively. These results were in correlation with the increase of scale removed determined by the image analysis. Coverage quantification by the image analysis technique indicated approximately of 1.4 % and 3.0 % of scale

were removed from an electrode surface for applied potential -1.2 V and -1.8 V respectively.

These results also show the percentage of scale removed increases with the increase of applied potential, which is expected. When the applied potential increases more hydrogen gas is generated and more scale is removed from the electrode surface. However, increasing the electrochemical potential, could also cause surface modification of the electrode. This finding is supported by the significant discrepancy of the scale removed determined by the electrochemical technique and image analysis as shown in Figure 8-1, even taking into consideration of a correction factor 1.6 for the image analysis technique (described in Chapter 6 "An Investigation of SIJ as A Means of Detecting Mineral Scaling", approximately 2.3 % (-1.2 V) and 5.0 % (-1.8 V) of removal coverage were estimated. Also no significant different levels of scale covered the sensor's surface before or after the cleaning process as shown in Figure 8-2 (a) and (b) but results from both quantification methods indicated certain percentage of scale was removed as shown in Figure 8-1. This could be explained that small quantity of scale may have removed. However it was very difficult to spot any significant changes of crystal levels on the electrode's surface by comparing the images.

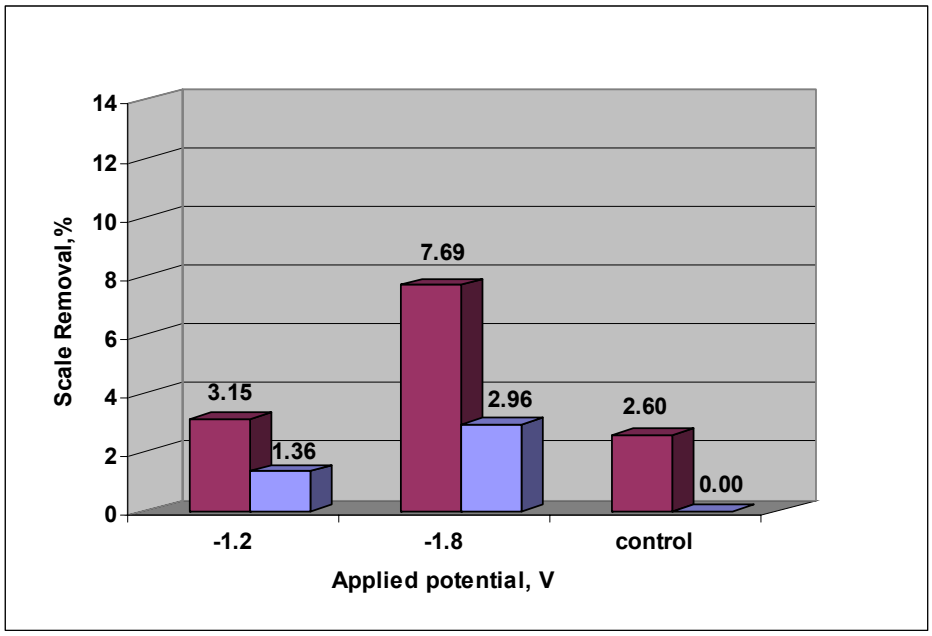

Figure 8-1 Percentage of scale removal determined by the electrochemical techniques (red) and image analysis (blue) for various applied potentials

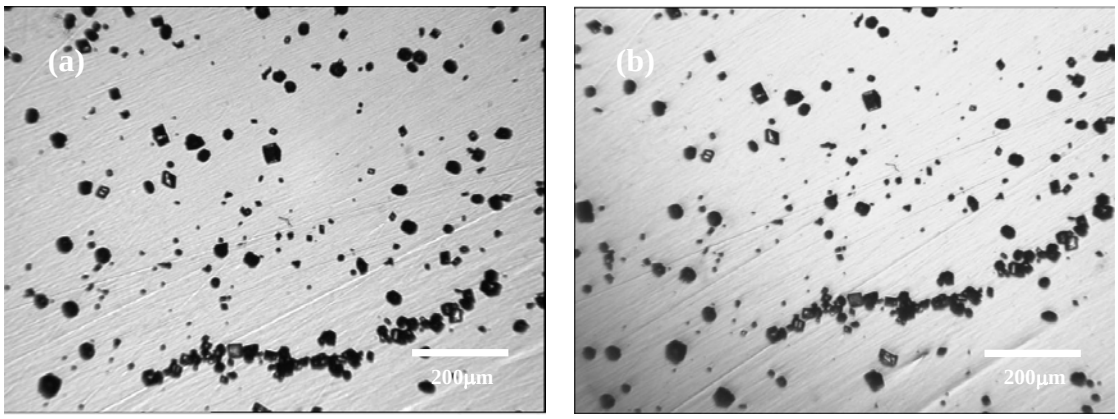

Figure 8-2 Scale covered on the specimen surface (a) before cleaning and (b) after 900 seconds of electrochemical cleaning with an applied potential of -1.8 V

8.2.1.2 Remarks of Electrochemical Cleaning

The calcium carbonate covered on the surface of the electrode can be removed by electrochemical cleaning at potential -1.8 V. However, electrochemical cleaning could have also modified the surface conditions after a cleaning process. This is clearly supported by the discrepancy coverage result between scale removed quantified by the image analysis with correction factor included and the scale removed determined by the electrochemical technique, which is less. This implies surface modification may have occurred on the surface of the electrode. It is difficult to compare the image before cleaning to after cleaning by searching for any sign of crystal removal; visibility not many differences between samples. Moreover, 900 seconds of cleaning time may be too short to remove any scale on specimen surfaces under static conditions. Therefore, further investigations were carried out to increase the polarisation time (cleaning time) for a selected potential under dynamic conditions to confirm if the percentage mineral scale removal is caused by surface medication rather the removal of small mineral scale .

8.2.1.3 Application of Submerged Impinging Jet

This experiment was carried out to investigate the effectiveness of the electrochemical cleaning under dynamic conditions using the submerged impinging jet as a means of generating the flow. The results obtained in section 8.2.1.1 for 900 seconds of cleaning potential at –1.8 V showed a significant amount of scale removal from the specimen surfaces, but only under a static condition. Therefore, a further investigation was carried out under a dynamic condition so more scale could be removed. A scaled specimen was then placed in the cell rig and was subjected to SIJ at a flow rate of 190

ml/min while it was cathodically polarised the specimen to –1.8 V (Ag/AgCl) for 60 or 120 minutes.

The current density versus the square root of the Reynolds number is shown in Figure 8-3. The plot values obtained from the initial, final and cleaning analyses are presented in Table 8-1. For 60 minutes cleaning experiment, the initial analysis of the bare specimen showed the initial-plot value of 0.0246 and a decrease in value of 0.018 for the final-plot (after deposited with mineral scale). Hence, the percentage of scale coverage prior cleaning was 26. When the specimen was subjected to 60 minutes cleaning, an increase of slope value 0.0256 was obtained for the clean-plot. The slope value exceeded the initial slope value of a bare specimen. After the cleaning process, the coverage quantified by the electrochemical technique showed -4 %, where approximately 30 % of mineral scale on the electrode was removed. Similar conditions were observed for the 120 minutes of cleaning, the slope value of the cleaning analysis indicated 0.0368 (cleaned-plot) compared to the final-plot value, 0.0205. For a longer cleaning time, the current density as shown in Figure 8-3 and its slope value the cleaned-plot as presented in Table 8-1 showed increases of current density. The slope value was restored back to its original value and exceeded the initial slope value as shown in Table 8-1. However, results from light microscope images showed no sign of any large crystals being removed and most of the crystals were remained on the electrode surface as presented in Figure 8-5. This implies the sensitivity of the technique is affected by the change of surface conditions as a result of the electrochemical cleaning. This is to be discussed in greater detail later in this chapter regarding the surface modification.

Cleaning Time (min)	Initial-plot (bare)	Final-plot (scaled)	Clean- plot (cleaning)	Electrochemical			Images Analysis		
				Before cleaning	After cleaning	% Remove	Before cleaning	After cleaning	% Remove
60	0.0246	0.0180	0.0256	26.83	-4.07	30.89	10.72	5.47	5.25
120	0.0241	0.0205	0.0268	14.94	-11.20	26.14	5.63	2.51	3.12
Control	0.0238	0.0237	0.0234	0.42	1.68	-1.26	/	/	/

Table 8-1 Results of the slope values and scale coverage before and after cleaning for various cleaning times under impingement conditions that were determined by the electrochemical and image analysis techniques

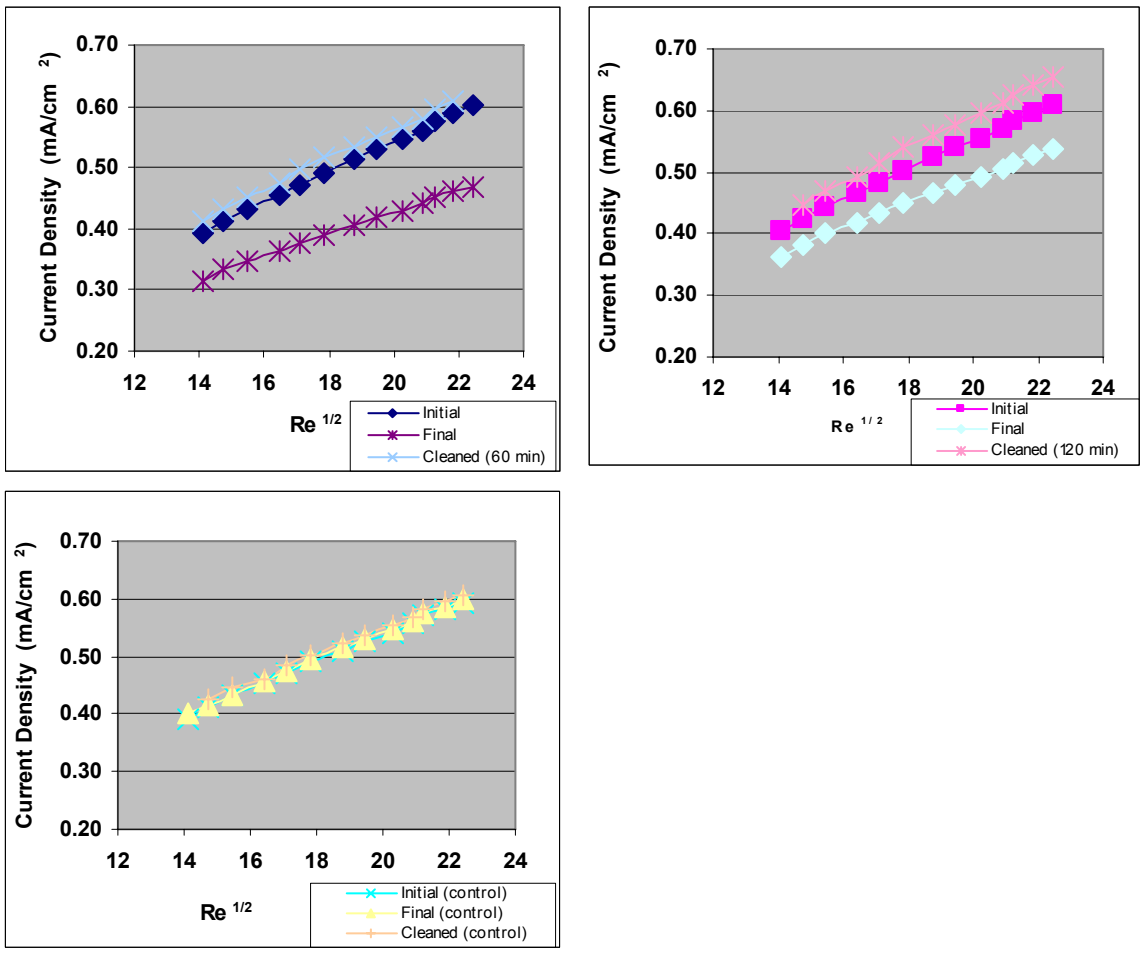

Figure 8-3 The current versus the square root of the Reynolds' number of the initial, final and cleaning analyses for cleaning times of 60 and 120 minutes under dynamic conditions

Figure 8-4 shows the percentage of scale removal determined by the electrochemical and the image analysis techniques for acetic acid electrolytes of different cleaning times. The percentage of scale removed was determined by the electrochemical technique indicating approximately 30 % scale was removed under the dynamic condition after 60 minutes of cleaning. The increase of cleaning time did not increase the scale removal but it caused the surface modification process, as shown in Figure 8-4.

Figure 8-5 and Figure 8-6 show images of the specimen before cleaning (scaled-specimen) and after the cleaning processes where the specimen was subjected to an impinging jet with a flow rate of 190 ml/min for 60 and 120 minutes of cleaning respectively. Although scale removal quantified by the electrochemical technique indicated that some mineral scale were removed from the specimen's surface, but the image analysis showed the specimen surface was not completely cleaned, there were still some mineral scale remaining on the specimen surfaces as shown in Figure 8-5 and

Figure 8-6. There is an indication of a slight decrease of scale on the specimen surface for both cleaning times 60 and 120 minutes when the specimens were subjected to electrolyte impingement at 190 ml/min during the cleaning process. This implies that an increase in the flow rate in this study has no effect on surface cleaning.

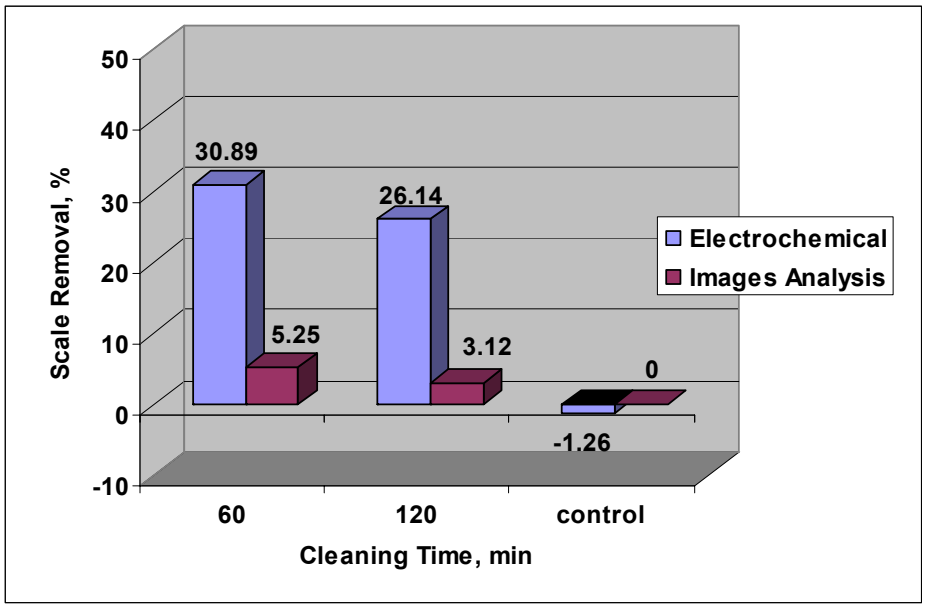

Figure 8-4 Percentage of scale removal determine by the electrochemical and the images analysis techniques for acetic acid electrolyte of different cleaning times

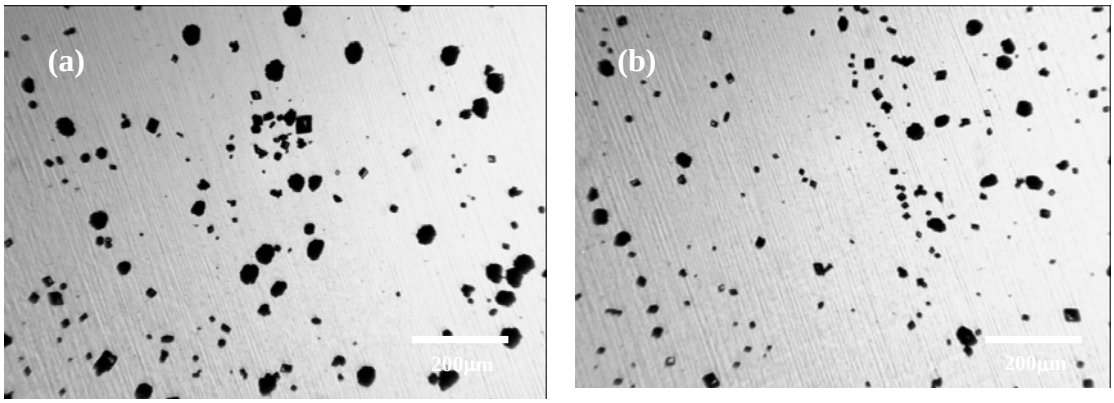

Figure 8-5 Scale covered on the specimen surfaces a) before cleaning and b) after 1 hour of cleaning with an applied potential of -1.8V

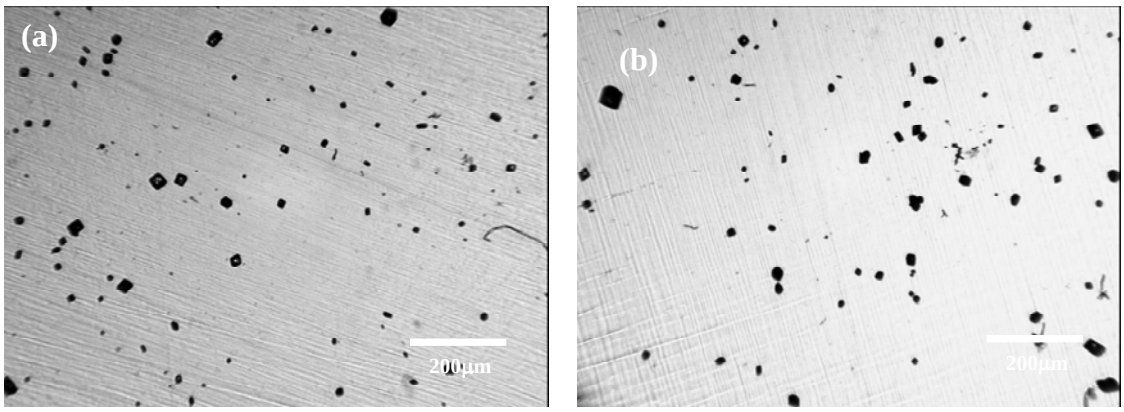

Figure 8-6 Represents the specimen surface condition on specimen surfaces a) before cleaning and b) after 2 hours of cleaning with an applied potential of -1.8V

8.2.1.4 Remarks of Electrochemical Cleaning Technique

Calcium carbonate scale on the surface of the specimen can be removed by electrochemical cleaning when the specimen is subjected to a potential at -1.8 V for 60 minutes. However, this cleaning technique is not effective as most of calcium carbonate scale remained on the surface of the electrode. It is believed the loose crystals as well as sub-micro crystals may be removed from the electrode surface with the large crystals (size approximately 30 μm) remaining on its surface. As the cleaning time increases, more scale is removed from the electrode's surface, but at the same time, the surface condition of the electrode is changed. The surface modification has led to some sensitivity issues on electrodes for the electrochemical measurement. This will be discussed in more detail later in this chapter.

8.2.2 The Understanding and Effect of Electrochemical Cleaning on Surface Coverage Quantification

The percentage of scale removal was quantified by the electrochemical and image analysis technique. There were a few inconsistencies of scale removal results from the scale removed measured by the image analysis and scale removed quantified by the electrochemical technique as presented in Figure 8-1 and Figure 8-4. The inconsistency could be related to the surface modification caused by scale removal process through electrochemical or polarisation process. When a specimen is cathodically polarised to a potential where oxygen or hydrogen evolution occurs, two possible reactions take place; the removal of scale by gas generated at electrode surface and surface modification on electrode surface to be more reactivity to oxygen reduction process.

Firstly, the mineral scale can be removed by gas generated on the surface, in this case, hydrogen gas. This gas establishes mechanical scrubbing action that loosens and lifts the mineral scale on the specimen surface. As a consequence of this, it exposes more active areas for oxygen reduction to be taken place on the specimen surface. As a result, the current density is expected for surface area covered with scale after cleaning compared to current density of the area covered with scale before cleaning.

Secondly, cathodic polarisation of the specimen may change the ionic properties of the oxide film. The ionic property is strongly related to the number of electrons involved for oxygen reduction.

This finding is supported by the experimental results obtained for 1 hour and 2 hours of electrochemical cleaning at -1.8 V (refer to section 8.2.1.3). The slope value was restored back to its original value and in some cases exceeded the initial slope value under dynamic conditions (after 1 and 2 hours of polarisation). The slope also increased with an increase in polarisation times but image analysis showed only small amount of scale removed. This implies the surface modification by the oxide film reduction on the electrode surface has taken place that contributes to the increase of current density rather the removal of the scale since some calcium carbonate remained on the specimen surface. This subsequently affects the electrochemical measurement used for scale coverage quantification and the percentage of coverage after cleaning is more than the coverage before cleaning. This also explains the discrepancy in coverage determination between the electrochemical technique and the image analysis technique.

The longer the polarisation time, the more the Fe (III) on the oxide film is reduced to Fe (II) and the higher the content of Fe (II) in the oxide film. Thus, it favours the oxygen reduction reaction. The outer oxide layer of the passive film, ferric oxide, Fe_2O_3 could be reduced or reducible at potential -0.5 to -0.8 V/ SCE [171] and -1.1 V /SCE [159] but not with the chromium oxide, Cr_2O_3. A pre-reduced surface of stainless steel is formed when oxygen reduction occurs at potential -1.1 V /SCE under aerated conditions was reported [159]. Under these conditions, the oxygen reduction mechanism mainly follows a 4-e^- pathways, even the surface is partly covered by non-reduced chromium oxide. Hence, both of these contribute to the increased slope value after cleaning when the specimen is subjected to more negative potential where hydrogen evolution occurs.

8.2.3 The Effectiveness of Electrochemical Cleaning

Generally, the image analysis technique proves to be a better method for scale removal quantification since it is not affected by the surface modification compared to the electrochemical technique. The results obtained from image analysis can be used for coverage quantification. Image analysis found the scale removal increased as the applied potential increased, as more hydrogen gases are generated as shown in Figure 8-1. The longer the cleaning time, the more scale removed. However, the percentage of scale removed was only slightly improved by dynamic conditions (impinging jet). It is expected the electrolytes under dynamic conditions can produce shear stress to remove scale. In addition, flow rate increases the diffusion of oxygen/ hydrogen towards the specimen's surface and promotes more hydrogen evolution. This leads to higher mechanical scrubbing generated by hydrogen in conjunction with shear stress produced by the electrolyte movement to remove the loosened scale. However, this is not the case as the scale removal determined by the image analysis was of a similar magnitude. This suggests the hydrogen evolution is only able to remove small amounts of scale in the presence of hydrodynamic conditions because it is believed that the shear stress used in the existing study is less than the critical shear stress reported in literature for the impinging jet to be effectively removed any deposited calcium carbonate. The use of SIJ to study the persistency of the inhibitor film was reported by Esteban *et al.* [111]. It was reported that a critical speed (1.2 m/s) was required to remove weakly absorbed species was reported. The adsorption of inhibitor film is less than mineral scale deposition. Therefore, a higher flow would be expected to remove any mineral scale. In this study, calcite removal is only slightly affected by the electrolyte impinging on the specimen surface. In order to remove scale deposited on specimen surface by jet electrolyte, more than 190 ml/min is required.

Overall, the electrochemical cleaning causes an increase in the slope value and the limiting current density. This is not only the removal of calcium carbonate by the hydrogen gases but also increased the surface reactivity toward oxygen reduction. The longer the polarisation times the more prominent the effect on the surface modification of the electrode.

8.2.4 Acid Cleaning

The purpose of this section was to demonstrate an alternative way to remove or clean the specimen/ sensor surfaces. Acid cleaning was considered since most of the calcium carbonate could be easy dissolved in an acidic environment. Furthermore, acid cleaning is common practise in the oil and gas industry to remove mineral scale such as calcium carbonate. Hence, the optimal conditions (pH and immersion time) to remove mineral scale and its effect on the sensor surfaces were investigated. Two specific acids were used to remove calcium carbonate scale deposited on the specimen surfaces; a) strong acid, hydrochloric acid (HCl) and b) weak acid, acetic acid (CH_3COOH). Acid solution was prepared by adding a certain amount of acid into distilled water to form a different concentration or pH solution.

8.2.4.1 An Investigation of Hydrochloric Acid Cleaning (HCl)

In this section, the effectiveness of hydrochloric acid used as a cleaning medium was investigated. Only electrochemical technique was used to estimate or quantify the amount of scale removed on the specimen's surface. The cleaning was performed under static conditions by immersing the specimen into a prepared acid solution, HCl at pH value of 1.23. Three experiments were carried out:

i.) Control experiment was an experiment conducted where a bare specimen (specimen without treated with acid) was used;

ii.) Control-acid was an experiment conducted where specimen was pre-treated by immersing into HCl solution for 10 minutes;

iii.) Acid-clean was an experiment where the specimen was pre-treated by immersing into HCl solution for 15 minutes prior scale deposition. The pre-treated specimen was then deposited with calcium carbonate scale by RDE technique for 3 hours. Finally, the specimen was cleaned with HCl solution by immersing into the solution for 15 minutes.

Figure 8-7 represents the percentage of scale coverage determine by the electrochemical technique. For the control-acid experiment, specimen surface pre-treated with acid showed a significant change in surface conditions, approximately 20 % coverage. It was clearly indicated that acid immersion had caused some surface changes on the specimen. For a specimen where the surface was pre-treated and then scale deposited, a total surface coverage of 84 % was found and after cleaning with an acid solution, the surface coverage was 79 %, with only approximately 4 % of scale was removed. This

result is expected as some of the calcium carbonate was dissolved when exposing to acid solution consequently more active areas were available for oxygen reduction process. However, after the cleaning, a significant increase of surface coverage was noted. It is believed that the coverage mainly due to surface modification rather than scale coverage. This suggestion is supported with the images as presented in the following SEM image section as shown in Figure 8-10, almost no calcium carbonate scale on the surface of the electrode can be seen. Hence, the acid cleaning properly changes and diminishes the stainless steel surface reactivity against oxygen reduction.

Experiment	% Coverage BEFORE cleaning	% Coverage AFTER cleaning
Control	1.42 (bare specimen)	/
Control-acid	/	20.36
Acid-clean	83.82 (pre-treated and scale deposited)	79.25

Table 8-2 Results of surface coverage before and after cleaning the specimen by HCl conditions that are determined by the electrochemical technique

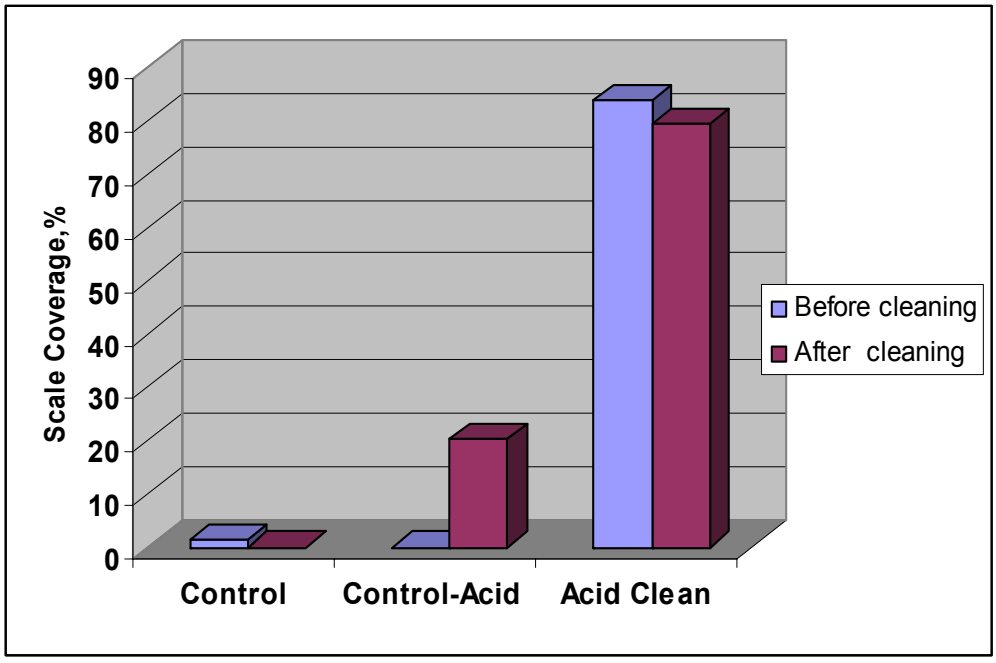

Figure 8-7 Percentage of scale coverage on a specimen surface before cleaning and after cleaning with HCl that are quantified by the electrochemical technique

SEM was used rather than a light microscope, since no significant crystal differences could be found on the electrode surface when the specimen was revealed under the light microscope. From the SEM image analysis, it is evident that the surface condition of

the specimen was changed after cleaning with HCI. By comparing the images between the specimen without acid treatment as shown in Figure 8-8 and specimens with acid treatment as shown in Figure 8-9, patches of grey colour coverage were found on sensor surfaces. After cleaning with HCl, calcium carbonate scale was completely removed from the electrode surfaces as shown in Figure 8-10. This further strengthens the evidence of surface modification as a result of acid immersion.

Figure 8-8 Represents the surface condition of a control specimen without treated with acid HCl

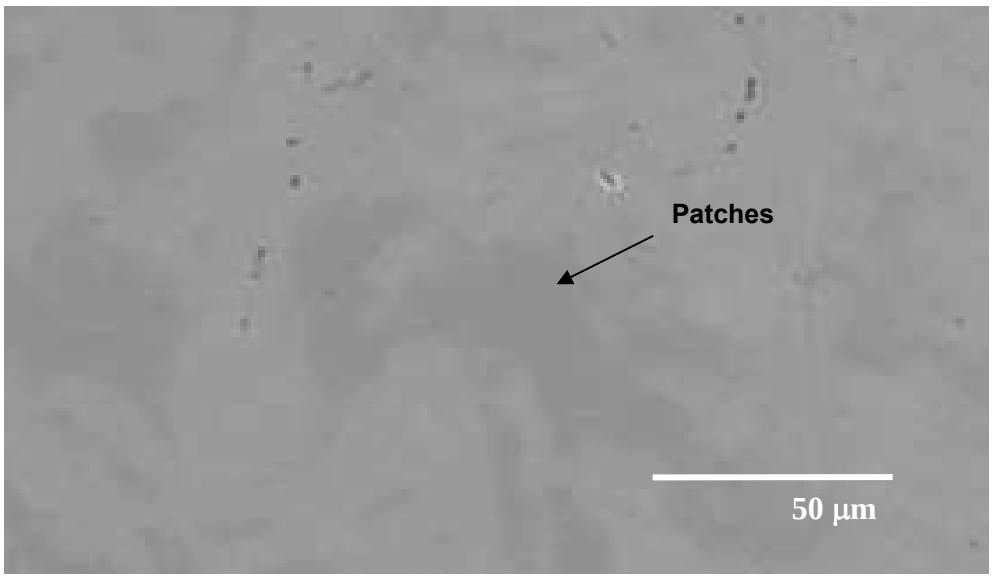

Figure 8-9 Represents the surface condition of an acid-control experiment where the specimen is treated with HCl by immersion for 15 minutes

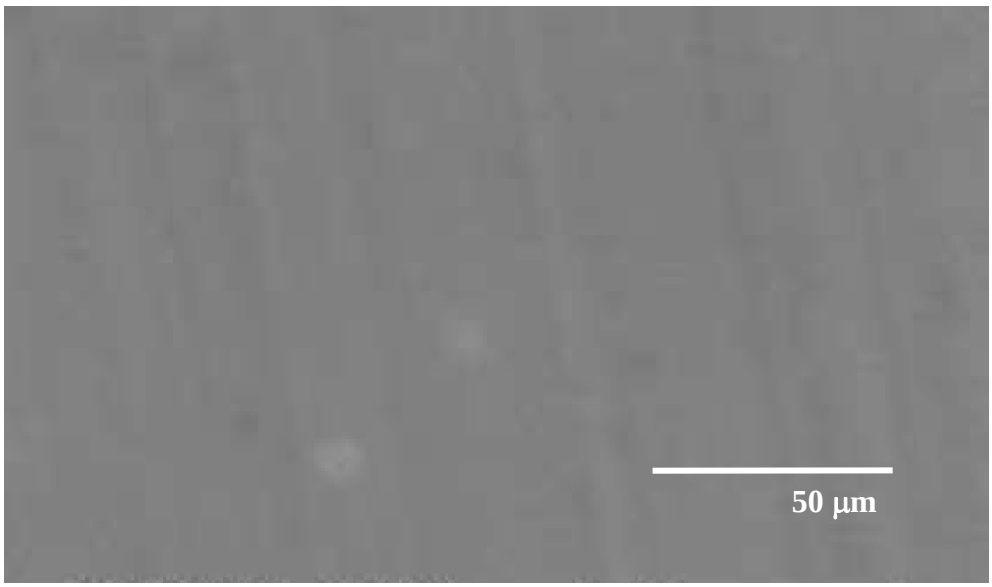

Figure 8-10 Represents the surface condition of a scaled-specimen after cleaning with HCl acid

8.2.4.2 Concluding Remarks on HCl acid Cleaning

HCl can be used to remove calcium carbonate scale deposited on the electrode surface however, the use of this acid has modified the surface conditions of the electrode. The sensivity of the electrode surface caused by surface modification as a result of acid immersion is explained more details in this chapter later. Currently the acid solution pH is 1.23 this may be due to too strongly acidic for cleaning and cause a significant change in surface conditions. Further investigation to explore the possibility of weaker acid usage such as acetic acid was carried out in the following section.

8.2.4.3 An Investigation of Acetic Acid Cleaning

Further investigation of acid cleaning was carried out using weak acid, acetic acid, since the use of strong HCl acid caused a change on the specimen surface. Tests were carried out under static conditions and using acetic acid with a pH value of 2.63 to remove mineral scale under static conditions. All specimens were pre-treated first, by immersion in the acetic acid for 10 minutes. The purpose of pre-treating the specimen was to investigate the surface condition or the effect of acid on a bare specimen (without mineral scale on the specimen surface). After pre-treating the specimens, calcium carbonate scale was deposited by RDE at 600 rpm for 3 hours. Then the scale on the surface of the specimen was removed or cleaned by immersion into acetic acid for 2, 5 and 60 minutes.

The current density versus the square root of the Reynolds number of the pre-treated specimen was in-between the value of the bare and scaled specimen as presented in Figure 8-11.

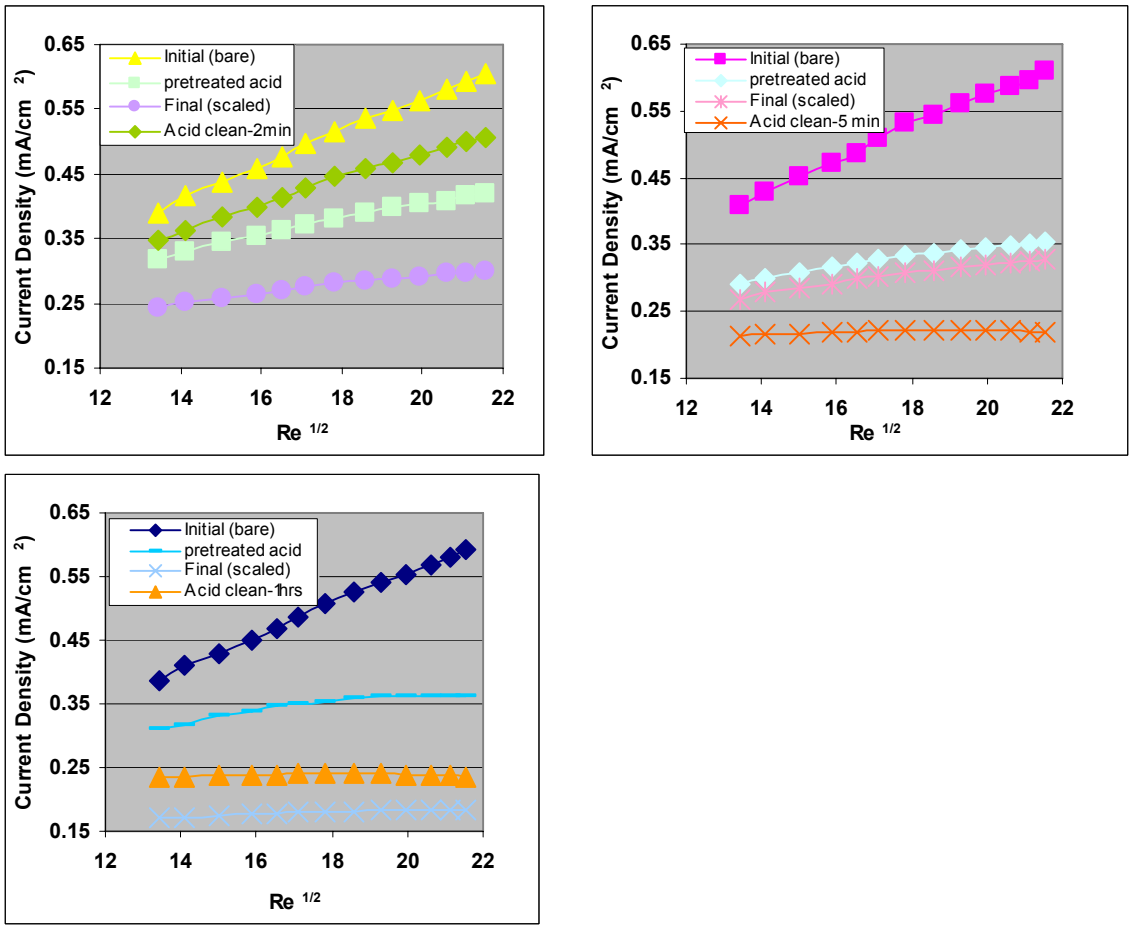

Figure 8-11 The current versus the square root of the Reynolds' number of the initial, final and cleaning analyses of acetic acid cleaning for 2, 5 and 60 minutes

The slope values and the coverage of various cleaning time experiments are presented in Table 8-3. After pre-treatment with acetic acid, the specimens showed a decrease in current densities as acid cleaning properly changed and diminished the stainless steel surface reactivity against oxygen reduction. As a consequence, a lower slope of current density versus the square root of the Reynolds' number, compared to a bare specimen could be expected for the pre-treated specimen as shown in Figure 8-11. These results correspond to a decrease of the slope values when comparing to the initial-plot's slope value. The surface coverage of the pre-treated specimens indicated 52 %, 70 % and 76 % for all the cleaning times as shown in Figure 8-12. After calcium carbonate was deposited on the specimen surfaces, a further decrease of all the current density and slope values of the final analysis was observed. This observation was related to surface

coverage due to mineral scale deposition and additional coverage due to surface modification by the acid treatment (indicated 73 %, 72% and 93% after mineral scale deposition on pretreated surface specimen). After cleaning, the specimen surface coverage determined using the electrochemical technique indicated 24 %, 97 % and 98 % (as result of surface modification). Again, it was clearly indicated that acid immersion, either by the pre-treatment or acid cleaning caused changes on the surface conditions and consequently resulted in a higher coverage.

Time, min	Initial slope (Bare)	Slope (pretreated)	Final slope (scaled)	Clean slope (Acid)	Coverage (Pre-treated)	Coverage before cleaning	Coverage after cleaning
2	0.0258	0.0123	0.0069	0.0195	52.33	73.26	24.42
5	0.0246	0.0074	0.0069	0.0007	69.92	71.95	97.15
60	0.0250	0.0061	0.0017	0.0003	75.52	93.20	98.80

Table 8-3 Results of the slope values and scale coverage before and after cleaning for different times determined by the electrochemical and the image analysis techniques

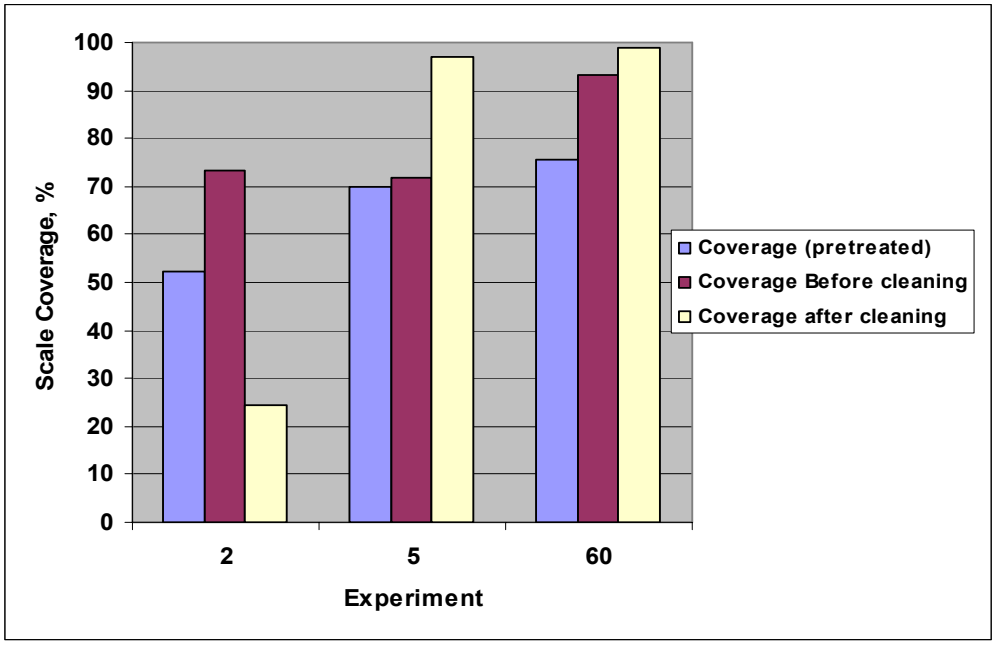

Figure 8-12 Percentage of coverage determined by the electrochemical technique for the pre-treated specimen, before and after cleaning for 2, 5 and 10 minutes

Generally, for all the cleaning time experiments, the use of acetic acid enables the removal and reduction of the calcium carbonate levels on the surface of the specimens. However, some residuals of calcium carbonate remained on the specimen surfaces for 2 and 5 minutes of cleanings. After 60 minutes of cleaning, the specimen surface was completely free of mineral scale. However, the percentage of scale removal determined by the electrochemical technique, showed -25 % and -5.6 % of scale removal for 5 and

60 minutes of cleanings respectively. A removal of 48.84 % was found for 2 minutes of cleaning as shown in Figure 8-13. Hence, it could conclude that a cleaning time of longer than 5 minutes results in not only calcium carbonate being completely removed from the surface but also causes changes to the surface's conditions. Although 2 minutes of cleaning showed a promising result from the electrochemical quantification, some scale remains on the specimen surface as this is supported by the light microscope image. Therefore, in the following section, further feasibility studies were carried out by employing a weaker concentration of acid or pH (more than 2.63) but with a longer cleaning time.

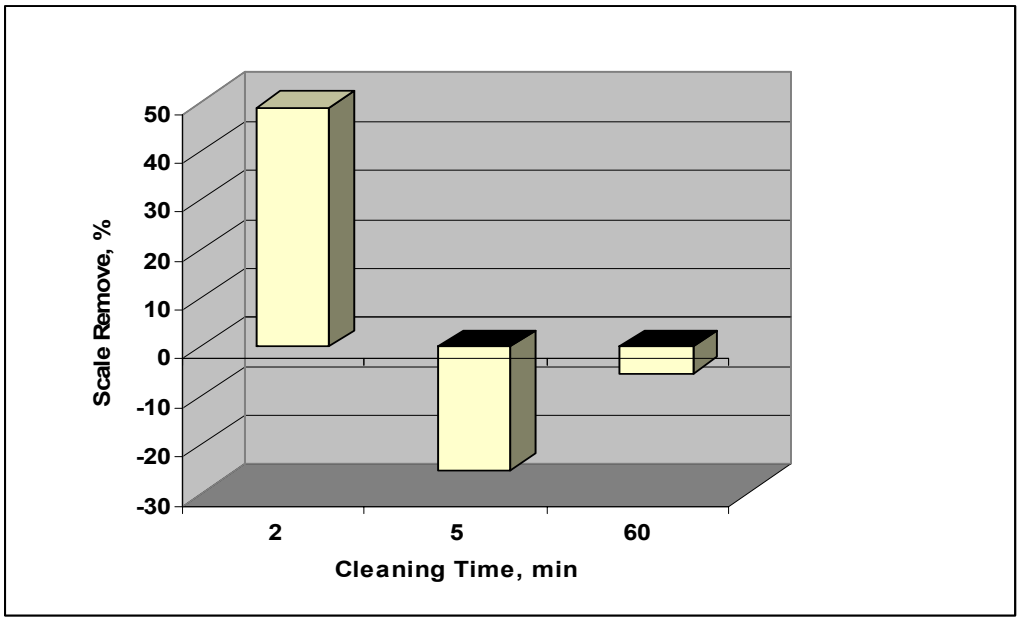

Figure 8-13 Percentage of mineral scale removed using acetic acid for various cleaning times

8.2.4.4 Acetic Cleaning with Different pH

Determination of the suitable pH is critical to ensure optimum cleaning conditions where mineral scale is deposited on the specimen can be removed without changing the specimen surface conditions. The previous section showed that pH 2.63 was too aggressive for the cleaning. Therefore, a higher pH solution were used for further investigation, three acid solutions, pH 3, 4 and 5 were used in this study to determine the optimal pH for cleaning. The pH solution was prepared by adding the acetic acid with distilled water until the required pH value was obtained. The specimens were subjected to 30 minutes of cleaning under static condition. All specimens were scale deposited by the RDE for 3 hours, including the control experiment.

pH	Initial slope (bare)	Final slope (scaled)	Cleaned slope (cleaning)	Electrochemical			Images Analysis		
				Before cleaning	After cleaning	% Remove	Before cleaning	After cleaning	% Remove
3	0.0310	0.0094	0.0145	69.68	53.23	16.45	47.40	13.60	33.80
4	0.0287	0.0120	0.0125	58.19	56.45	1.74	45.00	43.70	1.30
5	0.0285	0.0209	0.0222	26.67	22.11	4.56	7.00	5.60	1.40

Table 8-4 Results of the slope values and scale coverage before and after cleaning for different pHs that are determined by the electrochemical technique and image analysis technique

Two techniques, an electrochemical and image analysis were used to quantify the extent of mineral scale removed from the specimen's surface by different acetic pH. Results of the percentage of removal quantified by both techniques are shown in Figure 8-14 and Table 8-4. The scale coverage determined by the electrochemical technique showed that before cleaning (after being deposited with mineral scale), the coverage is 69 %, 58 % and 26 % which corresponds to the experiment pH 3, pH 4 and pH 5. This result is in agreement with the scale coverage estimated by the image analysis as shown in Table 8-4. The variation of percentage of scale coverage may be contributed to by the uncertainty of scale deposition such as surface finish, temperature and impurity of the scaling solution. For this specific study, the amount of scale deposited and its coverage were not of great importance since the main purpose was to demonstrate the range scale to be removed. The scale removal determination will not be affected by the uncertainty. According to the figure, it is clearly indicated among the pH electrolytes, the electrolyte with pH 3 removes most mineral scale on the specimen surface. Compared to other pHs, the percentage of scale removed quantified by the electrochemical technique and the image analysis for pH 3 is approximately 16 % and 34 % respectively.

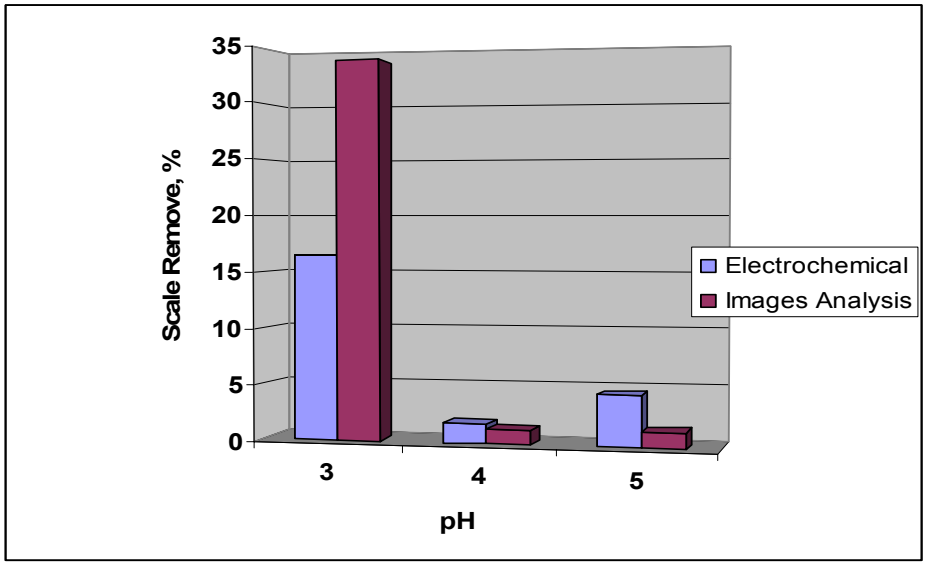

Figure 8-14 Percentage of scale removed determined by the electrochemical and image analysis techniques for different pH of acetic acid

Images taken by a light microscope with different magnification showed a significant reduction of mineral scale covering the specimen surface at pH electrolyte 3, but some mineral scale still remain on its surfaces as shown in Figure 8-15. Images of the specimen after cleaning with electrolyte pH 4 and 5 showed not many changes in scale coverage on the specimen surface when comparing the scale coverage before cleaning as shown in Figure 8-16 and Figure 8-17 respectively. As the pH solution increases, less hydrogen ions are available to react rather than dissolve the calcium carbonate scale, hence the cleaning effect reduces significantly.

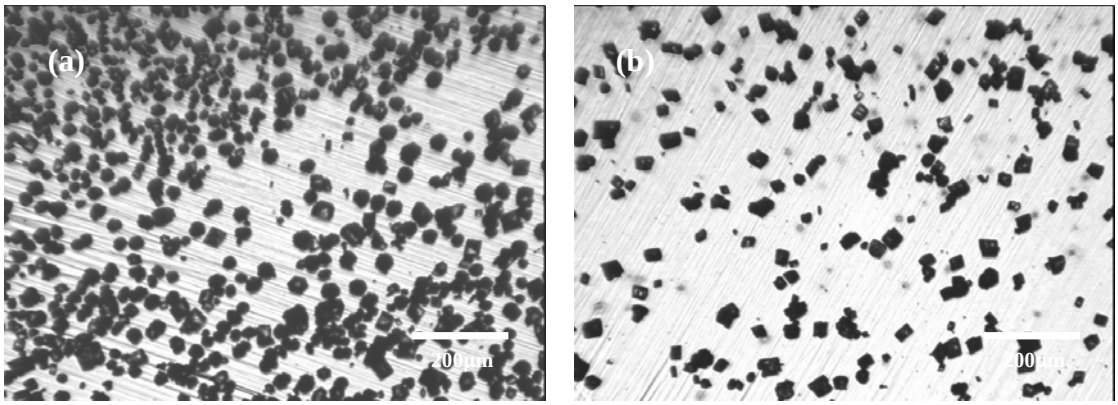

Figure 8-15 Scale covered on the specimen surfaces (a) before cleaning and (b) after cleaning with acetic acid of pH 3 for 30 minutes

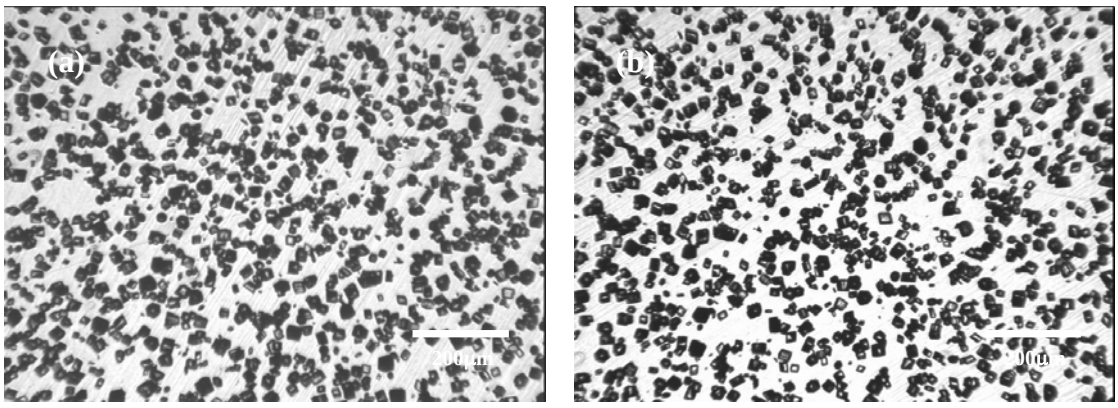

Figure 8-16 Scale covered on the specimen surface (a) before cleaning and (b) after cleaning with acetic acid of pH 4 for 30 minutes

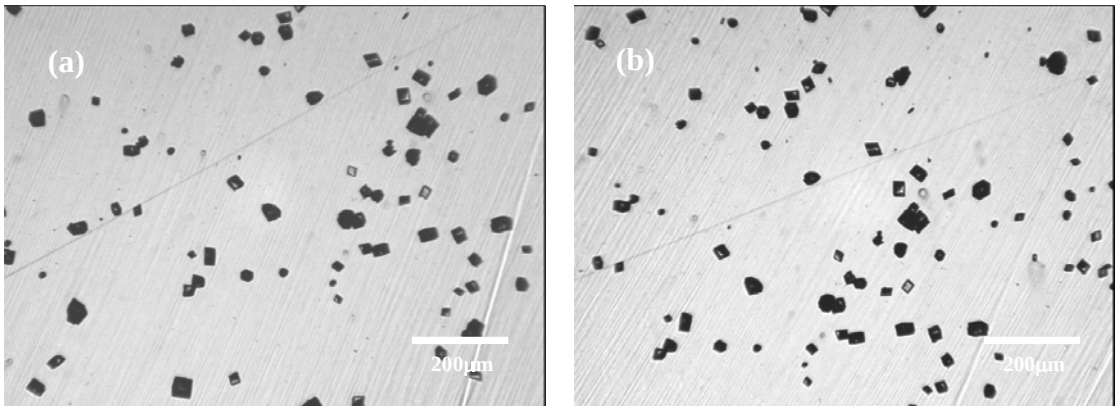

Figure 8-17 Scale covered on the specimen surface (a) before cleaning and (b) after cleaning with acetic acid of pH 5 for 30 minutes

8.2.4.5 Concluding Remarks on Acetic Acid Cleaning

In respect to acid pH and under static conditions, the surface can be modified by acid cleaning. The surface modifications are strongly dependent on the pH conditions and immersion times. The lower the pH and the longer immersion, the more significant the surface changes. One of the possible explanations is the acid cleaning process diminishes the stainless steel surface reactivity against oxygen reduction. This will be covered more details in later section.

Among the cleaning time 2, 5 and 60 minutes under static cleaning condition in acetic acid solution (pH = 2.63), 2 minutes of cleaning shows the optimum conditions of scale removed without affecting much of the electrode's surface condition. However, with this cleaning time, some crystals are not completely removed.

Cleaning process is enhanced under dynamic condition even higher pH is used (pH=3). Using this solution with 30 minutes cleaning time gives an optimum condition for calcium carbonate scale removal. When the pH is higher than 3, cleaning using acetic acid becomes less effective to dissolve any mineral scale.

8.2.5 The Effect of Acid Cleaning On Surface Coverage Quantification

In general, after the acid cleaning treatment with respect to the scaled specimen or bare specimen, a lower current density and slope values can be observed from the current density versus the square root of the Reynolds number. This suggests the O_2 reduction process on stainless steel surfaces is modified by acid cleaning process as discussed in section 8.2.4 and 8.2.5. The presence of the Fe (II) in the oxide film favours oxygen reduction reaction. Cleaning the electrode with acid solution oxides the Fe (II) to Fe (III) and the chromium species is not affected, thus it has a high content of chromium oxide and poor iron oxide in the passive film. Moreover, literature reported that the presence of acid in a solution tends to cause an enrichment effect, which promotes the formation of a chromium rich layer. The layer of chromium oxide and hydroxide acts as a barrier to oxygen reduction and the oxygen reduction reaction occurs at the Fe oxides only [159, 172]. Hence, acid cleaning changes and diminishes the stainless steel surface reactivity properly against oxygen reduction. Consequently, any specimen treated with acid solution acid has a lower slope of i_L versus $Re^{1/2}$, compared to a bare specimen. Subsequently it causes an increase of coverage quantification results determined by the electrochemical technique (overestimating the coverage).

For the scaled specimen, two competitive processes occur simultaneously when cleaning with acid solution. Firstly, the acid cleaning changes the surface ionic properties of the active areas (not covered with scale) by reducing the active sites of Fe (II) and subsequently decreases the reactivity of oxygen. Hence, a decrease in the slope value and current density can be seen. Secondly, it also increases the active area where the calcium carbonate is removed subsequently exposing a greater amount of active area for oxygen reduction, hence contributing to the increase in the slope value and current density. However, modification of the surface condition contributes to the major effect rather than to scale removed on the specimen surface. Hence, the overall reaction increases in the current density but reduces the slope value compared to the slope value for the scaled specimen.

Overall, the acid cleaning causes an increase in the slope value and the limiting current density compared to scaled specimen. This results in not only the removal of calcium carbonate by the hydrogen ions but also decreases the surface reactivity toward oxygen reduction.

8.2.6 The Effectiveness of Scale Removal by Acid Cleaning

In general, for a simple calcium carbonate such as calcite, the dissolution can proceed via a variety of mechanisms at the solid / water interface as listed below [114, 173]

$CaCO_3 \longleftrightarrow Ca^{2+} + CO_3^{2-}$ Hydration Equation 8-1

$CaCO_3 + H^+ \longrightarrow Ca^{2+} + HCO_3^-$ Protonation Equation 8-2

$CaCO_3 + H_2CO_3^* \leftrightarrow Ca^{2+} + 2HCO_3^-$ Carbonation Equation 8-3

Whereas the precipitation of calcium carbonate occurs accordance to a single reaction [109, 110]

$Ca^{2+} + CO_3^{2-} \rightarrow CaCO_{3(s)}$ Equation 8-4

Hence, the general dissolution rates for calcite r_c can be written as

$$r_c = k_1 + k_2 a_{H^+,s} + k_3 a_{H_2CO_3,s} - k_4 a_{Ca^{2+},s}.a_{CO_3^{2-},s}$$ Equation 8-5

where k_1, k_2, k_3 and k_4 stand for the chemical rate constants of reaction for Equation 8-1 to Equation 8-4 and $a_{i,5}$ refers to the activity of the i th aqueous species adjacent to the calcite surface. For any acid conditions pH <5, the terms $k_{a_{H^+,5}}$ on the right side of Equation 8-5 is the dominant reaction (Busenberg and Plummer [174], Chou *et al.* [81]). Hence, the dissolution rate of this pH is given as

$$r_c = k_2 a_{H^+,s}$$ Equation 8-6

Most of the calcium carbonate deposited on the electrode surface consists of predominantly of calcite crystals. Irrespective of whether strong or weak acid solutions are used, calcium carbonate deposited on the electrode can be completely removed accordance to Equation 8-6. The dissolution of calcite is under a protonation mechanism. However, the application of these acids caused an increase of scale coverage result, this is especially in the use of strong acid, HCl (pH=1.23) and weak acid, acetic acid (pH=2.63) as shown in Figure 8-7 and Figure 8-12 respectively. The influence of surface modification and the effectiveness of scale removal are obvious with the decrease of pH solution. Complete dissociation in aqueous solution is expected

for a strong acid (HCl) compared to a weak acid ($CHOOCH_3$) acid, which is only slightly dissociated when it dissolves in water. In other words, HCl is a good H^+ donor, hence it is more effective for removing scale deposited on the surface but it also causes changes to the surface of the electrode. The longer the immersion time, the higher the scale coverage result, an increase from 50 % of scale coverage to 70 % when the specimen was immersed in HCl from 2 minutes to 60 minutes as shown in Figure 8-12.

Further investigation on various acetic acid solutions, shows at pH range 3-5, sufficient H^+ is present in the solution to provide an adequate H^+ for protonation, subsequently calcite dissolution. One of main findings from this investigation is the electrochemical measurement is not affected by the acid immersion (30 minutes) irrespective to the pH solutions. However, the surface is not completely mineral scale free. The increase of magnitude dissolution rate with decreasing pH to 3 is due to protonation reaction occurring at the mineral surface. The dissolution rate of calcite is proportional to the activity of hydrogen ions and also the chemical rate constant, k. The hydrogen ion attacks and adsorbs the carbonate compound in the lattice rather than calcium compound, subsequently causing a dehydration of $CaCO_3$. As the solution pH decreases, more H^+ can reach the crystal's surface consequently the total amount of the carbonate present at the surface in the form of CO_3^{2-} decreases with decreasing pH, and the surface concentration of the reaction products increases. However, cleaning with a solution of pH 3 shows a significant amount of scale was removed when it was accessed by the electrochemical and the images analysis, compared to pH 4 and pH 5 where the amount scale removed is more or less the same. In the pH range between 4-5, the scale removal rate was similar, however once pH< 4 a sudden increase in removal rate (pH=3), this suggests the calcite dissolution is also governed by the chemical rate constants as described in Equation 8-6. This was reported by Sjoberg and Rickard [70] who noted that the rate of constant for calcite dissolution, k, could be represented by equation which has been reported by

$$k = \frac{k_c k_T}{k_c + k_T} \qquad \text{Equation 8-7}$$

where k_c is the chemically controlled rate constant and k_T is the transport controlled rate constant. When $k_T >> k_c$ the rate is chemically controlled and when $k_c >> k_T$ the rate is transport controlled. According to them, the rate of dissolution of calcite is simply proportional to the activity of proton at low pH and becomes constant in the neutral

range. They found that at a low pH (pH<4) regime, the rate of dissolution is under mass transfer control while at 4<pH<5 regimes are controlled by mixed kinetics (mass transfer and kinetics of the heterogeneous reaction on the carbonate surface). Berner *et al.* [78], Plummer *et al.* [175] also reported that at low pH, the rate is found to be controlled by mass transfer mechanisms between the surface of the mineral and the bulk of the solution.

In this study, the general trend observed during the calcite dissolution of calcite is very similar to the results reported by Sjoberg and Rickard [79]. This may explain the higher dissolution rate at pH 3 compared to other pHs. The dissolution rate is higher at pH 3, is most likely governed by the diffusion or mass transfer of H^+ to the surface carbonate and for pH>4 mixed kinetics (diffusion or chemically controlled) is involved. The rate decrease due to the backward precipitation reaction only occurs when the pH is high, usually pH above 7. Hence, the possible of backward $CaCO_3$ precipitation causing the decrease of the calcite dissolution for pH 4-5) is not possible under this study.

Generally, the electrochemical measurement quantifies the surface modification rather than the mineral scale remaining on the electrode surface after immersion into an acid solution. The surface modification may occur but depends on the aggressiveness of the pH solution. The lower the pH solution, the more aggressively the solution contributes toward the surface modification and also the scale removal is more effective. This is especially true for pH solutions below 3 (acetic acid 2.63 and HCl 1.23). However, this affects the electrochemical measurement less significantly using weaker acid solution pH at or above 3. The electrochemical measurement is less affected by the surface modification but the surface is not completely free of the scale. Among the pH solutions, pH 3 give the optimum condition for scale removal at the same the electrochemical measurements can be used as quantification.

8.3 Understand the Sensivity of Electrochemical Measurement on Surface Modifications

The sensivity of the electrochemical technique to quantify scale coverage depends on the surface properties of the electrode that often relates to oxygen reduction. The rate of the oxygen reduction is of great importance for the study of scale detection as it is used as a tracer. Often the oxygen reduction process governed by the properties of the

surface, may be affected by the composition of the alloy and the surface preparation such as a result of cathodic polarisation, polishing and acid treatment. Hence, the sensitivity of this technique as scale detection using the oxygen as a tracer was examined.

There are two possible sites where oxygen-reduction takes place 1) oxygen can diffuse through the chromium oxide layer to be reduced on the metal surfaces 2) direct oxygen reduction process on the oxide film are involved on reduced iron species particular Fe (II) [176, 177]. According to the observations from this study of the oxygen reduction reaction and the surface treatment, it appears that the oxides have an important role in the oxygen reduction kinetics. The electron pathway is often linked by the ionic property of the electrode. As demonstrated in Chapter 5, the O_2 reduction on bare metal electrodes follows a 4-electrons pathway. A pre-reduced surface (electrochemical cleaning) is particularly favourable to the oxygen reduction, as the oxygen is reduced through a 4-electrons pathway, the measured current is the highest. Though no surface analysis has been performed, the decrease in oxygen reduction is believed to be related to the presence of the amounts of Fe (II) and Fe (III) element found in the surface of the electrode. These species play an important role in oxygen reduction reaction and the rate is proportional to the amount of Fe (II) in iron oxide that has been reported to have good properties of conduction (electronic or ionic). Zecevic [178] claimed that the O_2 molecules co-ordinate to Fe (II) centres before the electrochemical reduction on iron.

Results of the experiments showed that acid treatment has significantly diminished the electrode surface reactivity against the oxygen reduction and the O_2 reduction rate is lower on the bare electrode. This is often linked to the formation of oxide film covering the electrode's surfaces. Generally, after being treated with acid solution, the Fe (II) site is oxidised to Fe (III) and also becomes passivated by forming chromium oxide rich film that acts as a barrier to oxygen reduction. This could be clearly observed from the SEM image presented in Figure 7.1. The patches of dark grey colour are believed to consist of Fe (III) and chromium rich oxide film. The formation mixture of chromium oxide and hydroxide constitutes a barrier to the oxygen diffusion, which has been reported in the literature [178, 179]. Whereas for the pre-reduced electrode, the electroreduction of O_2 on oxides requires the partial reduction of the Fe (III) to Fe (II) sites [176, 177]. Therefore, a higher Fe (II) is expected for the pre-reduced surface electrode. For the polished surface, the presence of a mixture of Fe (II) and Fe (III) is to

be responsible for a lower rate of O_2 reduction than on pre-reduced surfaces, but higher than on an acid treated surface. Jovancicevic and Bockris [180] discovered that in borate buffer (pH 8.4) solution, a 4-electrons pathway for O_2 reduction on bare iron and some small amount of hydrogen peroxide occurs, whereas on passive iron a two electron transfer occurs, with the formation of H_2O_2 as the final product. In artificial seawater, on a pre-reduced surface of AISI 316L or 904L austenitic stainless steels, the oxygen reduction proceeds via a 4-electrons pathway [159]. In 0.5 M NaCl solution (pH 4-10), O_2 reduction on bare 304 SS is under mixed activation-diffusion control and follows a four electron pathway [166]. According to Gojkovic *et al.*, 2.9 and 3.5-electrons involved and exchanged per O_2 molecule on passivated Duplex stainless in NaOH electrolyte and NaCl solution, respectively [172].

The occurrence of a specific two or four electrons process mainly depends on electrode surface composition and experimental conditions. The summary of various surface treatments and the calculated electron pathway assuming the following parameters is presented in Table 8-5.

$$i_L = 1.51 \mathrm{Re}^{0.5}\, Sc^{0.33} \left(\frac{H}{d}\right)^{-0.054} g(Sc) \frac{nAFCD}{d}$$

Diffusion Coefficient, D=2E-05 (cm^2/s)
Faraday constant, F=96500 (C/mol)
Oxygen concentration, C=2.5E-04 (mol/l)
Kinematics viscosity, ν =1E-02 (cm^2/s)
Sample Area, A=0.1963 cm^2
Nozzle Height to Target, H/d=1
Diameter of nozzle, d=0.8 cm
Schmidt number, Sc=ν /D
g (Sc) =1

Surface Treatment	Treated Condition	Slope value of i_L vs. $Re^{½}$	Possibility Explanation	Calculated Number of Electron Exchange	Number of electrons exchange reported in literature
Mechanical Polished Specimen	Cathodic Polarised at -0.8 V for 10 min, in NaCl and pH 10	0.0241	Air formed oxide film consists of Fe (II), Fe (III) sites and Cr_2O_3	3.30 (4 electrons pathway)	On bare 304 SS, in 0.5 M NaCl solution follows a 4-electrons pathway [119]. On passivated duplex stainless steel, Gojkovic and co-workers, 2.9 and 3.5-electrons in NaOH electrolyte and NaCl solution, respectively [172]. Freshly polished surface, both the 2 and 4-electrons pathways are involved.
Mechanical Polished Specimen	Immersed into a brine solution ($NaHCO_3$ and NaCl) pH 6.7 for 24 hours	0.0260	Oxide film consists of $FeCl^+$ or $(Fe,Cr)CO_3$	3.52 (4 electrons pathway)	
Polarised Specimen	Cathodic Polarised at -1.6 V for an hour in NaCl, pH 10	0.0268	Reduction of Fe (III) to Fe (II) sites, causing an increase in current and slope value	3.66 (4 electrons pathway)	In artificial seawater, on a pre-reduced surface of AISI 316L or 904L austenitic stainless steels, the oxygen reduction proceeds via a 4-electrons pathway [159].
Acid Treated Specimen	Immersed in HCl for 10 min, pH 1.23	0.0176	Oxidation of Fe (II) to Fe (III) sites and promotes Cr_2O_3 film formation, causing a decrease in current and slope value	2.40 (2 electrons pathway)	Jovancicevic and Bockris found a 2-electrons pathway for O_2 reduction on passive bare iron with the formation of H_2O_2 as the final product in borate buffer (pH 8.4) solution [180].

Table 8-5 Represents the influence of number of electron pathways by various surface conditions

8.3.1 Conclusions of the Sensivity of the Electrochemical Measurement on Surface Modifications

It is clearly demonstrated that the oxygen reduction reaction process is greatly influenced by the stainless steel surface treatment (cathodic pre-treatment, polishing, and acid treatment). It is a complicated process, the different intensity of oxygen reduction on 316L varied with various surface conditions that involves the number of electron pathway. Hence, the use of this technique may be affected under certain conditions as demonstrated in previous section. However, mechanical polished specimen, polarised specimen and brine immersed specimen, oxygen reduction the

electron pathways for the oxygen reduction is more or less similar which is close to the theoretical value, a 4-electrons pathway. At the opposite, the acid treated surface follows a 2-electrons pathway. This concludes that the surface electrode is not affected by polished, polarised and immersed treatments. Hence, the accuracy of scale coverage quantification using the electrochemical technique in a SIJ cell rig is not affected. However, this is not the case with the acid treated electrode, the scale coverage is overestimated as a result of oxide film formation that act as a barrier to oxygen reduction reaction.

In this study using 316L polarised in NaCl solution at pH 10, ambient temperature and pressure, the oxygen reduction reaction process is greatly influenced by the stainless steel surface treatment (cathodic pre-treatment, polishing, and acid treatment). The oxygen reduction process is decreased with the following surface treatment

Polarised specimen >mechanical polished specimen or brine immersed specimen> acid treated specimen.

Immersion and mechanical polished specimen showed also similar characteristics and the accuracy of scale coverage quantification using the electrochemical technique in a SIJ cell rig is not affected. However, this is not the case with acid treatment electrode the scale coverage is overestimated as a result of oxide film formation that acts as a barrier to oxygen reduction reaction. Surface modification by reduction of oxide film reduction at potential -1.8 V, polarised specimen through the electrochemical cleaning is slightly underestimated.

8.3.2 An Investigation of Different Materials

The possibility of employing other materials to prevent surface modifications during the cleaning process was considered. Two corrosion resistant materials were chosen for a preliminary experiment (i) Inconel and (ii) Hastelloy C-276. A comparison experiment on stainless steel 316L was also examined. The chemical compositions of each alloy is shown below

Alloy	C	Cr	Mn	Co	Mo	Ni	P	Fe	Others
Inconel 600	0.15	14-17	1		2.8-3.3	72	/	6-10	Si-0.5 Cu-0.5
Hastelloy C 276	0.02	15	1	2.5	16	57	/	5	V-0.35 Si-0.08 W-4
Stainless Steel 316 L	0.03	16.4	1.0	/	1.98	11.0	0.027	Remain	Si-0.045 P-0.03

Table 8-6 Chemical Compositions of Inconel 600, Hastelloy C-276 and 316L stainless steel

A potentiodynamic test was performed where the current density response to potential was recorded through three-cell electrodes system connected to a potentiostat machine. Data was monitored via a PC for these three materials. The electrochemical measurement was performed by polarising the material/specimen from cathodic toward anodic potential direction under static conditions in the analysis solution (5g/L NaCl). The purpose of potentiodynamic test was to determine the suitable applied potential where oxygen-reduction reaction takes place.

Figure 8-18 represents current density versus potential of 316L stainless steel, Hastelloy and Inconel. Plateau current density was observed in a potential range from -0.6 to -1.0 V (Ag/AgCl) for 316L stainless steel. However, this was not the case for nickel based alloys. The current response of the nickel based alloys showed a slow decrease of current density rather than constant current density in the potential range -0.3 to -0.9 V. The higher the potential above -0.9 V, the faster the decrease in current density irrespective to material being used as shown in Figure 8-18. This can be attributed to the hydrogen generation that is governed by kinetics controlled above this potential. Hence, an intermediate potential of -0.7 V was selected to be used in further investigations for the electrochemical measurement under diffusional controlled regime for both nickel alloys.

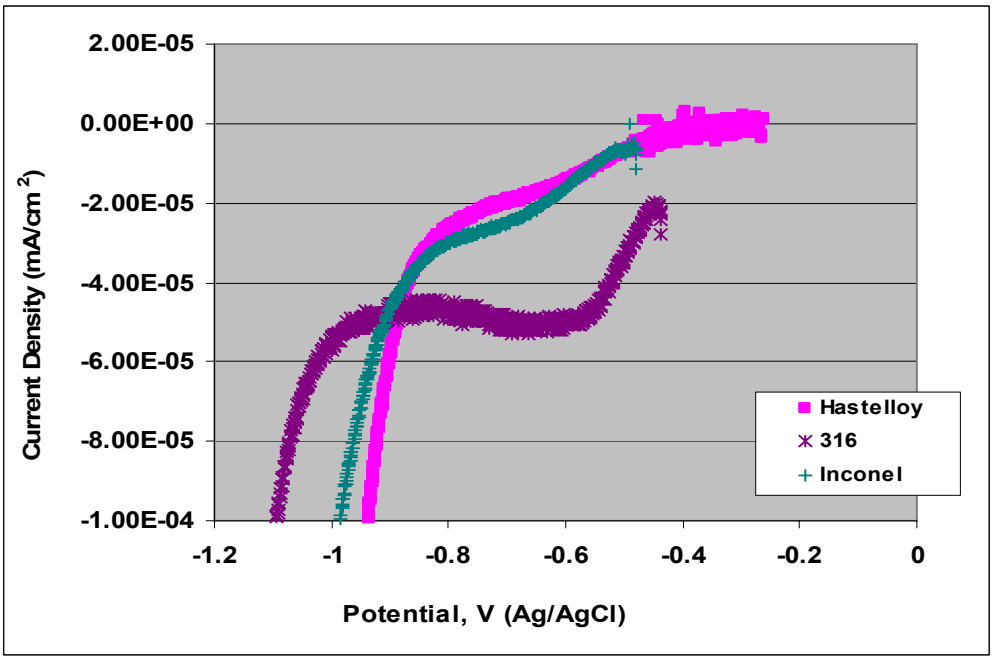

Figure 8-18 Potentiodynamic test of three different materials (a)stainless steel 316, (b)Hastelloy and (c) Inconel

The current density for Inconel and Hastelloy remain constant, approximately -5E-05 mA/cm2 and were not affected by the change of the electrolyte flows, compared to stainless steel 316L. The oxygen was not limited by the mass transport in the solution, since the oxygen reduction on passive film was not affected by the increases of flows on both nickel alloys as shown in Figure 8-19. The magnitude of the limiting current also depends on the nature of the substrate and the electrolyte medium. Both materials Inconel and Hastelloy C-276 are nickel based alloys consisting of approximately of 72 % and 56 % of nickel respectively. Having a higher nickel alloy content caused the oxygen reduction to shift to kinetics control (activation control) rather than to mass transport control.

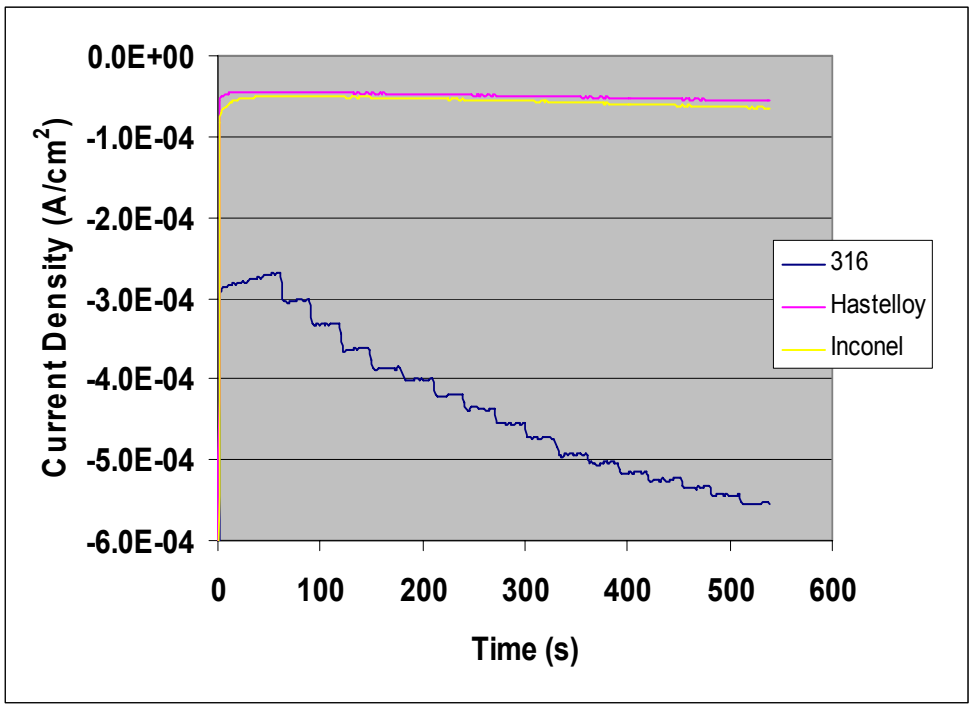

Figure 8-19 Represents the current density versus time of stainless steel 316, Hastelloy and Inconel under various flows

8.3.3 The Use of Different Materials on Oxygen Reduction

The nature of the surface oxide film strongly influences the oxygen reduction mechanism and the number of exchange electrons during polarisation as described in 8.3. The possible explanation of the lower limiting current density of the nickel based alloys is mainly due to a lack of iron oxide. Iron oxide sites especially Fe (II) are required in order to allow better oxygen-reduction. These sites play an important role in the oxygen-reduction reaction and the rate is proportional to the amount of number sites of Fe (II) in an iron oxide film. Therefore, the nickel based alloy shows a lower limiting current density. The possible nature and structure of the divalent iron oxides may have good properties of conduction (electronic or ionic) compared to nickel based alloys. This is supported by similar findings reported that for pure Fe the limiting current density is dependent on the electrode pre-treatment. A lower number of electrons was exchanged per O_2 molecule and has been associated with limiting current density [172].

The difference in the oxygen reduction process on the surface can be explained from an electronic point of view, the oxide film acts as semi conductive barrier that has different electronic properties related to its chemical composition of the oxide film. No surface analysis and investigation were carried out to confirm the chemical composition and

type of semiconductor of these three materials. However, a number of studies on the semi conducting properties of Ni oxides have been reported, that Ni (II) oxides, both hydrated and dehydrated forms, behave like p-type semiconductors. Nickel (II) oxide is generally the main component responsible for the passivity of film in an acidic and alkaline environment. Recent XPS studies on nickel and its alloy showed the existence of a bi-layer structure which consists of an inner layer, NiO and outer layer, $Ni(OH)_2$ [181-184]. Stainless steel, which is an iron base alloy, behaves as an n-type semiconductor. Several authors reported that the passive film of stainless steel and iron behave as an n-type semiconductor [185, 186]. Therefore, it is believed that both materials, nickel based alloys and iron based alloys behave as p-type semiconductors and n-type semiconductors respectively. Hence, the different types of semiconductor behaviour that influence the ionic/electron transfer between the oxide film/electrolyte and cause the difference in the oxygen-reduction kinetics.

8.3.4 Conclusion of Acid Cleaning and Electrochemical Polarisation

Electrochemical and acid cleaning , both technique have significant influence the accuracy of the technique to detect mineral scale on the specimen surface. Electrochemical cleaning by generation of hydrogen gases is not an effective cleaning. Acid cleaning is effective but it changes the surface condition toward reactivity of oxygen for reduction process. It is believed that the amount of Fe (II) makes the oxygen reduction easier. The iron oxidation state depends on the surface treatment on the stainless steel, on a polarised surface, the iron is divalent whereas, after the acid treatment, the surface is exclusively covered by ferric oxides; the polished surface contains ferric oxides and an important contribution for ferrous oxides. The polarised surface, which contains the highest amount of Fe (II), shows high currents for oxygen reduction.

Although HCl solution is a good proton donor, the use of HCl has significantly changed the surface of the electrode and the sensivity of the electrochemical measurement. Scale coverage quantification is overestimated as a result of oxide film formation that acts as a barrier to the oxygen reduction. A weaker acid, acetic acid with various pH solutions were used for this study, among the pH solution used, solution pH 3 appears to provide the optimum conditions for removing calcium carbonate scale deposited on the surface of the electrode without causing any significant surface modification.

Chapter 9 Conclusions and Future Work

9.1 Introduction

The goal of this research work is to develop a methodology to detect as well as to quantify the mineral scale deposition on an electrode. This is completed in three main sections. This first section is to develop and validate of the methodology. The second and third part of the research focuses on the scale coverage quantification on the specimen surface and scaling tendency measurement. The summary of this work is presented in the subsequent section.

9.1.1 Summary of Scale Detection and Quantification

In this study, the impinging jet electrode system was used to perform electrochemical measurement study using oxygen as a tracer. The study has verified the use of submerged impinging jet equipment (SIJ) setup for the electrochemical measurement. The range of area of uniform mass transfer was established with the nozzle geometry arrangement H/d=1 and r/d=0.3125. Laminar flow is most used in the practical applications of SIJ because the equations of mass transfer are well defined under this regime. The combination of electrochemical measurement with these SIJ configurations, have proven the hypothesis and also have validated the use of the mathematical equation below as a means of scale coverage and scaling tendency measurement. The electrochemical measurement has an accuracy of 10%.

$$i_L = 1.51\mathrm{Re}^{0.5}\, Sc^{0.33} \left(\frac{H}{d}\right)^{-0.054} g(Sc) \frac{nAFCD}{d}$$

9.1.2 Summary of Scale Detection and Quantification

This methodology is clearly demonstrated that mineral crystals can be detected and quantified by using the electrochemical technique and submerged impinging jet. The application of the electrochemical technique in combination with SIJ enables the possibility of quantifying and determining the scale deposited on the specimen surface in particular, calcium carbonate scale in the presence or absence of magnesium ions. The scale coverage determined by the electrochemical technique shows that the scale deposited in the presence of magnesium ions, produces approximately 1.2 times higher compared to scale coverage determined in the absence of magnesium ions.

There was a discrepancy of mineral scale coverage between mineral scale coverage quantified using an image analysis technique and an electrochemical technique. The discrepancy was mainly attributed the limitation of image analysis to detect the small mineral scale. The usage of the electrochemical technique is better than light microscope image analysis for scale detection purposes. The use of image analysis technique could also provide an effective way to study and investigate the first layer of scale deposited on the specimen however a correction factor of 1.65 is required to give a good surface quantification accuracy under normal deposition processes.

9.1.3 Summary of Scaling Tendency Quantification

Scale tendency can be quantified by the electrochemical data from the current versus time using the SIJ cell rig. As a rule of thumb, an increase in the concentration of calcium ions increases the scaling rate and scale deposition. An increase in the flow rate tends to increase three main parameters in determining the scaling tendency of brine for all the supersaturated brine: i) scaling tendency slope ii) scaling time and iii) scale deposition. A good correlation of scaling tendency slope versus saturation ratio with different flow rate is established. The scaling tendency slope is proportional to the saturation index of the brine. Hence, this technique can be used as a monitoring tool to determine brine condition.

9.1.4 Summary of Surface Cleaning and Surface Sensivity

Specimens subjected to electrolyte impingement with a flow rate of 190 ml/min while polarised to a potential of -1.8V for 3 hours showed no signs of having large size mineral crystals removed from the specimen's surface. This suggests that the electrochemical technique to generate hydrogen on specimen surfaces is not an effective technique for scale removal. Generally, it is agreed with reported literature that calcium carbonate dissolution increases as the pH decreases, scale can be removed by acid cleaning irrespective to acid being used in this research study. The acetic acid solution, pH 3 with immersion time of 30 minutes proved to enable significant scale removal from the specimen's surface without causing any surface modification. However, it was not a completely clean surface since some calcium carbonate scale still remained on the surface. Acid solution below pH 3, completely removed the scale however, the acid cleaning process changes the surface condition of the specimen.

The use of oxygen as a tracer for oxygen reduction process has great influenced on the sensivity of this technique. Oxygen reduction process is a complicated process, the different intensity of oxygen reduction on various materials and surface conditions (cathodic pre-treatment, polishing, and acid treatment).

It is believed that different ionic properties as well as well as the presence of Fe (III) sites play an important role on the oxygen reduction process. The application of highly corrosion resistant materials, such as a nickel-based alloy is being dominated by kinetics control rather than mass transfer at potential -0.75 V/(Ag/AgCl). This severe affect this sensivity and also as an methodology to quantify mineral scaling on specimen surface.

When a specimen is cathodically polarised in a NaCl solution, a favourable oxygen reduction occurred. However, acid cleaning tends to reduce the oxygen-reduction reaction taking place on the specimen's surface. For the existing study, the oxygen reduction process decreased with the following surface treatment

Polarised specimen >mechanical polished specimen or brine immersed specimen> acid treated specimen.

It can be concluded that the oxygen-reduction reaction is influenced by various surface treatments or materials. For an accurate assessment using the electrochemical technique to detect and quantify the amount of scale coverage, separate calibration is required for the use of different materials and surface treatment process. However, in this study the methodology can be easily quantified to the amount of scale deposited using 316 mechanically polished specimen.

9.2 Contributions of this Research Work toward Industry and Academics

The following are some of the contributions and highlights of this research;

- it has proven the concept and hypothesis using SIJ to detect and quantify the scale coverage. This contributes to a better understanding and also an alternative technique used in laboratory or industry to quantify the surface scaling;
- the surface condition of an electrode plays a significant role on the electrochemical measurement where ionic properties of the metallic electrode

has a great influence on the oxygen reduction. The oxygen reduction process exhibits similar properties for the mechanically polished specimen and short polarisation specimen. The scale coverage quantification and detection can be quantified for under these surface treatments;

- the developed scale detection technique can be used in conjunction with other scale prediction models, to provide scale monitoring as well as verification purposes for a predicted system;
- this technique has demonstrated a simple approach for quantify the amount of calcium carbonate deposited on component surface. It is fast only required 15 minutes for a measurement.
- it overcomes some of the complicated techniques to detect mineral scale formed on the component surface. The data obtained is easily interpreted and not complicated;
- this technique is not only capable of detecting mineral scale covered on the component surface but is also able to monitor the scaling tendency of a calcium carbonate brine system in a fairly clean system for the same equipment set up.
- crystal mineral removal using an electrochemical cleaning by polarising specimen to a potential more negative than -1 V (AgAg/Cl) is ineffective. Acid cleaning is an effective way to remove crystal mineral on an electrode's surface. However the sensivity of the electrode are affected by both cleaning method. The variation of the surface treatment such as acid treatment, pre-reduction required specially calibration for more accurate surface quantification;

9.3 Concept the use of SIJ Unit in a Field Trial

Though there are still some issues need to be addressed in order for this technique to be used to detect and monitor mineral scaling especially the electrode cleaning, the installation in field trial and the sensor operation conceptual are presented. This sensor or technology can be used in water transportation or oil and gas production (producing water from the separators). A side stream where the flow is controlled by the inlet and outlet valve or a pump, and a combination of three-cell electrode can be used. A stand-alone unit or mounted on the system with a data logger and a potentiostat is used to apply the potential and collect all the information as shown in Figure 9-2. A filter is to be installed to filter the impurities such as sand, particles and oil prior to the fluid entering the system.

Basically, an initial assessment on the active surface is performed using the electrolyte. Then the production fluid is filtered at the inlet of the bypass and passing the SIJ rig for a period. The valve is closed and the production fluid is drained out then reintroduced to the electrolyte and perform electrochemical measurement. The electrolyte is to be replenished when the specimen changes out. The summary is shown in Figure 9-1.

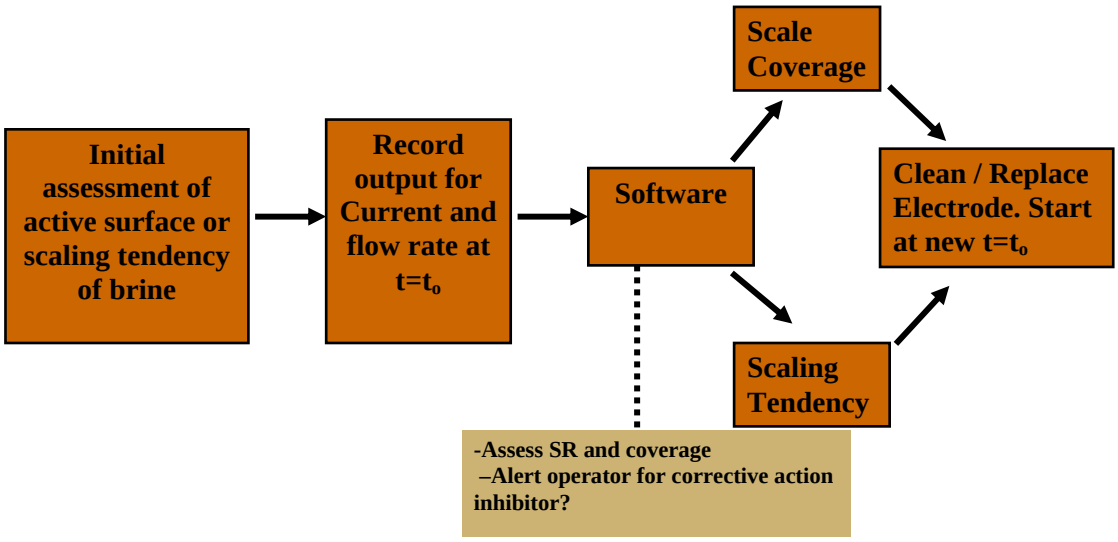

Figure 9-1 Summary of the sensor operation

Indication of the scale deposition from the electrode surface profile can be noticed by the large increase in coverage value as illustrates in Figure 9-2. The scale coverage quantification can therefore be used as an indicator of scale deposition. This highlights the importance of monitoring by electrochemical data.

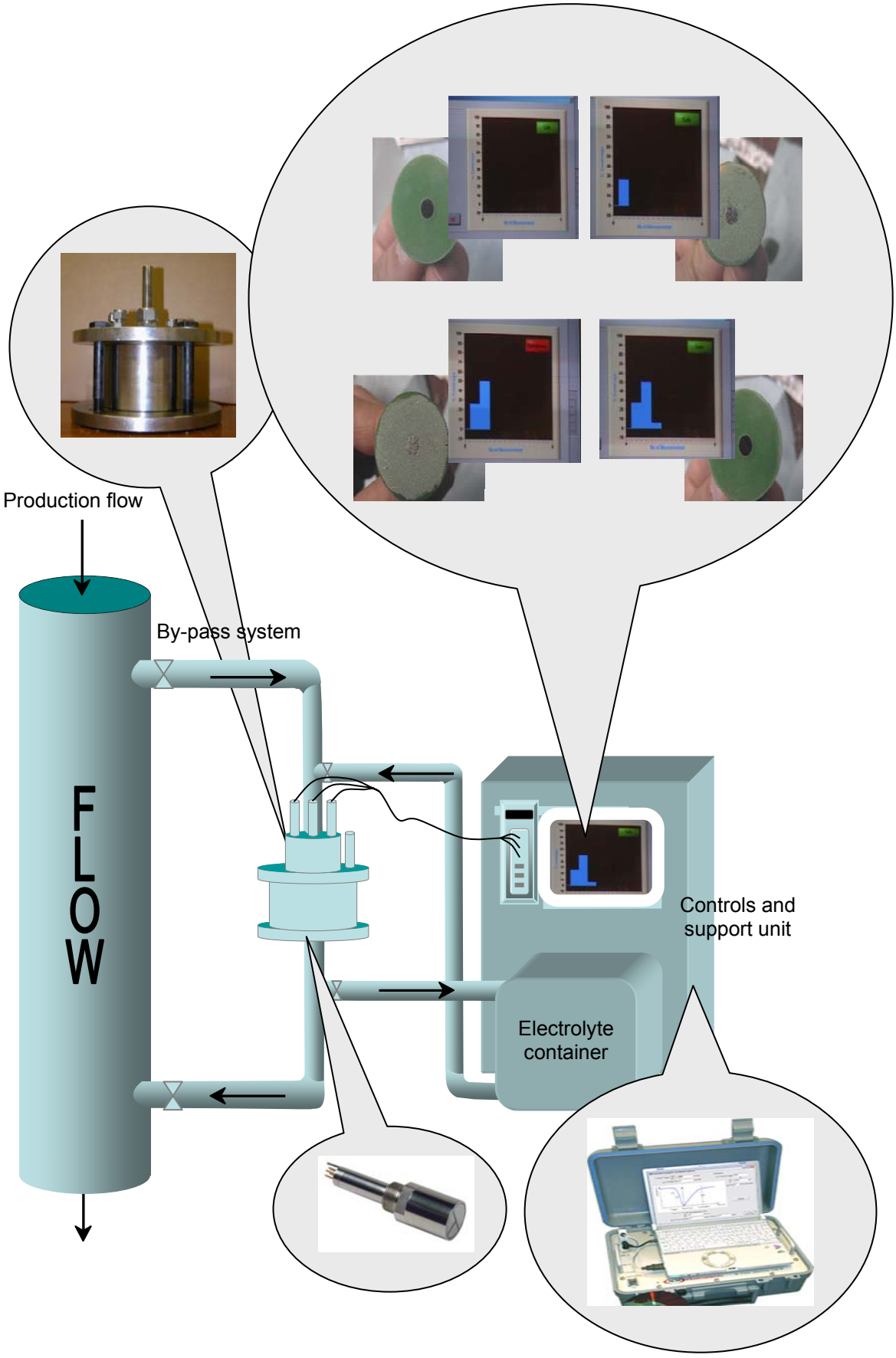

Figure 9-2 Schematic representation of the SIJ unit installed in production system, this is not according to scale.

9.4 Future Work

The study and further investigation the surface condition of the electrode through various surface treatments may provide a better understanding of the hypothesis described in this study especially when the surface is pre-treated with acid, or there is surface pre-reduction by polarisation or surface modification by high chloride immersion.

Verification and confirmation of the hypothesis on each regime of the formation process during polarisation such of Mg-Ca rich, bicarbonate film formation as well as oxide film reduction may form part of future work. This could lead to a better understanding and contribute toward the scaling tendency measurement process.

In future work an improvement to the experiment should be conducted to quantify the synergistic effect by selecting more noble material where no oxide film reduction should occur during polarisation.

Though the majority of the works are concentrated on the most common mineral scale (calcium carbonate and barium sulphate) found in the oil and gas sector, the study could be extended to any mineral scale including the exotic mineral scales strontium sulphate and calcium sulphate that can found at higher temperatures etc. In addition to mineral scale, oxide scale is formed on metal surfaces due to corrosion. The presence of any oxide scale may influence the scale detection. Hence, work can be carried out solely on oxide scale or on a combination of oxide and mineral scale.

This study has concentrated on the fundamental understanding and calibration of the technique as a method to detect mineral scale deposited on a sensor surface. This study can be used as a guide for further studies of mineral scale, especially with the presence of different types of inhibitors, commonly used in the oil and gas industry to avoid scaling problems. Studying and understanding the response of this technique in other real environments such as in the presence of the impurities of sand, oil, three phase systems and others are important. The current methodology is investigated under ambient temperature and atmospheric pressure conditions. In order to adapt this technology in downhole conditions, a series of feasibility studies is needed. Two important parameters in determining the amount of mineral scale deposited on

component surface are temperature and pressure, therefore a small laboratory simulation or investigation test at high temperature and pressure is necessary

It is interesting to investigate scale deposition and monitoring in a de-aerated system (with low level of oxygen in ppb of oxygen). As currently, this technique is based on oxygen as a tracer to determine the electrochemical reduction process and to determine the amount of scale covered on component surfaces. The change of the level of oxygen may influence the accuracy of this technique.

Nevertheless, electrochemical and acid cleaning indicated scale can be removed from the sensor's surface, both methods are not effective enough to completely clean the surface once scale has been deposited. More work is required in the sensor cleaning section to search for other alternative techniques that would be able to improve cleaning technique.

References

[1] Brown, M., *Full scale attack*, in *The BP Technology Magazine*. Oct-Dec1988. p. 30-32.

[2] Tjomsland, T., M.N. Grotle, and O. Vikane. *Scale control strategy and economical consequences of scale at Veslefrikk*. in *International Symposium on Oilfield Scale*. 2001. Aberdeen, United Kingdom: Society of Petroleum Engineers.

[3] Cranfield University's School of Water Sciences.

[4] Langelier, W.F., *Chemical equilibria in water treatment* Journal of the American Water Works Association, 1946. **38**: p. 169-182.

[5] Langelier, W.F., *The analytical control of anti-corrosion water treatment.* Journal of the American Water Works Association, 1939. **28**: p. 1500-1521

[6] Ryzar, J.W., *A new index for determining the amount of calcium carbonate scale formed by water.* Journal of the American Water Works Association, 1944. **36**: p. 472-486.

[7] Davis, H.A.S.J.a.L.E., *A method for predicting the tendency of oil field waters to deposit calcium carbonate.* Published in Petroleum Transactions, AIME, 1952. **195**: p. 213-216.

[8] Oddo, J.E. and M.B. Tomson, *Scale control prediction and treatment of how companies evaluate a scaling problem and what they do wrong.* CORROSION, NACE International, 1992(Paper No 34.).

[9] Oddo, J.E. and M.B. Tomson, *Why scale forms and how to predict it.* SPE Production & Facilities, 1994. **9**(1): p. 47-54.

[10] Tomson, M.B., Amy, T. Kan., Gongmin Fu and Musaed Al-Thubaiti. *Norm scale formation, control and relation to gas hydrate control*. in *10th International Petroleum Environmental Conference* November 11-14, 2003. Houston, TX.

[11] Ferguson, R.J., Freedman, A. J., Fowler, G., Kulik, A. J., Robson, J.and Weintritt, D. J., *The practical application of ion association model saturation indices to commercial water treatment problem solving.* American Chemical Society Paper, 1994.

[12] Hasson, D., et al., *Influence of the flow system on the inhibitory action of $CaCO_3$ scale prevention additives.* Desalination, 1997. **108**(1-3): p. 67-79.

[13] Arkam, C., et al., *Quartz-crystal electrogravimetry with controlled hydrodynamics - Applications to the study of nickel electrodeposition.* Journal of the Electrochemical Society, 1994. **141**(9): p. L103-L105.

[14] Compton, R.G. and C.A. Brown, *AC impedance spectroscopy of calcium carbonate.* Journal of Applied Electrochemistry, 1993. **23**: p. 203-211.

[15] Morizot, A.P., *Electrochemically based study of mineral scale formation and inhibition*, in *School of Mechanical*. 1999, Heriot Watt University: Edinburgh.

[16] Gabrielli, C., et al., *Nucleation and growth of calcium carbonate by an electrochemical scaling process.* Journal of Crystal Growth, 1999. **200**(1-2): p. 236-250.

[17] Gabrielli, C., et al., *Quartz crystal microbalance investigation of electrochemical calcium carbonate scaling.* Journal of the Electrochemical Society, 1998. **145**(7): p. 2386-2396.

[18] Gabrielli, C., et al., *Study of calcium carbonate scales by electrochemical impedance spectroscopy.* Electrochimica Acta, 1997. **42**(8): p. 1207-1218.

[19] Deslouis, C., et al., *Impedance techniques at partially blocked electrodes by scale deposition.* Electrochimica Acta, 1997. **42**(8): p. 1219-1233.

[20] Jean-Pierre Poyet, G.S., and Eric Toskey,. *Real-time method for the detection and characterization of scale*. in *International Symposium on Oilfield Scale*. 2002. Aberdeen, United Kingdom: Society of Petroleum Engineers.

[21] *Time Resolved Electrochemical Quartz Crystal Microbalance: for electro-deposition, adsorption, and chemical and biological sensor studies.* (IJ Cambria Scientific Ltd.).

[22] Neville, A. and A.P. Morizot, *A combined bulk chemistry/electrochemical approach to study the precipitation, deposition and inhibition of $CaCO_3$.* Chemical Engineering Science, 2000. **55**(20): p. 4737-4743.

[23] Deslouis, C., et al., *Interfacial pH measurement during the reduction of dissolved oxygen in a submerged impinging jet cell.* Journal of Applied Electrochemistry, 1997. **27**(4): p. 482-492.

[24] Loveday, D., P. Peterson, and B. Rodgers, *Evaluation of organic coatings with electrochemical impedance spectroscopy.* JCT CoatingsTech, 2004.

[25] Bousselme, L., et al., *The characterization of the coated layer at the interface carbon steel-natural salt by impedance spectroscopy.* Corrosion Science, 1997. **39**: p. 9.

[26] Gabrielli, C., et al., *Dynamic analysis of charge transport in fluidized bed electrodes: Impedance techniques for electro-inactive beds.* Journal of Applied Electrochemistry, 1992. **22**(9): p. 801-809.

[27] Candy, J.-P., et al., *The characterization of porous electrodes by impedance measurements.* Electrochimica Acta, 1981. **26**(8): p. 1029-1034.

[28] Gabrielli, C., et al., *An electrochemical method for testing the scaling susceptibility of insulating materials.* Journal of the Electrochemical Society, 2001. **148**(12): p. B517-B521.

[29] Lester, S.R.L., VA), *High frequency ultrasonic technique for measuring oxide scale on the inner surface of boiler tubes*. 1987, The Babcock & Wilcox Company (New Orleans, LA): United States.

[30] Okabe, Y.T., JP), Iwamoto, Keiichi (Nagasaki, JP), Torichigai, Masaaki (Nagasaki, JP), Kaneko, Shozo (Nagasaki, JP), Ichinari, Joji (Nagasaki, JP), Koizumi, Kiyoshi (Tokyo, JP), *Automated ultrasonic examination system for heat transfer tubes in a boiler*. 1989, Tokyo Electric Power Co. (Tokyo, JP),Mitsubishi Jukogyo Kabushiki Kaisha (Tokyo, JP): United States.

[31] Gunarathne, G.P.P. and R.W. Keatch. *Novel techniques for monitoring and enhancing dissolution of mineral deposits in petroleum pipelines* in *Offshore Europe*. 1995. Aberdeen, United Kingdom: Society of Petroleum Engineers.

[32] Slough, C.M., *Scale monitoring means and method*. 1988, Texaco Inc. (White Plains, NY): United States.

[33] Eaton, P.E., *Fouling test apparatus*. 1981, Petrolite Corporation (St. Louis, MO): United States.

[34] *Apparatus for measuring fouling on metal surfaces*. 1975, Universal Oil Products Company (Des Plaines, IL): United States.

[35] Fajhan Hilal, A. and R.D. David, *Detection of Scale Deposition Using Distributed Temperature Sensing*, in *SPE International Oilfield Scale Conference*. 2008, Society of Petroleum Engineers: Aberdeen, UK.

[36] S., B., et al., *Revitalizing Production logging.* Oilfield Review. **8**(4): p. 44-60.

[37] Kraus, P.R.B., IL), Mcclain, Robert D. (Sugar Land, TX), Poindexter, Michael K. (Sugar Land, TX), *Method to monitor and control chemical treatment of petroleum, petrochemical and processes with on-line quartz crystal microbalance sensors*. 1998, Nalco/Exxon Energy Chemicals, L.P. (Sugar Land, TX): United States.

[38] Emmons, D.H., et al. *On-site, near-real-time monitoring of scale deposition*. in *SPE Annual Technical Conference and Exhibition*. 1999. Houston, Texas: Society of Petroleum Engineers.

[39] Bertrand Theuveny, G. Ségéral, and P.O. Moksnes. *Detection and identification of scales using dual energy / venturi subsea or topside multiphase flow meters* in *Offshore Technology Conference*. 2001. Houston, Texas: Society of Petroleum Engineers.

[40] Welford, K.R., J.R. Sambles, and M.G. Clark, *Guided modes and surface plasmon-polaritons observed with a Nematic Liquid-Crystal using attenuated total reflection.* Liquid Crystals, 1987. **2**(1): p. 91-105.

[41] Smith, K.J.H., TX, US), Means, Mitch C. (Richmond, TX, US), Yuan, Mingdong (Missouri City, TX, US), Przybylinski, John L. (Missouri City, TX, US), Lopez, Thomas H. (Houston, TX, US), Ponstingl, Michael James (St. Louis, MO, US), *Real-time on-line sensing and control of mineral scale deposition from formation fluids*. 2005, Baker Hughes Incorporated (Houston, TX, US): United States.

[42] Smith, J.K., et al., *Real-time and in-situ detection of calcium carbonate scale in a West Texas oil field.* SPE Production & Facilities, 2004. **19**(2): p. 94-99.

[43] Mansoori, G.A., *Arterial blockage in the petroleum and natural gas industries - heavy organics (asphaltene / bitumen, resin, organometallics, paraffin / wax, diamondoids, etc.) deposition from petroleum fluids.* An INTERNET publication: http://www.uic.edu/~mansoori/HOD_html, 1995.

[44] Patel, S. and M.A. Finan, *New antifoulants for deposit control in MSF and MED plants.* Desalination, 1999. **124**(1-3): p. 63-74.

[45] Tracy, S.L., C.J.P. Francois, and H.M. Jennings, *The growth of calcite spherulites from solution - I. Experimental design techniques.* Journal of Crystal Growth, 1998. **193**: p. 374-381.

[46] Dunn, K., et al., *Mechanisms of surface precipitation and dissolution of barite: A morphology approach.* Journal of Colloid and Interface Science, 1999. **214**(2): p. 427-437.

[47] Blount, C.W., *Barite solubilities and thermodynamic quantities up to 300 degrees C and 1400 bars.* American Mineralogist, 1977. **62**(9-10): p. 942-957.

[48] Raju, K. and G. Atkinson, *Thermodynamics of scale mineral solubilities .1. $BaSO_{4(S)}$ in H_2O and aqueous NaCl.* Journal of Chemical and Engineering Data, 1988. **33**(4): p. 490-495.

[49] Patton, C.C., *Applied water technology*. 2007: John M. Campbell and Company.

[50] Todd, A.C. and M.D. Yuan, *Barium and strontium sulfate solid-solution scale formation at elevated temperatures.* SPE Production Engineering, 1992. **7**(1): p. 85-92.

[51] Gardner, G.L. and G.H. Nancollas, *Crystal-growth in aqueous-solution at elevated-temperatures - barium-sulfate growth-kinetics.* Journal of Physical Chemistry, 1983. **87**(23): p. 4699-4703.

[52] Liu, S.T., G.H. Nancollas, and E.A. Gasiecki, *Scanning electron microscopic and kinetic studies of the crystallization and dissolution of barium sulfate crystals.* Journal of Crystal Growth, 1976. **33**(1): p. 11-20.

[53] Suito, E. and K. Takiyama, *Formation and aging of precipitates I- electron microscopic studies of the formation of barium sulfate precipitate.* Bulletin of the Chemical Society of Japan, 1954. **27**(3): p. 121-123.

[54] Blanco, M., et al. in *Msc 96 Meeting*. 1996. Pasadena.

[55] Morizot, A., P. and A. Neville. *Barium sulfate deposition and precipitation using a combined electrochemical surface and bulk solution approach*. in *CORROSION*. 2000. Houston, TX, ETATS-UNIS: NACE International.

[56] Yokota, M., et al., *Formation and structure of round-shaped crystals of barium sulfate.* Chemical Engineering Science, 2000. **55**(19): p. 4379-4382.
[57] Plummer, L.N. and E. Busenberg, *The solubilities of calcite, aragonite and vaterite in CO2-H2O solutions between 0 and 90°C, and an evaluation of the aqueous model for the system CaCO3-CO2-H2O.* Geochimica et Cosmochimica Acta, 1982. **46**(6): p. 1011-1040.
[58] Appelo, C.A.J. and D. Postma, *Geochemistry groundwater and pollution*. 1993. 315-318.
[59] Mullin, J., *Crystallisation*. 3rd ed. 1993: Butterworth-Heinemann, London.
[60] Gibbs, J.W., *Thermodynamics*. Vol. 1. 1948: Yale University Press, New Haven
[61] Volmer, M., *Kinetic der Phasenbildung*. 1944: Stinkopff, Leipzig.
[62] Becker, R. and W. Döring, *Kínetische Behandlung der Keimbildung in übersättigten Dämpfen.* Annalen der Physik, 1935. **24**: p. 719.
[63] Jaouhari, R., et al., *Influence of water composition and substrate on electrochemical scaling.* Journal of The Electrochemical Society, 2000. **147**(6): p. 2151-2161.
[64] Kossel, W., *Zur Energetik von Oberflächenvorgängen.* Annalen der Physik, 1934. **413**(5): p. 457-480.
[65] Shooter, D., *Aqueous environmental chemistry of metals, Allen J. Rubin, Ann Arbor Science Publishers, Inc. (1974). 390 pages. $20.00.* AIChE Journal, 1976. **22**(1): p. 202-202.
[66] Burton, W.K., N. Cabrera, and F.C. Frank, *The growth of crystals and the equilibrium structure of their surfaces.* Philos. Trans. Roy. Soc. London. Ser. A., 1951. **243**: p. 299-358. .
[67] Noyes, A.A. and W.R. Whitney, *Rate of solution solid substances in their own solution.* Journal of the American Chemical Society, 1897. **19**(12): p. 930-934.
[68] Berthoud, A., *Theorie de la formation des faces d'un crystal.* Journal de Chimique Physique, 1912. **10**: p. 624–635.
[69] Valeton, J.J.P., *Wachstum und Auflosung der Kristalle.* Zeitschrift für Krystallographie, 1924. **59**: p. 483.
[70] Sjöberg, E.L. and D.T. Rickard, *Calcite dissolution kinetics: Surface speciation and the origin of the variable pH dependence.* Chemical Geology, 1984. **42**(1-4): p. 119-136.
[71] Söhnel, O. and J.W. Mullin, *Precipitation of calcium carbonate.* Journal of Crystal Growth, 1982. **60**(2): p. 239-250.
[72] Davies, C.W. and A.L. Jones, *The precipitation of silver chloride from aqueous solution Part 2-kinetics of growth of seed crystals.* Trans. Faraday Soc. , 1955. **51**: p. 812 - 817.
[73] Nancollas, G.H. and M.M. Reddy, *The crystallization of calcium carbonate. II. Calcite growth mechanism.* Journal of Colloid and Interface Science, 1971. **37**(4): p. 824-830.
[74] Plummer, L.N., T.M.L. Wigley, and D.L. Parkhurst, *The kinetics of calcite dissolution in CO_2-water systems at 5 to 60^{o}C and 0 to 1.0 atm CO_2.* American Journal of Science, 1978. **278**(2): p. 179-216.
[75] Zhang, Y. and R. Dawe, *The kinetics of calcite precipitation from a high salinity water.* Applied Geochemistry, 1998. **13**(2): p. 177-184.
[76] Zhang, Y., et al., *The kinetics of carbonate scaling--application for the prediction of downhole carbonate scaling.* Journal of Petroleum Science and Engineering, 2001. **29**(2): p. 85-95.
[77] Seidner, D.S., *Method for monitoring and controlling scale formation in a well*. 1989, Conoco Inc. (Ponca City, OK).

[78] Berner, R.A. and J.W. Morse, *Dissolution kinetics of calcium carbonate in sea water; IV, Theory of calcite dissolution.* Am J Sci, 1974. **274**(2): p. 108-134.
[79] Rickard, D.T. and E.L. Sjoberg, *Mixed kinetic control of calcite dissolution rates.* American Journal of Science, 1983. **283** (8): p. 815-830.
[80] Compton, R.G. and P.R. Unwin, *The dissolution of calcite in aqueous-solution at pH less-than-4 - kinetics and mechanism.* Philosophical Transactions of the Royal Society of London Series a-Mathematical Physical and Engineering Sciences, 1990. **330**(1609): p. 1-&.
[81] Chou, L., R.M. Garrels, and R. Wollast, *Comparative study of the dissolution kinetics and mechanisms of carbonates in aqueous solutions.* Chemical Geology, 1988. **70**(1-2): p. 77-77.
[82] Plummer, L.N., D.L. Parkhurst, and T.M.L. Wigley, *Critical review of the kinetics of calcite dissolution and precipitation.*, in *Chemical Modeling—Speciation, Sorption, Solubility and Kinetics in Aqueous Systems*, E. Jenne, Editor. 1979, American Chemical Society, Washington, DC. p. 537– 573.
[83] Morse, J.W. and R.S. Arvidson, *The dissolution kinetics of major sedimentary carbonate minerals.* Earth-Science Reviews, 2002. **58**(1-2): p. 51-84.
[84] Compton, R.G., P.J. Daly, and W.A. Houses, *The dissolution of iceland spar crystals: The effect of surface morphology.* Journal of Colloid and Interface Science, 1986. **113**(1): p. 12-20.
[85] Schott, J., et al., *Dissolution kinetics of strained calcite.* Geochimica et Cosmochimica Acta, 1989. **53**(2): p. 373-382.
[86] Van Cappellen, P., et al., *A surface complexation model of the carbonate mineral-aqueous solution interface.* Geochimica et Cosmochimica Acta, 1993. **57**(15): p. 3505-3518.
[87] Harding, K., D.A. Brikdle, and F. Thorne, *Chemical descaling of acid dosed desalination plants.* Desalination, 1978. **27**(3): p. 273-282.
[88] Dudley, L.Y. and J.S. Baker. *The role of antiscalants and cleaning chemicals to control membrane fouling*. in *Water Asia* 1999. New Delhi, India: PermaCare. ®. Reprint. R-799.
[89] Amjad, Z., *Science and Technology of Industrial Water Treatment*. 2010: The International Water Association (IWA),Co-Published with CRC Press.
[90] Tomson, M.B., et al. *Mechanisms of mineral scale inhibition*. in *International Symposium on Oilfield Scale*. 2002. Aberdeen, United Kingdom: Society of Petroleum Engineers.
[91] Xyla, A.G., J. Mikroyannidis, and P.G. Koutsoukos, *The inhibition of calcium carbonate precipitation in aqueous media by organophosphorus compounds.* Journal of Colloid and Interface Science, 1992. **153**(2): p. 537-551.
[92] Verwey, E.J.W. and J.T.G. Overbeek, *Theory of the stability of lyophobic colloids.* Journal of Colloid Science, 1955. **10**(2): p. 224-225.
[93] Derjaguin, B.V., *A theory of the heterocoagulation, interaction and adhesion of dissimilar particles in solutions of electrolytes.* Progress in Surface Science, 1993. **43**(1-4): p. 60-73.
[94] Epstein, N., *Elements of particle deposition onto nonporous solid surfaces parallel to suspension flows.* Experimental Thermal and Fluid Science, 1997. **14**(4): p. 323-334.
[95] Oliveira, R., *Understanding adhesion: A means for preventing fouling.* Experimental Thermal and Fluid Science, 1997. **14**(4): p. 316-322.
[96] van Oss, C.J., M.K. Chaudhury, and R.J. Good, *Monopolar surfaces.* Advances in Colloid and Interface Science, 1987. **28**: p. 35-64.

[97] Harris, A. and A. Marshall. *The evaluation of scale control additives*. in *Proceedings of Symposium on progress in the prevention of fouling in industrial plant*. 1981. Nottingham.

[98] Sohnel, O. and J. Garside, *Precipitation—basic principles and industrial applications*. 1992: Butterworth-Heinemann Ltd.

[99] Abdel-Aal, N., K. Satoh, and K. Sawada, *Study of the adhesion mechanism of $CaCO_3$ using a combined bulk chemistry/QCM technique.* Journal of Crystal Growth, 2002. **245**(1-2): p. 87-100.

[100] Vetter, O.J. and V. Kandarpa. *Prediction of $CaCO_3$ scale under downhole conditions*. in *SPE Oilfield and Geothermal Chemistry Symposium*. 1980 Stanford, California: American Institute of Mining, Metallurgical, and Petroleum Engineers, Inc.

[101] Vetter, O.J., Farone, W.A., . *Calcium carbonate scale in oilfield operations*. in *SPE Annual Technical Conference and Exhibition*. 1987. Dallas, Texas: Society of Petroleum Engineers

[102] Deslouis, C., et al., *Characterization of calcareous deposits in artificial sea water by impedance techniques—I. Deposit of $CaCO_3$ without $Mg(OH)_2$.* Electrochimica Acta, 1998. **43**(12-13): p. 1891-1901.

[103] Deslouis, C., Festy, D., Gil, O. Maillot, V., Touzain, S., Tribollet, B., *Characterization of calcareous deposits in artificial sea water by impedances techniques: 2-Deposit of $Mg(OH)_2$ without $CaCO_3$.* Electrochimica Acta, 2000 **45**(11): p. 1837-1845.

[104] Barchichea, C., et al., *Characterization of calcareous deposits in artificial seawater by impedance techniques: 3—Deposit of CaCO3 in the presence of Mg(II).* Electrochimica Acta, Volume 48, Issue 12, 30 May 2003, Pages 1645-1654, 2003. **48**(12): p. 1645-1654.

[105] Kobayashi, T. *Effect of environmental factors on the protective potential of steel*. in *Proceeding of 5th International on Metallic Corrosion NACE*. 1974.

[106] Hort, C. and H. Roques, Tribune l'Eau, 3, 1997. **3**: p. 587.

[107] Yan, J.F., R.E. White, and R.B. Griffin, *Parametric studies of the formation of calcareous deposits on cathodically protected steel in seawater.* Journal of The Electrochemical Society, 1993. **140**(5): p. 1275-1280.

[108] Loste, E., et al., *The role of magnesium in stabilising amorphous calcium carbonate and controlling calcite morphologies.* Journal of Crystal Growth, 2003. **254**(1-2): p. 206-218.

[109] Meldrum, F.C. and S.T. Hyde, *Morphological influence of magnesium and organic additives on the precipitation of calcite.* Journal of Crystal Growth, 2001. **231**(4): p. 544-558.

[110] Fitzgerald, J.A. and S.V. Garimella, *A study of the flow field of a confined and submerged impinging jet.* Int. J. Heat Transfer, 1998. **14**: p. 1025-1034.

[111] Esteban, J.M., G.S. Hickey, and M.E. Orazem, *The impinging jet electrode measurement of the hydrodynamic constant and its use for evaluating film persistency.* CORROSION, NACE International, 1990. **46**: p. 896-901.

[112] Chin, D.T. and C.H. Tsang, *Mass transfer to an impinging jet electrode.* Journal of the Electrochemical Society, 1978. **125**(9): p. 1461-1470.

[113] Bouet, V., et al., *Application of electrochemical impedance analysis to the characterization of mass-transfer in a submerged impinging jet cell.* Journal of Electroanalytical Chemistry, 1992. **340**(1-2): p. 325-331.

[114] Coeuret, F., *Transfert de matiere lors de l'impact normal de jets liquides circulaires immerges.* Chemical Engineering Science, 1975. **30**(10): p. 1257-1263.

[115] Chen, T., A. Neville, and M. Yuan. *Comparison of calcium carbonate scale formed in the bulk solution and on surface of metal*. in *1st IWA Conference on Scaling and Corrosion in the Water and Waterwaste System* 2003. Cranfield University, UK.

[116] Filinovsky, V.Y., *The limiting diffusion current value on a macroscopically inhomogeneous electrode.* Electrochimica Acta, 1980. **25**(3): p. 309-314.

[117] Chin, D.T. and R.R. Chandran, *Ring Disk Electrodes with an Impinging Jet.* Journal of The Electrochemical Society, 1981. **128**(9): p. 1904-1912.

[118] Alkire, R.C. and T.-J. Chen, *High-speed selective electroplating with single circular jets.* Journal of The Electrochemical Society, 1982. **129**(11): p. 2424-2432.

[119] Babic, R. and M. Metikoshukovic, *Oxygen reduction on stainless steel.* Journal of Applied Electrochemistry, 1993. **23**(4): p. 352-357.

[120] Morizot, A.P. and A. Neville. *A novel approach for monitoring of $CaCO_3$ and $BaSO_4$ scale formation*. in *International Symposium on Oilfield Scale*. 2000. Aberdeen, United Kingdom: Society of Petroleum Engineers.

[121] Yang, Q., et al., *Investigation of calcium carbonate scaling inhibition and scale morphology by AFM.* Journal of Colloid and Interface Science, 2001. **240**(2): p. 608-621.

[122] Ramadan, S. and H. Idrissi, *In situ monitoring of deposition and dissolution of calcium carbonate by acoustic emission techniques associated to electrochemical measurements.* Desalination, 2008. **219**(1-3): p. 358-366.

[123] Moller, P. and C.S. Sastri, *Estimation of the number of surface layers of calcite involved in Ca-45Ca isotopic exchange with solution.* Z. Physik. Chem. N. F., 1974. **89**(80): p. 80.

[124] Tao Chen, Anne Neville, and Mingdong Yuan, *Influence of Mg^{2+} on $CaCO_3$ formation--bulk precipitation and surface deposition.* Chemical Engineering Science, 2006. **61**(16): p. 5318-5327.

[125] Reddy, M.M. and K.K. Wang, *Crystallization of calcium carbonate in the presence of metal ions : I. Inhibition by magnesium ion at pH 8.8 and 25°C.* Journal of Crystal Growth, 1980. **50**(2): p. 470-480.

[126] Ahlberg Tidblad, A. and F. Herlitz, *Initial growth of calcic deposits on the cathode of a chlorate cell. Surface characterization using scanning electron microscopy and X-ray microanalysis (SEM/EDS).* Electrochimica Acta, 1999. **44**(13): p. 2251-2261.

[127] Reddy, M.M. and G.H. Nancollas, *The crystallization of calcium carbonate : IV. The effect of magnesium, strontium and sulfate ions.* Journal of Crystal Growth, 1976. **35**(1): p. 33-38.

[128] Gutjahr, A., H. Dabringhaus, and R. Lacmann, *Studies of the growth and dissolution kinetics of polymorphs calcite and aragonite II. The influence of divalent cation additives on the growth and dissolution rates.* Journal of Crystal Growth, 1996. **158**: p. 310-315.

[129] Lippmann, F., *Sedimentary carbonate minerals*. Minerals, rocks and inorganic materials ; 6. 1973, Berlin, New York: Springer-Verlag.

[130] Berner, R.A., *The role of magnesium in the crystal growth of calcite and aragonite from sea water.* Geochimica et Cosmochimica Acta, 1975. **39**(4): p. 489-494, IN3, 495-504.

[131] Tao Chen, A. Neville, and M. Yuan. *Influence of Mg^{2+} on the kinetics and morphology of scale formation on the metal surfaces and in the bulk solution.* in *CORROSION*. 2004 New Orleans, La: NACE International.

[132] Ogino, T., T. Suzuki, and K. Sawada, *The formation and transformation mechanism of calcium carbonate in water.* Geochimica et Cosmochimica Acta, 1987. **51**(10): p. 2757-2767.
[133] Clifford, Y.T. and F.B. Chen, *Polymorphism of $CaCO_3$, precipitated in a constant-composition environment.* AIChE Journal, 1998. **44**(8): p. 1790-1798.
[134] Sedriks, J., *Corrosion of stainless steels* 2nd ed. 1996: John Willey& Sons, Inc., New York.
[135] Fossati, A., et al., *Corrosion resistance properties of glow-discharge nitrided AISI 316L austenitic stainless steel in NaCl solutions.* Corrosion Science, 2006. **48**(6): p. 1513-1527.
[136] Yang, Q. and J.L. Luo, *Effects of hydrogen and tensile stress on the breakdown of passive films on type 304 stainless steel.* Electrochimica Acta, 2001. **46**(6): p. 851-859.
[137] Abd El Meguid, E.A., N.A. Mahmoud, and S.S. Abd El Rehim, *The effect of some sulphur compounds on the pitting corrosion of type 304 stainless steel.* Materials Chemistry and Physics, 2000. **63**(1): p. 67-74.
[138] Ameer, M.A., A.M. Fekry, and F.E.-T. Heakal, *Electrochemical behaviour of passive films on molybdenum-containing austenitic stainless steels in aqueous solutions.* Electrochimica Acta, 2004. **50**(1): p. 43-49.
[139] El-egamy, S.S. and W.A. Badaway, *Passivity and passivity breakdown of 304 stainless steel in alkaline sodium sulphate solutions.* Journal of Applied Electrochemistry, 2004. **34**(11): p. 1153-1158.
[140] Kim, J.D. and S.I. Pyun, *The effects of applied potential and chloride ion on the repassivation kinetics of pure iron.* Corrosion Science, 1996. **38**(7): p. 1093-1102.
[141] Morizot, A., A. Neville, and T. Hodgkiess, *Studies of the deposition of $CaCO_3$ on a stainless steel surface by a novel electrochemical technique.* Journal of Crystal Growth, 1999. **198-199**(Part 1): p. 738-743.
[142] Devos, O., C. Gabrielli, and B. Tribollet, *Nucleation-growth process of scale electrodeposition--Influence of the mass transport.* Electrochimica Acta, 2006. **52**(1): p. 285-291.
[143] Devos, O., C. Gabrielli, and B. Tribollet, *Simultaneous EIS and in-situ microscope observation on a partially blocked electrode application to scale electrodeposition.* Electrochimica Acta, 2006. **51**(8-9, 20): p. 1413-1422.
[144] Lédion, J., P. Leroy, and L.J. P., *Détermination du caractère incrustant d'une eau par essai d'entartrage accéléré.* TSM - L'eau, 1985. **80**(7-8): p. 323-328.
[145] Gabrielli, C., et al., *Characterization of the efficiency of antiscale treatments of water Part I: Chemical processes.* Journal of Applied Electrochemistry, 1996. **26**(11): p. 1125-1132.
[146] Gabrielli, C., et al., *Investigation of electrochemical calcareous scaling: Potentiostatic current- and mass-time transients.* Journal of Electroanalytical Chemistry, 2002. **538-539**: p. 133-143.
[147] Qiu, J.H., *Passivity and its breakdown on stainless steels and alloys.* Surface and Interface Analysis, 2002. **33**(10-11): p. 830-833.
[148] Okuyama, M. and S. Haruyama, *The cathodic reduction of oxygen on stainless steels in a neutral solution.* Corrosion Science, 1990. **31**: p. 521-526.
[149] Schmuki, P., et al., *Electrochemical behavior of Cr_2O_3/Fe_2O_3 artificial passive films studied by in situ XANES.* Journal of the Electrochemical Society, 1998. **145**(3): p. 791-801.
[150] Devito, E. and P. Marcus, *XPS study of passive films formed on molybdenum-implanted austenitic stainless-steels.* Surface and Interface Analysis, 1992. **19**(1-12): p. 403-408.

[151] Macdonald, D.D., S.R. Biaggio, and H. Song, *Steady-state passive films.* Journal of The Electrochemical Society, 1992. **139**(1): p. 170-177.
[152] Abreu, C.M., et al., *Comparative study of passive films of different stainless steels developed on alkaline medium.* Electrochimica Acta, 2004. **49**(17-18): p. 3049-3056.
[153] Bouttemy, M., et al. *Ageing of passivated Fe-Ni and Fe-Cr alloys : study of formation and growth's mechanisms of passive films*. in *EUROCORR*. 2004. Nice, France,.
[154] Yang, W.P., D. Costa, and P. Marcus, *Chemical composition, chemical states, and resistance to localized corrosion of passive films on an Fe-17%Cr alloy.* Journal of Electrochemical Society., 1994. **141**(1): p. 111-116
[155] Latimer, W.M., *Oxidation Potentials*. 1964, Prentice Hall, Englewood cliffs, NJ. p. 319.
[156] Kunjapur, M.M., W.H. Hartt, and S.W. Smith, *Influence of temperature and exposure time upon calcareous deposits.* CORROSION, NACE International, 1987. **43**(11): p. 674-679.
[157] Humble, R.A., *Cathodic Protection of Steel in Seawater with Magnesium Anodes.* Corrosion Nace International, 1948. **4**(7): p. 358.
[158] Shams El Din, A.M., *The problem of "red waters": A new approach to its solution.* Desalination, 1986. **60**(1): p. 75-88.
[159] Le Bozec, N., et al., *Influence of stainless steel surface treatment on the oxygen reduction reaction in seawater.* Corrosion Science, 2001. **43**(4): p. 765-786.
[160] Barchiche, C., et al., *Characterisation of calcareous deposits by electrochemical methods: role of sulphates, calcium concentration and temperature.* Electrochimica Acta, 2004. **49**(17-18): p. 2833-2839.
[161] Ambrose, J.R., A.E. Yaniv, and U.R. Lee. *Nucleation, growth and morphology of calcereous deposits on steel in seawater*. in *CORROSION*. 1983. Anaheim, Calif ; U.S.A: NACE International.
[162] Euvrard, M., C. Filiatre, and E. Crausaz, *A cell to study in situ electrocrystallization of calcium carbonate.* Journal of Crystal Growth, 2000. **216**(1-4): p. 466-474.
[163] Domingo, C., et al., *Calcite precipitation by a high-pressure CO_2 carbonation route.* The Journal of Supercritical Fluids, 2006. **36**(3): p. 202-215.
[164] García Carmona, J., J. Gómez Morales, and R. Rodríguez Clemente, *Rhombohedral-scalenohedral calcite transition produced by adjusting the solution electrical conductivity in the system $Ca(OH)_2$-CO_2-H_2O.* Journal of Colloid and Interface Science, 2003. **261**(2): p. 434-440.
[165] Gómez-Morales, J., J. Torrent-Burgués, and R. Rodríguez-Clemente, *Nucleation of calcium carbonate at different initial pH conditions.* Journal of Crystal Growth, 1996. **169**(2): p. 331-338.
[166] Jung, W.M., et al., *Particle morphology of calcium carbonate precipitated by gas-liquid reaction in a Couette-Taylor reactor.* Chemical Engineering Science, 2000. **55**(4): p. 733-747.
[167] Montes-Hernandez, G., et al., *Calcite precipitation from CO_2-H_2O-$Ca(OH)_2$ slurry under high pressure of CO_2.* Journal of Crystal Growth, 2007. **308**(1): p. 228-236.
[168] Kitano, Y., N. Kanamori, and A. Tokuyama, *Effects of Organic Matter on Solubilities and Crystal Form of Carbonates.* Amer. Zool., 1969. **9**(3): p. 681-688.
[169] Legrand, L. and P. Leroy, *Prevention of corrosion and scaling in water supply systems*. Ellis Horwood series in water and wastewater technology, Ellis

Horwood series, water and wastewater technology. 1990: E. Horwood (New York)
[170] Lin, S. and S.C. Dexter, *Effects of temperature and magnesium ions on calcareous deposition.* Corrosion Science, 1988. **44,**(9): p. 615-622.
[171] Ramasubramanian, N., N. Preocanin, and R.D. Davidson, *Analysis of passive films on stainless steel by cyclic voltammetry and auger spectroscopy.* Journal of The Electrochemical Society, 1985. **132**(4): p. 793-798.
[172] Gojkovic, S.L., et al., *Oxygen reduction on a duplex stainless steel.* Corrosion Science, 1998. **40**(6): p. 849-860.
[173] Oddo, J.E. and M.B. Tomson, *Simplified calculation of $CaCO_3$ saturation at high temperatures and pressures in brine solutions.* Journal of Petroleum Technology, 1982. **34**(7): p. 1583-1590.
[174] Buesnberg, E. and N.L. Plummer, *A comparative study of the dissolution and crystal growth kinetics of calcite and aragonite*, in *Studies in Diagenesis*, F.A. Mumptoon, Editor. 1986, U.S. Geological Survey (Washington) p. 139-168.
[175] Plummer, L.N. and T.M.L. Wigley, *The dissolution of calcite in CO2-saturated solutions at 25°C and 1 atmosphere total pressure.* Geochimica et Cosmochimica Acta, 1976. **40**(2): p. 191-202.
[176] Vago, E.R., E.J. Calvo, and M. Stratmann, *Electrocatalysis of oxygen reduction at well-defined iron oxide electrodes.* Electrochimica Acta, 1994. **39**(11-12): p. 1655-1659.
[177] Stratmann, M. and J. Müller, *The mechanism of the oxygen reduction on rust-covered metal substrates.* Corrosion Science, 1994. **36**(2): p. 327-359.
[178] Zecevic, S., D.M. Drazic, and S. Gojkovc, *Oxygen reduction on iron--V. Processes in boric acid-borate buffer solutions in the 7.4-9.8 pH range.* Corrosion Science, 1991. **32**(5-6): p. 563-576.
[179] Calvo, E.J. and D.J. Schiffrin, *The reduction of hydrogen peroxide on passive iron in alkaline solutions.* Journal of Electroanalytical Chemistry, 1984. **163**(1-2): p. 257-275.
[180] Jovancicevic, V. and J.O.M. Bockris, *The mechanism of oxygen reduction on iron in neutral solutions.* Journal of The Electrochemical Society, 1986. **133**(9): p. 1797-1807.
[181] Zhang, L. and D.D. Macdonald, *Segregation of alloying elements in passive systems--II. Numerical simulation.* Electrochimica Acta, 1998. **43**(18): p. 2673-2685.
[182] Zhang, L. and D.D. Macdonald, *Segregation of alloying elements in passive systems--I. XPS studies on the Ni-W system.* Electrochimica Acta, 1998. **43**(18): p. 2661-2671.
[183] Nishimura, R. and K. Kudo, *Pitting corrosion of nickel in borate and phosphate solutions.* CORROSION, NACE International, 1987. **43**(8): p. 486.
[184] Sato, N. and K. Kudo, *An ellipsometric study of anodic passivation of nickel in borate buffer solution.* Electrochimica Acta, 1974. **19**(8): p. 461-470.
[185] Sato, N., *An overview on the passivity of metals*. 1990, Elsevier: Oxford, ROYAUME-UNI. p. 793.
[186] Paola, A.D., *Semiconducting properties of passive films on stainless steels.* Electrochimica Acta, 1989. **34**(2): p. 203-210.